THE UNIVERSITY
of EDINBURGH

Developmental Pathways and Gene Function in Canine Myxomatous Mitral Valve Disease

Chih-Chien Lu

Thesis presented for the degree of

Doctor of Philosophy

Division of Veterinary Clinical Science
Royal (Dick) School of Veterinary Studies
College of Medicine and Veterinary Medicine
University of Edinburgh

Doctor of Philosophy – The University of Edinburgh – 2015

Declaration

I hereby declare that all the work included in this thesis, submitted for the degree of Doctorate of Philosophy at the University of Edinburgh, is my own original work and no part of this work has been, or will be, submitted for any other degree of qualification.

Chih Chien Lu

August 2015

Acknowledgement

Without great support, encouragement, understanding, and unconditional love from my father (Shiao-bin Lu), mother (Shu-ming Wu, 1950-2009), and brother (Chih-Gun Lu), I will not have been able to carry out my studies in the UK.

To my wife, Ye Fan, who is always by my side no matter how difficult the life is. Thank you for giving birth to our little baby (Aria). You are the reason to keep me always moving forward, and you are the one I am going to share any joy and tear in the rest of my life.

I would like to express my sincere appreciation and gratitude to my supervisors, Prof. Brendan M. Corcoran and Prof. David J. Argyle for their mentorship and guidance from the beginning to the end of my study. Special thanks to Geoff Culshaw and Anne French for their input in the early part of my PhD studies, and to Dr Michael Clinton who has guided me through the world of genomics.

I would also like to pay particular thanks to all the people in the Clinical Science Group at the Roslin Institute: Rhona, Karen, Lisa, Hannah, Adam, Tina, Tanveer, Craig, Julie, Mark, Julie, Emma, Breno, Teresa, Seungmee, Mathylda, and Daniela. You are my family in Edinburgh.

I express my gratitude to all the animals who contribute their valuable samples to the research, without whom this work would not have been possible.

This project was co-funded by the University of Edinburgh (Charles Darwin Scholarship), Cavalier King Charles Spaniel Club (UK), and the Taiwan Education Division and I would like to thank them for their support.

Abstract

Canine myxomatous mitral valve disease (MMVD) is the most common cardiac disease in dogs affecting all breeds, and it shares many similarities with the equivalent human disease. From the only transcriptomic report for canine MMVD published in 2006, serotonin signalling was identified as a contributing factor and has been widely studied since. Two transcriptomic profiling studies in human MMVD have also identified oxidative stress response and bone morphogenic protein signalling contributing to disease pathology. All studies at the transcriptional level have identified a variety of biological functions in MMVD suggesting dynamic extracellular matrix (ECM) remodelling processes are on-going. Moreover, cellular changes found in MMVD are somewhat reminiscent of the events seen in early heart valve, suggesting possible re-activation of signalling pathways of which those driving development and endothelial-to-mesenchymal transition (EndoMT) are particularly interesting. EndoMT, in which endothelial cells change their identity to mesenchymal phenotype and migrate into the cardiac jelly underneath the endothelium, is a crucial mechanism in valvulogenesis. Whether or not gene regulation of EndoMT and valve development also plays a role in MMVD is unknown.

In this study, the MMVD cellular changes in the Cavalier King Charles Spaniel (CKCS), a breed with the highest prevalence, earliest onset, and rapid progression of the disease, was investigated. Secondly, transcriptional profiling was conducted using the latest canine microarray chips, a single affected breed (CKCSs), stringent sample quality control and statistical thresholds, with quantitative polymerase chain reaction (Q-PCR) for data validation. After transcriptional mapping, multi-platform *in silico* analysis was conducted to identify relationship between differentially expressed genes and their relevant biological functions. Next, a comparison study using immunohistochemistry was performed on different severities of myxomatous valves to localize the proteins of interest. Finally, to model the transcriptional factors and their downstream targets, mitral valve endothelial cell (MVEC) clones were derived from the canine normal mitral valves for future *in vitro* studies.

Cellular changes of MMVD between CKCS and non-CKCS populations showed no difference in their distribution, number and phenotypic markers. Global genomic expression analysis identified similar (inflammation, up-regulation of serotonin receptor and bone morphogenic protein) and novel biological functions (epithelial-to-mesenchymal transition) compared to the previous study in 2006. Key transcriptional factors and genes associated with EndoMT including SNAI1, TAGLN, ACTA2, ACTG2, HAS2, and CTNNB1 were found up-regulated, and NID1, LAMA2, CDH5 were down-regulated in the MMVD group. In myxomatous mitral valves, increased expression of HAS2 in myofibroblasts, SNAI1 expression in endothelial cells, and co-expression of CDH5 and α-smooth muscle actin (α-SMA) also suggested the presence of EndoMT compared to normal valves. Nevertheless, there is also evidence of EndoMT in normal valves (α-SMA positive endothelial cells) which might suggest contribution to life-long valve re-modelling. In addition, there was a decreased expression of microRNAs associated with modulation of extracellular matrix transcripts, including miR-23, miR-29, and miR-218, indicating epigenetic regulation in MMVD.

Based on the cellular changes, MMVD in CKCS appears to be representative of MMVD in all breeds and the early-onset of MMVD in that breed does not lead to different end-stage pathology. Novel biological functions such as EndoMT, were identified by transcriptional profiling, and by using powerful bioinformatic tools providing insight into understanding gene regulation in MMVD. Furthermore, a relationship between developmental biology processes and MMVD pathogenesis was established, with a likely important role for epigenetics in disease pathogenesis.

Table of Contents

Abbreviations

5-HT	5-hydroxytryptamine
5-HT2B	5-hydroxytryptamine receptor 2B
ACTC	cardiac muscle actin
ADAMTS	a disintegrin and metalloproteinase with thrombospondin motifs
ANGPT1	angiopoietin 1
AV	atrioventricular
BM	basement membrane
BMP	bone morphogenic protein
BMPR	bone morphogenic protein receptor
BP	biological process
CAV	caveolin
CDH	cadherin
cfa-miRNA	canine familiaris microRNA
CHAD	chondroadherin
CILP	cartilage intermediate layer protein
CKCS	Cavalier King Charles Spaniel
CLDN	claudin
CRTAC1	cartilage acidic protein
CTGF	connective tissue growth factor
CTNNB	β-catenin
CTSK	cathepsin K
DCM	dilated cardiomyopathy
DNA	deoxyribonucleic acid
DTT	Dithiothreitol
ECM	extracellular matrix
EDN	endothelin or ET
EDNR	endothelin receptor
EGF	epithelial growth factor
ELN	elastin
EMT	epithelial-to-mesenchymal transition
EndoMT	endothelial-to-mesenchymal transition
ENG	endoglin
EPC	endothelial progenitor cells
FBLN	fibulin
FBN	fibrillin
FDR	false discovery rate
FGF	fibroblast growth factor

FLN	filamin
FN	fibronectin
GAG	glycosaminoglycan
GLCE	glucuronic acid epimerase
GO	gene ontology
GWAS	genome-wide association studies
HA	hyaluronan
HABP	hyaluronan-binding protein
HAPLN	hyaluronan and proteoglycan link protein
HARE	hyaluronan receptor for endocytosis
HAS2	hyaluronic acid synthase 2
HCM	hypertrophic cardiomyopathy
HSP47	heat shock protein 47
HSPG2	perlecan
HUVEC	human umbilical vein endothelial cell
ICAM	intercellular adhesion molecules
IHC	immunohistochemistry
IL-6	interleukine 6
IPA	Ingenuity Pathway Analysis
ITG	integrin
IVDD	intervertebral disc disease
KEGG	Kyoto Encyclopedia of Genes and Genomes
KERA	keratocan
LAMA	laminin
LAMB	laminin β
LDLR	low-density-lidoprotein receptor
MEndoT	mesenchymal-to-endothelial transition
MMP	matrix metalloproteinase
MMVD	myxomatous mitral valve disease
mRNA	messenger RNA
MT1/2	metallothioneins-1 and -2
MV	mitral valve
MVEC	mitral valve endothelial cell
NFATc1	nuclear factor of activated T-cells, cytoplasmic 1
NID	nidogen
NOS	nitric oxide synthase
OCLN	occludin
PBS	phosphate-buffered saline
PECAM	platelet endothelial cell adhesion molecule
PG	proteoglycan
PTN	periostin
QC	quality control

Q-PCR	quantitative polymerase chain reaction
RAAS	renin-angiotensin-aldosterone system
RBPJ	recombination signal binding protein for immunoglobulin kappa J region
RIN	RNA integrity index
RNA	ribonucleic acid
rRNA	ribosomal RNA
SCX	scleraxis
SELE	selectin
SL	semilunar
SLRP	small leucine-rich proteoglycan
SM22	smooth muscle cell marker, TAGLN
SMemb	embryonic smooth muscle myosin
SNP	single nucleotide polymorphism
TGF-β	transforming growth factor β
TIMP	tissue inhibitors of metalloproteinase
TLR	toll-like receptor
TNC	tenascin
tPA	tissue plasminogen activator
TPH1	tryptophan hydroxylase 1
tRNA	transfer RNA
UGDH	UDP-glucose dehydrogenase
VE-Cadherin	CD144, vascular endothelial cadherin, CDH5
VEGF	vascular endothelial growth factor
VIC	valve interstitial cell
VPS13B	vacuolar protein sorting 13 homolog B
vWF	von Willebrand factor
α-SMA	α-smooth muscle actin

List of Figures

List of Tables

1 Chapter 1 Introduction

From genesis to degeneration, the mitral valve is constantly in an active remodelling state, which is in response to uninterrupted and dynamic cues from both the internal and external environment such as normal aging, turbulent flow secondary to chamber geometry, and assaults from pathogens. The morphogenesis of valves is under sophisticated orchestration of cellular events including activation, migration, differentiation, and extracellular matrix deposition and organization. Mechanisms governing valve formation and extracellular matrix turnover also play important roles in myxomatous mitral valve degeneration. A well-described mechanism in valve development is endothelial-to-mesenchymal transition (EndoMT), in which endothelial cells switch their phenotype from endothelial to mesenchymal, and contribute to the formation of endocardial cushion and valves. [1,2] In a mouse model, EndoMT has also been shown to give rise to 25% of the fibroblasts in myocardial fibrosis, and this finding supports the idea that developmental pathways govern not only valvulogenesis, but could contribute to valve degeneration. [3] However, whether EndoMT is also involved or not in myxomatous degeneration is unknown. Therefore, a thorough understanding of heart morphogenesis is important in understanding disease pathogenesis and developing a hypothesis and inference on the role of valve developmental biology in disease.

1.1 Myxomatous Mitral Valve Disease

1.1.1 Historical Overview

Myxomatous mitral valve disease (MMVD) is the most common heart disease in dogs, and it has been known for more than a century. The earliest record of canine mitral valve disease can be traced back to 1817, when Delabere Blain identified an unusual thrill on the chest of a sick dog. [4] In humans, although the syndrome of a systolic murmur, now known as Barlow's disease, was first described in 1887 by Cuffer and Barbillon, it was not until the 1960s that these findings were recognized to be due to mitral valve prolapse. [5] Mitral valve prolapse due to mucoid degeneration in humans described by Read in 1965, shared similar pathology with canine MMVD, and was reported to feature fibroelastic degeneration. [5] In 1967, the

gross pathology grading system of canine MMVD was firstly introduced by Whitney. [6] The most common terminology used for the laminated mitral valve structure: atrialis, spongiosa, fibrosa, and ventricularis (not often used in mitral valve histopathology), was devised by Gross and Kugel. Pathological changes of MMVD have also been reported in an experimental heart failure canine model with ascites by Jarcho at Johns Hopkins Hospital. [7] In recent years, comparison between human and canine MMVD has suggested the potential role of dogs as a naturally occurring mitral valve degeneration model. [7]

1.1.2 Prevalence

MMVD accounts for ~75% of the cardiac disease in dogs, and the incidence increases with age in all canine breeds [8–11]. In general, geriatric animals and small breeds have the highest incidence of MMVD. Predisposed breeds include CKCS, Miniature Poodle, Miniature Schnauzer, Cocker Spaniel, Fox Terrier, Dachshund, Yorkshire Terrier, Chihuahua, Beagle, and Boston terrier, with highest frequencies in chondrodystrophoid breeds. [12] Although small breeds are most commonly affected, large breeds with dilated cardiomyopathy have been reported to be affected as well. [13,14] In one study, the incidence of clinical signs with MMVD was found to be positively associated with age, and more than one third of dogs were showing signs of congestive heart failure. Postmortem examination shows that nearly 93% of dogs aged between 9 and 12 years old are affected, and no dogs that are over 12 years old are free from MMVD (Table 1-1). [6] However, dogs that are younger than 5 years old are less likely to be affected by MMVD, with the exception of the cavalier King Charles spaniel (CKCS), which is reported to have 10% affected in dogs less than 1 year old, and particularly high prevalence and severe early onset characteristics. [15] The interesting and unusual CKCS-specific characteristics of MMVD have resulted in numerous research projects investigating the nature of MMVD in this breed.

Table 1-1 Incidence of MMVD with post-mortem prevalence in different age groups

Age	Incidence of Clinical Sign	Post-mortem (Whitney Grade I - IV)
5-8 Years Old	10%	n/a
9-12 Years Old	25%	93%
> 12 Years Old	35%	100%

1.1.3 Cavalier King Charles Spaniel

In the 16th century, several types of Spaniel were popular among the European aristocracy. However, it was under the Stuarts that the name of King Charles Spaniels was given to one breed of spaniel. It is said that King Charles II was seldom seen without a few spaniels at his heels (Figure 1-1). [16] The long nosed style of spaniel went out of popularity during the reign of King William III, and the Pug (a popular breed in the Netherlands) became popular in England as well. It is suspected that at this time cross-breeding may have occurred with pugs, or other flat nosed breeds, as the King Charles Spaniels took on some Pug-like characteristics (Figure 1-2). [16,17] It was not until a prize was set up by an American Spaniel lover in order to restore the original features of the King Charles Spaniel, and later the founding of the club (Cavalier King Charles Spaniel Club) in 1928, that the modern CKCS came into shape and received popularity with the public. [16]

In World War II, there was a drastic setback to the breed, with the most of the breeding facilities lost or destroyed. For example, in the Ttiweh Cavalier Kennel, CKCS numbers dropped from 60 to only 3 during the 1940s. Following the war, only six dogs would be used from which all CKCSs are descended. This narrow founder base with subsequent in-breeding inevitably passed heritable defects throughout the breed, of which MMVD is believed to be one. [17]

Figure 1-1 A Young King Charles II with his beloved Kings Charles Spaniels. Anthony van Dyck (1599–1641), Royal Collection.

Figure 1-2 Modern Cavalier King Charles Spaniel with a flat nose characteristics

The main breed-related health issues with CKCSs are myxomatous mitral valve disease, syringomyelia, and cataracts and multi-focal retinal dysplasia, and chronic fibrosing pancreatitis; disorders which suggest complex global connective collagenous disorders. More recently, two research groups in Scotland and Denmark have conducted genome-wide analysis of single nucleotide polymorphism (SNP) genetic variation for homozygosity mapping in groups of CKCS, and both groups

aimed to identify the genotype in early onset MMVD phenotype. French et al did not identify a single gene defect, whereas Madsen et al identified two loci suspected of contributing to early development of MMVD. [18,19] These findings also suggested the development of MMVD is governed by polygenic mode of inheritance rather than a single gene mutation, and this could partly explain why CKCS breeding schemes have failed to eliminate MMVD in the CKCS population. [20] The conflicting result between the two studies might also be due to the heterogeneous phenotypes of MMVD, or the early-advanced progression form of MMVD might be under control by multiple genes in response to epigenetic factors unique to the CKCS. Other abnormalities associated with CKCSs such as platelet dysfunction, macrothrombocytopenia, hypomagnesemia, natriuretic peptides, and serum serotonin level have been identified (Table 1-2). [21–29] With respect to MMVD the elevated serotonin levels is of greatest interest, due to its involvement in carcinoid syndrome valvulopathy in humans.

Table 1-2 CKCS specific research in recent years

Hypomagnesemia	Platelet Function	Natriuretic peptide	Serotonin
Pedersen, 1998 [25]	Olsen, 2001 [22] Pedersen, 2002 [29] Tarnow, 2003 [21] Cowan, 2004 [23] Davis, 2008 [24]	Tarnow, 2009 [26]	Arndt, 2009 [27] Ljungvall, 2013 [28]

Serotonin, 5-hydroxytryptamine (5-HT), is a neurotransmitter, and has been found to be linked to heart valve disease. In carcinoid tumors (serotonin producing tumors such as chromaffin cell adenocarcinoma) and experimentally-induced animal models, serotonin has been demonstrated to be linked to valvulopathy which shares some similarities with MMVD. [30] The other important finding is that serotonin related drugs such as the anorexogen fenfluramine (Fen, 5-HT receptor agonist and 5-HT-releasing activity) and phentermine (Phen, monoamine oxidase inhibitor) are reported to induce pathology of valves which resembles that seen with carcinoid syndrome. [31–33] Since platelets are the main storage of serotonin in the circulating

system and platelet abnormalities affect CKCS, one popular hypothesis is that the serotonin-TGF-β (transforming growth factor β) signalling pathway activates mitral valve interstitial cell activation and remodelling. Alternatively the 5-HT effect might be due to local production and have no platelet component (paracrine effect). Studies have shown that mitral valve interstitial cells undergo activation and phenotypic alteration in response to serotonin TGF-β signalling. The activated valve interstitial cells (VICs) show increased secretion of MMPs (matrix metalloproteinases) and ECM (extracellular matrix) deposition, which lead to mitral valve remodelling. [30,34–38]

1.1.4 Mitral Valve Complex

The normal mitral valve complex consists of six basic elements: 1) the posterior left atrial wall, 2) mitral valve annulus, 3) mitral valve leaflets, 4) chordae tendineae, 5) left ventricular papillary muscles and 6) associated left ventricular wall. (Figure 1-3) The synergistic interplay of each element determines the competence and integrity of the mitral valve during the cardiac cycle. Intact and correct orientation of chordae tendineae and papillary muscles with the valve leaflets and restraint of the annulus determines the tensile and compressive pressure loads created by ventricular and atrial systole. [39–41]

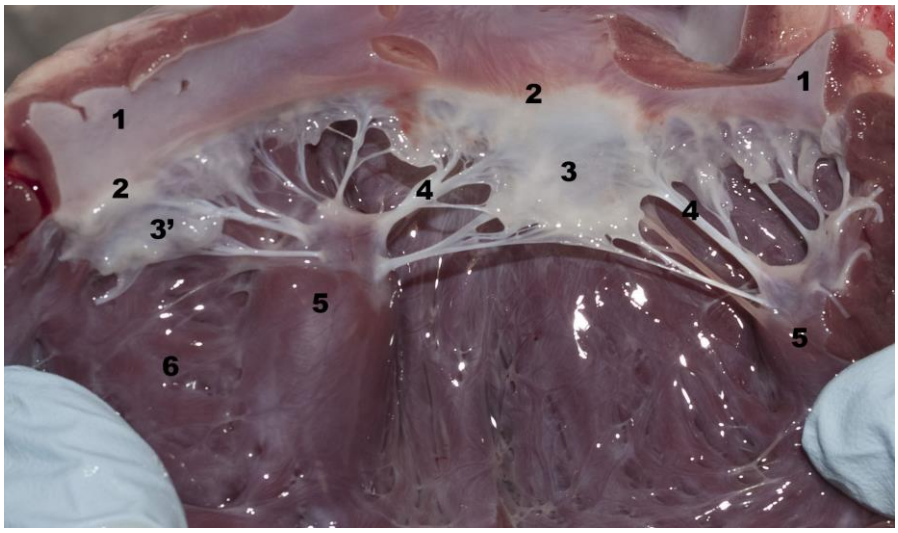

Figure 1-3 Mitral valve complex, canine.

1 posterior left atrial wall, 2 MV annulus, 3 MV anterior leaflet, 3'MV posterior leaflet, 4 chordae tendineae, 5 papillary muscle, 6 left ventricular wall.

The mitral valve

The mitral valve is composed of anterior (septal) and posterior (parietal, mural) leaflets, separated by commissures. Leaflets are defined as the structures with attached chordae tendineae anchored at the papillary muscles, and both leaflets are semicircular in shape. At the edges of leaflets, there is a rough zone where the leaflets come in contact during systole and chordae tendineae attach to. Normal appearance of mitral valves is thin and translucent without nodules and thickening at the tip of leaflets. The anterior mitral valve leaflet is larger and longer than the posterior leaflet. [7,12]

Heart Skeleton and Fibrous Annulus

The two leaflets are hinged at the supportive fibrous tissue in between the left atrium and left ventricle. Annulus fibrosus is a structure of elastin, dense collagen fibers, and scant cartilage, with various thicknesses in different anatomic locations, and is also referred to as the skeleton of the heart. [12,42] The functions of this fibrous skeleton include internal reinforcement of the myocardium, valve anchorage, restriction of valvular orifices, insertion of atrial and ventricular myocyte bundles, and insulation of electrical impulses between atria and ventricles. [42] The fibrous base lying around the caudal margin of aortic root is where the anterior leaflet is flanked by two main fibro-collagenous trigones (Figure 1-4). The fibrous extension of anterior mitral valve leaflet also forms part of the left ventricular outflow tract, and is joined by the continuity of the dorsal aspect of the non-coronary aortic valve cusps at the aortic root. This extensive fibrous continuity attached to both mitral and aortic valves has been described as the aortic mitral curtain (Figure 1-4). [12,43,44] The posterior mitral valve leaflet attaches to the endocardium at the left atrioventricular junction, and the posterior annulus is formed by merging of the left ventricular outflow tract and left ventricular posterior wall. In chronic volume overloading, annulus dilation further exacerbates valvular insufficiency. [45]

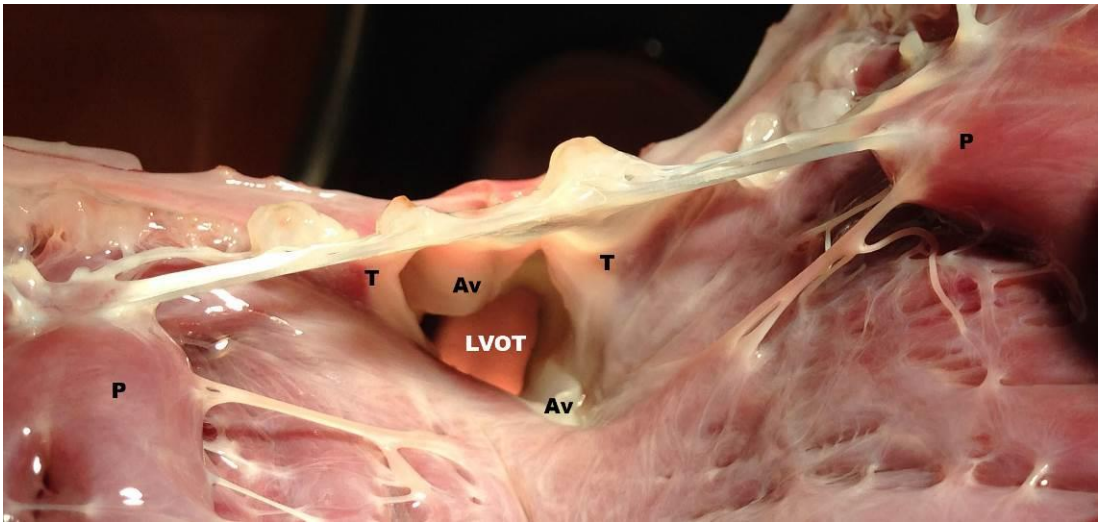

Figure 1-4 Fibro-collagenous trigones and aortic mitral curtain

LVOT: left ventricular outflow tract, T: fibro-collagenous trigone, Av: aortic valve, P: papillary muscle

The Chordae Tendineae and Papillary Muscles

The subvalvular apparatus helps to restrict mitral valve motion during systole and diastole. Both mitral valve leaflets are joined to two major papillary muscles (anterior and posterior) in the left ventricle through first- and second-order chordae, with occasional direct attachment to the ventricular wall by chordae tendineae. Coordination of these structures not only maintains adequate closure and left ventricle performance, but also prevents mitral regurgitation or mitral valve prolapse. Definition and function of the chordae tendineae are summarized in the Table 1-3. [46,47]

Table 1-3 Classification and function of the chordae tendineae. [46, 47]

Chordae Tendineae Classification	Definition	Function
First-order	Arise from papillary muscle Insertion on the free edges Originate from common or bifurcating chordae	Stiffer with higher stress, Prevent valve prolapse
Second-order	Arise from papillary muscle Larger than first-order chordae Insertion on the ventricular surface Originate from common or bifurcating chordae	Thicker, more elastic, less stress Tendon-like structure between annulus and myocardium Maintain geometry and systolic function
Third-order (less common in dogs)	Arise from septal wall Insertion on the ventricular surface	unknown

In general, papillary muscles are less likely to have geometrical and morphological variation. The anterior papillary muscle derives from the mid-area of the anterior left ventricular wall, whereas the posterior papillary muscle originates from the apical area of the posterior wall. Both the origins of papillary muscles are close to the sinuosal interventricular groove. During isovolumetric relaxation in the left ventricle, shortening of the papillary muscles assists mitral valve opening, while elongation of papillary muscles allows mitral valve closure during late diastole. [47]

1.1.5 Gross Morphology and Histopathology of the Mitral Valve

Normal Mitral Valve

The mitral valve leaflets are laminated and heterogeneous structures, and the distinct 3- (or 4) layered characteristics of mitral valve leaflets are most prominently seen at the mid-zone. From atrial to ventricular side, they are atrialis, spongiosa, fibrosa and ventricularis (the adopting of ventricularis as a 4^{th} mitral valve layer is not yet universal). The atrialis consists of a thin layer of endothelial cells with underlying loose collagen fibres and interstitial cells. At the proximal zone (closer to the annulus), adipocytes are usually present in the spongiosa. The fibrosa contains layers of dense collagen bundles with scattered spindle-shaped interstitial cells. The

ventricularis is used to describe the elastin-rich layer on the ventricular side of the aortic valve, but not found in mitral valve. So the use of the term "ventricularis" in mitral valve only implies a thin layer of endothelium without supportive collagen fibres and smooth muscle cell. The lining of endothelial cells on the ventricularis also extends to the surface of the chordae tendineae. The compositions of the different layers are summarized in Table 1-4. [6,12,42,48,49]. The spongiosa is a layer rich in glycosaminoglycans (GAGs), proteoglycans, supportive collagen fibres, elastic fibres, interstitial cells and rarely smooth muscle cells.

Table 1-4 Normal mitral valve composition and cell types with

Layer	Cell types	Composition
Atrialis (A)	Endothelial cells, smooth muscle cells, interstitial cells	Basement membrane: laminin, fibronectin, collagen I, III, IV, VI, and heparan sulphate, hyaluronan, elastin
Spongiosa (S)	Interstitial cells, adipocytes	Small amount of collagen I, III, laminin, fibronectin Glycosaminoglycans, proteoglycans, hyaluronan, elastin
Fibrosa (F)	Interstitial cells	Predominant collagen I, III, VI, and elastin
Ventricularis	Endothelial cells	Small quantity of collagen I, III, and elastin
Chordae Tendineae	Endothelial cells, interstitial cells, nerve cells	Loose meshed collagen Dense wavy collagen bundle Elastic fibers

Representative image of a normal canine mitral valve

Gross Mitral Valve Pathology in MMVD

The normal thin, translucent appearance of mitral valves is lost in the early stages of MMVD, where opaqueness and thickening of the valve edge are most prominent. With disease progression, thickened nodules coalesce and form a larger affected area, which rolls inward and bulges towards the atrial side. In severe cases, the distal

portion is remarkably thickened and protrudes into the left atrium causing mitral valve prolapse. In 1967, Whitney introduced a simple classification method (Whitney Grade I-IV) grading gross myxomatous lesions based on nodulariy, thickening, and deformity (Figure 1-5). [6,7] However, it is important to note that due to the pathologic heterogeneity of myxomatous degeneration, different grades can be often seen on the same affected leaflet. It is the extent of coverage of the valve edge by lesions that tends to give the most accurate grading. Illustrative examples are shown in Figure 1-6, Figure 1-7, and Figure 1-8.

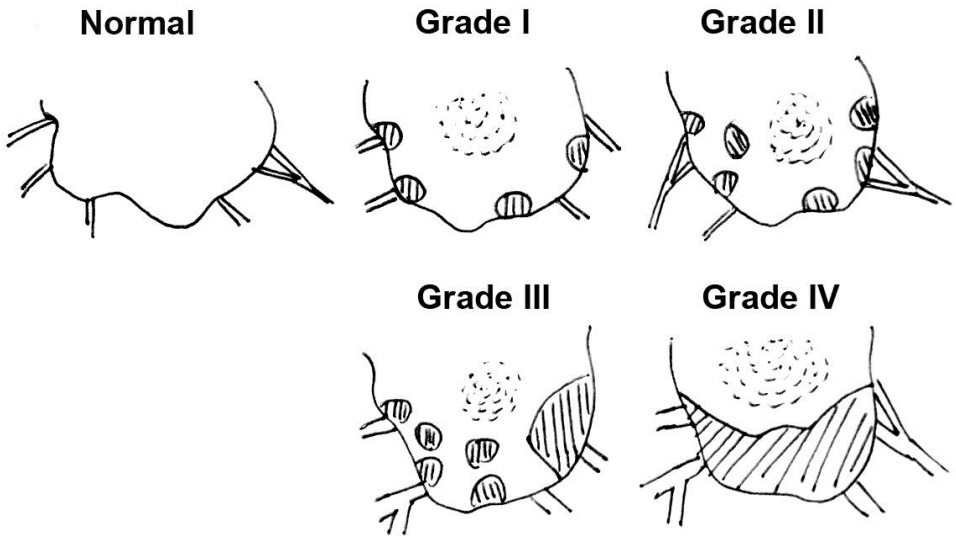

Grade	Description
Normal	Thin, translucent leaflet without chordae tendineae thickening
Grade I	A few small nodules at valve edge. Proximal leaflet area with opacity.
Grade II	Larger nodules, with coalescing. Diffuse area with Opacity.
Grade III	Larger nodules. Coalesced plaque-like deformity. Chordae tendineae thickened and elongated. Mitral competence affected.
Grade IV	Generalized distortion and ballooning of the cusps. Chordae tendineae thickened, elongated, and sometimes ruptured. Mitral competence affected.

Figure 1-5 Whitney Grading System. Modified from [7].

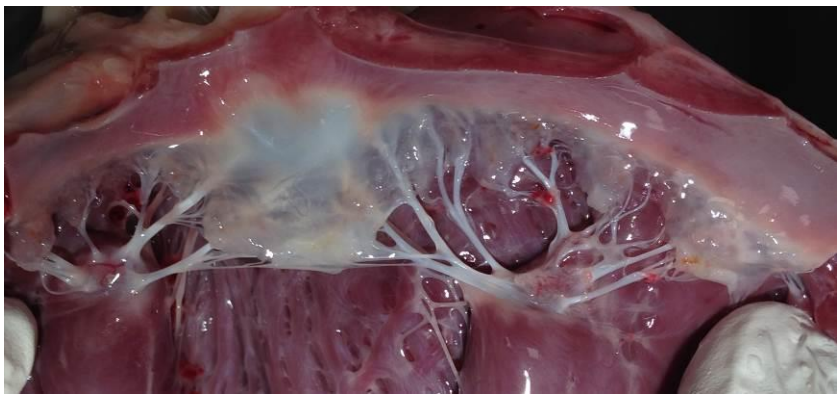

Figure 1-6 Normal mitral valve. Canine.

Figure 1-7 MMVD Grade I. Canine.

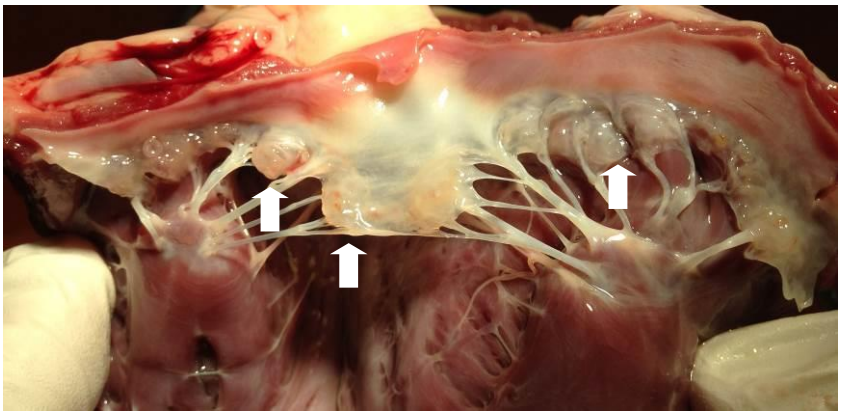

Figure 1-8 MMVD Grade II. White arrows indicate the nodular myxomatous lesions. Canine.

Histopathology

Histopathologic findings vary with the severity of myxomatous degeneration and location of the lesions, and the most prominent pathological changes are expansion of the spongiosa layer and destruction of the fibrosa layer. In the spongiosa, thickening of the layer with increased deposition of glycosaminoglycans, proteoglycans and oedematous ground substance are the main findings, while the normal alignment of dense collagen bundles in the fibrosa layer is disrupted and attenuated. Generally speaking, the distinct laminated structures are gradually lost with myxomatous progression. Aupperle and colleagues have reported a three tiered grading system based on the microscopic analysis and immunohistopathology, and this grading system is summarized in Table 1-5. [50]

Table 1-5 Immunohistopathology grading system by Aupperle. [50]

Grade	Histopathologic findings
Mild	Hyperplastic endothelium, activated interstitial cell, proliferation of fibroelastic tissue, production of laminin and collagen VI at the atrialis
	Disruption of basement membrane components: collagen IV, laminin
	Mild deposition of proteoglycans at the fibrosa
	Loss of dense collagen I and III structure, replaced by loose fibrils at the atrialis and spongiosa
Moderate	Remarkable increased glycosaminoglycan and proteoglycan deposition in the distal end of the valve
	Mild disarray of collagen bundles at the fibrosa
	Intact valve structure in the proximal half of the valve
Severe	Large quantity of glycosaminoglycan and proteoglycan deposition and complete destruction of the fibrosa layer in the distal end of the valve

Cellular and Morphological Changes

Changes in the extracellular matrix components and phenotypes of valve resident cells in myxomatous lesions are well described in this disease. In the myxomatous nodular lesions, there is a general reduction in connective tissue density and re-distribution of interstitial cells. [6,12,51,52] In the myxomatous nodules, relatively acellular central regions are rich in proteoglycans, collagen I and II, while in the

peripheral regions, they are surrounded by large spindle-shaped interstitial cells, which are responsible for collagen I, IV, fibronectin, and basement membrane component production. [53] Interestingly, ectopic deposition of basement membrane components such as laminin, elastin, and collagen IV implies the reorganization of the valve structure. Since valve interstitial cells and endothelial cells both contribute to the synthesis of the basement membrane, and endothelial cells show ability to regulate interstitial cell phenotypes under shear stress, it is important to understand the endothelial-interstitial-extracellular matrix interaction. [54,55]

The majority of the valve interstitial cells in normal mitral valves are vimentin+ and α-SMA- (alpha smooth muscle actin), and phenotypic alteration from a quiescent phenotype α-SMA- to and an activated α-SMA+ myofibroblast phenotype is prominent in MMVD. [56] These activated valve interstitial cells present a smooth-muscle-cell-like or myofibroblastic phenotype, and are positively associated with disease severity. [48,52,56] It has also been suggested that increased expression of the contractile proteins α-SMA and SMemb (embryonic smooth muscle myosin) in valve interstitial cells may be in response to gradual loss of integrity, competence, and increased mechanical stress in the mitral valve, in order to counteract the increased tensile strength. [57,58] Moreover, these activated interstitial cells also demonstrate higher extracellular matrix synthetic activity *in vivo* and *in vitro* compared to normal. In human myxomatous mitral valves, there is an increased expression of catabolic enzymes (MMPs, cathepsin K) which is thought to be responsible for valve remodelling. [56,58] Members of the TGF-β superfamily, which includes the bone morphogenic proteins (BMPs), have been shown to trigger valve interstitial cell differentiation and activation. [59–64] Autocrine serotonin-TGF-β signalling has also been demonstrated in myxomatous mitral valves. [36,65] The expression of SMemb by VICs is more closely correlated to MMPs expression than α-SMA expression. [38] Mechanical factors have also been shown to modulate phenotype differentiation, extracellular matrix synthesis, and catabolic enzyme production. [38] All these findings suggest that valve interstitial cells are likely to be constantly undergoing phenotypic changes, and this cell plasticity could be easily altered in response to different stimulation.

The valve endothelium is a single-cell-layer structure lying on both sides of the valve surface. [49] VECs are similar to those endothelial cells elsewhere in the circulation from a structural and functional perspective, in that endothelial cells maintain vessel and valve integrity by interacting with the underlying tissues and smooth muscle cells. [66] However, studies have identified the heterogeneity of endothelial cells across the different circulatory sites. [66] Surface morphology changes due to endothelial damage in myxomatous mitral valve have been identified by electron microscopy, and the surface morphology change is presented by patchy endothelial denudation with exposure of subendothelial basement membrane, while adjacent intact endothelium shows cell pleomorphism. [49,67] This endothelial damage might be secondary to altered mitral valve motion and turbulent flow with increased mechanical force during valve closure. [68] Also, endothelial cells generate endothelin, nitric oxide and other potent vessel tone regulators. Damaged endothelial cells will impair the endothelial synthesis of these mediators and affected their interaction with sub-endothelial tissues and interstitial cell functions. Butcher et al have demonstrated how endothelial cells regulate interstitial cell morphology and phenotype. [55] In a canine study increased endothelin receptor density at the tip of myxomatous valves has been identified. [69] Interestingly in valve development, foetal valve endothelial cells show higher expression of catabolic enzymes (MMPs), mesenchymal markers (α-SMA, SMemb), and cell adhesion molecules such as intercellular adhesion molecules (ICAM-1, CD54) and vascular cell adhesion molecule 1 (VCAM-1, CD106) compared to adult valve endothelial cells, features that are in-part also apparent in MMVD.[70] The role of developmental pathways in embryogenesis of the heart valves and in adult valves is discussed later.

1.1.6 Aetiology

The cause of myxomatous mitral valve disease is unknown. In small breed dogs, myxomatous valve disease is thought to be inherited. In the Cavalier King Charles spaniel, studies have suggested a polygenic threshold trait, and parental heart condition (onset of murmur and murmur intensity) is an important determinant of the prevalence of murmur in 5-year-old offspring. [20,71]

Similar pathology of the mitral valve is also noticed in human mitral valve prolapse patients with congenital abnormalities, such as Marfan syndrome. [11,72] In fact, chondrodystrophoid breeds such as Dachshunds, have already been shown to be prone to have connective tissue associated disorders like tracheobronchomalacia (trachea collapse), intervertebral disc disease (IVDD), cranial cruciate ligament rupture. [7,9–12,15,73] These observations suggest a global collagenous abnormality might be present. The histologic lesions seen in the valves of human patients with connective tissue abnormalities suggest that a similar pathogenesis might be the cause of MMVD in dogs, but such comparisons need to be treated with caution as there are differences between the two species. For example, tissue overlays are a common pathological feature of human MMVD but are not present in dogs. [74]

Barlow's Disease and fibroelastic deficiency are the two types of degeneration leading to mitral valve prolapse in human. The manifestation of both diseases includes thickening of the leaflet due to deposition of myxomatous material, but there are differences in aetiology. In fibroelastic deficient mitral valves, myxomatous degeneration is secondary to insufficient production of collagen and elastin which leads to mitral valve prolapse. It is usually associated with aging, and the myxomatous lesions are localized at the prolapsed segments. In Barlow's Disease, the aetiology is also unknown. The generalized myxoid infiltration and disruption of the normal mitral valve three layer structures are similar to pathologic findings in canine MMVD. [5] In canine MMVD, the pathology shows a more homogeneous pathology without calcific and fibrotic lesions compared to Barlow's Disease and fibroelastic deficiency (Table 1-6). Overall, because of the prevalence of MMVD and the asymptomatic presentation of early myxomatous degeneration, it is challenging for both humans and dogs to be able to differentiate age-related myxomatous changes from normal aging processes. [7,74]

Table 1-6 Classification and comparison of degenerative mitral valve disease in human and dogs. Modified from [5].

	Barlow's Disease	Fibroelastic Deficiency	Canine MMVD
Pathology	Myxoid infiltration	Reduced connective tissue production	Myxomatous degeneration
Age	Young (<60 years old)	Older (>60 years old)	Older (> 5years old)
Long history of murmur	Yes, usually present	No	Present and gradual progress
Familial history	Sometimes present	No	Yes
Echocardiography	Bulky, billowing leaflets, multi-segmental prolapse	Thin leaflets, prolapse of single segment, ruptured chord(s)	Thickening, prolapse of leaflets
Surgical lesions	Thickened leaflets Thickening, elongation, or rupture of chordae Calcification, fibrosis or fusion of chords, papillary muscle	Thin leaflets Leaflet thickening limited to prolapsed segment Rupture chordae	Leaflet thickening Rupture and elongation of chordae tendineae. No fibrotic or calcific lesions

1.1.7 Pathophysiology

Myxomatous lesions affect the coaptation of the leaflets, leading to mitral valve incompetence and regurgitation. A fraction of stroke volume from the left ventricle then is ejected into the left atrium through the regurgitant orifice, and this will raise the left atrial pressure which results in left atrial dilatation. Since the left ventricular filling in diastole is from the left atrium, the additional regurgitant volume with the normal blood return from the lung will impose volume load on the left ventricle and the left atrium. Increased end-diastolic pressures and volume lead to eccentric hypertrophy of the left ventricle. The increased filling pressure will also reflect backwardly to the pulmonary vein pressure, and results in pulmonary oedema in decompensated heart. In dogs with mitral regurgitation, neuroendocrine (renin-angiotensin-aldosterone system, RAAS) activation and other compensatory mechanisms (eg. Frank-Starling's Law) allow the heart to cope with the mitral regurgitation and the disease can remain clinically silent for years until the disease is advanced. [7-10] In severe mitral regurgitation, patient starts showing signs of congestive heart failure like exercise intolerance, weakness, cough, and dyspnea, and

this is due to progressive maladaptation of neuroendocrine response and loss of myocardium contractility. [9–11]

1.1.8 Clinical Presentation

In most mildly affected dogs, MMVD itself does not cause clinical signs, and it could be an incidental finding in a patient presented for annual health check or for other non-cardiac disease. When clinical signs emerge in patients with MMVD, coughing is one of the signs that may be observed by owners. Dry cough could be due to bronchial compression by enlarged left atrium due to volume overload. Productive and moist cough due to pulmonary edema (left side congestive heart failure) may be accompanied by other signs including exercise intolerance and tachypnea. [9–11] Syncope is occasionally reported by owners in MMVD dogs. Syncopal episodes could be the result of insufficient cerebral perfusion owing to impaired cardiac function, where the cardiac output does not increase adequately in order to meet the physiological demands like exercise. Another pathophysiology of syncope could be due to arrhythmia secondary to chamber enlargement. [11]

During auscultation, a systolic murmur with maximal point of intensity over the left cardiac apex can be heard in MMVD dogs. Crackles may also be auscultated in dogs with pulmonary edema due to congestive heart failure.[10]

1.1.9 Diagnosis

The diagnosis of mitral regurgitation due to MMVD can be based on signalment, history, physical examination, and thoracic radiographs. Echocardiography is the most useful diagnostic tool for MMVD. Measurement of enlarged chamber and quantification of mitral regurgitant jet can be obtained from echocardiography. [11]

1.1.10 Treatment

Medical management of congestive heart failure secondary to MMVD is case-dependent. In brief, the four most common drugs used in veterinary cardiology to treat congestive heart failure are angiotensin converting enzyme inhibitor (ACEi), loop diuretic (furosemide), aldosterone antagonist (spironolactone), and inodilator (pimobendan). The actions of these drugs and indications for use are summarized in Table 1-7.

Table 1-7 Common drugs used in veterinary medicine to treat congestive heart failure

Drug Trade Name	Action	Indication
Benazepril	ACE inhibitor	Volume overload Decrease pre-load
Furosemide	Inhibits sodium and potassium reabsorption at the thick ascending Henle's loop	Volume overload Decrease pre-load
Spironolactone	Aldosterone inhibitor Potassium sparing diuretic	Volume overload Mild effect of diuretics
Pimobendan	Phosphodiesterase II inhibitor and calcium sensitizer which shows both inotropic and vasodilation effect	Systolic dysfunction Decrease afterload Increase contractility

Mitral valve repair is the optimal and curative way to treat myxomatous mitral valve disease in humans. With the assistance of the robotic technology and interventional radiology techniques, specialized cardio-surgeons can achieve mitral valve repair with minimal invasiveness. [75] In veterinary medicine, surgical interventions have been attempted but with a low success rate and questionable clinical improvement in dogs affected by MMVD. [76] Nevertheless, Uechi has recently reported the highest success rate in mitral valve repair on 48 dogs with significant resolved clinical sign, longer life expectancy, and reverse cardiac remodelling. [77] However, due to the predisposed breeds (small size), cost-benefit (cardiopulmonary by-pass, life-expectancy), animal welfare (invasive surgery), and post-operative management (systemic thromboembolism, dysfunction of prosthetic valves and chordae), mitral valve repair procedures remain controversial in veterinary medicine and are unlikely to become widespread. More innovative approaches are required to develop novel treatments for both humans and dogs, and these are likely to be based around understanding of the molecular events that occur on diseased valves and the application of molecular tools as therapy.

1.2 Heart Valve Development

1.2.1 Overview

Formation of the Heart Tube

At the early three- to four-somite stage, the heart arises in the mesoderm from the paired endocardial tubes (consisting of endocardium only). Later they are enclosed by thickened splanchnic mesoderm (epimyocardium). Epimyocardium then differentiates into epicardium and myocardium. These paired endocardial tubes migrate centrally and fuse to form a single straight cardiac tube (Figure 1-9). [9]

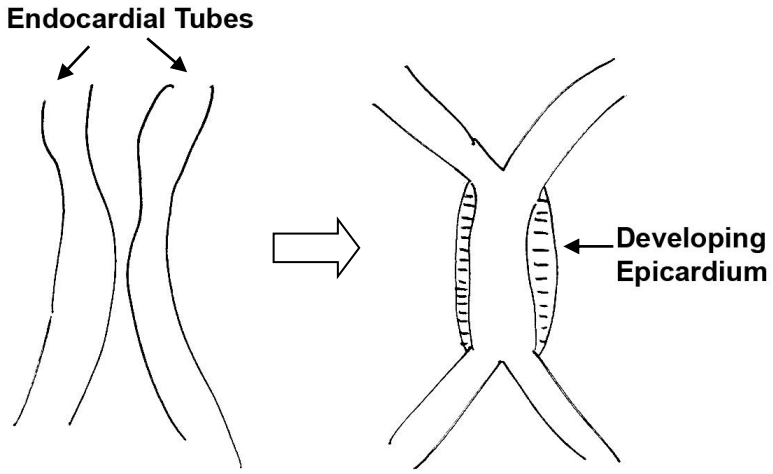

Figure 1-9 Endocardial tube formation. Modified From[78].

Convolution of the Heart Tube

The straight cardiac tube contains ventral aortae (cranial) and omphalomesenteric veins (caudal), which firmly anchor within the pericardial sac. Therefore, elongation is only possible by folding and bending the cardiac tube into an S-shaped loop. During the looping of the heart, primary subdivisions of the heart are gradually defined (Figure 1-10). [9]

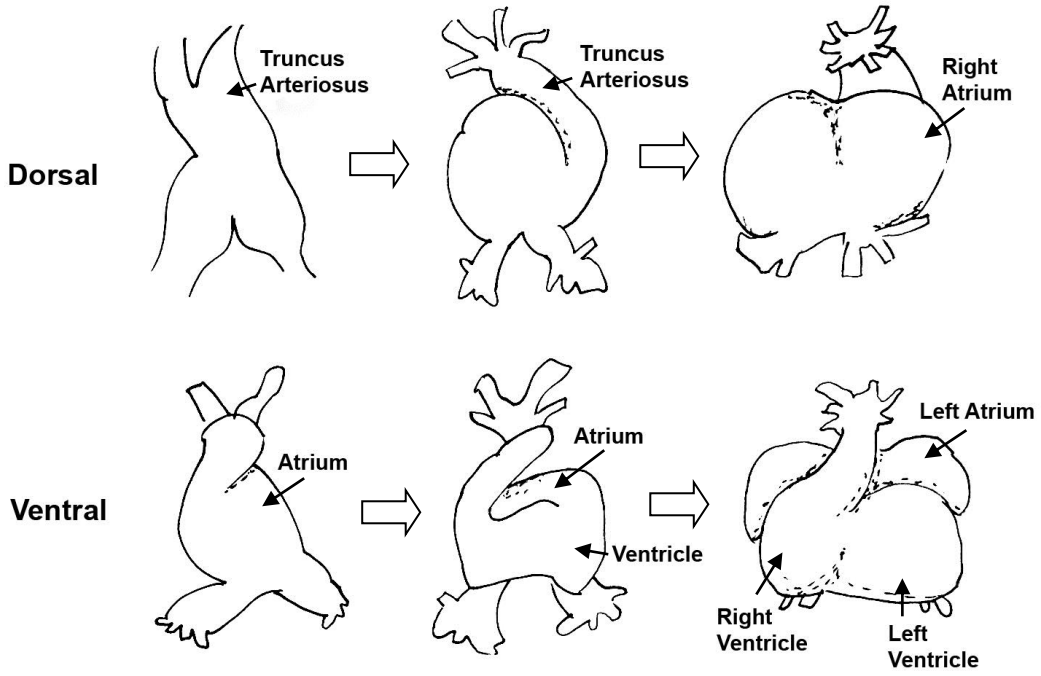

Figure 1-10 Looping of the heart. Modified from [79]**.**

Formation Primitive 4-Chambered Heart

After the stage of cardiac looping, a series of septations occur in order to divide the left and right sides of the chambers. The primitive atrium joins with the primitive ventricle through a common atrioventricular canal. During heart septation, the cranial and caudal atrioventricular (AV) endocardial cushions grow towards each other and fuse, dividing the primitive common atrioventricular canal into left and right atrioventricular canals. In ventricular septation, tissue grows from trabeculation processes at the heart apex towards the atrioventricular canal to form the primary inter-ventricular foramen, which is later closed by fusion with the atrioventricular endocardial cushion growth. In the atrium, extension of the septum primum from atrial wall towards AV canal forms the ostium primum. This opening is closed when the septum primum fuses with the endocardial cushion. At the same time perforations from the superior portion of the septum coalesce to form the ostium secundum. Another septum originates from atrial wall, descends down the right side of the septum primum and joins the AV cushion. On the septum secundum the fossa ovalis is a persistent opening and is normally covered by the septum primum. Defects in this region mainly cause atrial septal defect.[9,11,78]

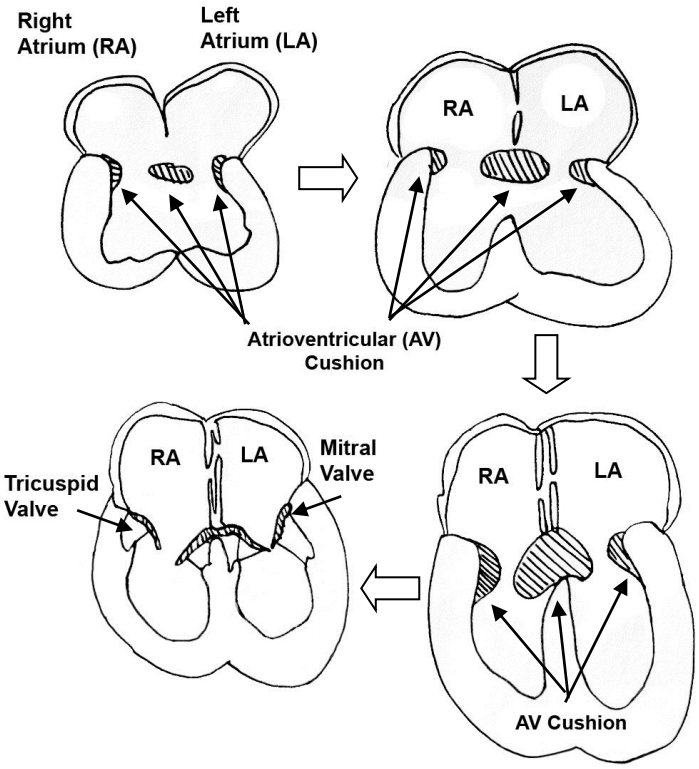

Figure 1-11 Development of the AV valve and septation of the heart. Modified from [9]

1.2.2 Valve Morphogenesis

The AV and semilunar (SL) valve have the same developmental mechanisms occurring at the endocardial cushions. The only difference is the anatomical location. The sites of the valve morphogenesis are the main sites of EndoMT. Under the effect of factors such as TGF-β and BMP secreted by the adjacent myocardial cells, endocardial endothelial cells undergo phenotypic transition by losing endothelial phenotype markers such as platelet endothelial cell adhesion molecule (PECAM-1, CD31), and vascular endothelial cadherin (VE-cadherin, CD144, CDH5) and acquiring a mesenchymal α-SMA positive phenotype. The migratory ability is also obtained by losing cell-cell contact and secreting MMPs which degrade the endocardial basal lamina (collagen IV) allowing invasion. At the endocardial cushion, EndoMT contributes to the mesenchymal cells by the migration of the transformed endothelial cells into the underlying hyaluronan- and chondroitin sulfates-rich cardiac jelly. [80–84] Under continual effects of growth factors such as TGF-β, BMPs, fibroblast growth factor (FGF), epithelial growth factor (EGF)

secreted from the endocardium and the myocardium, these cells contribute to the early expansion and elongation of the primitive valves by ECM deposition and cell proliferation. Finally, atrioventricular valve maturation is achieved by delamination from the muscular walls (Figure 1-12), whereas in semilunar valves, there are excavations of cushions from the aortic and pulmonary sides inward. [83,85]

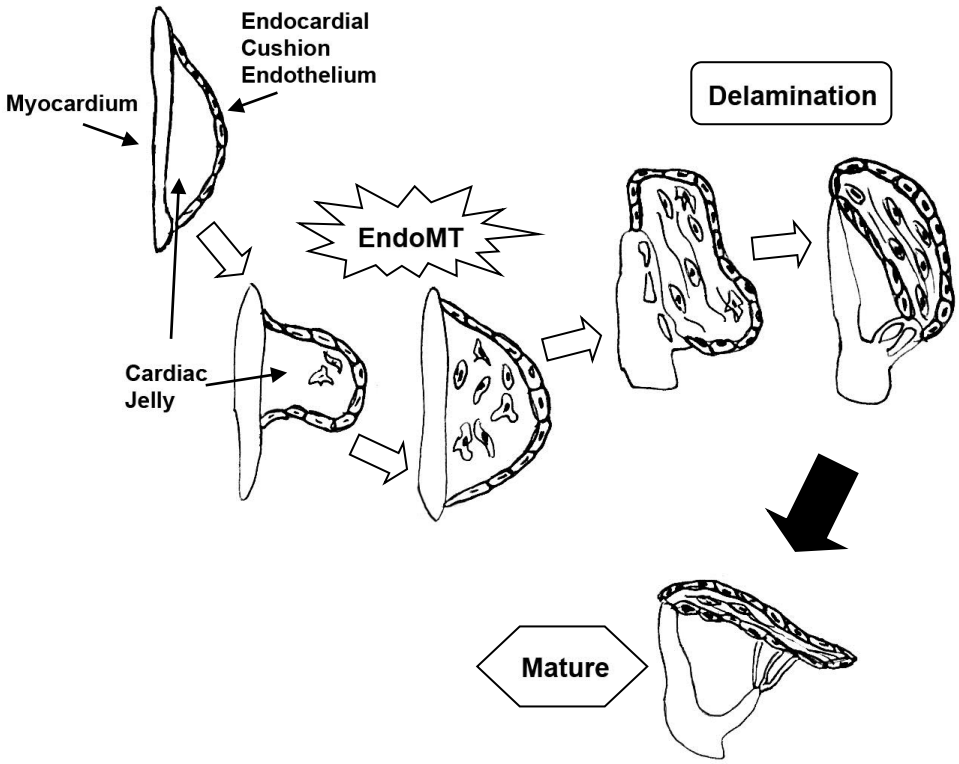

Figure 1-12 Morphogenesis of atrioventricular valve. Modified from [83].

Although septation of the heart occurs early in embryogenesis, atrioventricular valves development is observed in the first trimester in mammals. At the atrioventricular canal, fusion of the ventral and dorsal atrioventricular endocardial cushion with the atrial and ventricular septa gives rise to the mitral and tricuspid valves. [9] For the semilunar valves, protrusion of three endocardial cushions at the aortic and pulmonary lumen forms the aortic valves and pulmonic valves.

1.2.3 Endothelial Mesenchymal Transition

During valvulogenesis, the term "endothelial mesenchymal transition" describes the process where the endocardial endothelial cells at the valve–developing region undergo a series of transformations including activation, migration, and invasion into

the cardiac jelly, a hyaluronan-rich space underlying the valvulogenic endocardial cushion. The initiation of EndoMT is closely regulated by several growth factor-mediated signalling pathways including vascular endothelial growth factor (VEGF), TGF-β, BMP and NOTCH. [83]

VEGF. Vascular endothelial cell growth factor regulates endothelial cell proliferation during valve development, and is expressed by endocardium and myocardium near the valve forming region. Though VEGF has been shown to have some EndoMT antagonist activity, basal level of VEGF expression is indispensable for endocardial cushion formation, possibly due to the maintenance of endocardial integrity and endothelial cell population during EndoMT. [80,83,86]

Wnt/β-catenin. Wnt/β-catenin signalling is expressed locally at the valve forming region, and is important in patterning of the heart-forming field. In addition, β-catenin acts as a link between actin and VE-cadherin that constructs the adherens junction, which mediates cell-cell adhesion and cell polarity in endothelial cells. In animal models, inhibition of Wnt signalling results in no EndoMT, whereas overexpression leads to excessive endocardial cushion formation. Wnt/β-catenin signalling also triggers expression of EndoMT associated genes during the phenotype transition. [86]

NOTCH. NOTCH is a cell fate determining factor expressed in embryonic and adult tissues alike. Expression of NOTCH at the valve forming region induces EndoMT. The mechanism is by selective induction of the TGF-β signalling pathway, and Snail is the downstream transcription factor which represses expression of endothelial markers (VE-Cadherin, PECAM1), but increases mesenchymal markers (α-SMA, fibronectin). Therefore, NOTCH transforms the regional endocardium into active and unstable mesenchyme. [83,85,87] Finally, functional studies on animal models show that disruption of NOTCH results in no EndoMT, and constitutive activation of NOTCH leads to hypercellular valves. [83]

TGF-β. Transforming growth factors and BMPs are part of the TGF-β superfamily. TGF-β ligands play an important role mediating cell differentiation in physiological and pathological states in multiple tissues. [83] In atrioventricular valve formation, expression of TGF-β is observed at the endocardium and myocardium. It is

suggested that endocardial expression of TGF-β2 is essential for endothelial cell separation and hypertrophy, and expression of TGF-β3 is important for mesenchymal transformation and migration. [88] Degradation of basal lamina component collagen IV by MMPs is also triggered by TGF-β3. [89] Simultaneously with the acquired mesenchymal phenotype of the endocardium, this permits the migration of the transformed endothelial cells. In animal models, blocking of the TGF-β receptors results in complete inhibition of EndoMT, and in a mouse model TGF-β2 has been showed to activate mesenchymal transformation through activation of Snail/Slug. [87,90,91] .

BMP. BMPs, as the name suggested, are osteogenic cytokines, but also crucial for cellular differentiation in early valvulogenesis with BMP2 and BMP4 expression particularly noticed in the valve forming region. [82,83,86] In general, BMPs are expressed in the myocardium earlier than the onset of EndoMT, and BMP signalling also triggers multiple pathways including TGF-β, HAS2 (hyaluronic acid synthase 2) and NOTCH, as well as the transcription factors Snail and Twist. [92–94] Because of the pre-EndoMT expression of BMPs, the action of BMPs could be divided into two phases. Initially, before the onset of EndoMT, BMP stimulates HAS2 expression and creates an hyaluronan-rich environment which permits the activation and migration of endocardium by other growth factors. Later, synergistic signalling with TGF-β and NOTCH drive the EndoMT and allow invasion of cells into the cardiac jelly. [59] Experimentally, inhibition of BMP signalling results in complete silencing of EndoMT in atrioventricular cushion explants. [95]

Extracellular Matrix. Underlying the valve forming endocardial cushion, cardiac jelly is mainly composed of hyaluronan (HA), initially produced from adjacent myocardium through HAS2 and UDP-glucose dehydrogenase (UGDH). [96] The accumulation of hyaluronan causes expansion of the extracellular space by binding to salt and water. The hyaluronan-rich environment also favors migration of transformed endothelial cells, and induces PI3K and ErbB2/3 signalling and valve mesenchyme formation. [97] In cultured embryos, disruption of hyaluronan synthesis leads to no endocardial cushion formation, and a similar result is found in HAS2-null cushion explants. [98]

Another important proteoglycan found in cardiac jelly is versican, which links protein between hyaluronan and collagen, and versican-null mice do not form endocardial cushions at the valvulogenic region. [99]

1.2.4 Extracellular Matrix (ECM) Maturation and Organization

The dynamic environment during valve development contains numerous molecules, which play crucial roles in the regulation of cellular events. The main components found in valve formation include hyaluronan, fibronectin, fibrillin, proteoglycans and collagens. [100] The mesenchymal cells regulate valve elongation, expansion, fusion, stratification and maturation by ECM remodelling during valve formation. This process involves a tight balance between degradation and deposition of extracellular matrix. Detailed information of ECM genes associated with development and disease phenotypes is summarized in Table 1-8. [82,100]

Table 1-8 Animal models of extracellular matrix genes associated with cardiovascular development. All studies performed on mouse except aggrecan (chicken). Modified from [100]

Extracellular Matrix	Expression during Heart Formation	Cardiovascular Phenotype in animal models
Hyaluronan, Proteoglycans and Link Proteins		
Aggrecan	Epicardium, mesenchyme of the OFT and AVC	None reported
Cartilage link protein (CRLT1)	Endocardium, mesenchyme of the OFT AVC	ASD, VSD, AVSD
Hyaluronic acid synthase 2 (HAS2)	Myocardium, endocardium of heart tube, OFT cushions, AV valves	Fail to form AVC
Perlecan	Basement membrane, OFT, SMCs of Ao and pulmonary artery	Defects in OFT rotation
Versican	AV and OFT cushions, mesenchyme of the PAS	Fail to form RV, OFT, AVC
Collagens		
Collagen I	AV valves, vasculature	Vascular defects, aortic dissection
Collagen II	AV valves	Cartilage and bone disease
Collagen III	AV valves, vasculature	Vessel rupture
Collagen IV	AV valves	Vascular defect
Collagen V	Ao, annulus fibrosus, MV mural leaflet	Decreased Ao stiffness
Collagen VI	AV valves, myocardium, epicardium, Ao, and pulmonary artery	None reported
Collagen XI	Not reported	Thickened heart valves
Collagen XV	BM, myocardial capillaries	Vascular defects, cardiomyopathy
Collagen XVIII	BM, endocardium, semilunar valves	Broadened AV valves
Proteases		
ADAMTS1	Endocardium, myocardium, AV cushion	Hypertrabeculation
ADAMTS5	Endocardium, myocardium, pericardium, Ao, aortic valves	Normal
ADAMTS9	Myocardium, right-sided OFT cushion, SLV, Ao, MV	Myxomatous mitral valve
Others		
Periostin	Endothelium, cushion of OFT and AVC, AV valves	Leaflet abnormalities and valve disease
Fibronectin	Embryonic mesoderm, AVC, endocardium	Vascular defect, failure of heart tube formation
Fibrillin 1	Endocardium, AVC and cushion of OFT, AV valves	Fail to form EC, mitral valve prolapse, aortic aneurism
Laminins	Basement membrane	Compromised cardiovascular function
Tensacin	AV valves	Mitral valve prolapse
Elastin	AV valves	Malformation of aortic valve

SMC, smooth muscle cell; OFT, Outflow tract; AVC, atrioventricular cushion; AV, atrioventricular; ASD, atrial septal defect; VSD, ventricular septal defect; AVSD, atrioventricular septal defect; CT, chordae tendineae; Ao, aorta; RV, right ventricle; SLV, semilunar valve; MVP mitral valve prolapse

The mechanisms controlling post-EndoMT valve remodelling are understudied and poorly understood. Before EndoMT, the endocardial cushion is rich in hyaluronan and versican. After the endocardial cushion is cellularized through EndoMT, migrated mesenchymal cells start to synthesize network collagens (mainly fibrillar collagen I, III, V), and proteases as well as cartilage- and tendon- related ECM proteins such as aggrecan and tenascin, during valve maturation. [80,86] Over time, increased cellularity and collagen deposition directly contribute to rigidity and elongation of the valves. The mechanisms contributing to patterning and stratification of each specialized layer in valves remain unknown. Based on transcriptional patterns, a regulatory model controlling atrioventricular valve stratification was proposed by Combs. [81] In the atrialis, NOTCH expression is localized to the flow side. In the spongiosa, Sox-9 up-regulation is mediated by BMP2 signalling, and this triggers cartilage-related ECM (aggrecan) deposition. In the fibrosa layer, fibroblast and preosteoblast associated ECM proteins (such as periostin) are positively controlled by Wnt expression and signalling. Finally, chordae tendineae and other subvalvular apparatus development is initiated by FGF4 signalling. FGF4 signalling increases expression of the tendon-related transcriptional factor SCX (scleraxis) and other ECM components (tenascin) alike. [82]

In the matured and laminated valves, structurally distinct layers have unique biomechanical properties. Elastin fiber is abundant in the atrialis, and it gives valve elasticity responding to the blood flow. The spongiosa layer is rich in chondroitin sulfate proteoglycans that provide valve compressibility which is biomechanically similar to cartilage. The collagen-rich fibrosa layer provides stiffness and strength of the leaflets against tension and flexure. [80] Mutations in ECM genes associated with valve abnormalities have been reported in human literature and give a clear insight into the role of various ECM products (Table 1-9). [80] However, very few are known in dogs.

Table 1-9 Gene mutations associated with valve abnormalities in human. Modified from [80].

Gene	Valve phenotype
Fibrillin-1, FBN1	Aortic root dilation, BAV, MVP
Elastin, ELN	SVAS, BAV, MVP
TGF-β Receptor, TGFBR1	Aortic aneurism, MVP
Collagen I, COL1A1	Aortic valve prolapse, MVP
Collagen III, COL3A1	Aortic root dilation, BAV, MVP
NOTCH1	BAV, CAVD, CVM
α-smooth muscle actin, ACTA2	Aortic aneurism, BAV
Myosin heavy chain 11, MYH11	Aortic aneurism, BAV
Filamin A, FLNA	BAV, MVP

BAV, bicuspid aortic valve; MVP, mitral valve prolapse. SVAS, supravalvular aortic stenosis. CAVD, calcific aortic valve disease. CVM, cardiovascular malformation.

1.2.5 Biomechanics

Both atrioventricular and semilunar valves maintain the unidirectional flow of blood in the heart. The normal average human heart rate is 60 beats per minute, and accounts for more than 100,000 beats per day and approximately 3 billion beats throughout a 70 year lifespan. In dogs, depending on breed size, the average heart rate varies from 70-100, and also contributes to approximately half a billion beats in a 10 -15 years of life expectancy. [101]

The movement of valves (opening and closing) is primarily passively controlled by the pressure differences in the heart chambers, with a contribution from the papillary muscles, valve associated myocardium and valve annulus, and the left side of the heart maintains higher pressures than the right side in the normal heart. [101] The three main mechanic forces affecting heart valves are flexure, shear and tension. Flexure occurs during valve opening and closing. Shear stress is created when blood flow passes through the opening valve surface. Tension occurs when the valve is stretched by the annulus and sub-valvular apparatus at coaptation. [85] Hence, the cellular and matrix composition are crucial for considering valve dynamics and loading force endurance.

Using α-SMA and heat shock protein 47 (HSP47) to quantify cellular stiffness and monitoring collagen synthesis, Sacks and Yoganathan found the mitral valve

interstitial cells to have higher quantities of both α-SMA and HSP47, and this finding implies that valve interstitial cells are exposed to higher forces. In response to the greater forces created by left side of the heart, the valve interstitial cells increase collagen and cellular (cytoskeletal) stiffness in order to maintain homeostasis. [101] Another study by Aikawa also demonstrated similar cellular events; during the postnatal valve development, interstitial cells gradually become quiescent in accordance with the collagen maturation and biomechanical adaptation. [70] By manipulating the papillary muscle tethering and mitral valve geometry in a sheep model, localized thickening (collagen deposition) and EndoMT (migration and increased α-SMA expression) of the mitral valve in adaptation to increased mechanical force was identified to be associated with reactivation of developmental pathways. [102] These studies all point out the unique plasticity of mitral valves and their adaptive potential to haemodynamics.

Study Aims and Hypothesis

The aim of this study was to evaluate changes in the mitral valves of cavalier King Charles spaniels, with particular reference to cell and gene profiles.

The first aim was to characterise the cellular changes in CKCS with the hypothesis that there are no differences between CKCS and other equally affected dogs and that the valve pathology is the same irrespective of breed. With that in mind the CKCS could be used examined as a model of MMVD in the dog.

The second aim was to evaluate expression of developmental genes in CKCS valves with the hypothesis that endothelial-to-mesenchymal transition is a component of disease pathogenesis.

2 Chapter 2 Cellular changes in Myxomatous Mitral Valve Disease in Cavalier King Charles Spaniel

2.1 Introduction

The CKCS breed is recognised to be particularly pre-disposed to the development of MMVD in terms of age of onset, progression and severity. [15,20,29,71] MMVD is highly heritable in the CKCS breed and it is reasonable to suppose heritability also has a role in disease appearance and progression. [18–20] Additionally, there are CKCS-specific traits that might be implicated in the development of MMVD, such as differences in platelet numbers and platelet aggregation tendency and higher serum magnesium and 5-HT levels compared to other dogs. [21,23,24,26,27,29,103] CKCS are also more predisposed to chronic fibrosing pancreatitis, multi-focal retinal dysplasia, syringomyelia, which with MMVD might reflect a breed-specific global connective tissue abnormality. [20,67]

Cellular changes that occur with MMVD are well described in canine and human MMVD. In general, there is an increase in α-SMA positive VICs (activated myofibroblasts) which locate mainly towards the valve free-edge (valve tip) in a linear cluster pattern and beneath endothelium. [51,56,104] In normal valve stroma the majority of cells are quiescent vimentin-positive VICs (qVIC), with a few desmin-positive cells. [52,104] In overtly myxomatous areas of affected valves some cells also appear to be activated myofibroblasts based on their expression of myosin SMemb, and SMemb positive cells are shown to be more associated with catabolic serotonin synthesis. [36,38,51] A small increase in mast cell numbers is also noted, but there is no increase in macrophage numbers and no inflammatory cell infiltration is evident. [51,104] Changes in endothelial cell morphology, coupled with endothelial cell denudation are also reported. [49,57,104]

Of the histopathology studies to date, all have presented data from a mix of pedigree and cross-bred dogs. Considering the susceptibility of the CKCS to MMVD, the aim of this study was to determine if there are differences in valve cellular changes in the CKCS compared to non-CKCS dogs.

2.2 Material and Methods

2.2.1 Tissue samples

Mitral valve leaflets were obtained from six elderly CKCS (12-14 years) and six elderly mixed breed dogs (8-12 years) with MMVD. Control samples were obtained from four young adult mixed breed dogs (1-2 years) with no evidence of disease. Briefly, after removal of the heart the mitral valve leaflets were exposed by opening from left atrium and ventricle through the lateral wall between the two papillary muscles. The mitral valve leaflets were examined for MMVD lesions and photographed. The whole mitral valve leaflets were then surgically dissected from the attachments of annulus and pupillary muscles, and immediately immersed in 4% paraformaldehyde and fixed at 4^{o}C for 36 hours. Samples were then rinsed in PBS and stored in 70% ethanol at 4^{o}C until required. All samples were collected with full owner consent and the study conformed to national (UK) and institutional ethical guidelines for the use of animals in research.

Affected valves were pathologically graded Whitney Grade 3 or 4 by at least two observers. [6] Representative samples of similar gross pathological appearance (nodular and thickening at valve tip) were cut from each valve, paraffin-embedded and 4 consecutive 5µm sections were collected onto slides.

2.2.2 Hematoxylin & Eosin (H&E)

Sections were de-waxed in xylene for 5 minutes and rehydrated through 100% ethanol, 95% ethanol, 90% ethanol, 70% ethanol, and distilled water for 2 minutes each. Standard H&E staining was performed using a programmed autostainer (Autostainer XL Leica ST5010). Briefly, slides were immersed in hematoxylin reagent for 4 minutes before rinsing in running tap water for 30 seconds. Sections then were rinsed with acid alcohol for 2 seconds and rinsed with running tap water for 30 seconds. Sections were then counterstained in eosin for 2 minutes. Before mounting with mounting medium (DePex; Gurr-BDH Chemicals Ltd), sections were dehydrated through the same graded ethanols for 2 minutes each, and xylene for 5 minutes.

2.2.3 Immunohistochemistry

Sections were de-waxed firstly in xylene for 10 minutes. The slides were then rehydrated through graded ethanol: 100% ethanol, 95% ethanol, 90% ethanol, 70% ethanol, and distilled water for 5 minutes each. All slide rehydration was done in a programmed autostainer (Autostainer XL Leica ST5010). For antigen retrieval, sections were heated in citrate buffer (0.01M, pH 6.0) or Tris-EDTA (10mM Tris base, 1mM EDTA solution, pH 8.0) for 5 minutes at 120˚C by HISTO5 Rapid Microwave Histoprocessor (Milestone). After antigen retrieval, slides were rinsed 2 times for 5 minutes in distilled water. At this stage slides were ready to be mounted using sequenza cassettes (Thermo Scientific, Shandon Sequenza Immunostaining Cassettes) with 200 µm of 0.5% PBS-Tween20 with the following steps.

Peroxidase Method: For the peroxidase technique, sections were incubated with 1% hydrogen peroxide (H_2O_2 in phosphate-buffered saline (PBS pH 7.4) for 10 minutes to block the endogenous peroxidase. Next, permeabilization and non-specific-block of antigens were performed with 10% goat serum (diluted in 0.5% Tween 20) (Vector Laboratories Inc.) for 30 minutes at room temperature. Sections were then incubated for 60 minutes at room temperature with the primary antibodies. Slides were washed with 0.5% PBS-Tween20 5 times for 5 minutes and incubated for 30 minutes at room temperature with biotinylated secondary antibodies (goat anti-mouse or anti-rabbit IgG; Vector Laboratories Inc.). After another 5-times-5-minute washes, slides were incubated with avidin-biotin complex (VECTASTAIN ABC system, Vector Labs Inc.) for 30 minutes. After ABC reagent complex conjugation, slides were developed with NovaRED (NovaRED peroxidase substrate kit, Vector Labs Inc.) as a chromagen. Mayer's Haematoxylin solution (Sigma-Aldrich) was used for counterstaining for 90 seconds followed by 10 seconds in Scott's tap water. Finally, slides were manually dehydrated in a glass slide stainer through distilled water, 70% ethanol, 90% ethanol, 95% ethanol, fresh 100% ethanol for 5 minutes each and fresh xylene for 10 minutes. After dehydration, slides were mounted in a xylene-based medium (DePex; Gurr-BDH Chemicals Ltd).

Indirect fluorescence: For immunofluorescence, the basic protocol was the same for the peroxidase technique, without addition of H_2O_2. The secondary fluorescent dye

conjugated antibody (AlexaFluor488 and 568, Invitrogen) was applied for 60 minutes at room temperature in a dark humid chamber. Slides were washed in 0.5% PBS-Tween20 (5x 5min) between primary antibody probing, secondary antibody probing, and mounting. Mounting medium with nuclear counterstain DAPI was used to mount slides (ProLong Gold Antifade Reagent, Invitrogen). Briefly, Prolong Gold was brought to room temperature 10 minutes before use. After the slides were mounted and sealed with nail polish, they were left in a tin-foil wrapped paper box at room temperature to cure overnight. The next morning, sealed slides were ready to be viewed or stored at -20 ˚C.

Double indirect fluorescence: For double-labelling methods, two primary antibodies targeting two antigens were selected (from different species, mouse and rabbit), and were mixed up in one buffer for the primary antibody incubation. The secondary antibodies were also mixed up in one buffer for incubation, and species specific secondary antibodies were designed to bind the designated primary antibodies. In addition, the fluorescent tags on secondary antibodies were different in excitation range for antigen differentiation (AlexaFluor488, 568). The incubation time for primary and secondary antibodies, washing, and mounting in double labelling method were the same as indirect single fluorescent labelling method.

Sections were examined for the presence of the universal mesenchymal cell marker vimentin, the inflammatory cell markers CD11c and CD45, the VEC markers Von Willebrand factor (vWF) and CD31, the activated myofibroblasts (aVIC) markers α-SMA, SMemb and the cell proliferation marker Ki-67. The details for each antibody are shown in Table 2-1. Double staining was carried out for α-SMA and SMemb using indirect immunofluorescence.

Table 2-1 Details of each antibody used in this study

Name	Clonality	IHC	Supplier	Cat. No.
Primary Antibody				
α-SMA	Ms monoclonal	1:400	Sigma	A2547
SMemb	Rb polyclonal	1:1000	Abcam	Ab24761
Vimentin	Ms monoclonal	1:1600	Sigma	V6389
vWF	Rb polyclonal	1:1000	Abcam	Ab6994
CD31	Rb polyclonal	1:100	Abcam	Ab28364
Ki-67	Rb polyclonal	1:200	Abcam	Ab15580
CD-11c	Ms monoclonal	1:100	Abcam	Ab76911
CD-45	Ms monoclonal	1:100	AbD Serotec	MCA2035S
Secondary Antibody				
Alexafluor 488	Goat anti-Ms IgG (H+L)	1:100	Invitrogen	A10667
Alexafluor 568	Goat anti-Rb IgG (H+L)	1:100	Invitrogen	A11011
Biotinylated Antibody	Goat anti-Ms IgG (H+L)	1:1000	Vector	BA-9200
Biotinylated Antibody	Goat anti-Rb IgG (H+L)	1:1000	Vector	BA-1000

*Abbreviation: H+L, heavy and light chain. Ms, mouse. Rb, rabbit.

For each dog a minimum of four sections were examined for each antibody. Positive controls included canine spleen, lymph node and duodenum, and for negative controls the primary antibody was omitted. Images were taken using a light microscope with fluorescent capability (Leica-DMRB, Leica Microsystems, Leitz).

2.2.4 Image capture and Statistical analysis

For quantitative assessment (ImageJ cell counter plug-in; National Institutes of Health) nine selected (x400 magnification) images, from the same region of interest for each valve, were digitally captured from close to the valve edge (tip of leaflet) to the valve base (zone adjacent to the annulus). Qualitative assessment only was carried out on the NovaRed stained sections (longitudinal and horizontal), and quantitative assessment on the fluorescent labelled sections (longitudinal only).

The positive cell counts for α-SMA, SMemb, and vimentin for all groups of mitral valves were analysed using GraphPad Prism® . Data were expressed as mean ± standard deviation of the mean. Inferential statistical analysis involved one-way analysis of variance testing with a p-value of <0.05. Where ANOVA detected significant difference, inter-group differences were compared using the post-hoc Tukey Simultaneous test. Due to small sample size (n= 4 to 6) in this study, normality testing was not performed and non-parametric testing was not considered (no power). [105]

2.3 Results

2.3.1 Gross histology

Gross and histological changes in myxomatous mitral valves from CKCS and non-CKCS were not appreciably different, and not dissimilar to previous reports (Figure 2-1). In general, there was marked thickening at the valve tip in both CKCSs and non-CKCSs. In the myxomatous nodular lesion sites, there was higher cellularity at the periphery than in the centre. Intact fibrosa layer with dense collagen bundle was seen in the mid portion in both MVs (Figure 2-1). Chordae tendineae attachments were also identified in Figure 2-1A.

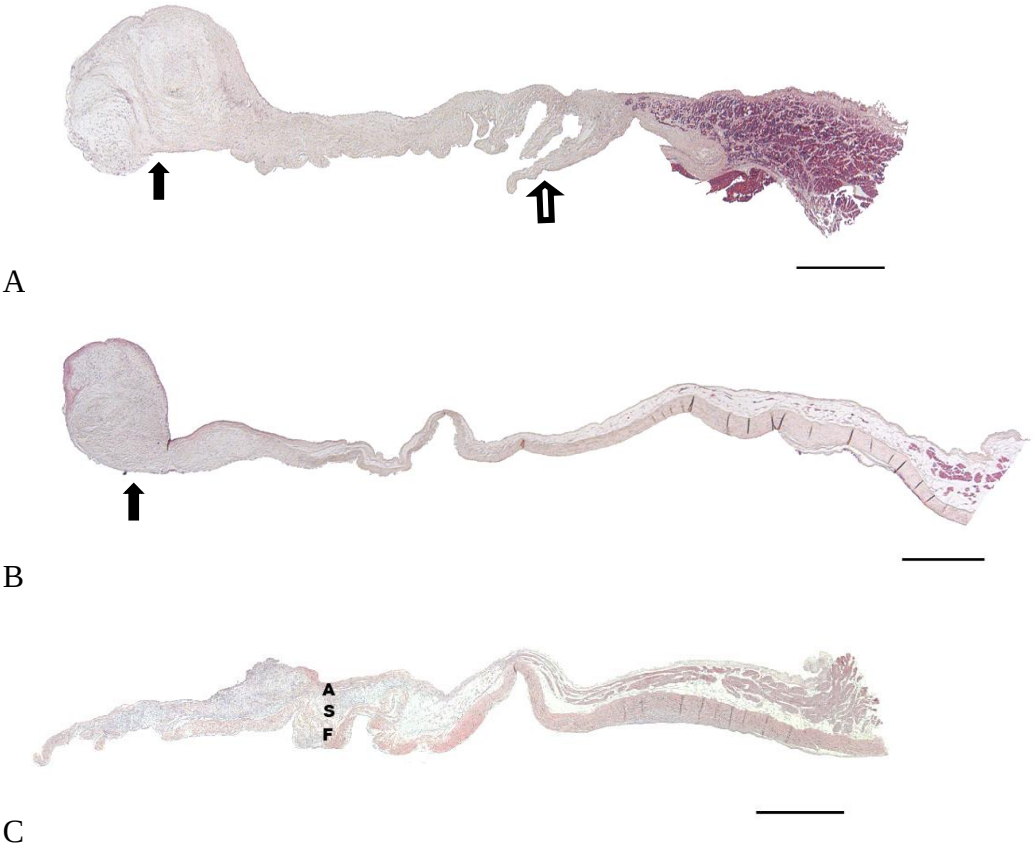

Figure 2-1 H&E staining of myxomatous mitral valve from (A) a CKCS (B) a non-CKCS dog, and (C) a normal mitral valve from a Beagle. Note at the valve tip (black arrow), loss of distinct laminated structures was found on both myxomatous mitral valves, and it is featured by thickening and nodular changes at the valve edge. Hollow arrow indicates chordae tendineae. A, atrialis; S, spongiosa; F, fibrosa Scale bar = 1mm.

2.3.2 Cellular changes in myxomatous mitral valve disease

Similar changes in the distribution of immunoreactive cells were noted for longitudinal and horizontal sections.

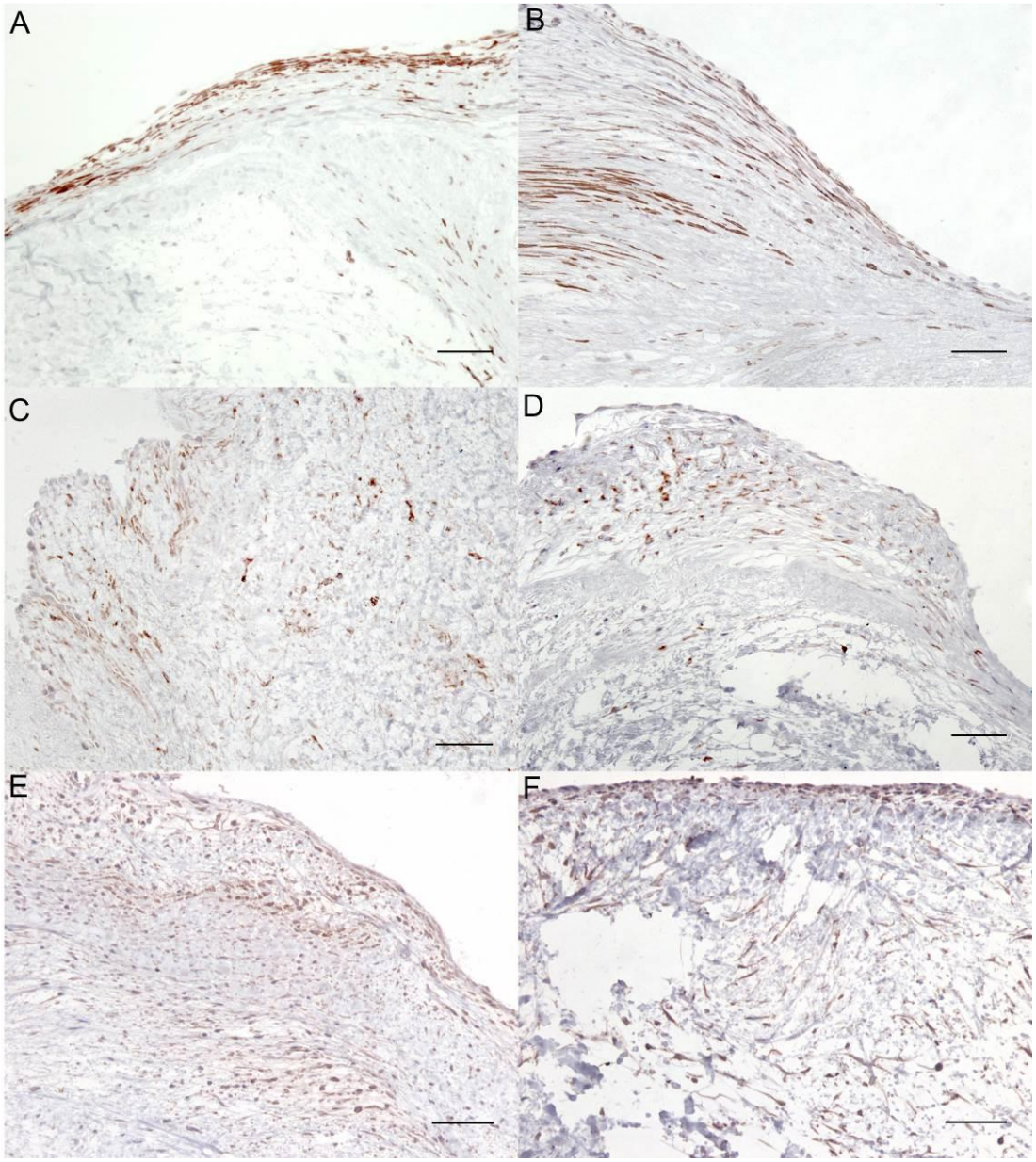

Figure 2-2 Photomicrograph immunostaining for (A)(B)α-SMA, (C)(D) SMemb, and (E)(F) vimentin of myxomatous mitral valve tip from (A)(C)(E) CKCS and (B)(D)(F) non-CKCS. Tip of the leaflet. Scale bar = 50µm.

In the normal mitral valves, most cells were vimentin positive and evenly distributed, and presumed to be quiescent VICs. In the diseased valves, vimentin positive cells

were also evenly distributed but the highest density was adjacent to the endothelial layer (Figure 2-2). In the diseased and normal mitral valves, the endothelial cells at atrialis and ventricularis sides of the leaflet were both vimentin positive.

No cell staining was observed in any valve for the inflammatory cell markers CD11c or CD45, but positive staining was found in lymph node (Figure 2-3).

A

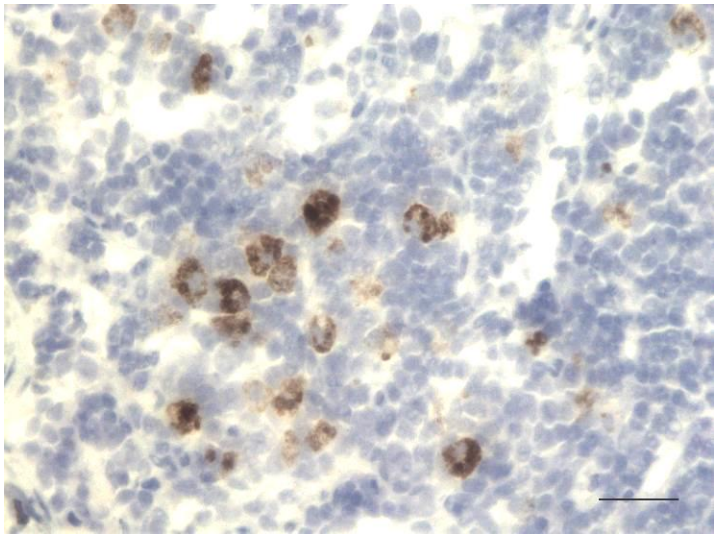

B

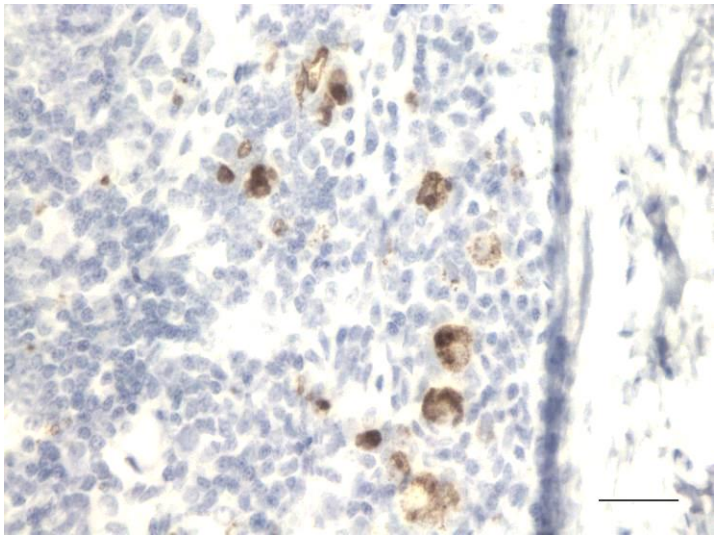

Figure 2-3 Positive staining control for (A) CD45 and (B) CD11c. Canine cortex of pre-scapular lymph node. Scale bar = 25µm.

In normal mitral valves, very few α-SMA or SMemb positive cells were seen and these were typically located adjacent to the endothelium in the mid zone. In diseased valves α-SMA positive cells were generally found lying beneath the endothelium,

clustering mostly at the free edge with a few cells present in the valve stroma. SMemb positive cells were also found clustering around the myxomatous areas and close to the free edge, but there was positive staining throughout the leaflet depth. There were no clear differences comparing CKCS and the non-CKCS (Figure 2-4). In addition, both SMemb positive cells and α-SMA positive cells were observed in the spongiosa in the diseased mitral valves, and a spindle-shaped, elongated cell morphology was noted (Figure 2-4).

A

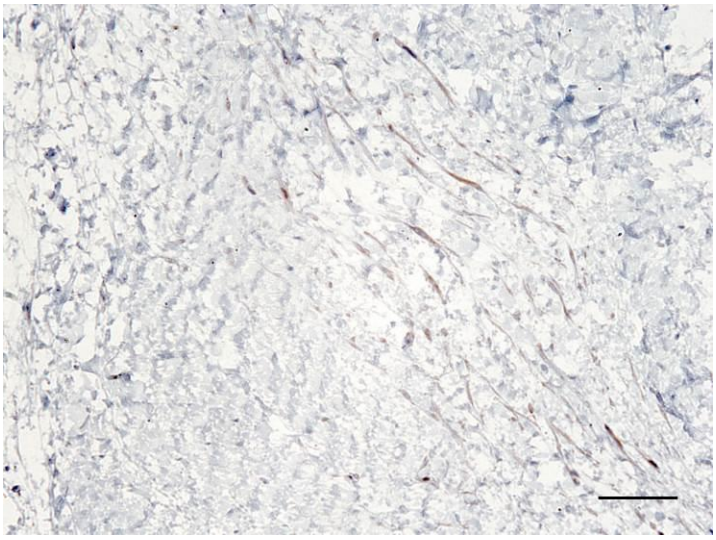

B

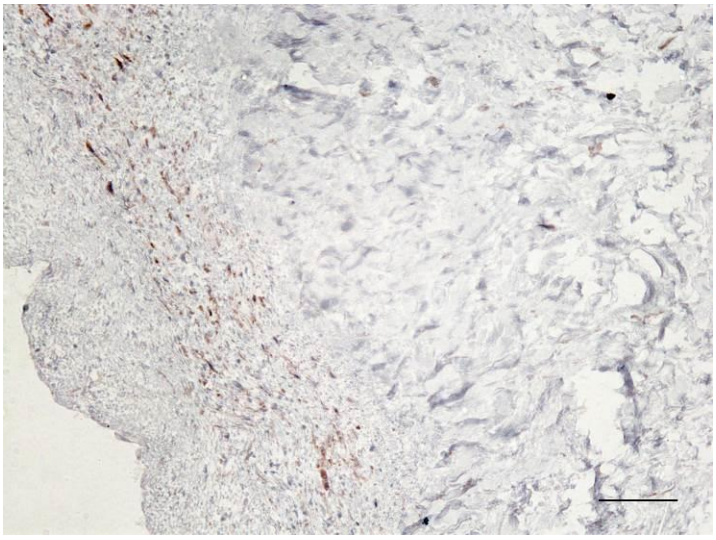

Figure 2-4 Immunostaining for (A) α-SMA and (B) SMemb. Mid-portion of canine myxomatous mitral valves. CKCS. Scale bar = 50µm.

A

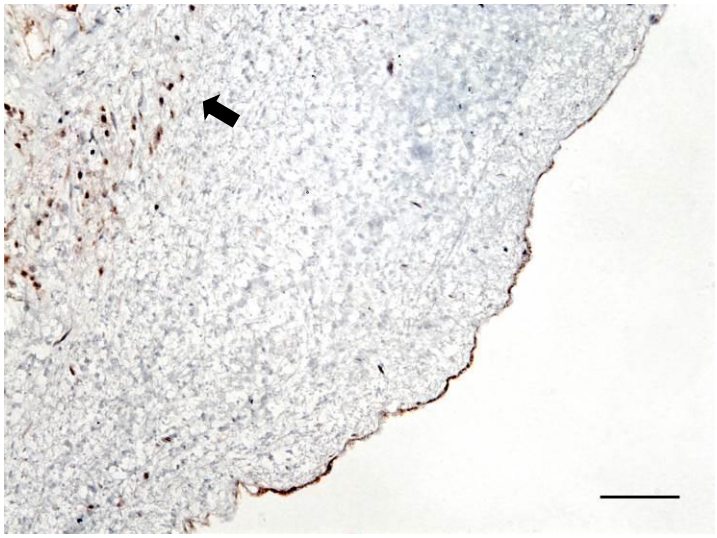

B

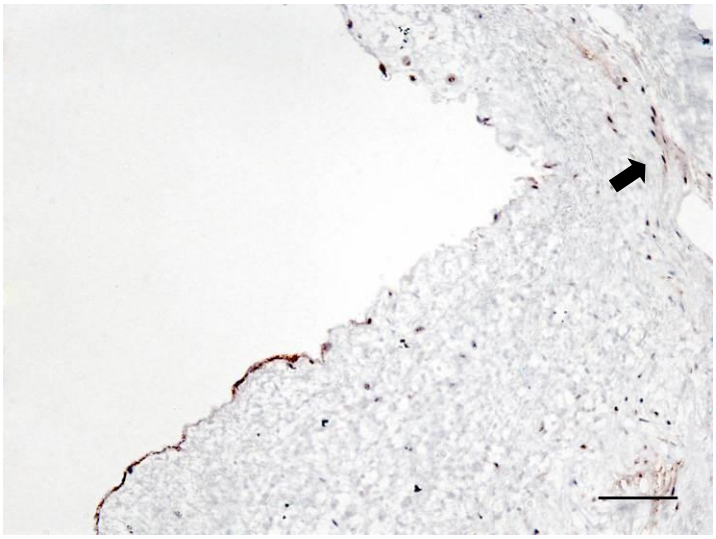

Figure 2-5 Photomicrograph for (A) continual and (B) interrupted expression of vWF staining. Canine myxomatous mitral valves. Scale bar = 50µm. Arrows show mild staining of interstitial cells in myxomatous region (A) and spongiosa (B).

vWF positive endothelial cells were found along the whole leaflet length, but with areas of discontinuity in the diseased dogs (Figure 2-5). A consistent finding in both diseased groups (5/6 CKCS; 6/6 non-CKCS) was clusters of vWF-positive cells in the myxomatous sites away from the valve edge (Figure 2-6). In addition, mild vWF positive staining was also present in the interstitial cells in the spongiosa layer. Polymorphism and denudation of the endothelium was also noted in the diseased mitral valves (Figure 2-6).

A

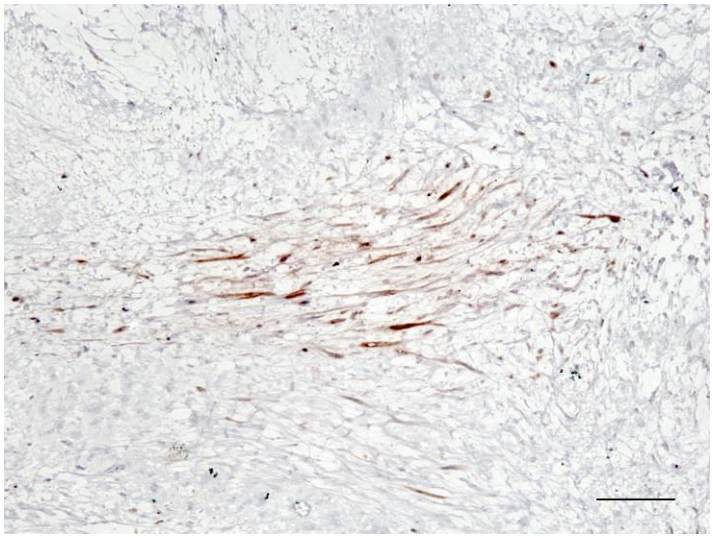

B

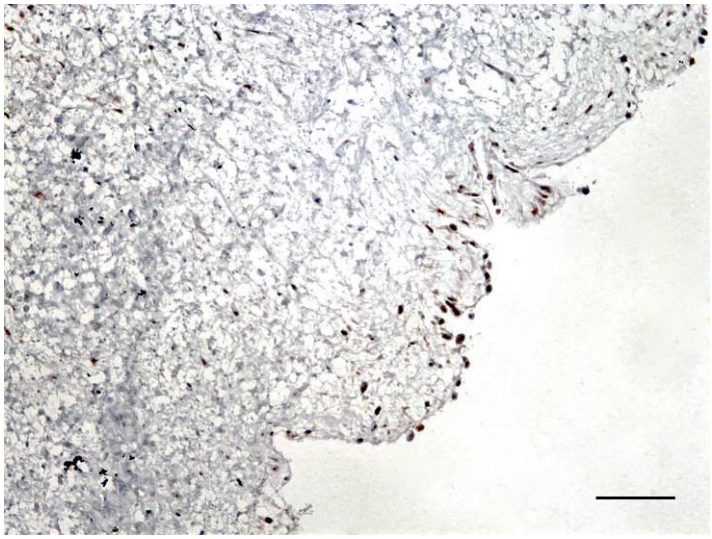

Figure 2-6 Photomicrography of vWF immunostaining. (A) Clusters of spindle-shaped interstitial cells were positive for vWF. Scale bar = 50µm. (B) Polymorphism of endothelial cells with evidence of endothelial denudation. Canine myxomatous mitral valve (CKCS). Scale bar = 25µm.

No CD31 positive cells were seen in any sample examined. (Note: identifying CD31 positive cells in any canine paraformaldehyde fixed tissues has not been possible, but the antibody used has been effective in acetone fixed canine valve endothelial cell cultures).

A

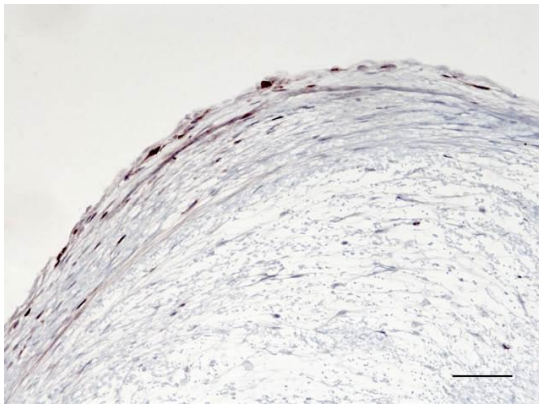

B

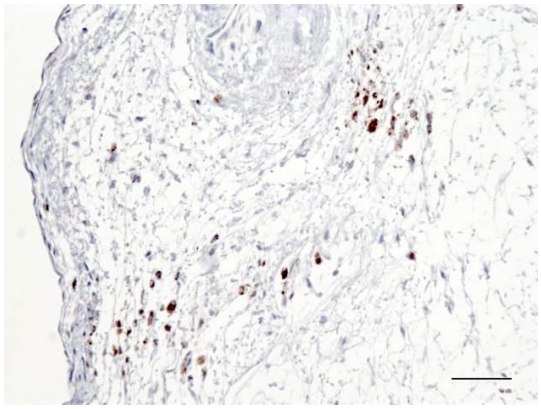

C

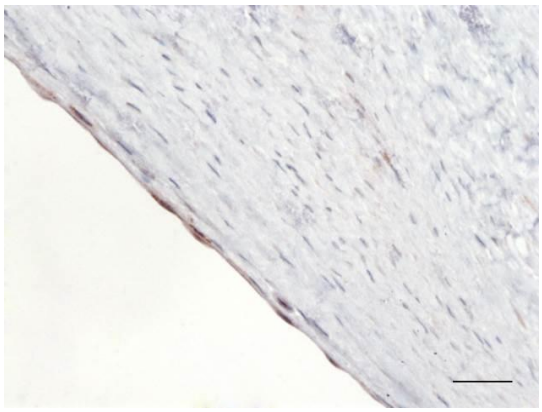

Figure 2-7 Photomicrograph of Ki-67 immunostaining. Canine (CKCS) myxomatous mitral valves. Scale bar = 50µm (A)(B), and 25 µm (C). (A) Hyperplastic endothelium at the valve tip showed Ki-67 reactivity, and this pattern is similar to staining pattern of α-SMA and SMemb. (B) Clusters of Ki-67 positive interstitial cells in the overtly myxomatous lesion site. (C) Endothelial expression of Ki-67.

In normal mitral valve, Ki-67 staining was mild and negligible (non-specific staining). Ki-67 positive cells formed linear clusters typically at the leaflet tip, but also were distributed sparsely throughout the myxomatous valves of both groups (Figure 2-7). This patchy distribution was similar to that seen for α-SMA and SMemb positive cells (linear clusters under endothelium). Ki-67 positive staining was also found occasionally in small clusters in the overtly myxomatous region. In affected valves, flattened elongated cells at the valve surface (presumed to be VECs) also showed positive staining for Ki-67 (Figure 2-7).

2.3.3 Immunofluorescence; Qualitative and Quantitative Analysis

In myxomatous mitral valves from both CKCS and non-CKCS, linear clusters of α-SMA positive cells were discovered at the myxomatous valve tip under endothelium, and the majority of these cells were elongated, spindle-shaped (Figure 2-8A). Similarly, SMemb positive cells appeared to be clustered linearly at the myxomatous valve tip, and the morphology was spindle-shaped. However, round-shaped SMemb positive cells were occasionally seen under the endothelium (Figure 2-8B). The staining of vimentin was generalized and vimentin was expressed by almost all cells in the mitral valve. In myxomatous mitral valve, higher cellularity with polymorphism was noted at the endothelium, whereas in the stroma most valve cells were elongated and spindle-shaped (Figure 2-8C). Co-expression of SMemb and α-SMA was identified in the linear clusters along the tip of the leaflet (Figure 2-9).

A

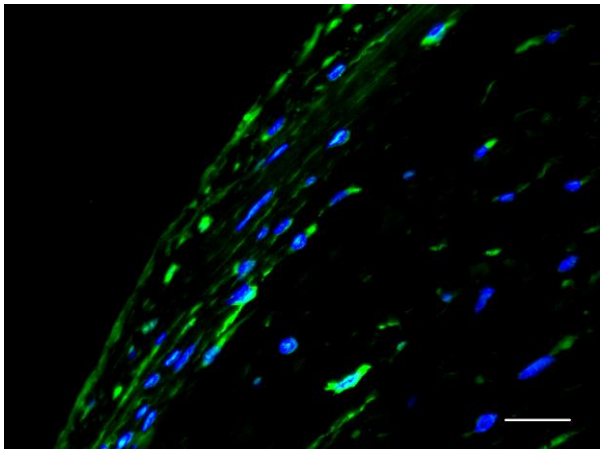

B

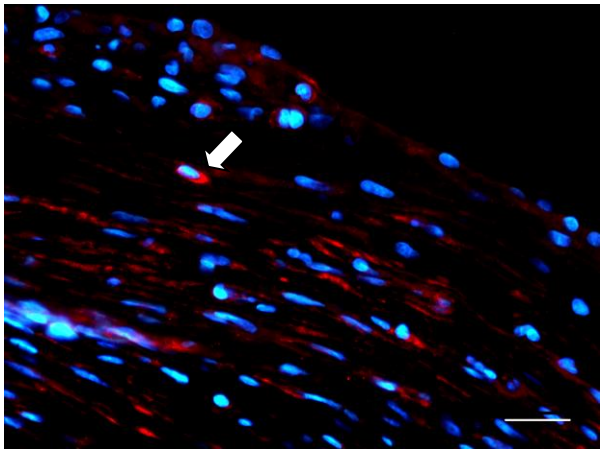

C

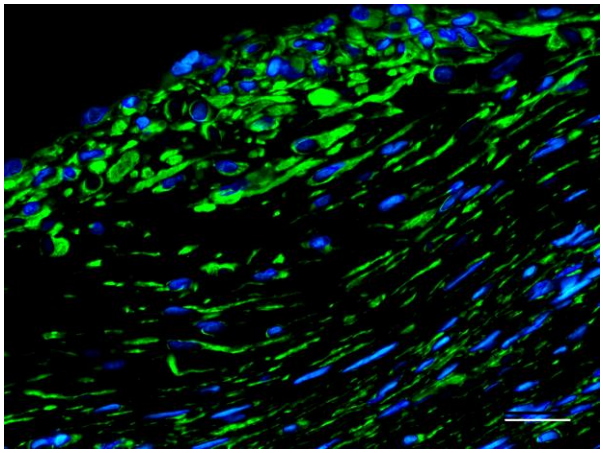

Figure 2-8 Photomicrograph for (A) α-SMA in green, (B) SMemb in red, and (C) vimentin in green immunostaining. Canine (CKCS) myxomatous mitral valve (tip). In B, the white arrow indicates a round SMemb positive cell. Scale bar= 25µm.

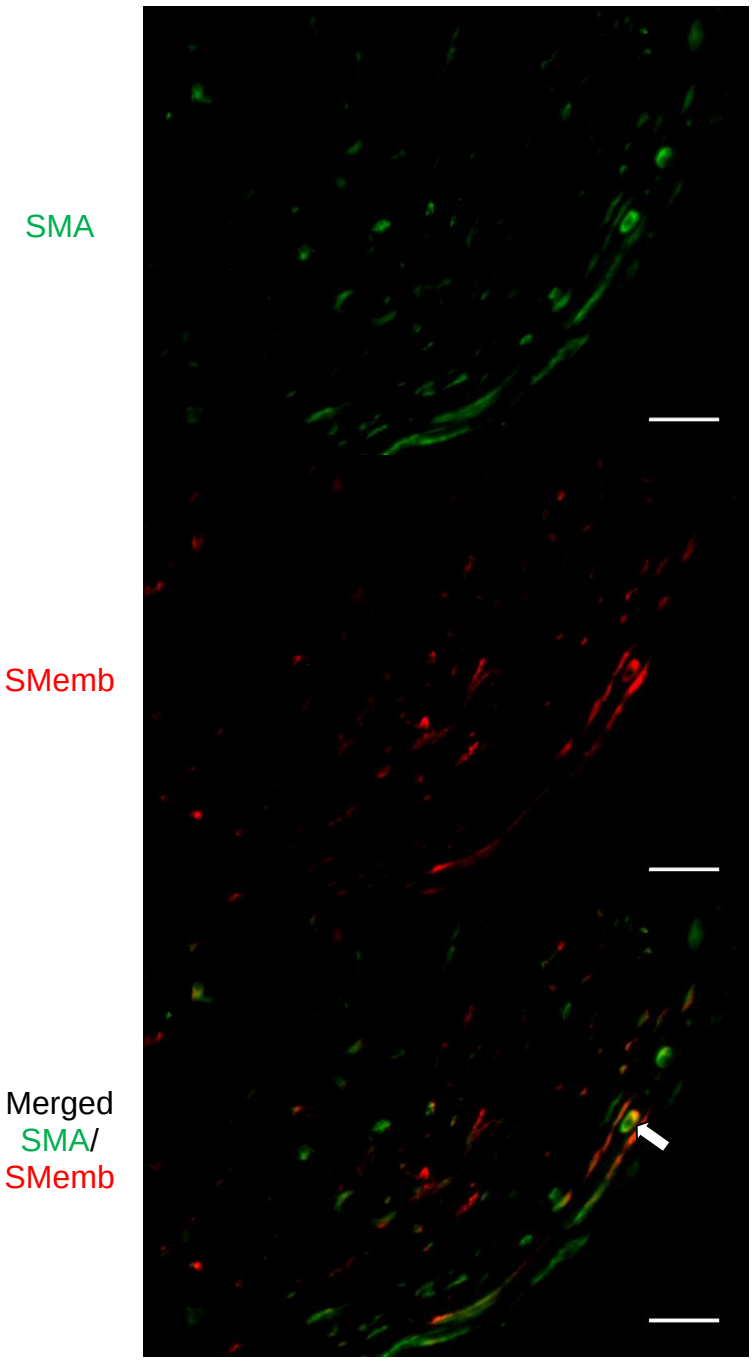

Figure 2-9 Photomicrograph for double immunofluorescence staining of α-SMA and SMemb. White arrow indicates a round-shaped cell co-expressing α-SMA and SMemb. Scale bar= 25µm.

While the pattern of staining for α-SMA and SMemb at the valve edge was similar in both affected groups, only a few of those cells co-expressed both antigens (Figure 2-9). In overtly myxomatous areas, the overall pattern of cellular staining (indirect immunofluorescence) for α-SMA and SMemb was similar in the CKCS and non-CKCS, and was in agreement with staining pattern using the peroxidase method.

The total cell counts for α-SMA, SMemb, and vimentin of CKCS, non-CKCS, and normal control (section 2.2.4) are summarized in Table 2-2. The total number of cells positive for α-SMA was significantly increased in the CKCS group and non-CKCS group compared to normal (CKCS vs control, p=0.0052; non-CKCS vs control, p=0.0005), and there was no difference between CKCS and non-CKCS (p=0.5376). SMemb positive cells were significantly increased in the two diseased groups compared to normal (CKCS vs control, p=0.0126; non-CKCS vs control, p=0.0012), and there was no difference between CKCS and non-CKCS. Vimentin positive cells made up the largest number in all groups of valves, and cell numbers in both diseased valves approached twice that seen in normal valves (Figure 2-10). However, statistically there was no difference between any of the groups sampled (CKCS vs control, p=0.4669; non-CKCS vs control, p=0.2265; CKCS vs non-CKCS, p=0.7612).

Table 2-2 Quantification of positive staining cells for α-SMA, SMemb, and vimentin in the diseased mitral valves from CKCS, Non-CKCS, and the normal mitral valves.

	α-SMA	SMemb	Vimentin
CKCS (n=6)	33.95 ± 12.13	23.13 ± 5.72	40.52 ± 18.41
Non-CKCS (n=6)	25.70 ± 2.67	29.55 ± 3.06	46.95 ± 17.65
Control (n=4)	10.75 ± 2.95	14.53 ± 3.96	26.75 ± 7.24

The data is presented as mean ± standard deviation

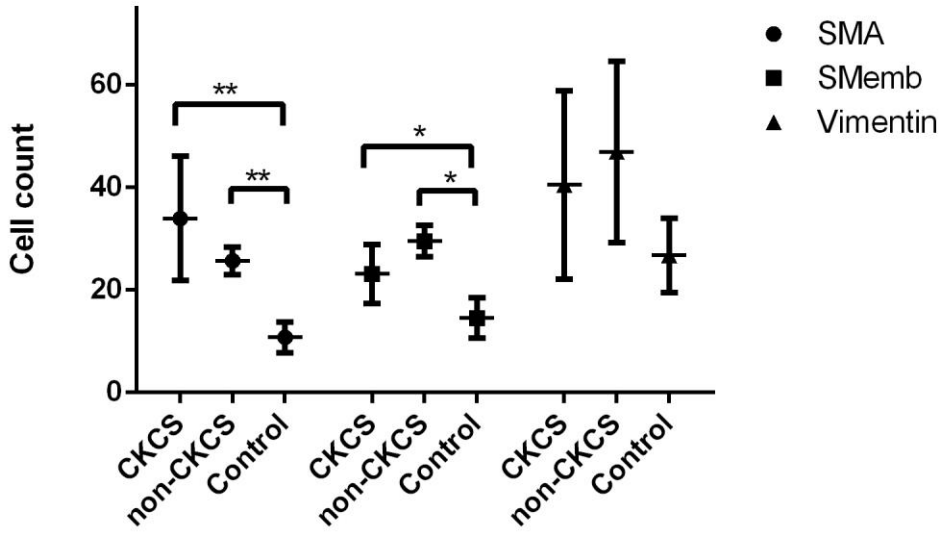

Figure 2-10 Total positive cell counts for α-SMA, SMemb, and vimentin. The data is presented as mean ± standard deviation. * $p < 0.05$, ** $p < 0.01$.

2.4 Discussion

The CKCS breed predisposition to MMVD is well recognised and heritability has a role in disease appearance and progression. [18,20] Certain CKCS-specific traits are associated with MMVD, and it is not known if this may result in a disease phenotype and pathology different to that seen in other dogs. [21,23–25,27] By assessing for a range of markers for inflammation, proliferation and mesenchymal cell phenotypic differentiation no evidence was found that cell changes in the CKCS valve are fundamentally different to that seen in other dogs.

There was no evidence of inflammatory cells in any of the samples examined and this is in agreement with the only other report. [104] Small numbers of macrophages and mast cells have been previously found in MMVD valves and there was an increased expression of some inflammatory cytokine transcripts in affected valves

[106], but there still is no clear evidence that inflammation has an important role in the aetio-pathogenesis of this disease. [52,106]

Aggregation of activated α-SMA positive valve interstitial cells in canine MMVD is well recognised, particularly in the distal portion of the valve and close to the valve edge, and this was again noted in the present study in all affected dogs. [52,104] Increased α-SMA positive cells numbers were seen in the two affected groups. In MMVD, the increased expression of α-SMA by valve interstitial cells may be a compensation to maintain mitral valve stiffness secondary to mitral valve incompetence. [101,107] SMemb is expressed in synthetic phenotypes of mesenchymal cells, or myofibroblasts, and myofibroblasts play multiple physiological roles in heart development and tissue repair (myocardial infarction). [80,108,109] Increased SMemb positive cell numbers have also been previously reported and were found again to be increased in this study. [104] An association between SMemb positive interstitial cells, tryptophan hydroxylase 1 (TPH1) expression and serotonin synthesis has also been reported in MMVD [38] Pleomorphism of myofibroblasts positive for SMemb was noted in the current study and this might imply heterogeneity of the myofibroblast population. Using vimentin as a general mesenchymal cell marker, total cell numbers in the two affected groups were similar. However, it should be noted the normal valves were not age-matched and increased cell numbers associated with aging cannot be discounted. The lack of age-matched normal controls is a study limitation, but finding normal mitral valves in aged dogs is not readily achievable.

While vimentin expression is widespread in many cell types, interstitial cells expressing vimentin are generally considered to be a quiescent phenotype form of VIC in the normal mitral valve. [52,104] In the diseased valve cells retaining vimentin expression and/or not expressing the two activation markers (α-SMA and SMemb) may represent an expanded population available for phenotypic alteration in response to appropriate triggers, such as TGF-β and serotonin. There was localized expression of the cell proliferation marker Ki-67 in the MMVD valves and this was most noticeable where there was the largest number of α-SMA positive cells close to the free edge. This finding contrasts with the only other study where Ki-67 showed

minimal expression in diseased valves. [104] This contradictory finding may reflect the heterogeneous pathology of MMVD or could be a temporal effect. For example, in a valve injury model myofibroblast proliferation peaked at the 4th day post injury. [110,111]

The co-expression of α-SMA and SMemb in a small number of cells close to the valve edge identifies a population that has greater differentiation potential than those expressing α-SMA or SMemb alone, and such cells are believed to have greater phenotypic differentiation capability in response to injury. [108] In the case of MMVD, a similar capacity for phenotypic versatility might exist where endothelial damage has occurred.

Von Willebrand factor expression demonstrated the presence of the endothelium in all valves and the loss of endothelial cells along some sections of affected valve edges. Endothelial damage and denuding is now recognised to be a cardinal feature of MMVD, and might be a major triggering event driving the phenotypic changes seen with VICs and proliferation of aVICs close to the valve edge. [21,49,57] Recently, one study found that the secretion of haemostatic proteins such as vWF, tissue plasminogen activator (tPA), and tissue factor pathway inhibitor by aortic valve endothelial cells is age-dependent. [112] The localised expression of vWF in cells within the stroma of the diseased valves was an unexpected finding. Possible explanations might be migration of endothelial cells or the presence of mesenchymal-endothelial transition (MEndoT) of stromal VICs. This finding needs to be investigated further as it might also due to extravasation. Successful staining for CD31 would have been helpful in clarifying the cell identity as endothelial.

In conclusion, this study confirms that there is no evidence for inflammatory cell involvement in canine MMVD, that the cell changes are not different for CKCS compared with other dogs and that the changes in cell numbers in MMVD are due to cell proliferation. This study further suggests MMVD is not a heterogeneous disease (detailed assessment of pathology and ECM changes is still required) and the CKCS form of the disease differs only in its time of onset and speed of progression. It is this temporal presentation that is likely to be the inherited feature of MMVD in the cavalier King Charles spaniel. A summary of the results is provided in Table 2-3.

Table 2-3 Summary of IHC findings

Markers	Myxomatous Mitral Valves		Normal Mitral Valves
	CKCS	Non-CKCS	
CD11c	No staining	No staining	No staining
CD45	No staining	No staining	No staining
vWF	Discontinuous staining EC	Discontinuous staining of EC	EC (continual)
α-SMA*	Linear clusters mainly found at the tip, increased expression (vs normal)	Linear clusters mainly found at the tip, increased expression (vs normal)	Small numbers of positive cells found at atrialis and spongiosa in middle portion
SMemb*	Similar to α-SMA and increased expression (vs normal)	Similar to α-SMA and increased expression (vs normal)	Similar to α-SMA and no change (vs MMVD)
Vimentin*	Diffuse but no change (vs normal)	Diffuse but no change (vs normal)	Diffuse but no change (vs MMVD)
Ki-67	Spindle-shaped cells at myxomatous area and in EC	Spindle-shaped cells at myxomatous area and in EC	Negligible

EC, endothelial cells. *Quantitative study

3 Chapter 3 Transcriptional Profile of Canine Myxomatous Mitral Valves

3.1 Introduction

Transcriptomics is the study of overall ribonucleic acid (RNA) such as messenger RNA (mRNA), ribosomal RNA (rRNA), transfer RNA (tRNA) transcribed from the genome in a single cell or from a heterogeneous population of cells in a certain organ or tissue at a specific time point. By studying the transcriptome, it not only helps us to understand the relationship between gene activities within the functional cells, but also provides insight into the transcriptional regulation of diseases. Proteomics is the quantitative study of the set of proteins and their diversity. However, proteins are technically challenging to characterise because, for example, they have post-translational modifications and may interact with other molecules. [113] Measuring the intermediate step between genes and proteins, that is the expression of transcripts of mRNA, helps connecting the gap between genome and functional molecules.

Microarrays have been reliably utilized for many kinds of studies due to the their cost-effectiveness and the ability to screen and compare more than 20,000 transcripts at once. The only genomic study of canine MMVD to date used the Affymetrix Canine Gene 1.0 array covering approximately 23,000 gene transcripts, but did not include transcripts for microRNAs (miRNAs). [106] This study only compared mixed breed dogs. Since that study there have been significant advances in the quality of canine gene microarrays (Affymetrix Canine Gene 1.0 ST Array based on Genome database CanFam2.0) with much improved transcript annotation (27,681 genes), transcript sensitivity (590,097 probes, 24 probes/gene) and bioinformatics. The study by Oyama et al in 2006 [106] identified only 229 probe sets that were differentially expressed in MMVD compared to normal valves (at least 2-fold change; 70% up-regulated and 30% down-regulated) of which 166 could be assigned to recognised genes. The main functional classes attributed to the affected genes, in descending order, included cell signalling, metabolism extracellular matrix, inflammation, cell defence, immunity, cell transport and cell structure. [106] Of particular note was the ~4-fold increase in the 5-HTR2B (5-hydroxytryptamine receptor 2B) receptor gene,

which fits in with the serotonin hypothesis of MMVD pathogenesis. [34,106] Limited numbers of studies of gene expression have also been undertaken in human MMVD with the number of differentially expressed genes reported varying between 400 and 2000 [114,115]. One study demonstrated changes in metallothioneins and ADAMTS (a disintegrin and metalloproteinase with thrombospondin motifs) genes, processes that are implicated in extracellular matrix remodelling. [115] The other study found higher expression for bone morphogenic protein 4 (BMP-4, TGF-β superfamily), proteoglycans (bigylcan, decorin, lumican, and versican), collagens (collagen I, and collagen III), and chondrogenic associated transcripts such as Sox-9, CRTAC1 (cartilage acidic protein). [114] However, the number of reported differentially expressed genes in any transcriptomic study is markedly affected by the corrected Benjamini-Hochberg false discovery rates (FDR) [116,117], fold change thresholds (correction for signal intensity) and batch effects. Although a single snap-shot of the genomic expression will not reflect the whole dynamic remodelling process and cellular events during the myxomatous degeneration, transcriptomic profiling remains a useful tool to identify key genes regulating MMVD pathogenesis.

The aim of this study, therefore, was to use more stringent threshold criteria and quality control, than used in previous studies, in line with current recommended protocols and with the affected group all from the same breed (cavalier King Charles spaniel) to identify gene regulation in canine MMVD. While this study would give information on changes in the entire transcriptome, a particular aim was to investigate the possible changes in expression of genes typically associated with developmental pathways, valvulogenesis and endothelial-to-mesenchymal transition.

3.2 Material and Methods

3.2.1 Tissue Sample

Myxomatous mitral valve anterior leaflets (n=10, Whitney grade ≥ 3) from CKCS were either collected by the author from CKCS presenting to the Hospital for Small Animals, Royal (Dick) School of Veterinary Study, the University of Edinburgh, or received from pathology units from the Queen's Veterinary Hospital, Cambridge Veterinary School, University of Cambridge, and The Veterinary Teaching Hospital, School of Veterinary Medicine, University College Dublin, through a CKCS club

tissue collection scheme. All dogs previously had been clinically confirmed to have MMVD and were on a range of treatments for congestive heart failure. Control normal anterior mitral valve leaflets (n=6) were collected from young adult dogs (beagles) euthanized for reasons other than cardiac disease. Based on the same protocol, all samples were collected within 10 minutes of death and classified by two investigators according to Whitney's MMVD grading system. [6] After removal of the heart and flushing with cold PBS (phosphate-buffered saline), the mitral valve leaflets were exposed by opening from the left atrium and ventricle through the lateral wall between the two papillary muscles. The mitral valve leaflets were examined for MMVD lesions and photographed. The whole mitral valve leaflets then were surgically dissected from the annulus and papillary muscles, and immediately immersed in RNAlater (Invitrogen). After overnight incubation at 4 ˚C, samples were transferred to -20˚C freezer for long-term storage. All tissue samples were collected with full owner consent and the study conformed to national (UK) and institutional ethical guidelines for the use of animals in research.

3.2.2 RNA Extraction

Mitral valve leaflets in RNAlater tubes were taken from -20˚C freezer and thawed on ice. The dis-membranator equipment (ball, lid, and flask) was submerged in liquid nitrogen for a few minutes. Mitral valve anterior leaflets were weighed and minced with a sterile scaple blade. A hundred mg of tissue was then gathered in an eppendorf tube and snap-frozen in liquid nitrogen. Shortly after removing the dis-membranator from liquid nitrogen, snap-frozen tissues and 500 µl of phenol/guanidine HCl reagents (TriReagent, Sigma) and the ball were transferred to the flask, the lid closed and tightly screwed into the dis-membranator. (Braun Mikro Dis-membranator Vessel, Braun Biotech International, Melsungen, Germany). Next, speed of the machine was set at 30 m/s, and the duration of vibration was 90 seconds. After pulverising, tissue-TriReagent powdered samples were scraped into an Eppendorf tube containing 0.5 ml of TriReagent (1ml/100mg tissue weight) and mixed thoroughly, left to stand for 45 minute at room temperature and spun at 12,000 rpm (in a microfuge) for 10 minutes at 4˚C. The supernatant was carefully transferred into another clean tube. and the cell and matrix debris were discarded. 200 µl of chloroform was added followed by vigorous mixing for a few seconds. The mixture

was left at room temperature for 10 minutes then spun at 12,000 rpm at 4˚C for 15 minutes. The supernatant was again transferred to another clean tube and 400µl of 70% ethanol was added in with gentle pipetting to mix with the RNA sample. RNA extraction, purification and DNA digestions were carried out using commercially available kits (RNeasy Mini Kit & RNase-Free DNase Set Qiagen). Detailed protocols for the column-based RNA extraction and DNA digestion can be found in the manufacturer manual. Final elution was completed by adding 30µl of RNase-free water. The RNA samples were stored at -80℃ prior to reverse transcription.

3.2.3 RNA Quality Assessment

The RNA sample purity and quantity was analysed by spectrophotometery (Thermo Scientific NanoDrop™ 1000). 1µl of each sample was pipetted onto the pedestal and the ratio of absorbance at 260 nm and 280 nm (260/280, pure RNA = 2.0) was used to assessed the purity of RNA. The ratio of 260 nm and 230 nm (260/230, normal range 2.0-2.2) was used for secondary assessment of RNA purity. [118]

For final standardization of RNA quality, the sample RNA quantity and integrity were further characterized by using Agilent 2100 Bio-analyser and RNA 6000 LabChip. Degradation of total RNA, mRNA and ribosomal RNA contamination could be identified by electropherogram, electrophoretic trace of the RNA sample, and the given RNA integrity number (RIN). RIN $\geq$ 7 was considered acceptable for further analysis. [119]

3.2.4 Microarray Analysis

The two cycle RNA-cDNA amplification, hybridization, and chip scanning were undertaken by ARK-Genomics (Roslin Institute, UK). Affymetrix Gene Chip WT Terminal Labelling Kit, combined with Ambion WT Expression Kit, was used to generate amplified and biotinylated sense-strand DNA targets for the Affymetrix Canine Gene 1.0 ST Array.

Differential gene expression analysis and signal intensity profile for each array were also performed by ARK-Genomics (Roslin Institute, UK). First, all the raw Affymetrix CEL files representing each array were imported into Partek Genomic Suite 6.6 (PGS). In the PGS post-hybridization quality control was conducted by principal component analysis (PCA plot) to identify any outliers, and histogram plots

were produced for general array expression patterns. The volcano plot and the heat map were also generated by PGS. Robust Multi-array Average (RMA) was used for data normalization and final summarization. [120] The ANOVA was used to identify differentially expressed genes between the two groups. To determine the differentially expressed genes, $p < 0.05$ with Benjamini-Hochberg false-discovery correction and at least a 1.5 fold change in expression were used. [117] Normalized signal intensity data for whole probe sets and attributed transcripts were produced by Affymetrix Expression Console. Seasonal annotation-updates for canine transcripts were released from Affymetrix, and were also applied to the data set to synchronize with the latest online database.

The initial differentially expressed gene list produced by ARK-Genomics was further filtered by an signal intensity stringency filter as following:

1. Signal Intensity ≥ 1000, fold change ≥ 1.5 or ≤ -1.5
2. Signal intensity between 1000 and 500, fold change ≥ 2.5 or ≤ -2.5
3. Signal intensity ≤ 500, fold change ≥ 3.5 or ≤ -3.5
4. Remove transcripts without annotation, non-protein coding RNA

3.2.5 Multi-platform Data Mining

ToppFun. ToppFun is web-based gene list enrichment tool for transcriptome, ontology, phenotype, proteome using ToppGene Suite. The IDs of differentially expressed genes without fold-change values were uploaded to the platform followed by manually modifying the unmatched gene ID The statistical correction used the Bonferroni method with the cutoff set to be $p = 0.05$. The submitted gene lists were analysed and the associated results assigned to different categories: GO (gene ontology): molecular function, GO: biological process, GO: cellular component, human phenotype, mouse phenotype, pathway, microRNA, drug, and disease. [121]

DAVID. The database for annotation, visualization and integrated discovery (DAVID 6.7) was another gene network analysis tool used to identify gene connections. Finalized gene lists were submitted to the DAVID web-based bioinformatics resources for function annotation analysis. Candidate genes were firstly matched and converted to the human gene symbol according to the DAVID

database. Functional annotation clustering analysis was conducted at "high" classification stringency with cutoff set for enrichment score (no less than 1.5) and p-value ($p > 0.05$). [122]

IPA. Pathway analysis was undertaken using the Ingenuity Pathways Analysis (IPA, Qiagen) database by uploading the differentially expressed gene list (finalized gene list including transcript ID, fold-change, and p-value) to the online server. Core analysis was performed at the default settings, and this included canonical pathways, disease and biological functions, gene networking, up-stream analysis and toxicity. Functional analysis of a network identified the biological functions that were most attributable to the genes in the network.

BioLayout *Express3D*. Network analysis and visualization was conducted using BioLayout Express^{3D} version 3.3. Briefly, signal intensity value ($\geq$ 100) for all probes for all samples were formatted in an excel file following the software manual instructions. [123] The network graph was then illustrated using a correlation threshold of $r \geq 0.94$. Markov clustering algorithm (MCL) analysis was conducted at an inflation value 1.6 (controlling granularity of clustering) according to recommendations. [123] Clustered genes were analysed using the ToppFun as described previously.

3.3 Results

3.3.1 RNA Quality Assessment

Using the standardized RNA extraction technique and the final elution volume (30 µl), the yield of RNA from mitral valve leaflets was variable (303.23 ± 127.21 ng/ µl). The highest RNA concentration was 541.6 ng/µl and the lowest was 78.5 ng/µl. The values for absorbance of 260/280 were between 1.99 and 2.10 (2.046 ± 0.031, pure RNA ≈ 2). Another indicator for RNA purity was 260/230 absorbance, and the values were generally consistent and acceptable except 5 samples, 811M_003, 811m_006, 811M_010, 811M_011, and 811M_012 that were far below the reference range (2.0 – 2.2) (Table 3-1).

Table 3-1 Summary of RNA assessment for 10 diseased (CKCS) and 6 control mitral valves.

Barcode	ID	Breed	Con. (ng/µl)	Volume (µl)	260/280	260/230	RIN
811M_001	Cam	CKCS	325	28	2.04	2.15	5.00
811M_002	Han	CKCS	461.5	28	2.01	2.01	5.50
811M_003	Dublin	CKCS	78.5	28	1.99	1.56	6.30
811M_004	Dublin **R**	CKCS	407.6	28	2.00	1.98	6.00
811M_005	Shay (MMVD005)	CKCS	349	28	2.05	2.01	7.30
811M_006	Cam R	CKCS	122.8	28	2.03	1.76	4.10
811M_007	Dublin **R**	CKCS	541.6	28	2.10	1.99	6.60
811M_008	Han R	CKCS	431.1	28	2.01	1.98	6.20
811M_010	Control05	Beagle	275.5	28	2.04	1.42	7.20
811M_011	Control02	Beagle	338.8	28	2.05	1.68	8.50
811M_012	Control06	Beagle	112.7	28	2.08	1.00	7.00
811M_013	Control03	Beagle	304.1	28	2.05	2.11	6.70
811M_014	Control04	Beagle	449.4	28	2.02	2.07	7.80
811M_015	Control01	Beagle	420.3	28	2.02	2.09	7.60
811M_016	Bonnie (MMVD016)	CKCS	265.7	28	2.07	2.18	7.60
811M_017	Cinders	CKCS	192.3	28	2.06	2.13	6.90
811M_018	Emily	CKCS	129.5	28	2.08	2.15	6.40
811M_019	Joe (MMVD019)	CKCS	465.7	28	2.01	2.19	8.10
811M_020	Cinders **R**	CKCS	247.1	28	2.08	2.21	6.40
811M_021	Emily **R**	CKCS	140.5	28	2.10	2.12	5.70
811M_022	Eric	CKCS	260.5	28	2.08	2.16	7.10
811M_023	Eric **R**	CKCS	351.6	28	2.06	2.04	6.80
811M_024	Tom (MMVD024)	CKCS	303.5	28	2.05	2.16	7.80

*Con. = Concentration. RIN = RNA integrity number. R= repeat RNA extraction.

From the electrophoresis studies of RNA samples, 18S and 28S ribosomal RNA could be identified as the thickest bands at 2000 and 4000 nucleotides (nt) respectively, and there were variable degrees of mRNA degradation in 6 of 23 samples (smearing below 2000 nt), and poor integrity in 7 of 23 samples (multiple bands) (Figure 3-1).

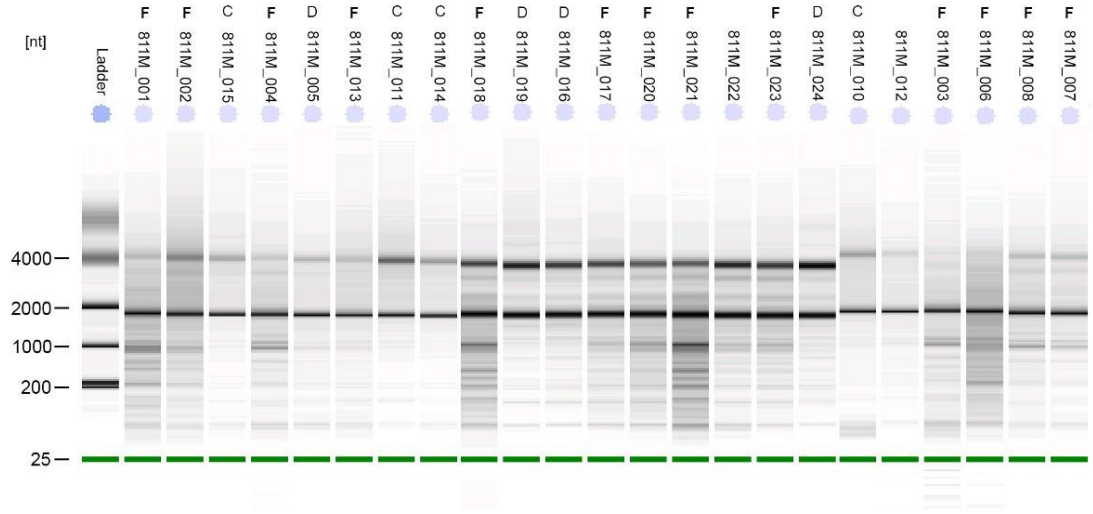

Figure 3-1 Electrophoresis of RNA samples. C (control) and D (diseased) RNA samples were selected for the microarray hybridization and labelling. F (failed RIN test) were excluded, and blanks were borderline.

Electrophoresis and associated fluorescence signals were captured and transformed into electropherogram. Based on the electropherogram the RIN (RNA integrity index) was determined by the Bioanalyser (Figure 3-1). Only 10 samples passed the RIN cutoff (RIN $\geq$ 7) and one sample was borderline (RIN = 6.9). The remaining 5 valve samples failed to pass the pre-hybridization quality control (Figure 3-2), after multiple RNA extractions.

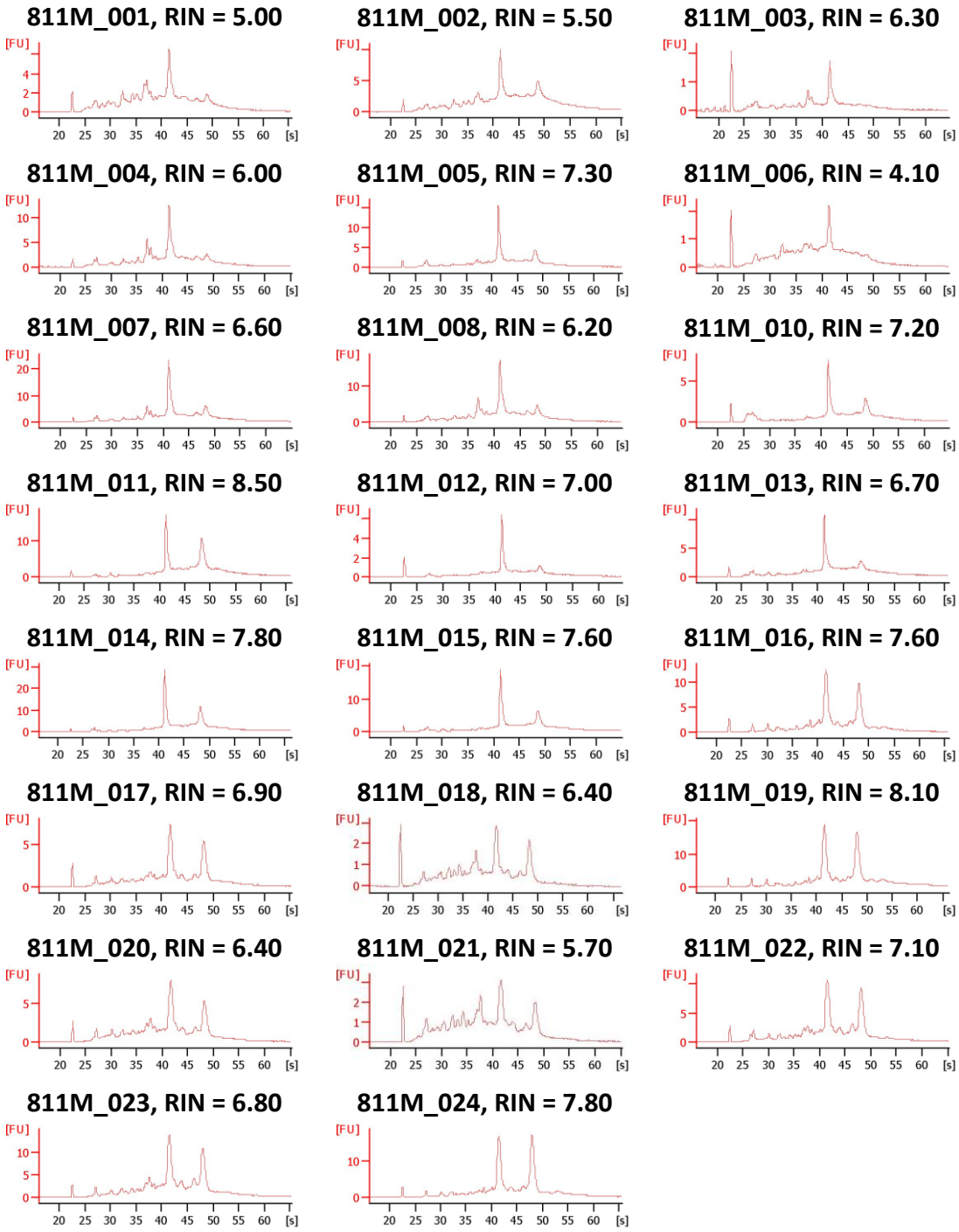

Figure 3-2 RNA integrity numbers (RIN) for pre-hybridization quality assessment.

By evaluating the spectrophotometer measurements (260/280), RNA electrophoresis (visual representation), and electropherogram (RIN), a final four samples for each group (MMVD: 811M_005, 811M_016, 811M_019, 811M_024. Control:

811M_010, 811M_011, 811M_014, 811M_015) were selected for transcriptomic analysis. The details of the 8 samples can be found in Table 3-2.

Table 3-2 Details of final RNA samples for the diseased and the control group.

Barcode	ID	Age	Heart murmur [9]	Gender	Whitney Grade [6]	RIN	260/ 280
MMVD							
811M_005	Shay	11Y4M	4/6	Male	3/4	7.3	2.05
811M_016	Bonnie	12Y	4/6	Female	4/4	7.6	2.07
811M_019	Joe	11Y	6/6	Male	3/4	8.1	2.01
811M_024	Tom	12Y	3/6	Male	3/4	7.8	2.05
Control							
811M_010	Control05	1Y	0/6	Female	0/4	7.2	2.04
811M_011	Control02	1Y	0/6	Female	0/4	8.5	2.05
811M_014	Control04	1Y	0/6	Male	0/4	7.8	2.02
811M_015	Control01	1Y	0/6	Male	0/4	7.6	2.05

Y, year; M, month.

3.3.2 Overview of Microarray Data

Post-hybridization Quality Control

A PCA plot was produced for general array expression pattern and quality control (QC). Two major clusters representing diseased and control groups were identified, and one outlier within each group (811M_005 and 811M_011) was also noted (Figure 3-3A). The histogram plots of arrays showed the signal intensity distribution of each sample and the same samples in each group were again found to have a different distribution pattern and were confirmed as outliers (Figure 3-3B). The rest of the lines followed the same pattern indicating that there is no distributional difference in probe signal intensity. There was another signal intensity plot for Affymetrix internal control probe-sets. This graph gave quality control information from control and experimental probes on the Affymetrix chips. One sample showed abnormally signal intensity (Figure 3-3C). Together with all the evidence, post-hybridization QC provided confidence in the quality of the microarray data and identified two samples that do not meet QC criteria.

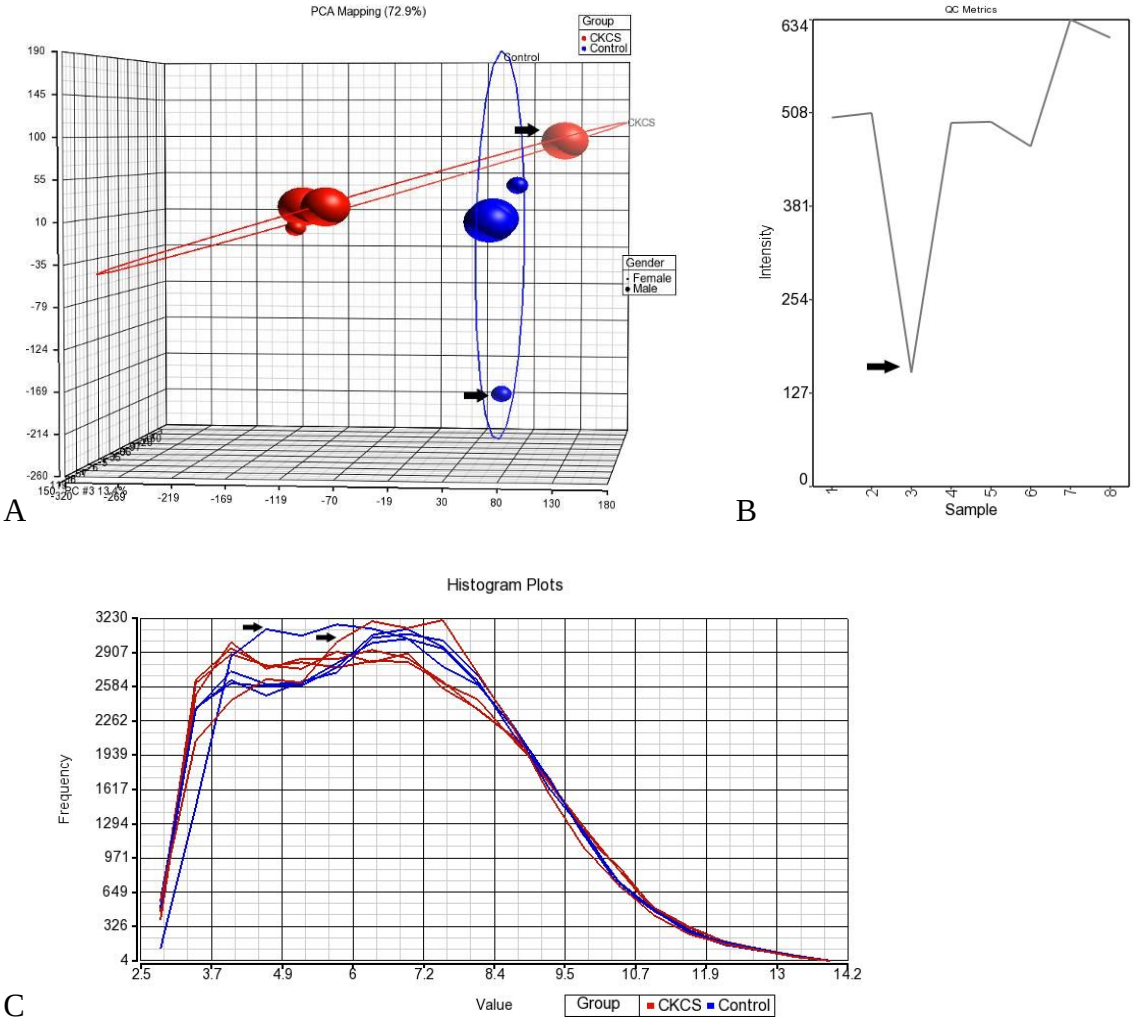

Figure 3-3 Post-hybridization QC (A) PCA plot, (B) Signal intensity plot for internal control. X-axis = intensity of the probes, Y-axis = frequency of the probe intensity (C) Histogram plot with summarized intensity value of Affymetrix control probe-sets. Arrows in each figure indicate the outliers.

Differentially Expressed Gene List

With inclusion of the two outliers, differential expression analysis was examined using One-way ANOVA comparing the 4 diseased CKCS and 4 control samples. This only identified 18 differentially expressed genes (p-value $p < 0.05$, FDR <0.05, and fold change ≥ 1.5 or ≤ -1.5). Excluding the two outliers, 5397 transcripts were identified to be differentially expressed passing the following cut-off: fold-change (>1.5 or <-1.5), false discovery rate (FDR, <0.05), and p-value (<0.05). A volcano plot was generated to visualize the overall gene expression pattern. (Figure 3-4). Two

vertical (fold-change value at 1.5 and -1.5) and one horizontal (p-value = 0.05) cut-off lines were also applied to the plot. In general, the plot was equally distributed, but the significantly down-regulated genes in zone 3 were more diffusely distributed compared with the significantly up-regulated genes in zone 4. In zone 1 and 2, the majority of the genes were unchanged. A heat map of the differentially expressed genes (excluding outliers) was also generated, and there were two clusters of up- (red) and down-regulated (blue) genes in each group (Figure 3-4).

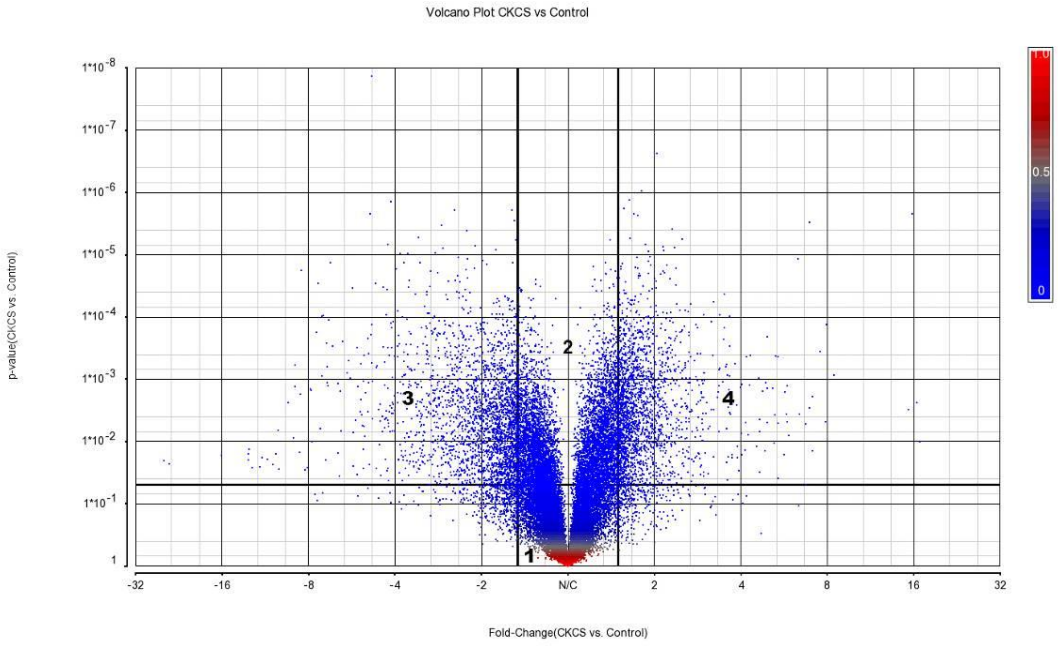

Figure 3-4 Volcano plot (section 3.2.4). Every dot represents one gene. The X-axis is the fold-change value) and Y-axis is the p-value.

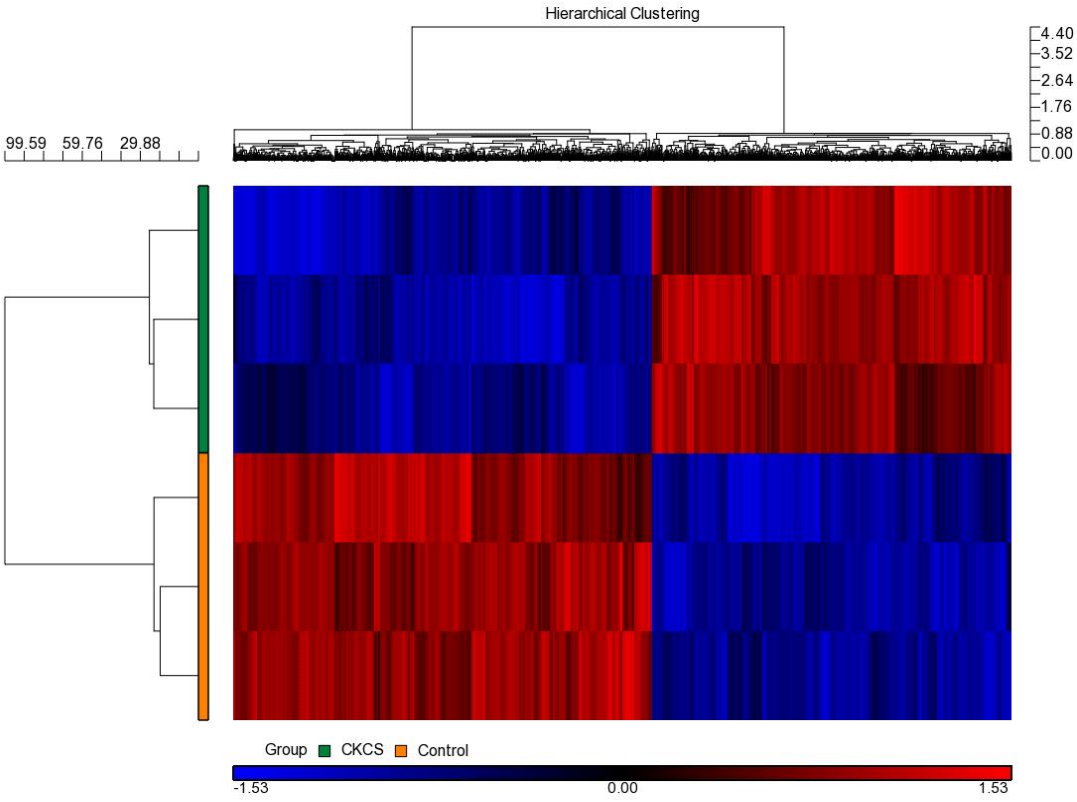

Figure 3-5 Heat map (section 3.2.4) of the microarray excluding two outlier samples from MMVD and control groups. The vertical axis represent 6 different samples (green, CKCS; orange, controls). The bar in red represents up- (red) and down-regulation (blue) in fold-change.

In 5397 differentially expressed transcripts, 4002 were annotated, whereas 1395 probes were not assigned to a specific transcript in the Affymetrix canine database . For these unknown transcripts sequences were downloaded in a batch from the Affymetrix website and matched with the public genomic information by NCBI nucleotide BLAST and miRBase BLAST. [124] Sequences were considered matched with the transcript only if the E-score was $\leq 1x10^{-20}$. [106] After pairing, only 139 additional probes were successfully identified as transcript homologs to other species, canine microRNAs or a duplicate or triplicate of already annotated transcripts (Table 3-3). Within 139 manually annotated transcripts, 59 were matched with *Canis familiaris* microRNA family (cfa-miRNA) (see Chapter 6).

The gene list (including manually annotated genes) was further narrowed down to 591 genes using more stringent thresholds based on signal intensity and fold-change

value and exclusion of microRNAs (described in 3.2.4). Within the finalized gene list, 322 genes were up-regulated and 269 genes were down-regulated in the diseased group compared with the normal control group. The complete list of differentially expressed genes can be found in the appendix 9.1 and 9.2.

Table 3-3 Summary of identified differentially expressed transcripts

Differential expressed Genes	5,397
Annotated transcripts	4,002
Uncharacterized, or non-coding	1,395
Manual pairing	139
Transcripts in other species	80
miRNAs	59
Finalized by signal intensity cutoff	591
Up-regulated	322
Down-regulated	269

3.3.3 ToppFun

The list of 591 genes was uploaded to the ToppFun in ToppGene Suite, and 571 of 591 genes were identified with the HGNC symbol and synonyms. After gene list enrichment, 28 significant terms for gene ontology (GO) biological process (BP) were derived. The top ten most significant GO: BP terms were inflammatory response, response to wounding, biological adhesion, cell adhesion, positive regulation of cellular component movement, positive regulation of cell migration, positive regulation of cell motility, positive regulation of immune system process, blood vessel morphogenesis, and positive regulation of locomotion (Figure 3-6). "Positive regulation" in GO terms means the overall biological function is likely to be active compared to the control group.

The GO terms were further categorized into six functional sub-groups: inflammation and immune response, cellular adhesion and movement, cardiovascular development, extracellular matrix, osteogenesis, and epithelial cell proliferation (Table 3-4) based on the biological functions of each gene ontology terms. In addition, there were three major clusters of GO: BP terms according to the p-value classification ($p < 0.005$, $0.005 < p < 0.03$, and $0.03 < p < 0.05$) (Table 3-5). The most significant GO: BP terms in the first group ($p < 0.005$) were associated with injury (inflammatory response, response to wounding), cell movement, and vasculature development.

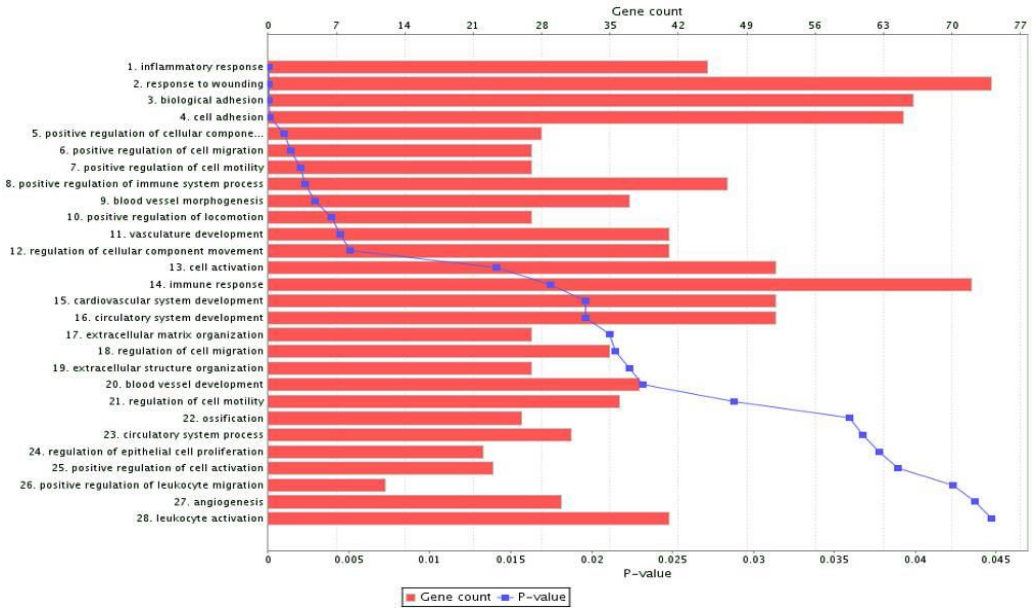

Figure 3-6 Significant terms for gene ontology: biological process

Table 3-4 Gene ontology terms for biological process

Name	Term	p-value	Count in term	
Inflammation and immune response				
GO:0006954	Inflammatory response	3.17E-05	45	566
GO:0009611	Response to wounding	4.04E-05	74	1202
GO:0002684	Positive regulation of immune system process	2.31E-03	47	699
GO:0001775	Cell activation	1.41E-02	52	861
GO:0006955	Immune response	1.75E-02	72	1353
GO:0050867	Positive regulation of cell activation	3.89E-02	23	264
GO:0002687	Positive regulation of leukocyte migration	4.24E-02	12	83
GO:0045321	Leukocyte activation	4.47E-02	41	642
Cellular adhesion and movement				
GO:0022610	Biological adhesion	5.73E-05	66	1028
GO:0007155	Cell adhesion	1.11E-04	65	1023
GO:0051272	Positive regulation of cellular component movement	1.01E-03	28	300
GO:0030335	Positive regulation of cell migration	1.42E-03	27	287
GO:2000147	Positive regulation of cell motility	2.00E-03	27	292
GO:0051270	Regulation of cellular component movement	5.10E-03	41	588
GO:0030334	Regulation of cell migration	2.15E-02	35	493
GO:2000145	Regulation of cell motility	2.88E-02	36	521
Cardiovascular development				
GO:0048514	Blood vessel morphogenesis	2.90E-03	37	492
GO:0040017	Positive regulation of locomotion	3.88E-03	27	302
GO:0001944	Vasculature development	4.48E-03	41	585
GO:0072358	Cardiovascular system development	1.96E-02	52	871
GO:0072359	Circulatory system development	1.96E-02	52	871
GO:0001568	Blood vessel development	2.32E-02	38	559
GO:0003013	Circulatory system process	3.68E-02	31	421
GO:0001525	Angiogenesis	4.37E-02	30	404
Extracellular matrix				
GO:0030198	Extracellular matrix organization	2.11E-02	27	330
GO:0043062	Extracellular structure organization	2.23E-02	27	331
Osteogenesis				
GO:0001503	Ossification	3.59E-02	26	320
Epithelial proliferation				
GO:0050678	Regulation of epithelial cell proliferation	3.78E-02	22	245

Table 3-5 Three major clusters of GO: terms identified based on p-value

GO: BP	Terms	p-value
p < 0.005		
GO:0006954	Inflammatory response	3.17E-05
GO:0009611	Response to wounding	4.04E-05
GO:0022610	Biological adhesion	5.73E-05
GO:0007155	Cell adhesion	1.11E-04
GO:0051272	Positive regulation of cellular component movement	1.01E-03
GO:0030335	Positive regulation of cell migration	1.42E-03
GO:2000147	Positive regulation of cell motility	2.00E-03
GO:0002684	Positive regulation of immune system process	2.31E-03
GO:0048514	Blood vessel morphogenesis	2.90E-03
GO:0040017	Positive regulation of locomotion	3.88E-03
GO:0001944	Vasculature development	4.48E-03
0.005 < p < 0.03		
GO:0051270	Regulation of cellular component movement	5.10E-03
GO:0001775	Cell activation	1.41E-02
GO:0006955	Immune response	1.75E-02
GO:0072358	Cardiovascular system development	1.96E-02
GO:0072359	Circulatory system development	1.96E-02
GO:0030198	Extracellular matrix organization	2.11E-02
GO:0030334	Regulation of cell migration	2.15E-02
GO:0043062	Extracellular structure organization	2.23E-02
GO:0001568	Blood vessel development	2.32E-02
GO:2000145	Regulation of cell motility	2.88E-02
0.03 < p < 0.05		
GO:0001503	Ossification	3.59E-02
GO:0003013	Circulatory system process	3.68E-02
GO:0050678	Regulation of epithelial cell proliferation	3.78E-02
GO:0050867	Positive regulation of cell activation	3.89E-02
GO:0002687	Positive regulation of leukocyte migration	4.24E-02
GO:0001525	Angiogenesis	4.37E-02
GO:0045321	Leukocyte activation	4.47E-02

GO:BP terms relating to endothelial function, developmental pathways and basic mitral valve biology included response to wounding, biological adhesion, positive regulation of cell migration, cardiovascular system development, extracellular matrix organisation, ossification, and regulation of epithelial cell proliferation. Genes associated with these terms are listed in the following tables. In each sub-group, GO: BP terms selected were response to wounding, biological adhesion, positive regulation of cell migration, cardiovascular system development, extracellular matrix organization, ossification, and regulation of epithelial cell proliferation. Genes involved in these terms are listed in the following tables. (Table 3-6 to Table 3-12)

Table 3-6 Identity of differentially expressed genes for the response to wounding

Transcript ID	Fold-change	Gene Symbol	Gene Name
14291033	7.87	IL6	Interleukin 6 (interferon, beta 2)
14409533	6.93	IL18	Interleukin 18 (interferon-gamma-inducing factor)
14429457	6.74	C4BPA	Complement component 4 binding protein, alpha
14452716	6.40	CCL13	Chemokine (C-C motif) ligand 13
14387651	5.40	CXCL10	Chemokine (C-X-C motif) ligand 10
14324893	5.39	CD180	CD180 molecule
14276379	4.76	IRGM	Immunity-related GTPase family, M
14364302	4.64	OLR1	Oxidized low density lipoprotein (lectin-like) receptor 1
14433991	3.98	PTGS2	Prostaglandin-endoperoxide synthase 2
14306037	3.87	FCGR1A	Fc fragment of IgG, high affinity Ia, receptor
14409809	3.82	MMP12	Matrix metallopeptidase 12
14265296	3.67	MIA	Melanoma inhibitory activity family
14298963	3.66	FGG	Fibrinogen gamma chain
14287764	3.65	ANGPT1	Angiopoietin 1
14457347	3.56	TLR8	Toll-like receptor 8
14430646	3.02	SELE	Selectin E
14366798	2.95	C3AR1	Complement component 3a receptor 1
14375983	2.92	TLR1	Toll-like receptor 1
14316910	2.90	SLC7A11	Solute carrier family 7 (anionic amino acid transporter light chain, xc- system), member 11
14305354	2.81	TACR1	Tachykinin receptor 1
14401130	2.79	CD48	CD48 molecule
14330808	2.71	ACP5	Acid phosphatase 5, tartrate resistant
14430287	2.67	PLA2G4A	Phospholipase A2, group IVA (cytosolic, calcium-dependent)
14388619	2.67	CFI	Complement factor I
14455870	2.60	MUSTN1	Musculoskeletal, embryonic nuclear protein 1
14394611	2.58	F13A1	Coagulation factor XIII, A1 polypeptide
14355262	2.58	ALOX5AP	Arachidonate 5-lipoxygenase-activating protein
14404160	2.47	KCNMB1	Potassium large conductance calcium-activated

			channel, subfamily M, beta member 1
14262002	2.44	SOD2	Superoxide dismutase 2, mitochondrial
14457934	2.44	CYBB	Cytochrome b-245, beta polypeptide
14360356	2.40	P2RX7	Purinergic receptor P2X, ligand-gated ion channel, 7
14279411	2.39	AIF1	Allograft inflammatory factor 1
14393925	2.38	BMP6	Bone morphogenetic protein 6
14276284	2.35	TLR4	Toll-like receptor 4
14370194	2.29	BLNK	B-cell linker
14309451	2.27	CTSS	Cathepsin S
14257638	2.21	JAK2	Janus kinase 2
14269753	2.20	PLEK	Pleckstrin
14387085	2.20	BMPR1B	Bone morphogenetic protein receptor, type IB
14387277	2.18	AIMP1	Aminoacyl tRNA synthetase complex-interacting multifunctional protein 1
14296247	2.17	GUCY1B3	Guanylate cyclase 1, soluble, beta 3
14329619	2.14	CCR1	Chemokine (C-C motif) receptor 1
14279522	2.14	CFB	Complement factor B
14370250	2.13	PIK3AP1	Phosphoinositide-3-kinase adaptor protein 1
14447044	2.12	CCL5	Chemokine (C-C motif) ligand 5
14341803	2.11	LCP1	Lymphocyte cytosolic protein 1 (L-plastin)
14347364	2.09	P2RY12	Purinergic receptor P2Y, G-protein coupled, 12
14326966	2.09	PDPN	Podoplanin
14434527	2.01	ATP1B1	ATPase, Na+/K+ transporting, beta 1 polypeptide
14265178	1.90	RPS19	Ribosomal protein S19
14400410	1.75	SERPINE2	Serpin peptidase inhibitor, clade E, member 2
14437994	1.67	HIF1A	Hypoxia inducible factor 1, alpha subunit (basic helix-loop-helix transcription factor)
14343958	1.66	GAS6	Growth arrest-specific 6
14379164	1.60	RBPJ	Recombination signal binding protein for immunoglobulin kappa J region
14319137	1.52	ITGB1	Integrin, beta 1 (fibronectin receptor, beta polypeptide, antigen CD29 includes MDF2, MSK12)
14427965	1.51	GNAI3	Guanine nucleotide binding protein, alpha inhibiting activity polypeptide 3
14262925	1.50	ANXA1	Annexin A1
14449024	-1.52	ENG	Endoglin
14295467	-1.64	ELK3	ELK3, ETS-domain protein
14446155	-1.66	NFE2L1	Nuclear factor, erythroid 2-like 1
14306172	-1.70	ECM1	Extracellular matrix protein 1
14429473	-1.98	CD55	CD55 molecule, decay accelerating factor for complement (Cromer blood group)
14305965	-2.01	BCL9	B-cell CLL/lymphoma 9
14357744	-2.10	ATP2A2	ATPase, Ca++ transporting, cardiac muscle, slow twitch 2
14281639	-2.12	NT5E	5'-nucleotidase, ecto (CD73)
14449897	-2.23	ITGB4	Integrin, beta 4
14448168	-2.33	NOTCH1	NOTCH 1
14330901	-3.01	DOCK6	Dedicator of cytokinesis 6

14266793	-3.10	KIF5A	Kinesin family member 5A
14347367	-4.43	IGSF10	Immunoglobulin superfamily, member 10

Table 3-7 Identity of differentially expressed genes for biological adhesion

Transcript ID	Fold-change	Gene Symbol	Gene Name
14356140	16.43	ADAMDEC1	ADAM-like, decysin 1
14298902	7.11	SFRP2	Secreted frizzled-related protein 2
14409533	6.93	IL18	Interleukin 18 (interferon-gamma-inducing factor)
14389567	4.66	CSTA	Cystatin A (stefin A)
14364302	4.64	OLR1	Oxidized low density lipoprotein (lectin-like) receptor 1
14265296	3.67	MIA	Melanoma inhibitory activity family, member
14287764	3.65	ANGPT1	Angiopoietin 1
14388813	3.34	EPHA3	EPH receptor A3
14408542	3.16	CDH6	Cadherin 6, type 2, K-cadherin (foetal kidney)
14392321	3.07	CLDN1	Claudin 1
14430646	3.02	SELE	Selectin E
14316910	2.90	SLC7A11	Solute carrier family 7, member 11
14266174	2.83	SCN1B	Sodium channel, voltage-gated, type I, beta subunit
14336520	2.83	EMR1	Egf-like module containing, mucin-like, hormone receptor-like 1, macrophage marker F480
14295395	2.64	PLXNC1	Plexin C1
14307331	2.58	CGREF1	Cell growth regulator with EF-hand domain 1
14311075	2.47	LPXN	Leupaxin
14423570	2.39	GBP7	Guanylate binding protein 7
14425484	2.29	ITGAD	Integrin, alpha D
14257638	2.21	JAK2	Janus kinase 2
14304046	2.20	EMILIN1	Elastin microfibril interfacer 1
14269753	2.20	PLEK	Pleckstrin
14387085	2.20	BMPR1B	Bone morphogenetic protein receptor, type IB
14387277	2.18	AIMP1	Aminoacyl tRNA synthetase complex-interacting multifunctional protein 1
14288059	2.18	HAS2	Hyaluronan synthase 2
14329619	2.14	CCR1	Chemokine (C-C motif) receptor 1
14447044	2.12	CCL5	Chemokine (C-C motif) ligand 5
14290397	2.09	ADAM22	ADAM metallopeptidase domain 22
14347364	2.09	P2RY12	Purinergic receptor P2Y, G-protein coupled, 12
14326966	2.09	PDPN	Podoplanin
14342436	2.06	ITGBL1	Integrin, beta-like 1 (with EGF-like repeat domains)
14303184	2.02	CDKN2A	Cyclin-dependent kinase inhibitor 2A
14434527	2.01	ATP1B1	ATPase, Na+/K+ transporting, beta 1 polypeptide
14400410	1.75	SERPINE2	Serpin peptidase inhibitor, clade E (member 2
14343958	1.66	GAS6	Growth arrest-specific 6
14379164	1.60	RBPJ	Recombination signal binding protein for

			immunoglobulin kappa J region
14344504	1.60	RPSA	Ribosomal protein SA
14398657	1.55	ARPC2	Actin related protein 2/3 complex, subunit 2
14319137	1.52	ITGB1	Integrin, beta 1 (fibronectin receptor, beta polypeptide, antigen CD29 includes MDF2, MSK12)
14387670	1.52	SCARB2	Scavenger receptor class B, member 2
14449024	-1.52	ENG	Endoglin
14436816	-1.53	MMP14	Matrix metallopeptidase 14 (membrane-inserted)
14402043	-1.54	DDR2	Discoidin domain receptor tyrosine kinase 2
14318073	-1.56	FAT4	FAT atypical cadherin 4
14444308	-1.73	SOX9	SRY (sex determining region Y)-box 9
14310205	-1.80	LAMB1	Laminin, beta 1
14453163	-2.04	FLOT2	Flotillin 2
14357744	-2.10	ATP2A2	ATPase, Ca++ transporting, cardiac muscle, slow twitch 2
14449897	-2.23	ITGB4	Integrin, beta 4
14320231	-2.27	PCDHB6	Protocadherin beta 6
14363340	-2.28	NELL2	NEL-like 2 (chicken)
14448168	-2.33	NOTCH1	NOTCH 1
14282609	-2.38	TNXB	Tenascin XB
14263835	-2.44	TTYH1	Tweety family member 1
14356848	-2.47	COL6A3	Collagen, type VI, alpha 3
14277414	-2.69	FREM1	FRAS1 related extracellular matrix 1
14392321	-2.87	CLDN11	Claudin 11
14409246	-2.88	MPZL2	Myelin protein zero-like 2
14311489	-3.00	MYBPC3	Myosin binding protein C, cardiac
14402587	-3.09	NID1	Nidogen 1
14452015	-3.15	CHAD	Chondroadherin
14408526	-3.22	PDZD2	PDZ domain containing 2
14256801	-5.16	LAMA2	Laminin, alpha 2
14432404	-5.18	DSC2	Desmocollin 2

Table 3-8 Identity of differentially expressed genes for positive regulation of cell migration

Transcript ID	Fold-change	Gene Symbol	Gene Name
14291033	7.87	IL6	Interleukin 6 (interferon, beta 2)
14452716	6.40	CCL13	Chemokine (C-C motif) ligand 13
14387651	5.40	CXCL10	Chemokine (C-X-C motif) ligand 10
14433991	3.98	PTGS2	Prostaglandin-endoperoxide synthase 2
14265296	3.67	MIA	Melanoma inhibitory activity family
14287764	3.65	ANGPT1	Angiopoietin 1
14430646	3.02	SELE	Selectin E
14366798	2.95	C3AR1	Complement component 3a receptor 1
14305354	2.81	TACR1	Tachykinin receptor 1
14279411	2.39	AIF1	Allograft inflammatory factor 1
14281184	2.36	PTP4A1	Protein tyrosine phosphatase type 4A, member 1
14257638	2.21	JAK2	Janus kinase 2

14288059	2.18	HAS2	Hyaluronan synthase 2
14329619	2.14	CCR1	Chemokine (C-C motif) receptor 1
14447044	2.12	CCL5	Chemokine (C-C motif) ligand 5
14326966	2.09	PDPN	Podoplanin
14437994	1.67	HIF1A	Hypoxia inducible factor 1, alpha subunit (
14343958	1.66	GAS6	Growth arrest-specific 6
14445842	1.65	MIEN1	Migration and invasion enhancer 1
14319137	1.52	ITGB1	Integrin, beta 1 (fibronectin receptor, beta polypeptide, antigen CD29 includes MDF2, MSK12)
14278691	-1.51	LPAR1	Lysophosphatidic acid receptor 1
14436816	-1.53	MMP14	Matrix metallopeptidase 14 (membrane-inserted)
14402043	-1.54	DDR2	Discoidin domain receptor tyrosine kinase 2
14444308	-1.73	SOX9	SRY (sex determining region Y)-box 9
14310205	-1.80	LAMB1	Laminin, beta 1
14448168	-2.33	NOTCH1	NOTCH 1

Table 3-9 Identity of differentially expressed genes for cardiovascular system development

Transcript ID	Fold-change	Gene Symbol	Gene Name
14291033	7.87	IL6	Interleukin 6 (interferon, beta 2)
14298902	7.11	SFRP2	Secreted frizzled-related protein 2
14409533	6.93	IL18	Interleukin 18
14452716	6.40	CCL13	Chemokine (C-C motif) ligand 13
14356695	5.78	HTR2B	5-hydroxytryptamine receptor 2B
14387651	5.40	CXCL10	Chemokine (C-X-C motif) ligand 10
14421671	4.94	MYH11	Myosin, heavy chain 11, smooth muscle
14433991	3.98	PTGS2	Prostaglandin-endoperoxide synthase 2
14287764	3.65	ANGPT1	Angiopoietin 1
14397988	3.51	CASP8	Caspase 8, apoptosis-related cysteine peptidase
14388813	3.34	EPHA3	EPH receptor A3
14366798	2.95	C3AR1	Complement component 3a receptor 1
14393476	2.45	PDCD10	Programmed cell death 10
14262002	2.44	SOD2	Superoxide dismutase 2, mitochondrial
14452113	2.26	TMEM100	Transmembrane protein 100
14387277	2.18	AIMP1	Aminoacyl tRNA synthetase complex-interacting multifunctional protein 1
14288059	2.18	HAS2	Hyaluronan synthase 2
14447044	2.12	CCL5	Chemokine (C-C motif) ligand 5
14326966	2.09	PDPN	Podoplanin
14311483	2.08	SPI1	Spleen focus forming virus (SFFV) proviral integration oncogene
14432910	1.73	PLXDC1	Plexin domain containing 1
14397472	1.72	FRZB	Frizzled-related protein
14437994	1.67	HIF1A	Hypoxia inducible factor 1, alpha subunit
14379164	1.60	RBPJ	Recombination signal binding protein for

			Immunoglobulin kappa J region
14360089	1.52	TMED2	Transmembrane emp24 domain trafficking protein 2
14319137	1.52	ITGB1	Integrin, beta 1 (fibronectin receptor, beta polypeptide, antigen CD29 includes MDF2, MSK12)
14449024	-1.52	ENG	Endoglin
14436816	-1.53	MMP14	Matrix metallopeptidase 14 (membrane-inserted)
14318073	-1.56	FAT4	FAT atypical cadherin 4
14322498	-1.60	ECE1	Endothelin converting enzyme 1
14295467	-1.63	ELK3	ELK3, ETS-domain protein (SRF accessory protein 2)
14306172	-1.70	ECM1	Extracellular matrix protein 1
14383275	-1.70	MYO1E	Myosin IE
14444308	-1.73	SOX9	SRY (sex determining region Y)-box 9
14390820	-1.74	HEG1	Heart development protein with EGF-like domains 1
14269237	-1.78	EPAS1	Endothelial PAS domain protein 1
14433723	-1.86	PTPN14	Protein tyrosine phosphatase, non-receptor type 14
14260690	-1.87	NFATC1	Nuclear factor of activated T-cells, cytoplasmic, calcineurin-dependent 1
14426693	-1.94	MKL2	MKL/myocardin-like 2
14269730	-2.06	MEIS1	Meis homeobox 1
14319305	-2.06	NEBL	Nebulette
14322014	-2.08	WASF2	WAS protein family, member 2
14259044	-2.19	RASIP1	Ras interacting protein 1
14451257	-2.27	RAMP2	Receptor (G protein-coupled) activity modifying protein 2
14368859	-2.28	TCF7L2	Transcription factor 7-like 2 (T-cell specific, HMG-box)
14299531	-2.32	HIPK2	Homeodomain interacting protein kinase 2
14448168	-2.33	NOTCH1	NOTCH 1
14441890	-2.84	ZFP36L1	ZFP36 ring finger protein-like 1
14403626	-2.84	ZMIZ1	Zinc finger, MIZ-type containing 1
14311489	-3.00	MYBPC3	Myosin binding protein C, cardiac
14459309	-5.48	TNMD	Tenomodulin

Table 3-10 Identity of differentially expressed genes for extracellular matrix organization

Transcript ID	Fold-change	Gene Symbol	Gene Name
14298902	7.11	SFRP2	Secreted frizzled-related protein 2
14421671	4.94	MYH11	Myosin, heavy chain 11, smooth muscle
14296316	4.24	RXFP1	Relaxin/insulin-like family peptide receptor 1
14409809	3.82	MMP12	Matrix metallopeptidase 12(macrophage elastase)
14265296	3.67	MIA	Melanoma inhibitory activity family

14304046	2.20	EMILIN1	Elastin microfibril interfacer 1
14288059	2.18	HAS2	Hyaluronan synthase 2
14343958	1.66	GAS6	Growth arrest-specific 6
14319137	1.52	ITGB1	Integrin, beta 1 (fibronectin receptor, beta polypeptide, antigen CD29 includes MDF2, MSK12)
14449024	-1.52	ENG	Endoglin
14436816	-1.53	MMP14	Matrix metallopeptidase 14 (membrane-inserted)
14402043	-1.54	DDR2	Discoidin domain receptor tyrosine kinase 2
14383275	-1.70	MYO1E	Myosin IE
14444308	-1.73	SOX9	SRY (sex determining region Y)-box 9
14310205	-1.80	LAMB1	Laminin, beta 1
14418313	-2.04	CRISPLD2	Cysteine-rich secretory protein LCCL domain containing 2
14455291	-2.15	OLFML2A	Olfactomedin-like 2A
14449897	-2.23	ITGB4	Integrin, beta 4
14451257	-2.27	RAMP2	Receptor (G protein-coupled) activity modifying protein 2
14448168	-2.33	NOTCH1	NOTCH 1
14282609	-2.38	TNXB	Tenascin XB
14356848	-2.47	COL6A3	Collagen, type VI, alpha 3
14373535	-2.58	MMP16	Matrix metallopeptidase 16 (membrane-inserted)
14402587	-3.09	NID1	Nidogen 1
14274287	-4.52	ADAMTSL4	ADAMTS-like 4
14256801	-5.16	LAMA2	Laminin, alpha 2

Table 3-11 Identity of differentially expressed genes for ossification

Transcript ID	Fold-change	Gene Symbol	Gene Name
14291033	7.87	IL6	Interleukin 6 (interferon, beta 2)
14298902	7.11	SFRP2	Secreted frizzled-related protein 2
14409533	6.93	IL18	Interleukin 18
14433991	3.98	PTGS2	Prostaglandin-endoperoxide synthase 2
14265296	3.67	MIA	Melanoma inhibitory activity family
14305354	2.81	TACR1	Tachykinin receptor 1
14360356	2.40	P2RX7	Purinergic receptor P2X, ligand-gated ion channel, 7
14393925	2.38	BMP6	Bone morphogenetic protein 6
14387085	2.20	BMPR1B	Bone morphogenetic protein receptor, type IB
14329619	2.14	CCR1	Chemokine (C-C motif) receptor 1
14374668	2.04	CHSY1	Chondroitin sulfate synthase 1
14437994	1.67	HIF1A	Hypoxia inducible factor 1, alpha subunit (basic helix-loop-helix transcription factor)
14379164	1.60	RBPJ	Recombination signal binding protein for immunoglobulin kappa J region
14436816	-1.53	MMP14	Matrix metallopeptidase 14 (membrane-inserted)
14402043	-1.54	DDR2	Discoidin domain receptor tyrosine kinase 2
14318073	-1.56	FAT4	FAT atypical cadherin 4

14299705	-1.56	PTN	Pleiotrophin
14306172	-1.70	ECM1	Extracellular matrix protein 1
14444308	-1.73	SOX9	SRY (sex determining region Y)-box 9
14403912	-2.12	PDLIM7	PDZ and LIM domain 7 (enigma)
14368859	-2.28	TCF7L2	Transcription factor 7-like 2
14448168	-2.33	NOTCH1	NOTCH 1
14409363	-2.42	SIK3	SIK family kinase 3
14400025	-2.65	IGFBP5	Insulin-like growth factor binding protein 5
14347367	-4.43	IGSF10	Immunoglobulin superfamily, member 10

Table 3-12 Identity of differentially expressed genes for regulation of epithelial cell proliferation

Transcript ID	Fold-change	Gene Symbol	Gene Name
14430334	7.93	ANGPT1	Angiopoietin 1
14291033	7.87	IL6	Interleukin 6 (interferon, beta 2)
14298902	7.11	SFRP2	Secreted frizzled-related protein 2
14452716	6.40	CCL13	Chemokine (C-C motif) ligand 13
14356695	5.78	HTR2B	5-hydroxytryptamine (serotonin) receptor 2B, G protein-coupled
14409809	3.82	MMP12	Matrix metallopeptidase 12(macrophage elastase)
14305354	2.81	TACR1	Tachykinin receptor 1
14393925	2.38	BMP6	Bone morphogenetic protein 6
14387277	2.18	AIMP1	Aminoacyl tRNA synthetase complex-interacting multifunctional protein 1
14447044	2.12	CCL5	Chemokine (C-C motif) ligand 5
14303184	2.02	CDKN2A	Cyclin-dependent kinase inhibitor 2A
14373072	2.02	CYP7B1	Cytochrome P450, family 7, subfamily B, polypeptide 1
14437994	1.67	HIF1A	Hypoxia inducible factor 1, alpha subunit
14449024	-1.52	ENG	Endoglin
14349213	-1.59	SRSF6	Serine/arginine-rich splicing factor 6
14306172	-1.70	ECM1	Extracellular matrix protein 1
14444308	-1.73	SOX9	SRY (sex determining region Y)-box 9
14310205	-1.80	LAMB1	Laminin, beta 1
14307431	-2.08	IFT172	Intraflagellar transport 172 homolog
14368859	-2.28	TCF7L2	Transcription factor 7-like 2
14448168	-2.33	NOTCH1	NOTCH 1
14459309	-5.48	TNMD	Tenomodulin

3.3.4 DAVID 6.7

The same list of 591 genes was submitted to the DAVID web-based bioinformatics resources for functional annotation and classification analysis. A total 504 of 591 genes were firstly matched and identified according to official gene symbol for human. In the general gene ontology, 16 biological categories were classified based on the gene functions (Table 3-13).

Table 3-13 Gene Ontology Chart for differentially expressed genes

Gene Ontology Term	Gene Counts	Gene %	p-value
Response to wounding	43	8.5	2.10E-08
Inflammatory response	31	6.2	9.50E-08
Immune response	42	8.3	4.70E-05
Cell adhesion	41	8.1	1.40E-04
Biological adhesion	41	8.1	1.40E-04
Defence response	37	7.3	1.80E-04
Vasculature development	20	4	3.10E-04
Positive regulation of cytoskeleton organization	8	1.6	4.30E-04
Blood vessel development	19	3.8	6.30E-04
Regulation of cell proliferation	42	8.3	7.50E-04
Blood vessel morphogenesis	17	3.4	8.90E-04
Regulation of cytoskeleton organization	13	2.6	1.10E-03
Innate immune response	13	2.6	1.20E-03
Response to oxygen levels	13	2.6	1.40E-03
Collagen metabolic process	6	1.2	1.50E-03
Epithelial to mesenchymal transition	5	1	2.00E-03

Functional annotation clustering analysis was conducted for the final 504 genes. In general, 35 clusters were initially classified by similar biological gene function ($p < 0.05$). After applying the cutoff (enrichment score with high stringency setting), 10 clusters remained on the list (Table 3-14).

Table 3-14 Functional annotation with cutoff

Annotation Clusters	Enrichment Score	Gene Count	p-value
Vasculature development	3.25	20	3.10E-04
Collagen metabolic process	2.57	6	1.50E-03
Protein processing	2.41	11	2.50E-03
Vacuole	2.36	18	2.20E-03
Positive regulation of cytoskeleton organization	2.24	10	4.30E-04
Regulation of cell motion	1.91	14	7.10E-03
Regulation of bone mineralization	1.71	5	1.30E-02
Positive regulation of cell motion	1.71	9	1.10E-02
Cysteine-type endopeptidase activity	1.61	9	5.40E-03
Epithelial to mesenchymal transition	1.52	5	2.00E-03

Differentially expressed genes related to these biological terms are listed in Table 3-15 to Table 3-24.

Table 3-15 Identity of differentially expressed genes for the vasculature development category

Transcript ID	Fold-change	Gene symbol	Gene identity
14409533	6.93	IL18	Interleukin 18 (interferon-gamma-inducing factor)
14287764	3.65	ANGPT1	Angiopoietin 1
14397988	3.51	CASP8	Caspase 8, apoptosis-related cysteine peptidase
14310860	2.28	LMO2	LIM domain only 2 (rhombotin-like 1)
14387277	2.18	AIMP1	Aminoacyl tRNA synthetase complex-interacting multifunctional protein 1
14326996	2.09	PDPN	Podoplanin
14432910	1.73	PLXDC1	Plexin domain containing 1
14437994	1.67	HIF1A	Hypoxia inducible factor 1, alpha subunit (basic helix-loop-helix transcription factor)
14379164	1.60	RBPJ	Recombination signal binding protein for immunoglobulin kappa J region
14449024	-1.52	ENG	Endoglin
14436816	-1.53	MMP14	Matrix metallopeptidase 14 (membrane-inserted)
14295467	-1.63	ELK3	ETS-domain protein (SRF accessory protein 2)
14383275	-1.70	MYO1E	Myosin IE
14269237	-1.78	EPAS1	Endothelial PAS domain protein 1
14426693	-1.94	MKL2	Myocardin-like 2
14322014	-2.08	WASF2	WAS protein family, member 2
14368859	-2.28	TCF7L2	Transcription factor 7-like 2 (T-cell specific, HMG-box)
14448168	-2.33	NOTCH1	NOTCH homolog 1, translocation-associated (Drosophila)
14441890	-2.84	ZFP36L1	Zinc finger protein 36, C3H type-like 1
14403626	-2.84	ZMIZ1	Zinc finger, MIZ-type containing 1

Table 3-16 Identity of differentially expressed genes for the collagen metabolic process category

Transcript ID	Fold-change	Gene symbol	Gene identity
14260509	2.44	PEPD	Peptidase D
14360356	2.40	P2RX7	Purinergic receptor P2X, ligand-gated ion channel, 7
14437994	1.67	HIF1A	Hypoxia inducible factor 1, alpha subunit (basic helix-loop-helix transcription factor)
14283991	-2.14	TRAM2	Translocation associated membrane protein 2
14282609	-2.38	TNXB	Tenascin XB; tenascin XA pseudogene
14373535	-2.58	MMP16	Matrix metallopeptidase 16 (membrane-inserted)

Table 3-17 Identity of differentially expressed genes for the protein processing category

Transcript ID	Fold-change	Gene symbol	Gene identity
14429457	6.74	C4BPA	Complement component 4 binding protein, alpha
14388619	2.67	CFI	Complement factor I
14326462	2.45	C1QC	Complement component 1, q subcomponent, C chain
14360356	2.40	P2RX7	Purinergic receptor P2X, ligand-gated ion channel, 7
14261042	2.23	SEC11C	SEC11 homolog C (S. cerevisiae)
14279522	2.14	CFB	Complement factor B
14436816	-1.53	MMP14	Matrix metallopeptidase 14 (membrane-inserted)
14333938	-1.56	SPCS1	Signal peptidase complex subunit 1 homolog (S. cerevisiae)
14322498	-1.60	ECE1	Endothelin converting enzyme 1
14429473	-1.98	CD55	CD55 molecule, decay accelerating factor for complement (Cromer blood group)
14307431	-2.08	IFT172	Intraflagellar transport 172 homolog (Chlamydomonas)

Table 3-18 Identity of differentially expressed genes for the vacuole category

Transcript ID	Fold-change	Gene symbol	Gene identity
14276379	4.76	IRGM	Immunity-related GTPase family, M
14337646	3.69	CTSC	Cathepsin C
14330808	2.71	ACP5	Acid phosphatase 5, tartrate resistant
14282827	2.42	HLA-DMB	Major histocompatibility complex, class II, DM beta
14309451	2.27	CTSS	Cathepsin S
14384036	2.27	HEXA	Hexosaminidase A (alpha polypeptide)
14330676	2.22	DNASE2	Deoxyribonuclease II, lysosomal
14366663	2.20	GABARAPL1	GABA(A) receptors associated protein like 3
14457364	2.03	RAB9A	RAB9A, member RAS oncogene family
1444139	1.83	NPC2	Niemann-Pick disease, type C2
14342161	1.66	CLN5	Ceroid-lipofuscinosis, neuronal 5
14461000	1.65	VAMP7	Vesicle-associated membrane protein 7
14292191	1.61	ATP6V1F	ATPase, H+ transporting, lysosomal 14kDa, V1 subunit F
14440227	1.55	LGMN	Legumain
14387670	1.52	SCARB2	Scavenger receptor class B, member 2
14370464	-1.67	GOT1	Glutamic-oxaloacetic transaminase 1, soluble (aspartate aminotransferase 1)
14451257	-2.27	RAMP2	Receptor (G protein-coupled) activity modifying protein 2
14421559	-2.91	SYT17	Synaptotagmin XVII; synaptotagmin VII

Table 3-19 Identity of differentially expressed genes for the positive regulation of cytoskeleton organization category

Transcript ID	Fold-change	Gene symbol	Gene identity
14430646	3.02	SELE	Selectin E
14305354	2.81	TACR1	Tachykinin receptor 1
14430287	2.67	PLA2G4A	Phospholipase A2, group IVA (cytosolic, calcium-dependent)
14360356	2.40	P2RX7	Purinergic receptor P2X, ligand-gated ion channel, 7
14350497	1.82	DSTN	Destrin (actin depolymerizing factor)
14398657	1.55	ARPC2	Actin related protein 2/3 complex, subunit 2, 34kDa
14438313	-2.37	PLEK	Pleckstrin
14293539	-2.52	CTTNBP2	Cortactin binding protein 2
14450321	-2.81	MAPT	Microtubule-associated protein tau
14316083	-3.35	CDC42EP2	CDC42 effector protein (Rho GTPase binding) 2

Table 3-20 Identity of differentially expressed genes for the regulation of cell motion category

Transcript ID	Fold-change	Gene symbol	Gene identity
14291033	7.87	IL6	Interleukin 6 (interferon, beta 2)
14387651	5.40	CXCL10	Chemokine (C-X-C motif) ligand 10
14305354	2.81	TACR1	Tachykinin receptor 1
14281184	2.36	PTP4A1	Protein tyrosine phosphatase type IVA, member 1
14257638	2.21	JAK2	Janus kinase 2
14326996	2.09	PDPN	Podoplanin
14265178	1.90	RPS19	Ribosomal protein S19 pseudogene 3; ribosomal protein S19
14400410	1.75	SERPINE2	Serpin peptidase inhibitor, clade E (nexin, plasminogen activator inhibitor type 1), member 2
14437994	1.67	HIF1A	Hypoxia inducible factor 1, alpha subunit (basic helix-loop-helix transcription factor)
14287965	-1.64	ENPP2	Ectonucleotide phosphodiesterase 2
14310205	-1.80	LAMB1	Laminin, beta 1
14315712	-2.01	BBS1	Bardet-Biedl syndrome 1
14400025	-2.65	IGFBP5	Insulin-like growth factor binding protein 5
14256801	-5.16	LAMA2	Laminin, alpha 2

Table 3-21 Identity of differentially expressed genes for the regulation of bone mineralization category

Transcript ID	Fold-change	Gene symbol	Gene identity
14430287	2.67	PLA2G4A	Phospholipase A2, group IVA (cytosolic, calcium-dependent)
14360356	2.40	P2RX7	Purinergic receptor P2X, ligand-gated ion channel, 7
14393925	2.38	BMP6	Bone morphogenetic protein 6
14387085	2.20	BMPR1B	Bone morphogenetic protein receptor, type IB
14444308	-1.73	SOX9	SRY (sex determining region Y)-box 9

Table 3-22 Identity of differentially expressed genes for the positive regulation of cell motion category

Transcript ID	Fold-change	Gene symbol	Gene identity
14291033	7.87	IL6	Interleukin 6 (interferon, beta 2)
14387651	5.40	CXCL10	Chemokine (C-X-C motif) ligand 10
14305354	2.81	TACR1	Tachykinin receptor 1
14281184	2.36	PTP4A1	Protein tyrosine phosphatase type IVA, member 1
14257638	2.21	JAK2	Janus kinase 2
14326966	2.09	PDPN	Podoplanin
14265178	1.90	RPS19	Ribosomal protein S19 pseudogene 3; ribosomal protein S19
14437994	1.67	HIF1A	Hypoxia inducible factor 1, alpha subunit (basic helix-loop-helix transcription factor)
14310205	-1.80	LAMB1	Laminin, beta 1

Table 3-23 Identity of differentially expressed genes for the cysteine-type endopeptidase activity category

Transcript ID	Fold-change	Gene symbol	Gene identity
14378900	3.73	UCHL1	Ubiquitin carboxyl-terminal esterase L1 (ubiquitin thiolesterase)
14337646	3.69	CTSC	Cathepsin C
14397988	3.51	CASP8	Caspase 8, apoptosis-related cysteine peptidase
14409755	2.42	CASP4	Caspase 4, apoptosis-related cysteine peptidase
14390084	2.33	SENP7	SUMO1/sentrin specific peptidase 7
14309451	2.27	CTSS	Cathepsin S
14440227	1.55	LGMN	Legumain
14265772	-1.51	CAPNS1	Calpain, small subunit 1
14458281	-1.74	USP11	Ubiquitin specific peptidase 11

Table 3-24 Identity of differentially expressed genes for the epithelial to mesenchymal transition category

Transcript ID	Fold-change	Gene symbol	Gene identity
14432035	2.96	S100A4	S100 calcium binding protein A4
14437994	1.67	HIF1A	Hypoxia inducible factor 1, alpha subunit (basic helix-loop-helix transcription factor)
14444308	-1.73	SOX9	SRY (sex determining region Y)-box 9
14260690	-1.87	NFATC1	Nuclear factor of activated T-cells, cytoplasmic, calcineurin-dependent 1
14448168	-2.33	NOTCH1	NOTCH homolog 1, translocation-associated

3.3.5 IPA

The list of 591 genes was uploaded to the Ingenuity Pathway Analysis (IPA), and 525 out of 591 genes were mapped. The top 10 up- and down-regulated mapped genes are listed in Table 3-25.

Table 3-25 Top 10 up- and down-regulated mapped genes in IPA

Fold-change up-regulated			Fold-change down-regulated		
Gene Symbol	Gene Identity	Fold-change	Gene Symbol	Gene Identity	Fold-change
ADAMDEC1	ADAM-like, decysin 1	16.43	CILP	Cartilage intermediate layer protein,	-6.20
ACTG2	Actin, gamma 2, smooth muscle, enteric	15.35	TNMD	Tenomodulin	-5.48
ANGPTL1	Angiopoietin-like 1	7.93	GJB6	Gap junction protein, beta 6	-5.27
IL6	Interleukin 6	7.87	DSC2	Desmocollin 2	-5.18
SFRP2	Secreted frizzled-related protein 2	7.11	LAMA2	Laminin, alpha 2	-5.16
IL18	Interleukin 18	6.93	IGSF10	Immunoglobulin superfamily, member 10	-4.43
C4BPA	Complement component 4 binding protein, alpha	6.74	HCN1	Potassium/sodium hyperpolarization-activated cyclic nucleotide-gated channel 1	-4.30
CCL13	Chemokine ligand 13	6.40	LPPR5	Lipid phosphate phosphatase-related protein type 5-l	-4.23
RGS2	Regulator of G-protein signalling 2	5.81	CBR1	Carbonyl reductase 1	-3.61
HTR2B	5-hydroxytryptamine receptor 2B	5.78	FSTL4	Follistatin-like 4	-3.53

Functional clustering showed 11 main categories using IPA, and they were endocrine system disorders, cellular movement, connective tissue disorders, inflammatory diseases, immune cell trafficking, cancer, haematological system development,

cardiovascular disease, humoral immune response, cardiovascular system development, and cell death and survival (Table 3-26).

Table 3-26 Diseases and functions annotation

Category	Disease or Function Annotation	Count	p-value
Endocrine System Disorders	Diabetes mellitus	71	1.70E-11
Cellular Movement	Migration of cells	134	1.53E-09
Connective Tissue Disorders	Arthropathy	78	1.8E-08
Inflammatory Disease	Arthritis	83	1.43E-08
Immune Cell Trafficking	Leukocyte migration	79	4.05E-08
Cancer	Uterine tumor	315	3.60E-07
Haematological System Development	Cell movement	122	5.32E-07
Cardiovascular Disease	Vascular disease	114	7.01E-07
Humoral Immune Response	Production of antibody	40	1.56E-06
Cardiovascular System Development	Angiogenesis	94	1.79E-06
Cell Death and Survival	Cell death	125	2.39E-06

Up-stream analysis by IPA identified the top 10 up-stream regulators, these ten molecules contribute to the up-regulation of the differentially expressed genes. They are IL-1B, IL-13, TGFβ1, DYSF, IFN-γ, TNF, LDLR, CSF2, NFκB, and NFE2L2, and they are summarized in Table 3-27 and Figure 3-7 (LDLR).

Table 3-27 Top 10 up-stream regulators identified by IPA

Upstream Regulator	Description	Molecule Type	Predicted State	Activation z-score	p-value of overlap
IL1B	Interleukin 1, β	Cytokine	Activated	3.274	3.55E-12
IL13	Interleukin 13	Cytokine		0.697	3.95E-11
TGFB1	Transforming growth factor β1	Growth factor		0.930	1.91E-09
DYSF	Dysferlin	Other			1.98E-09
IFN-γ	Interferon γ	Cytokine	Activated	4.876	2.77E-08
TNF	Tumor necrosis factor	Cytokine	Activated	2.683	1.13E-07
LDLR	Low-density lipoprotein receptor	Complex	Activated	3.006	1.68E-07
CSF2	Colony stimulating factor 2	Cytokine	Activated	3.024	7.64E-07
NFκB	nuclear factor kappa-light-chain-enhancer of activated B cells	Complex	Activated	3.387	8.63E-07
NFE2L2	Nuclear factor , erythroid 2-like-2	Transcription regulator		-0.535	8.66E-07

In Figure 3-7 (LDLR), only 4 downstream targets (down-regulation: MMP14, MMP16; up-regulation: IL6, CCL5 in MMVD) of LDLR were inconsistent with the published experimental findings (yellow interrupted arrow lines).

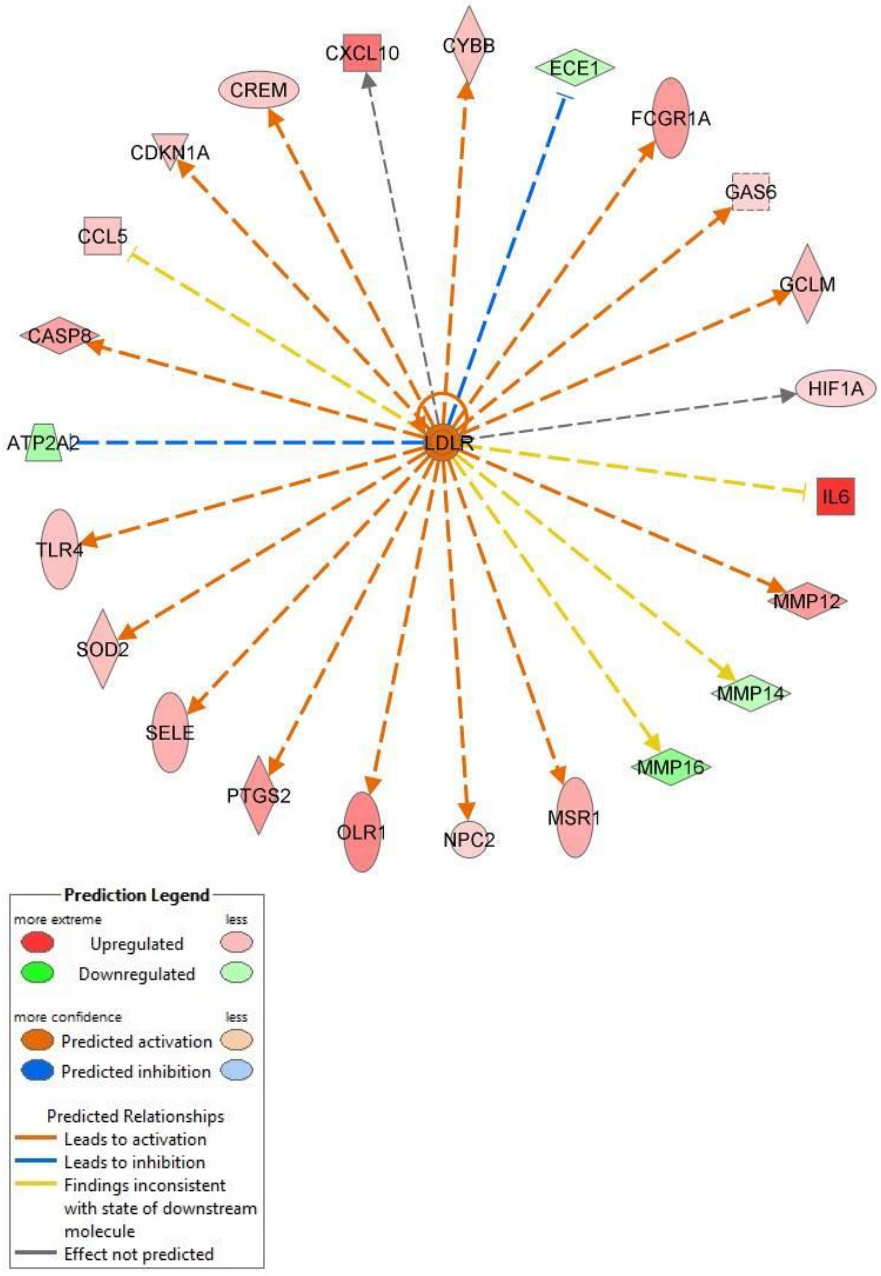

Figure 3-7 Example for one of the activated up-stream regulators, LDLR. The gene in the centre is LDLR, which up- or down-regulates the genes around the outer ring based on published experiments.

Canonical Pathway Analysis

In total, 33 canonical pathways passed the p-value cut-off in IPA (Table 3-28). Three functions identified that appeared biologically relevant to myxomatous mitral valve disease were caveolar-mediated endocytosis signalling, remodelling of epithelial adherens junctions and endothelin-1 signalling. Schematic representations of these three functions are shown in Figure 3-8, Figure 3-9, and Figure 3-10.

Table 3-28: Thirty three canonical pathways identified by IPA, cutoff –log(p-value) = 1.5

Ingenuity Canonical Pathways	-log(p-value)	Ratio
Communication between Innate and Adaptive Immune Cells	3.88E00	8.04E-02
Agranulocyte Adhesion and Diapedesis	3.63E00	7.81E-02
TREM1 Signalling	3.38E00	1.07E-01
Glucocorticoid Receptor Signalling	3.29E00	6.35E-02
Role of NFAT in Regulation of the Immune Response	3.19E00	7E-02
Complement System	3.10E00	1.43E-01
Pathogenesis of Multiple Sclerosis	2.82E00	3E-01
Granulocyte Adhesion and Diapedesis	2.79E00	7.14E-02
Systemic Lupus Erythematosus Signalling	2.62E00	5.08E-02
fMLP Signalling in Neutrophils	2.58E00	7.58E-02
Role of Hypercytokinemia/hyperchemokinemia in the Pathogenesis of Influenza	2.58E00	1.09E-01
Altered T Cell and B Cell Signalling in Rheumatoid Arthritis	2.49E00	8E-02
Dendritic Cell Maturation	2.46E00	5.69E-02
Graft-versus-Host Disease Signalling	2.43E00	9.8E-02
Role of Pattern Recognition Receptors in Recognition of Bacteria and Viruses	2.06E00	7.34E-02
CD28 Signalling in T Helper Cells	2.05E00	6.62E-02
NRF2-mediated Oxidative Stress Response	1.96E00	6.15E-02
Caveolar-mediated Endocytosis Signalling	1.93E00	8.24E-02
Adenine and Adenosine Salvage III	1.91E00	1.18E-01
Purine Ribonucleosides Degradation to Ribose-1-phosphate	1.91E00	1E-01
Pregnenolone Biosynthesis	1.91E00	1.54E-01
Fcγ Receptor-mediated Phagocytosis in Macrophages and Monocytes	1.85E00	7.55E-02
Remodelling of Epithelial Adherens Junctions	1.83E00	8.57E-02
γ-linolenate Biosynthesis II (Animals)	1.8E00	1.25E-01
PI3K Signalling in B Lymphocytes	1.67E00	6.29E-02
cAMP-mediated signalling	1.63E00	5.75E-02
HIF1α Signalling	1.62E00	7.14E-02
Endothelin-1 Signalling	1.61E00	5.73E-02
Crosstalk between Dendritic Cells and Natural Killer Cells	1.6E00	5.66E-02
B Cell Development	1.58E00	8.33E-02
Cdc42 Signalling	1.55E00	4.3E-02
Role of Macrophages, Fibroblasts and Endothelial Cells in	1.54E00	4.68E-02

Rheumatoid Arthritis		
IL-4 Signalling	1.54E00	7.5E-02
RhoGDI Signalling	1.52E00	5.45E-02

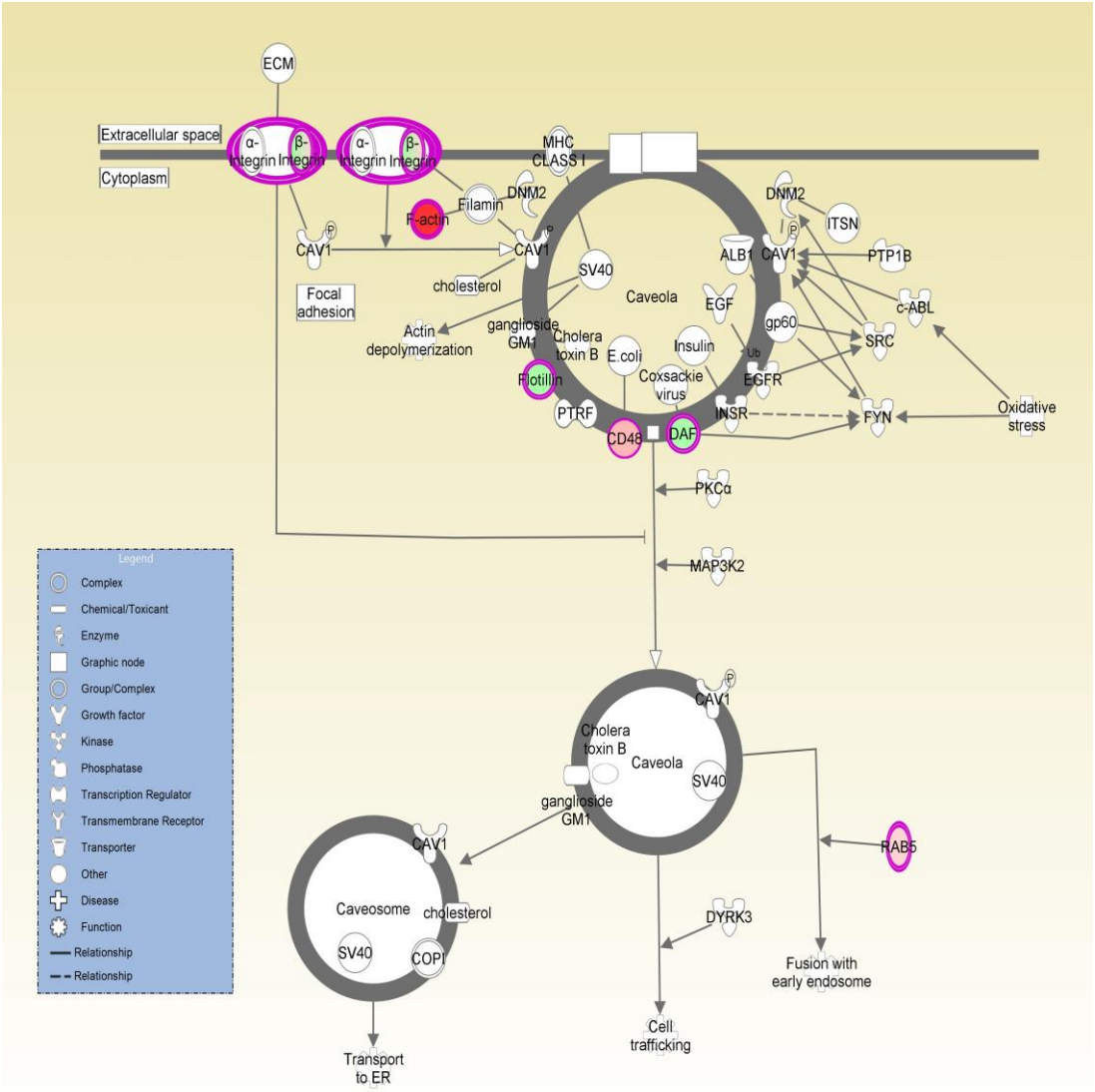

Figure 3-8 Diagram illustrating caveolar mediated endocytosis signalling. Genes are coded as red (up-regulation) and green (down-regulation). This figure was generated by IPA Pathway Designer.

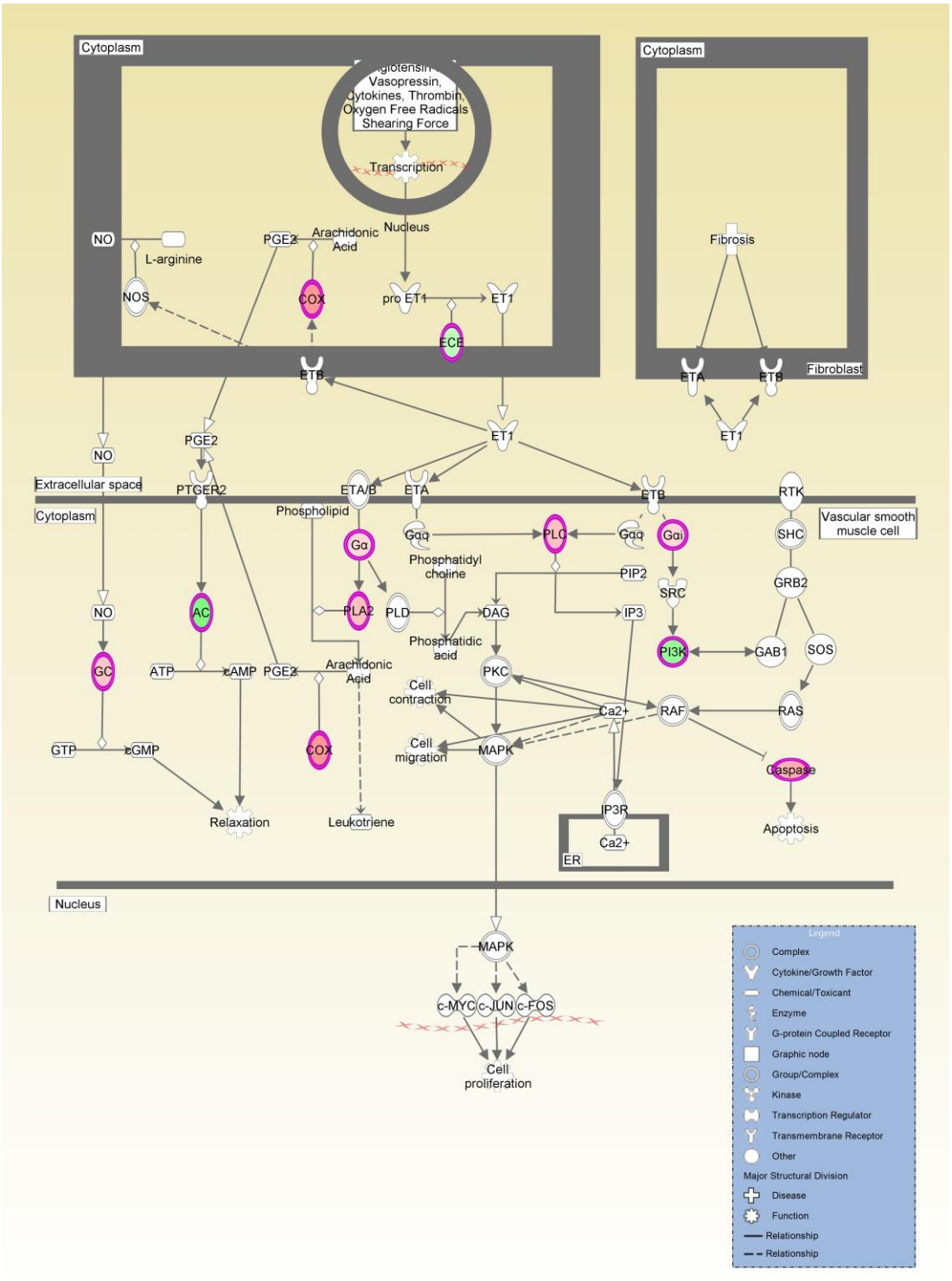

Figure 3-9 Diagram illustrating endothelin-1 signalling. Genes are coded as red (up-regulation) and green (down-regulation). This figure was generated by IPA Pathway Designer.

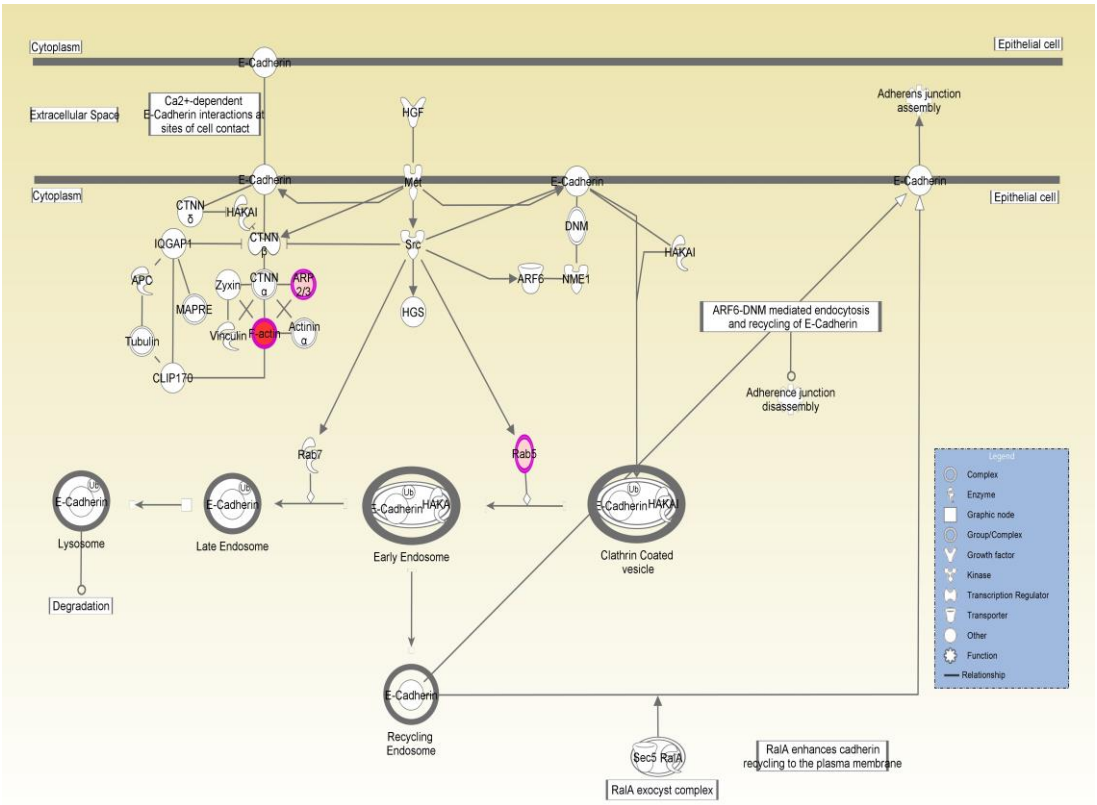

Figure 3-10 Diagram illustrating remodelling of epithelial adherens junctions. Genes are coded as red (up-regulation) and green (down-regulation). This figure was generated by IPA Pathway Designer.

Toxicity

IPA identified 16 categories under "toxicity" which contributes to a certain pathology based on the literature or experimental reports. Significant cardiac related toxic functions were cardiac hypertrophy, cardiac necrosis/cell death, oxidative stress, and cardiac dysfunction Table 3-29. A number of categories relating to renal function were also found, and could be expected to contribute to cardiovascular dysfunction.

Table 3-29 Ingenuity toxicity list identified by IPA

Toxicity List	-log(p-value)	Ratio
Cardiac Hypertrophy	3.78E00	7.07E-02
Increases Renal Proliferation	3.73E00	1.07E-01
Persistent Renal Ischemia-Reperfusion Injury	3.64E00	2E-01
Increases Liver Damage	2.79E00	1.01E-01
Acute Renal Failure Panel	2.57E00	1.13E-01
Cardiac Necrosis/Cell Death	2.23E00	6.45E-02
Oxidative Stress	2.2E00	1.05E-01
Long-term Renal Injury Pro-oxidative Response Panel	2.08E00	2.31E-01
NRF2-mediated Oxidative Stress Response	1.92E00	5.56E-02
Decreases Depolarization of Mitochondria and Mitochondrial Membrane	1.58E00	1.5E-01
Increases Cardiac Dysfunction	1.55E00	1.08E-01
Hepatic Fibrosis	1.4E00	7.29E-02
Renal Proximal Tubule Toxicity Biomarker Panel	1.35E00	1.11E-01
Increases Renal Damage	1.33E00	7.25E-02
Increases Liver Steatosis	1.12E00	7.04E-02

Gene Networking

The gene networking analysis was conducted based on the diseases and functions annotations in accordance with the fold-change for each gene identified by microarray. The three most significant and biologically relevant networks were identified and overlaid with the diseases/functions annotations and canonical pathways; they were cardiovascular system development and function (Figure 3-11), cellular movement (Figure 3-12), and cell-to-cell signalling (Figure 3-13).

The number under each shape is the fold-change. Shapes in red colour mean increased expression while shapes in green colour mean decreased expression.

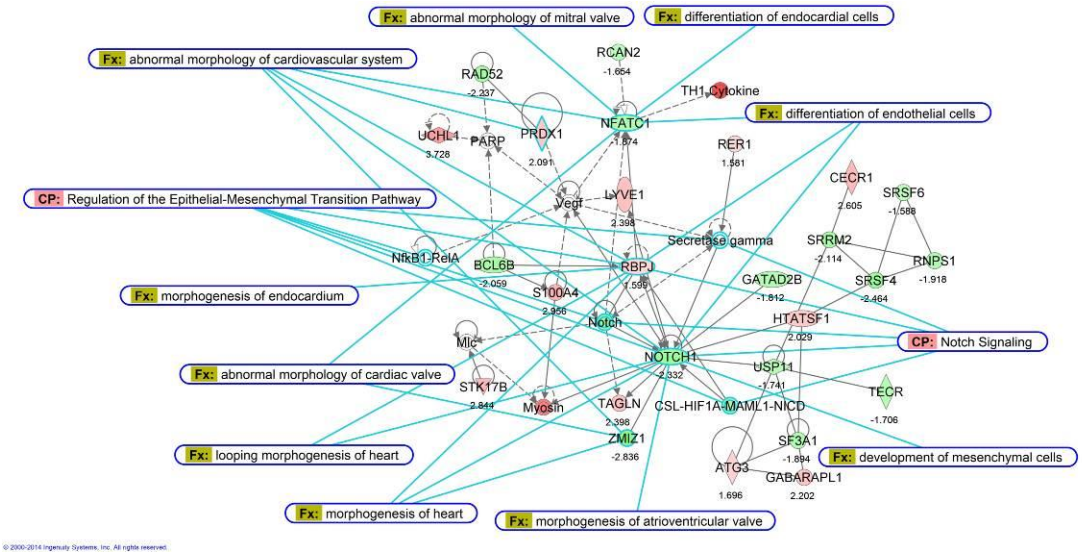

Diseases and functions	Genes
Abnormal morphology of mitral valve	NFATC1
Abnormal morphology of cardiovascular system	NFATC1, PPDX1, RBPJ, NOTCH1, ZMIZ1
Abnormal morphology of cardiac valve	NFATC1, ZMIZ1
Morphogenesis of endocardium	RBPJ
Morphogenesis of atrioventricular valve	NOTCH1
Morphogenesis of heart	NOTCH1, RBPJ, ZMIZ1
Looping morphogenesis of heart	NOTCH1, RBPJ
Differentiation of endocardial cells	NFATC1
Differentiation of endothelial cells	NFATC1, RBPJ, NOTCH1
Development of mesenchymal cells	NOTCH1

Canonical Pathway	Genes
Regulation of the epithelial-mesenchymal transition pathway	Secretase γ, RBPJ, NFκB1, NOTCH1, CSL-HIF-1A
NOTCH signalling	Secretase γ, RBPJ, NOTCH1, CSL-HIF-1A

Figure 3-11 Gene network for cardiovascular system development and function identified by IPA. This figure was generated by IPA Pathway Designer.

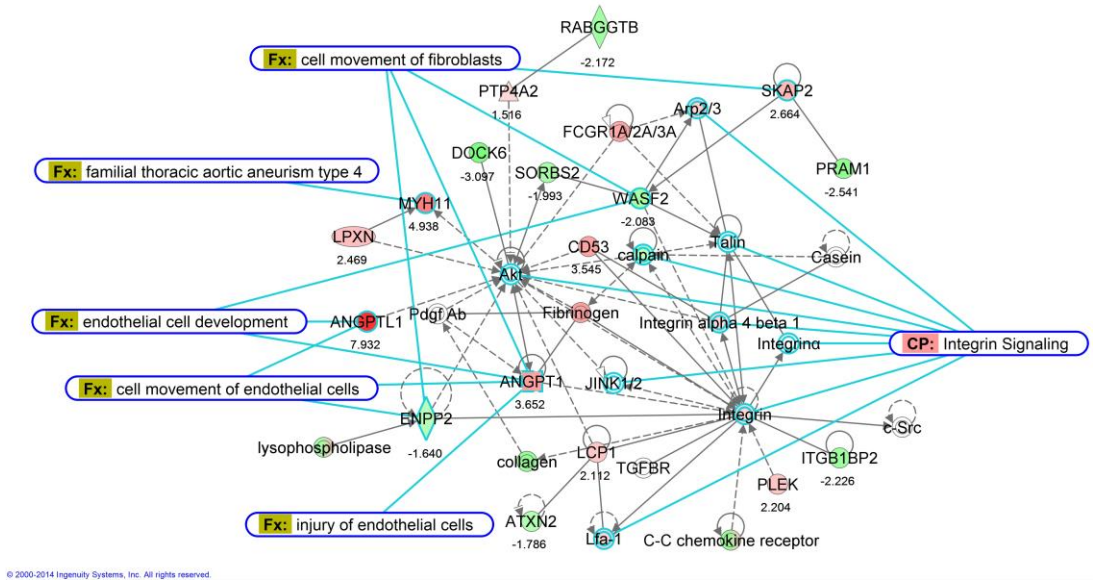

Diseases and functions	Gene
Cell movement of fibroblast	SKAP2, WASF2, ANGPT1, ENPP2
Familial thoracic aortic aneurism	MYH11
Endothelial cell development	ANGPTL1, ANGPT1
Cell movement of endothelial cells	ANGPT1, ENPP2
Injury of endothelial cells	ANGPT1

Canonical Pathway	Gene
Integrin Signalling	Arp2/3, Talin, calpain, Akt, integrin, JINK1/2, Lfa-1

Figure 3-12 Gene network for cellular movement and connective tissue development identified by IPA. This figure was generated by IPA Pathway Designer.

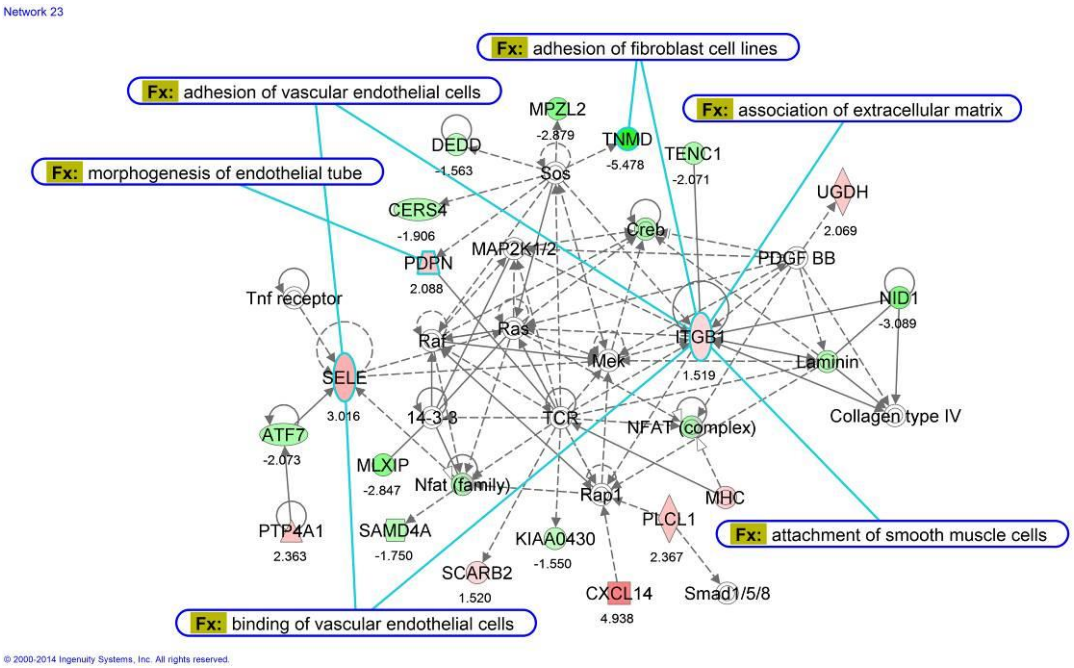

Diseases and functions	Gene
Adhesion of fibroblast cell lines	TNMD, TENC1
Adhesion of vascular endothelial cells	ITGB1, SELE
Association of extracellular matrix	ITGB1
Attachment of smooth muscle cells	ITGB1
Binding of vascular endothelial cells	ITGB1, SELE
Morphogenesis of endothelial tube	PDPN
Basement membrane disruption	NID1, Laminin

Figure 3-13 Gene network for cell-to-cell signalling and tissue development identified by IPA. This figure was generated by IPA Pathway Designer.

3.3.6 BioLayout *Express*^{3D}

BioLayout *Express*^{3D} is a network analysis tool that clusters genes based on coexpression patterns. In the graph (Figure 3-14), every node represents an annotated or un-annotated transcript. All clustered nodes are joined by edges (when the Pearson correlation coefficient between two transcripts was over 0.94), and weighted based on the correlations between similar expression patterns. Nodal clustering was based on the MCL method (Figure 3-14).

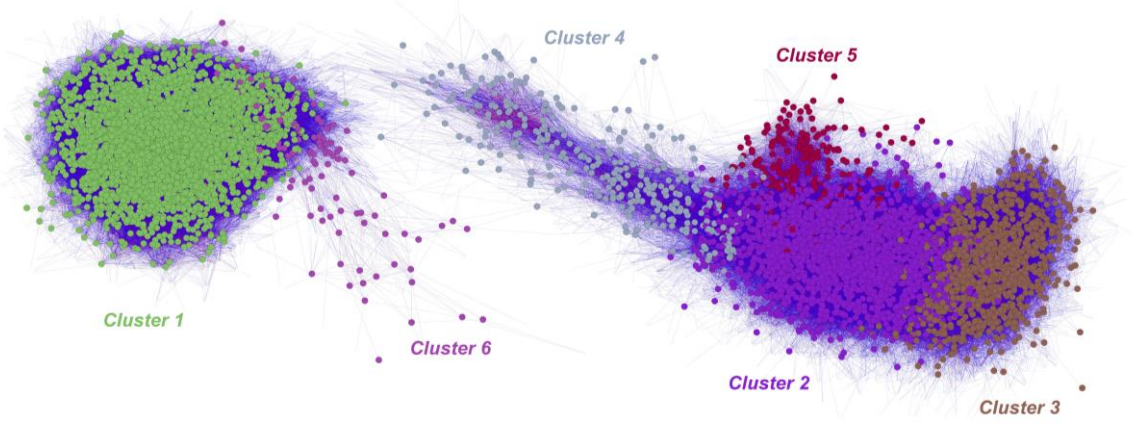

Figure 3-14 Two major groups of clusters were identified in BioLayout *Express* ^{3D}. Cluster 1 and 6 were genes with higher expression level in MMVD compared to controls, whereas Cluster 2, 3, 4, 5 were genes with lower expression level in MMVD compared to controls.

The two major clusters (1 and 2) with highest numbers of genes have distinct expression patterns, where cluster 1 showed relatively high expression in myxomatous mitral valves and cluster 2 showed relatively low expression in myxomatous mitral valves (Figure 3-15). One diseased valve sample (MMVD024) had a similar expression pattern to controls in cluster 1, 2, and 3. Genes with higher expression level in control group can be found in cluster 3, 4, and 5. In cluster 4, control02 was found exceptionally high compared to other samples in the control group, and this similar pattern can be found in cluster05 for control01 (Figure 3-15).

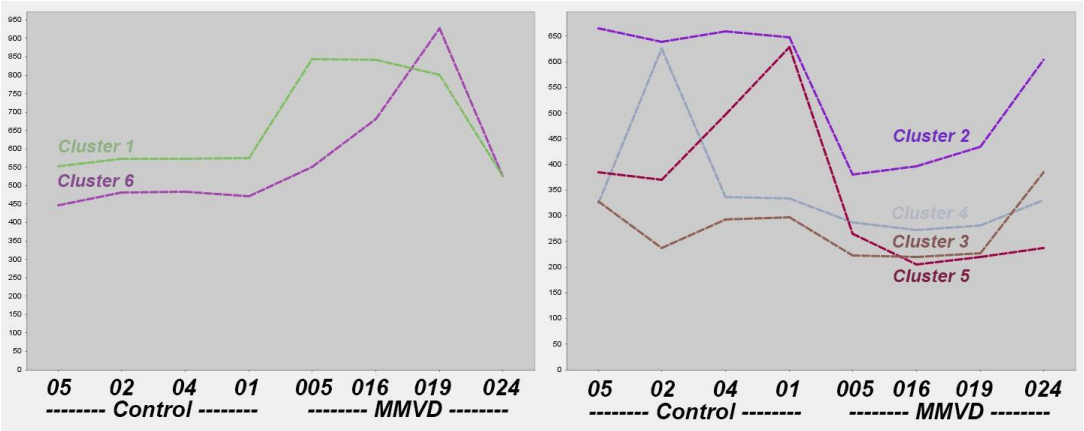

Figure 3-15 Mean signal intensity for main clusters (1 to 6) on two plots. Y axis- average intensity for the cluster. The plot on the left shows two clusters (1 and 6) of genes that have relatively higher expression level in MMVD, whereas the plot on the right shows 4 clusters (2, 3, 4, and 5) of genes that have relatively lower expression level in MMVD. In the three major clusters (1, 2, and 3), MMVD024 was identified as an outlier, which also showed in the PCA plot (Figure 3-3).

Further data mining for the genes associated with EndoMT can be found in Table 3-30. Genes underlined in the Table were not in the 591 genes identified by the initial microarray analysis.

Table 3-30 Summary of the Biolayout *Express3D* findings and genes associated with EndoMT in each cluster

Cluster	Expression Pattern	Genes associated with EndoMT	Annotation
Cluster 1	**↑MMVD, ↓Control**	HAS2, SNAI1, CTSS, TAGLN, BMP6, BMPR1B, BMPR2, CTNNB1, RBPJ1	69% (2420/3504)
Cluster 2	**↓MMVD, ↑Control**	NOTCH1, NOTCH2, NID1, NFATC1, NFATC2	54% (1137/2091)
Cluster 3	**↓MMVD, ↑Control**	CDH5	31% (342/1114)
Cluster 4	**↑Control02**	No gene	34% (120/357)
Cluster 5	**↑Control01**	LAMA2	70% (144/207)
Cluster 6	**↑MMVD019**	MYH11, ACTG2,	68% (92/136)

3.3.7 Transcriptomic Data Mining Based on Signal Intensity

Annotation clustering analysis of differentially expressed genes by gene ontology platforms provided insight into the functional aspects of MMVD, and the most biologically relevant functions identified were 1) inflammatory response, 2) cellular movement, 3) cardiovascular development, 4) extracellular matrix organization, 5) epithelial to mesenchymal transition. Genes associated with these five categories were sub-categorized with their signal intensity values (this value was converted from the digital pixels on the array) for further analysis and the detail is shown in 3.3.7.1 to 3.3.7.17. Down- or up-regulation of genes presented in this section were based on microarray analysis. Mining the data on their signal intensities provides extra insight into the trend and pattern of gene expression.

3.3.7.1 Collagens

The signal intensity for all collagen mRNA is shown in Figure 3-16. Briefly, the signal intensities for genes encoding subunits of collagen I, III, V, VI, XII, and XIV were higher than 1,000, but intensity for COL15A1 and COL16A1 was low. The only significantly altered gene was COL6A3 ($p < 0.001$).

A

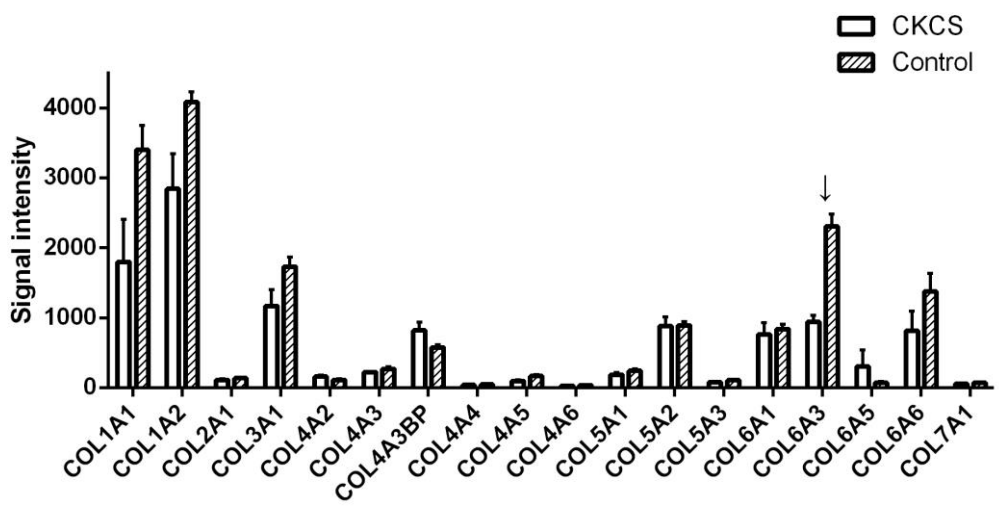

B

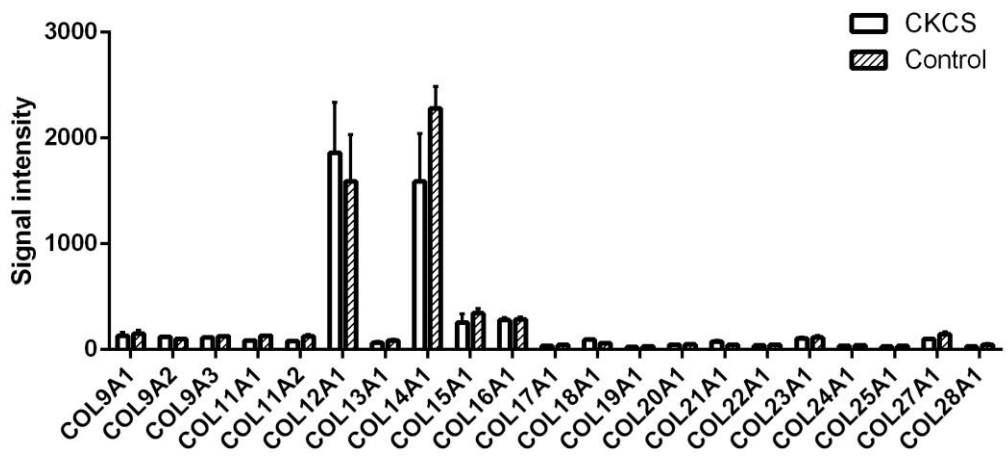

Figure 3-16 Signal intensity for collagens: (A) Genes encoding Collagen type I to type VII, and (B) Genes encoding collagen type IX to XXVIII. ↓ down-regulated ($p < 0.05$)

3.3.7.2 ADAMTS

ADAMTS is a family of peptidases. A homologous sub-family of ADAMTSL (ADAMTS-like) proteins which lack enzymatic activity was also included. The signal intensity values for ADAMTS and ADAMTSL were all below 1,000, and the three significantly decreased genes were ADAMTS2, ADAMTS19, and ADAMTSL4 (Figure 3-17).

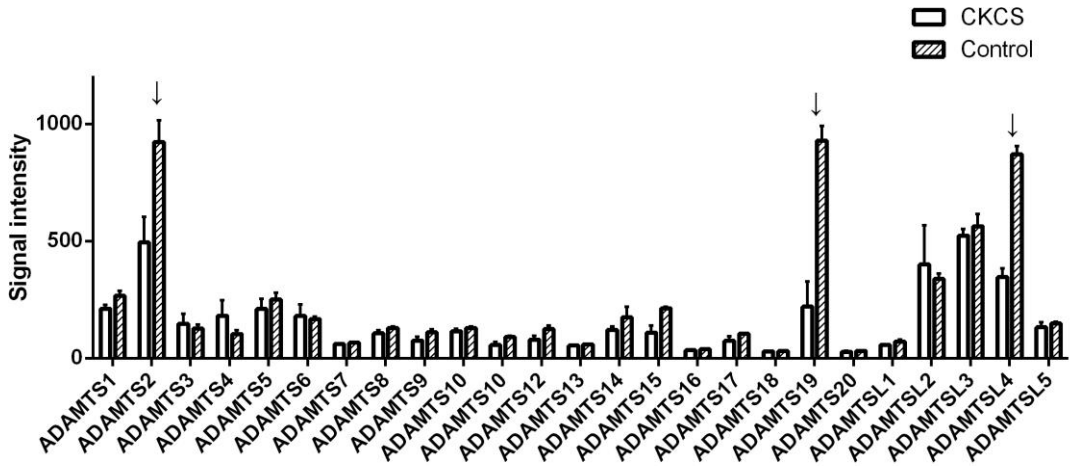

Figure 3-17 Signal intensity for ADAMTS and ADAMTSL. ↓ down-regulated ($p < 0.05$)

3.3.7.3 Proteoglycans and Glycosaminoglycans

The transcripts for proteoglycans and glycosaminoglycans had the highest signal intensity values among all the transcripts in the microarray. In general, lumican and versican had the highest signal intensity value (> 10,000), and the signal intensities for biglycan, decorin, asporin, fibromodulin, prolargin, keratocan, osteoglycin, and chondroadherin were between 3,000 and 10,000 (Figure 3-18). The two significantly down-regulated genes were KERA (keratocan) and CHAD (chondroadherin).

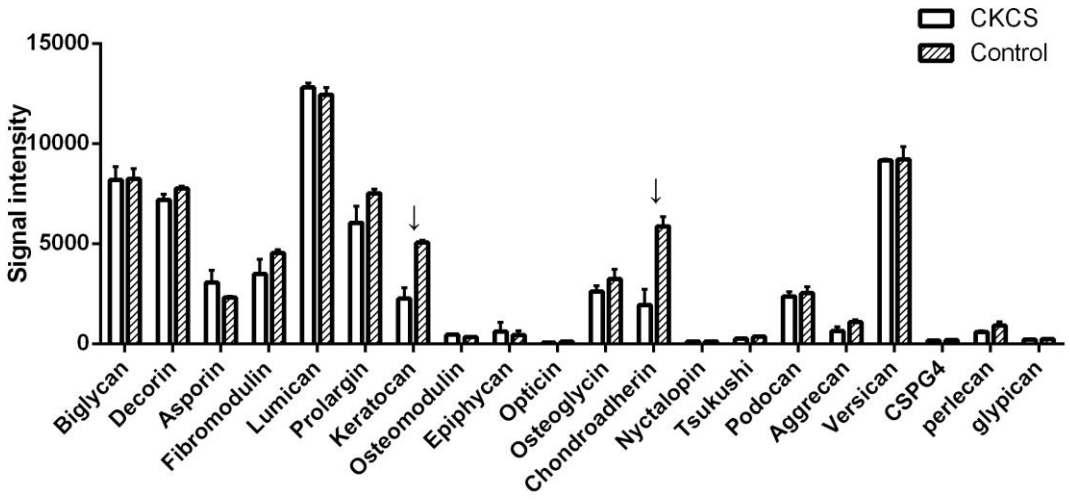

Figure 3-18 Signal intensity for PGs and GAGs. ↓ down-regulated ($p < 0.05$). Chondroitin sulphate proteoglycan 4 (CSPG4)

3.3.7.4 MMPs and TIMPs

MMPs and tissue inhibitors of metalloproteinases (TIMPs) were categorized into one group. The signal intensity for TIMPs was higher (TIMP1 > 1,000, TIMP2 and TIMP3 > 4,000) than for MMPs. (Figure 3-19).

MMP2 had the highest signal intensity value (> 4,000) among all the MMPs. MMP14 ($p < 0.001$) and MMP16 ($p < 0.01$) were significantly down-regulated, and MMP12 ($p < 0.001$) was significantly up-regulated (Figure 3-19).

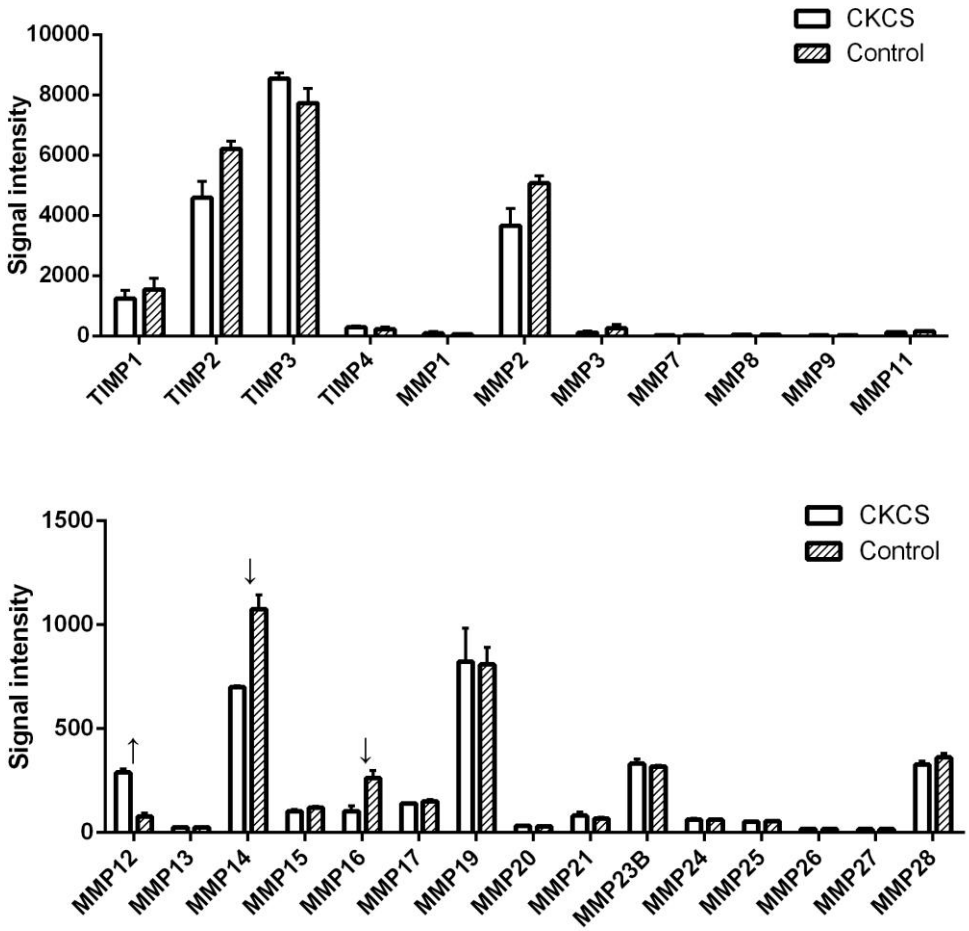

Figure 3-19 Signal intensity for TIMPs and MMPs. ↓ down-regulated, ↑ up-regulated.

3.3.7.5 Basement membrane (BM) components

Nidogen1 (NID1, $p < 0.01$), laminin2 (LAMA2, $p < 0.001$), and laminin4 (LAMA4, $p < 0.01$) were the three significantly down-regulated transcripts in this category (Figure 3-20).

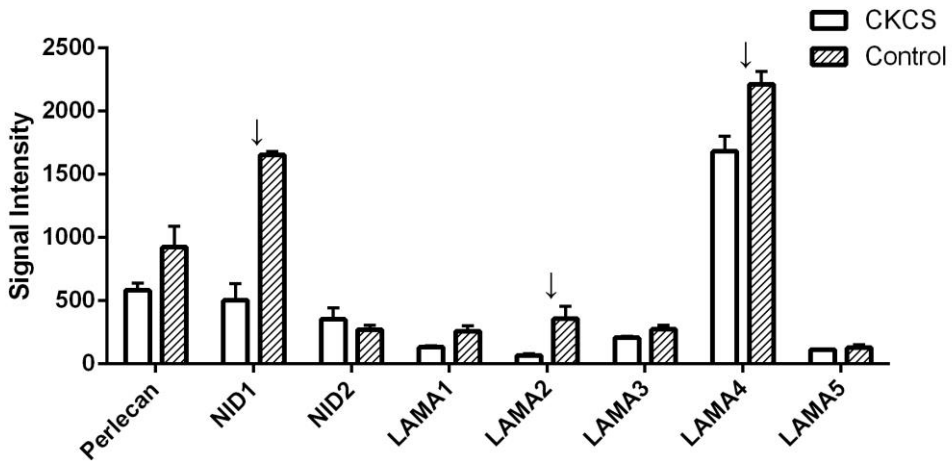

Figure 3-20 signal intensity for basement membrane components. ↓ down-regulated.

3.3.7.6 Cathepsins

Cathepsin K (CTSK) had the highest signal intensity value (> 5,000) for this category (Figure 3-21). Expression of cathepsin S (CTSS) (> 3,000) and Cathepsin C (CTSC) (< 1,000) were both significantly higher in CKCS than control.

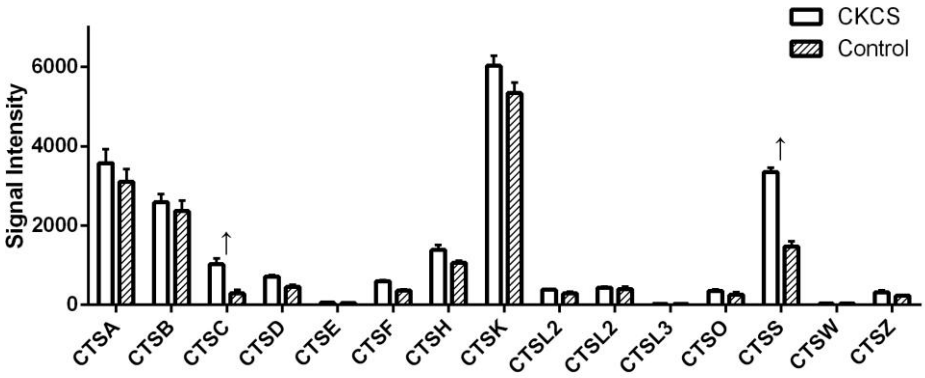

Figure 3-21 Signal intensity for cathepsins. ↑ up-regulated ($p < 0.05$)

3.3.7.7 Integrins

The top three highest signal intensity (> 2,000) values for members of the integrin family were integrin α FG-GAP repeat containing 1 (ITFG1), integrin α5 (ITGA5), and integrin β1 (ITGB1) (Figure 3-22). ITFG1 and ITGB1 were significantly up-regulated in CKCSs. The other significantly up-regulated integrin genes included

integrin α1 (ITGA1), integrin α8 (ITGA8) and integrin β1-like (ITGBL1), whereas integrin β4 (ITGB4) was the only significantly down-regulated gene in CKCSs.

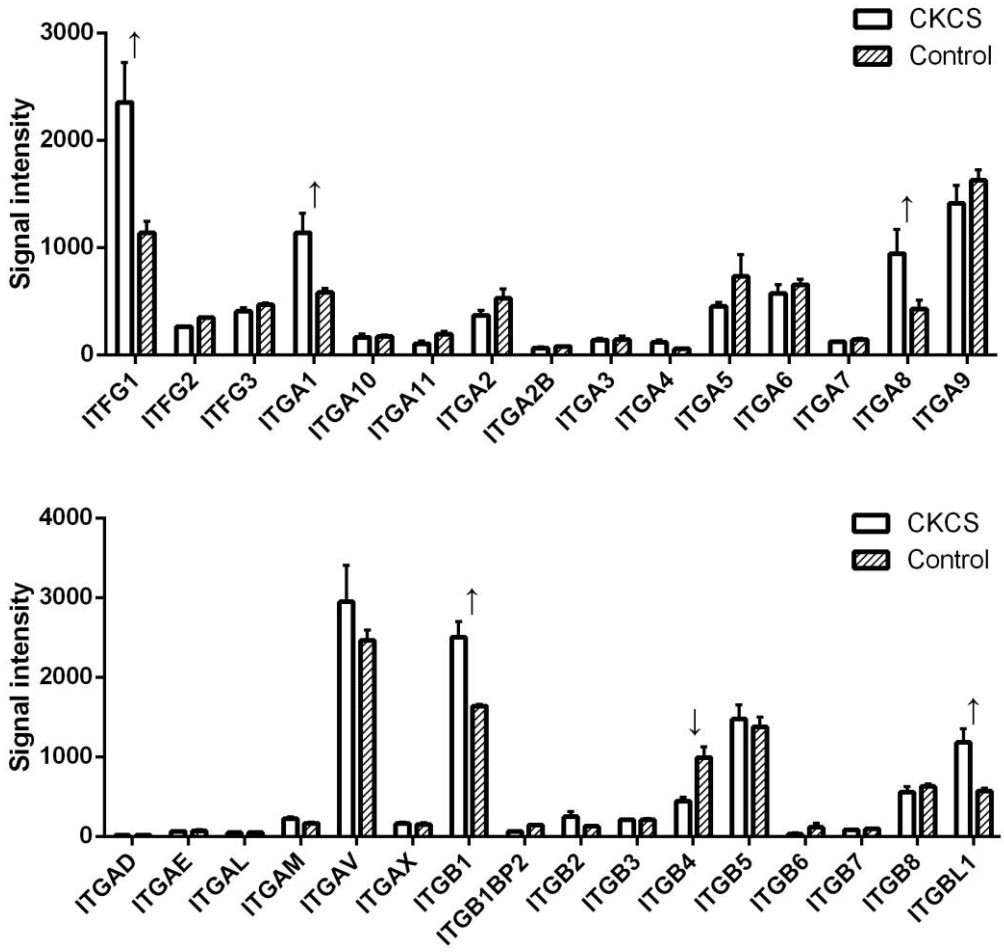

Figure 3-22 Signal intensity for integrins. ↓ down-regulated ($p < 0.05$), ↑ up-regulated ($p < 0.05$)

3.3.7.8 Claudins and Occludin

Claudin 1 (CLDN1), claudin 11 (CLDN11), and claudin 12 (CLDN12) had higher signal intensities compared with other claudins. Interestingly, CLDN1 was significantly up-regulated while CLDN11 was significantly down-regulated in CKCSs. The expression of occludin (OCLN) was minimal (Figure 3-23).

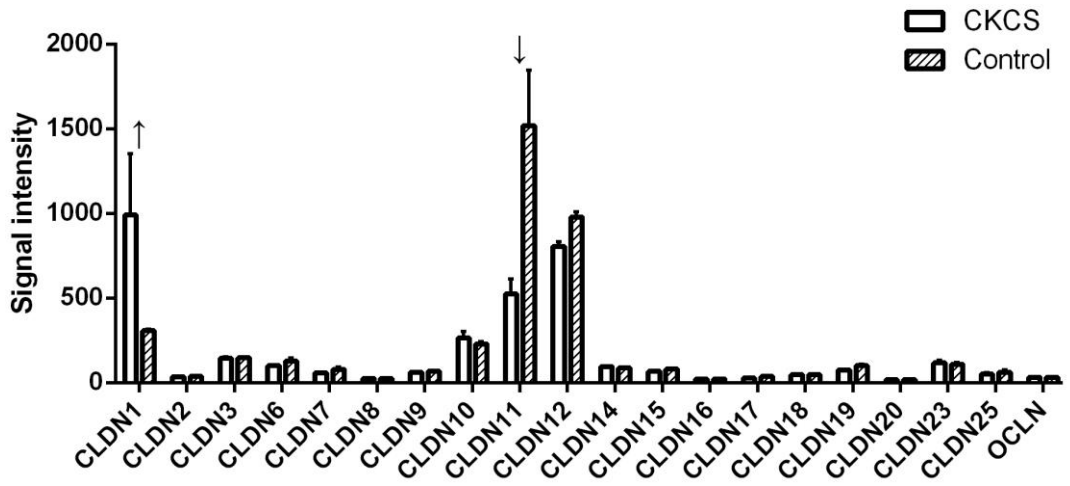

Figure 3-23 Signal intensity for claudins and occludin. ↓ down-regulated ($p < 0.05$), ↑ up-regulated ($p < 0.05$)

3.3.7.9 Cadherins

Cadherin (CDH) expression was high in signal intensity (> 1000), and CDH2, CDH5, CDH11, CDH13, and CDH23 were the highest cadherins expressed in both groups (Figure 3-24). CDH13 was the most expressed cadherin (> 3,000). CDH2, CDH5, CDH11, and CDH23 had similar expression levels (1,000 ~ 2,000).

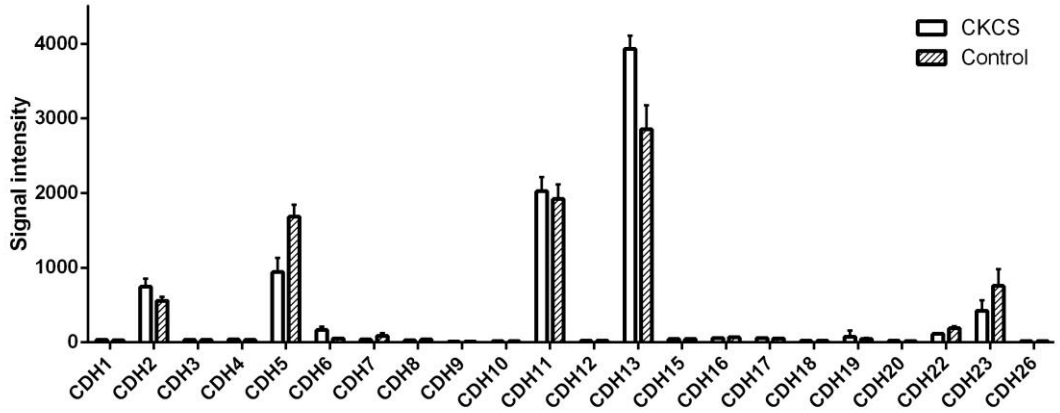

Figure 3-24 Signal intensity for cadherins

3.3.7.10 Fibrillins, Periostin, Fibronectin, and Fibulins

Signal intensities for periostin (PTN), fibronectin (FN), and fibulin1 (FBLN1) were generally high (> 5,000), and expression level for fibrillin (FBN1) and fibulin5 (FBLN5) were between 3,000 and 5,000 (Figure 3-25).

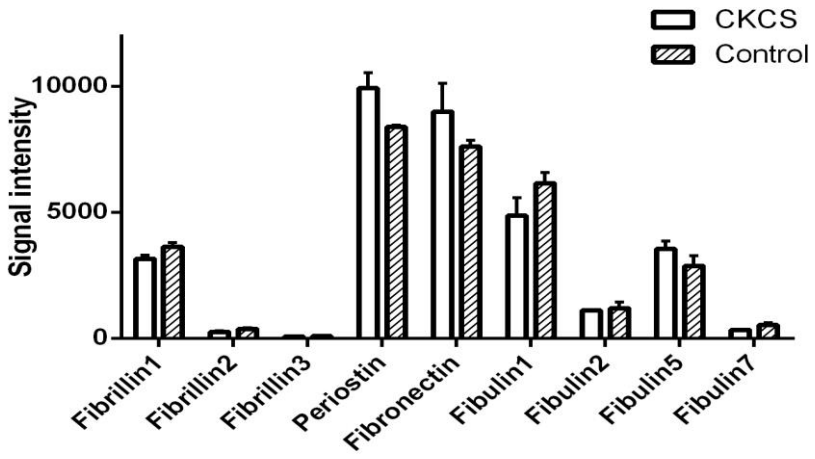

Figure 3-25 Signal intensity for fibrillins, periostin, fibronectin, and fibulins.

3.3.7.11 Others

In this category, cartilage intermediate layer protein (CILP), elastin (ELN), hyaluronic acid synthases (HAS), tenascin (TNC), filamin (FLN), and hyaluronan and proteoglycan link protein (HAPLN) were included. Expression of HAPLN1 had the highest expression (> 2,500), and CILP, HAS2, TNC, and FLNA had moderate expression (> 1,000) (Figure 3-26). Two significantly down-regulated genes were CILP and HAPLN1, whereas HAS2 had significantly higher expression.

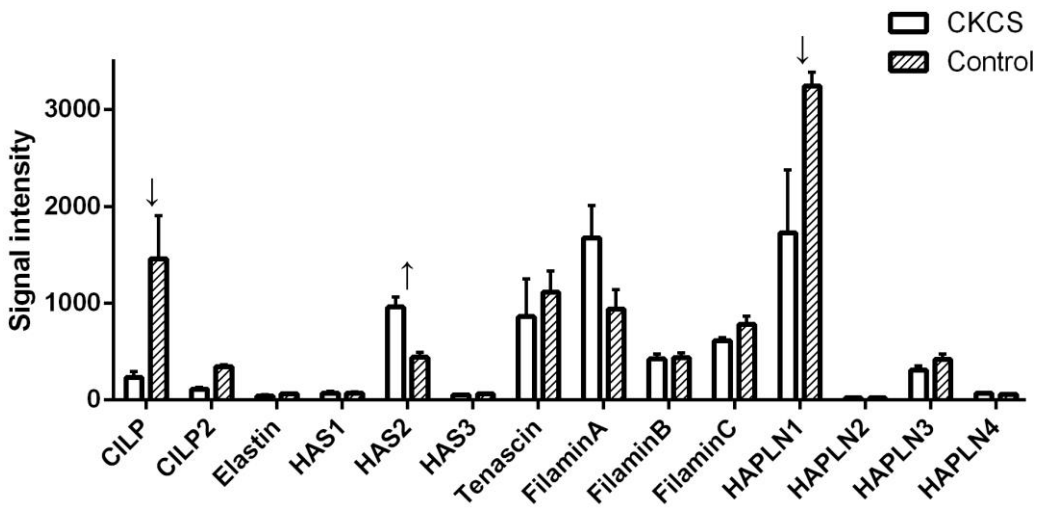

Figure 3-26 Signal intensity for CILP, ELN, Has, TNC, FLN, HAPLN, ↓ down-regulated ($p < 0.05$), ↑ up-regulated ($p < 0.05$).

3.3.7.12 Nitric oxide synthases and endothelins

Signal intensity for all three nitric oxide synthases and the three endothelins was low (< 500) (Figure 3-27). Nitric oxide synthase 1 (NOS1, neural NOS, nNOS) and nitric oxide synthase 3 (NOS3, endothelial NOS, eNOS) were similar in signal intensity.

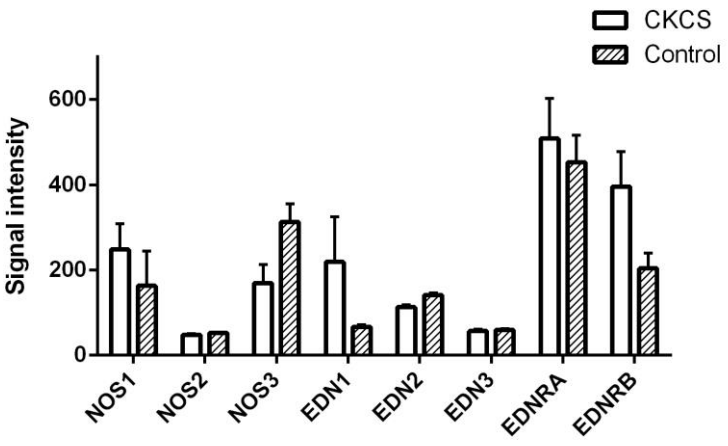

Figure 3-27 Signal intensity for NOSs and EDNs.

3.3.7.13 Caveolins, PECAM-1, selectin, ICAM-1, and VCAM-1

Signal intensities for caveolin1 (CAV1), caveolin (CAV2), platelet endothelial adhesion molecule-1 (PECAM1), and vascular cell adhesion molecule-1 (VCAM1) were high (> 1,000), whereas caveolin3 (CAV3), selectin (SELE), and intercellular cell adhesion molecule-1 (ICAM1) had low intensities (< 500) (Figure 3-28). Only SELE had significantly higher expression level in CKCSs.

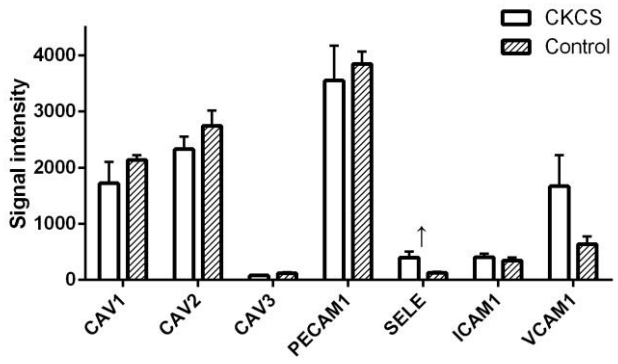

Figure 3-28 Signal intensity for CAVs, PECAM, SELE, ICAM1, and VCAM1. ↑ up-regulated ($p < 0.05$)

3.3.7.14 NOTCH and SNAI1

Signals for NOTCH2, recombination signal binding protein for immunoglobulin kappa J region (RBPJ) and SNAI2 (Slug) were medium to high (1,000~2,500), and signal for NOTCH1 and SNAI1 were low (<500) (Figure 3-29). There was lower expression of NOTCH1 in CKCSs, but higher expression of RBPJ in CKCSs.

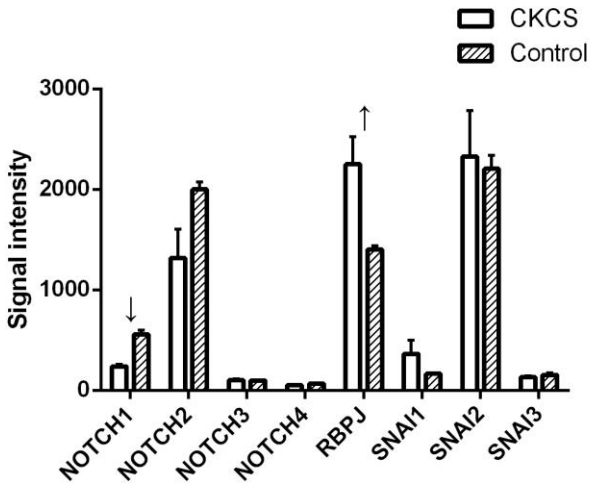

Figure 3-29 Signal intensity for NOTCH, RBPJ, and SNAI1. ↓ down-regulated ($p < 0.05$), ↑ up-regulated ($p < 0.05$).

3.3.7.15 Catenins, VEGFs, and NFATcs

Signal intensity for β-catenin (CTNNB1) was strong (>2,000). Expression of nuclear factor of activated T-cells, cytoplasmic 1 (NFATC1) and NFATC3 was moderate to low (500 ~ 1500). NFATC1 was significantly down-regulated in CKCS. Expression of vascular endothelial growth factors were low (> 500), and there was no difference between two groups (Figure 3-30).

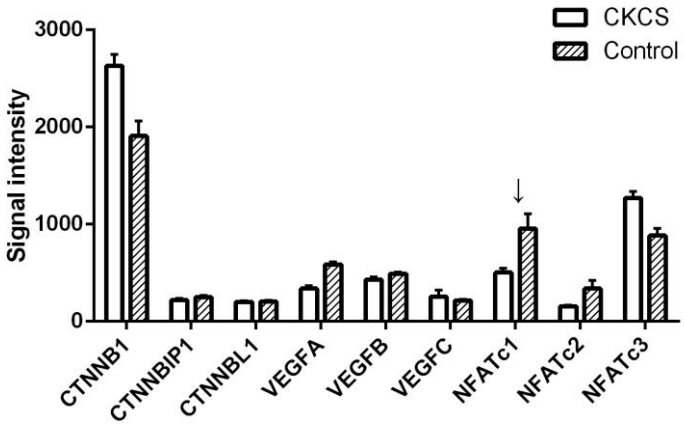

Figure 3-30 Signal intensity for catenins, VEGFs, and NFATcs. ↓ down-regulated ($p < 0.05$).

3.3.7.16 TGF-β and TGF-β Superfamily

Expression of members of the transforming growth factor β family was variable but not different between affected and normal dogs (Figure 3-31). The highest signal intensity was for TGFβI (transforming growth factor induced) (> 3,000), following by TGFβ receptors (TGFβR3, TGFβR2, and TGFβR1) and TGFβ (TGFβ2 and TGFβ3). TGFβ1 had the lowest expression. Endoglin (ENG) also showed high signal intensity (> 3,000).

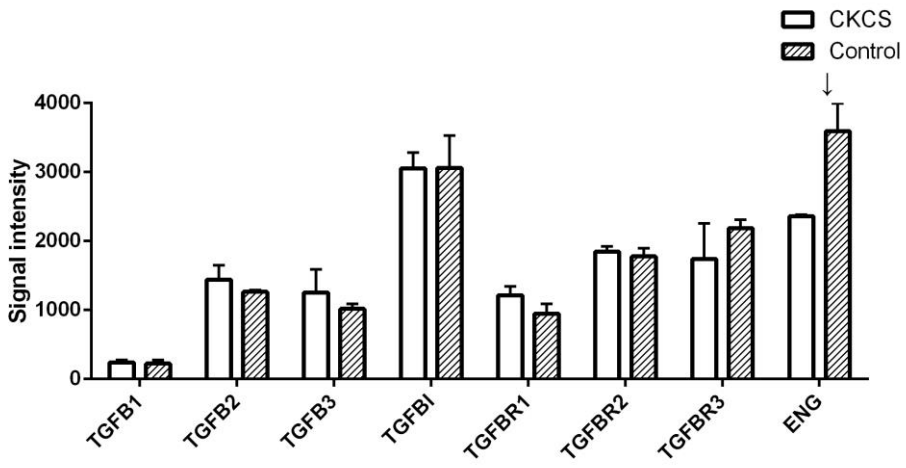

Figure 3-31 Signal intensity for TGF-βs, TGF-β receptors, and endoglin

Bone morphogenic proteins (BMPs) are also members of the TGF-β superfamily. Highest signal intensity was seen with bone morphogenic protein receptors (BMPR1A and BMPR2), and BMPs (BMP2, BMP4, BMP5, and BMP6) with BMPR1B having low to moderate expression (500 ~ 1,000) (Figure 3-32). BMP6 and BMPR1B were the only two significantly up-regulated genes in CKCSs, and the other BMPs and BMP receptors showed no difference in expression.

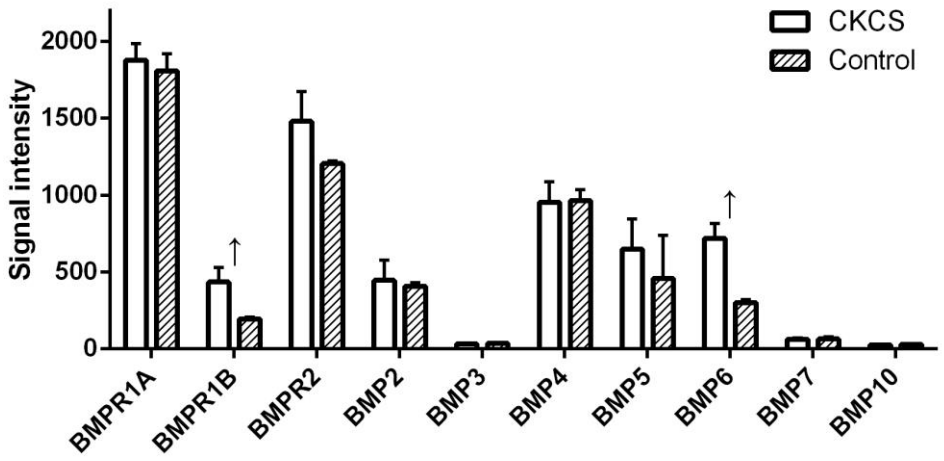

Figure 3-32 Signal intensity for BMPs and BMP receptors. ↑ up-regulated ($p < 0.05$).

3.3.7.17 Actins, Myosins and Smooth Muscle Cell Markers

Signal intensity for most actins, myosins and SM22 (smooth muscle cell marker, transgelin, TAGLN) was in general high (> 2,000) except α1 actin (ACTA1) and TAGLN3 (Figure 3-33). There was significantly increased expression of γ2 actin (ACTG2) and TAGLN1.

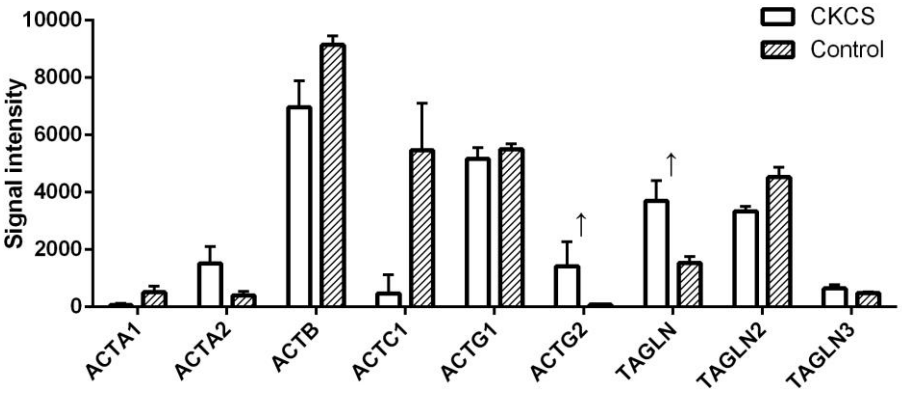

Figure 3-33 Signal intensity for actin and SM22 (transgelin, TAGLN). ↑ up-regulated ($p < 0.05$)

Genes associated with myosins overall had a low expression pattern (< 1,000) compared with actins (> 2,000) (Figure 3-34). Only myosin heavy chain 7 (MYH7), MYH9, MYH10, MYH11 had signal intensity above 200, which was the cutoff for

background noise. Nevertheless, MYH11 showed significant up-regulation in CKCSs.

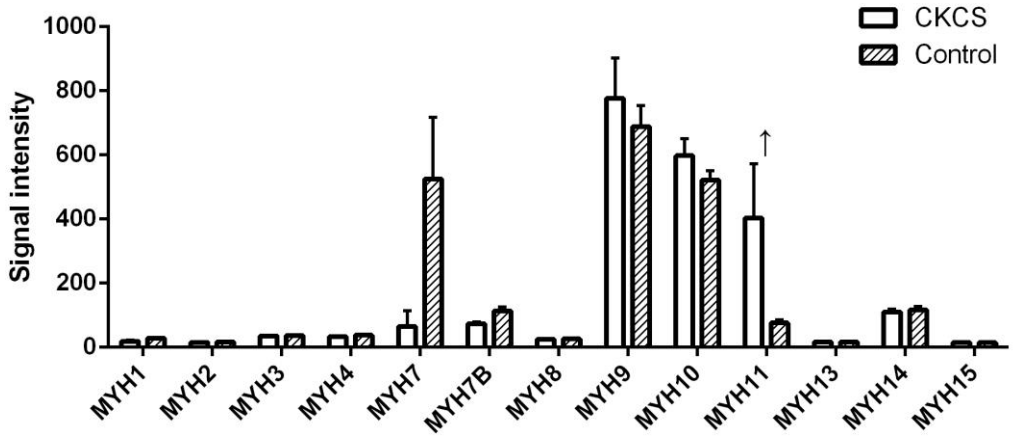

Figure 3-34 Signal intensity for myosin heavy chain genes. ↑ up-regulated ($p < 0.05$).

3.3.8 Final Categorization and Prioritization of Microarray Results

The gene list contained 591 differentially expressed genes which were analysed using the three major Gene ontology platforms (ToppFun, DAVID, and IPA), and the combined summarized results are shown in Table 3-31. The annotations that were biologically relevant to MMVD were selected and combined into the final functions list, and included inflammatory response, cellular movement, cardiovascular development, extracellular matrix organization, and epithelial to mesenchymal transition.

Table 3-31 Functions and diseases annotation identified by different platforms

Platform	Functions and Diseases
ToppFun	1. Inflammation and immune response 2. Cellular adhesion and movement 3. Cardiovascular development 4. Extracellular matrix organization 5. Osteogenesis 6. Epithelial proliferation
DAVID	1. Inflammatory response 2. Cell adhesion 3. Vasculature development 4. Cytoskeleton organization

	5. Collagen metabolic process 6. Epithelial to mesenchymal transition
IPA	1. Endocrine system disorders 2. Connective tissue disorders 3. Inflammatory disease 4. Cancer 5. Cardiovascular system development 6. Cell death and survival
Finalized	1. Inflammatory response 2. Cellular movement 3. Cardiovascular development 4. Extracellular matrix organization 5. Epithelial to mesenchymal transition

IPA alone also allowed prediction of upstream regulators, toxicity, and canonical pathways by analyzing fold-changes of the imported gene list. The finalized result are summarized in Table 3-32.

Table 3-32 Identified upstream regulators, toxicity, and canonical pathways

IPA	Description
Upstream regulator	IL1B, IL13, TGFB1, LDL
Toxicity	1. Cardiac Hypertrophy 2. Cardiac Necrosis/Cell Death 3. Oxidative Stress 4. Increases Cardiac Dysfunction
Canonical Pathway	1. Caveolar-mediated endocytosis signalling 2. Endothelin-1 signalling 3. Remodelling of epithelial adherens junctions

The genes showing significant signal differences between affected and unaffected dogs as outlined above in sections 3.3.7.1 to 3.3.7.17 are summarised in Table 3-33.

Table 3-33 Significant results from signal intensity analysis

Category	Gene, direction of change and intensity level
Collagen	COL6A3↓(H)
ADAMTS	ADAMTS2↓(M), ADAMTS19↓(M), ADAMTSL4↓(M)
PGs and GAGs	KERA↓(H), CHAD↓(H)
MMP and TIMP	MMP12↑(M), MMP14↓(M), MMP16↓(M)
BM	NID1↓(H), LAMA2↓(L), CTSS↑(H)
Cathepsin	CTSC↑(M), CTSS↑(H)
Integrin	ITFG1↑(H), ITGA↑(M), ITGA8↑(M), ITGB1↑(H), ITGB4↓(M), ITGBL1↑(M)
Claudin and occludin	CLDN1↑(M), CLDN11↓(H)
Others	CILP↓(H), HAS2↑(M), HAPLN1↓(H)
CAV, PECAM, ICAM, SELE, and VCAM	SELE↑(L)
NOTCH and SNAI1	NOTCH1↓(L), RBPJ↑(H)
Catenin, VEGF, and NFATc	NFATC1↓(M)
TGF-β superfamily	ENG↓(H), BMPR1B↑(L), BMP6↑(M)
Actin, myosin, and SM22	ACTG2↑(H), TAGLN↑(H)

↑ up-regulated, ↓ down-regulated, H = high signal intensity, M = medium signal intensity, L = low signal intensity

3.4 Discussion

The array used for transcriptional profiling in this study was the Affymetrix Canine Gene 1.0 ST Array. In total, 590,097 probes against 27,681 genes (both annotated

and predicted canine genes) were designed according to the updated genome information from canFam2. The specific design of 26 unique 25-mer probes for each transcript allowed the highest coverage yet and the potential for future updates on currently unannotated transcripts. This also yielded accurate detection of the transcribed genome and provided higher resolution compared with classical 3'-biased microarrays. Oyama et al first reported the transcriptional profile of canine MMVD in 2006 using the first generation of the array (Affymetrix GeneChip Canine Genome 1.0). [106] In that study, up-regulation of HTR2B and TGF-β superfamily molecules including endoglin and BMP6 highlighted the potential role of the serotonin-TGF-β signalling pathway in MMVD, which may play a role in VIC activation and ECM remodelling. [106]

For human MMVD there have been three transcriptomic studies so far (two published, and one abstract). Hulin et al identified the down-regulation of metallothioneins-1 and -2 (MT1/2) and ADAMTS family members. In cultured cells in the same study knocking out MT1/2, TGF-β2 was up-regulated, which then down-regulated ADAMTS19 resulting in excessive versican deposition. [115] The other two studies both identified increased expression of extracellular component genes (collagen, proteoglycans and MMPs) and ECM associated transcriptional factors (BMPs), with activation of valve interstitial cells by BMP4 in a culture system. [114] These findings suggest an important role for TGF-β and TGF-β superfamily signalling in controlling cellular activation and ECM remodelling in human mitral valves. In the current study expression of genes associated with collagen and proteoglycan was generally down-regulated (COL6A3, KERA, CHAD) or unchanged whereas in human MMVD they were all up-regulated (COL1A1, COL3A1, decorin, biglycan, versican, and lumican). [114] Another interesting difference between the dog and human is the absence of up-regulation of HTR2B in any of the human transcriptomic studies. This might suggest species-specific mechanisms for MMVD and that the two diseases differ at least at the transcriptome level. The up-regulation of collagen and proteoglycan expression in human MMVD may also explain why calcific and fibrotic lesions are rarely seen in severe canine MMVD compared with human MMVD. [12,15]

The microarray results (Appendix 9.1) confirmed the previous findings (Table 3-25) in dogs for up-regulation of HTR2B (5.783-fold increase) and BMP6 (2.378-fold increase) [106], but found no differences in the expression of TGF-βs or TGF-β receptors. Because of the complexity of regulation of the TGF-β superfamily, this result does not rule out involvement in control of valve cell differentiation and ECM turnover during valve development, valve remodelling and disease. [59,63] The gene ontology analysis in the current study found similar biological functions for the differentially expressed gene sets as has been previously reported, including genes involved in cell signalling, inflammation, extracellular matrix, immunity, cell defence, and metabolism, but additional novel functions, including cellular movement and epithelial to mesenchymal transition, were also identified. [106] The specific findings in the transcriptome of interest to MMVD are discussed in detail in the following sections.

TGF-β and TGF-β superfamily

Transforming growth factor β plays a key role in development, and diseases such as cancer, fibrosis, and calcification. [125] There are three isoforms of TGF-β: TGF-β1, TGF-β2, and TGF-β3, and TGF-β signalling through SMAD pathway triggers myofibroblastic differentiation of valve interstitial cells and increases expression of SMAD-targeted genes associated with extracellular matrix such as COL1A1, COL3A1, COL6A1, COL6A3, elastin, and TIMP1. [126,127]

In the current study none of genes encoding the TGF-βs and TGF-β receptors were differentially expressed in MMVD. TGFB1 had the lowest (signal intensity 200) expression level and was considered as background noise suggesting extremely low or no expression. Expression of TGFB2 and TGFB3 was moderate (signal intensity = 1,000) but more variable in MMVD. Expression of TGF-β receptors (TGFBR1, TGFBR2, and TGFBR3) was high (signal intensity > 1,000). Consistent expression of TGF-β genes suggested there is continual biological effect of TGF-β2 and TGF-β3, which is not surprising. This homeostasis maintained by TGF-β may be associated with ECM turnover, cell survival, and differentiation; although no sign of myofibroblastic differentiation was present in the normal mitral valve. [52,61] TGF-β was also identified as a potential upstream regulator by IPA. However, many of the

TGF-β downstream genes such as COL1A1, COL3A1, and TIMP1 were not differentially expressed, suggesting there was no excessive up-regulation of the target genes. In contrast, human myxomatous mitral valves were found to show higher transcriptional level of all isoforms of TGF-β, and TGF-β downstream genes (COL1A1, COL3A1 and elastin) were also up-regulated, suggesting activation of fibrosis. [125] Interestingly, Aupperle et al have also observed an increased expression (by immunohistochemistry) of TGF-β1 and TGF-β3 in the subendothelial stroma cells (proposed to be activated myofibroblasts) in canine myxomatous valves, but with minimal expression of TGF-β2 in both normal and myxomatous valves. [61] Post-transcriptional modification might be the reason that the expression of TGF-βs in the current study conflicts with these IHC (immunohistochemistry) results.

Low-density lipoprotein

The plasticity of valve cells implies an adaptive and homeostatic potential to the dynamically changing macro- and micro-environment. The upstream regulators analysis identified a positive association between LDLR and the downstream genes (17 out of 23), which predicted an activation of LDL signalling. One canine lipid profiling study identified an increased LDL-cholesterol concentration (mean = 145.7mg/dL) for the aging group (>7 years old) compared with young adult group (3.1 to 7 years old, cholesterol-LDL = 117.2 mg/dL), and this coincided with the MMVD prevalence in dogs. [7,12,15,128] It is not particularly surprising since control mitral valves were sampled from young adult dogs and diseased mitral valves were collected from elderly dogs. Moreover, CKCS has been recently identified as a breed predisposed to chronic fibrosing pancreatitis, and the abnormal lipid metabolism leading to intermittent LDL surge may be one of the contributing factors to the early onset of MMVD. [129,130]

It is generally believed that the degenerative pathways of mitral and aortic valve were shared and controlled by BMPs and TGFβ signalling [131], and it has been reported that coronary calcification and aortic valve calcification progress more rapidly in subjects with levels of LDL >130 mg/dL. [131] Together, LDL could be a potential factor contributing to MMVD in normal aging group and the early-onset population of CKCS.

Canonical pathways

Three canonical pathways deemed to be of potential interest to MMVD were identified, and included caveolar mediated endocytosis, endothelin-1 signalling, and remodelling of epithelial adherens junction. The remodelling of epithelial adherens junctions will be discussed together with EndoMT later.

Caveolae are lipid raft invaginations of the plasma membrane found in high numbers in endothelial cells, fibroblasts, smooth muscle cells, and adipocytes. They are believed to be involved in regulation of endothelial cell growth, endocytosis, and cell migration by internalizing important signalling molecules, such as TGF-β receptors, tyrosine kinase receptor, and endothelial nitric oxide synthase. [132] Due to their endosomal degradation of TGF-β receptors, caveolae are suggested to play an important role in reducing TGF-β induced fibroblast activation, leading to excess deposition of associated ECM in fibrotic disorders. [133] Down-regulation of this pathway (section 3.3.5) could mean increased TGF-β signalling. In migrating cells, focal adhesion is regulated by integrin-caveolae interaction, and the increased expression of integrin β1 (ITGB1, 1.519-fold increase) in the current study might suggest a change in cell polarity or directional migration through caveolae signalling in valve endothelial and interstitial cells. [134] Nevertheless, expression levels of caveolin1 (CAV1) and CAV2 were high (signal intensity > 2,000) in CKCSs and controls.

Endothelins (ET-1 encoded by EDN1, ET-2, encoded by EDN2, and ET-3 encoded by EDN5) are potent vasoconstrictor peptides synthesized from endothelium throughout the whole body and they have mitogenic effect on fibroblasts, smooth muscle cells, and endothelial cells. [135] ET-1 is the main isoform acting through ET_A-R (endothelin receptor A, vasoconstriction) and ET_B-R (endothelin receptor B, NO release) to maintain normal cardiovascular physiology. [136] It has been suggested that ET-1 modulates extracellular matrix remodelling in MMVD, since the expression of ET receptor is positively associated with canine MMVD severity and ET receptors are highly expressed in the stroma and endothelium of the myxomatous leaflet tips. [69] [69] In the current study, expression of endothelins, endothelin receptors (EDNRA and

EDNRB) and nitric oxide synthase (nNOS, iNOS, eNOS) was low (signal intensity < 500), and statistically there was no difference. Whether there is localized activation of endothelin signalling or not remains unknown. Further work is required to quantify and localize endothelin and eNOS expression in normal and affected valves. Finally, the low signal intensity of ET receptors coincides with the report by Pedersen et al, which found low levels and localized expression of endothelin receptor RNA both in diseased and normal mitral valves. Unfortunately, expression patterns of the ET_A-R (vasocontriction) and ET_B-R (vasodilation) could not be differentiated in their study. [69]

Inflammation

In general, there was evidence of an increased inflammatory response in the myxomatous mitral valves transcriptome, with increased expression of inflammatory cytokines, and these result are in agreement with the previous finding. [106] However, adhesion molecules expressed by endothelium (VCAM-1 and ICAM1) were not changed. The novel finding from the current study was the over-expression of toll-like receptors (TLRs) in CKCSs. In the gene networking analysis, two molecules central to the inflammation network were identified by IPA; toll-like receptor 4 (TLR4) and interleukin 18 (IL-18). Other up-regulated molecules associated with inflammation and immunity included interleukin 6 (IL-6), toll-like receptor 1 (TLR1), and toll-like receptor 8 (TLR8). The TLRs are the first line of defence against microbial infection and modulate innate and adaptive immunity. Moreover, TLRs can also recognize endogenous ligands (heat shock protein 70, fibronectin, hyaluronic acid, heparan sulfate, and hyaluronan), and may play a protective role in ischemic injury in heart and wound healing in skin. [137] However, in MMVD there is no evidence of inflammatory cell infiltration, and this was confirmed in the myxomatous mitral valves from CKCSs [52]. Pathological changes in myxomatous mitral valves are characterized by deposition of glycosaminoglycans, fragmentation of collagen bundles and elastic fibres. Taken together, excess breakdown of the ECM components in the mitral valve might be the endogenous factor that triggers TLR receptors signalling, which then further contributes to ECM remodelling and deteriorating valve structure [138]. This could also explain how mechanical injury from

mitral regurgitation alone could trigger leaflet remodelling leading to an inflammatory response. Recently, IL-6 has been shown capable of triggering EndoMT in the embryonic and adult aortic valve endothelium suggestive of an important role during valve development. [139] The continuous mechanical assault might initiate the developmental signal in adult valve endothelial cells, which could play a role in the pathogenic remodelling of valve tissues.

Collagens

There are 28 different types of collagen found in vertebrates. [140] Genes encoding subunits of all collagens except collagen VIII were screened in this study. In general, genes for collagen type I, III, IV, V, VI, XII, and XIV subunits were highly expressed (signal intensity 1,000 ~ 4,000) both in the diseased and normal mitral valves, and very minimum expression of collagen XV and XVI subunits was also found in the diseased and normal mitral valves. The only significantly down-regulated collagen gene was COL6A3. COL6A3 is a network-forming collagen expressed in developing the endocardial cushion and adult atrioventricular valves, and is thought to provide tensile strength to the surrounding tissues. [141,142] Lower expression of COL6A3 suggests disorganization of force-resistant collagen bundle formation in MMVD, and this could result in weakening of the mitral valve leaflet.

ADAMTS and ADAMTSL

ADAMTS family consists of 19 ECM metalloproteases. ADAMTS1, ADAMTS5, ADAMTS9 are reported to be expressed in the developing heart where they control atrioventricular endocardial cushion formation, trabeculation, and outflow tract remodelling.[143,144]

ECM degradation by ADAMTS also plays an important role in connective tissue formation, cancer, coagulation, arthritis, angiogenesis and cell migration. [145] In the current study there were 20 ADAMTS and 4 ADAMTSL genes identified in the canine microarray. The expression of all ADMATS and ADAMTSL family genes was generally low (signal intensity < 500), except for ADAMTS2, ADAMTS9, and ADAMTSL4 (ADAMTS-like 4), which were all significantly down-regulated in the diseased valves. ADAMTS2 is responsible for maturation of pro-collagen and extracellular proteolysis associated with morphogenesis, angiogenesis, ovulation,

cancer, and arthritis. [146] ADAMTS9 is one of the three ADAMTS expressed in the developing heart. [147,148] Haploinsufficient animal models of ADAMTS9 exhibit excessive versican deposition in myocardium and valves, and myxomatous degeneration is also noted in mitral valves. [147] This suggests lower expression of ADAMTS2 and ADAMTS9 in canine myxomatous mitral valves results in an inactive collagen turnover state with excessive extracellular matrix accumulation.

ADAMTSL4, which lacks the disintegrin-like domain, is thought to be catalytically inactive. However, ADAMTSL4 has been identified in distinct human genetic disorders including thrombotic thrombocytopenic purpura and acromelic dysplasia, and mutation of ADAMTSL4 results in ectopia lentis, which is also caused by mutation in FBN1 (Marfan Syndrome). [146] One study has also identified that ADAMTSL4 binds fibrillin microfibrils and stimulates microfibril biogenesis. [145,146] Diffuse expression of ADAMTSL4 in the fibrillar extracellular matrix region in ocular tissue also indicates its regulatory role for fibrillin-1. [145] Taken together data from these and the current study suggest lower expression of ADAMTSL4 in MMVD may contribute to decreased elastic fibre formation and leaflet elasticity.

MMPs and TIMPs

Matrix metalloproteinases are zinc-dependent endopeptidases, and can be roughly divided into 6 groups: (1) collagenases (MMP1, MMP8, MMP13), (2) gelatinases (MMP2, MMP9), (3) stromelysins (MMP3, MMP10, MMP11), (4) matrilysins (MMP7, MMP26), (5) enamelysin (MMP20), (6) membrane-type MMPs (MMP14, MMP15, MMP16, MMP17, MMP24, MMP25). Other unclassified MMPs include MMP19, MMP21, MMP23A, MMP23B, MMP27, and MMP28. The MMPs are inhibited by specific endogenous tissue inhibitors of metalloproteinases (TIMPs), which comprise a family of four protease inhibitors: TIMP1, TIMP2, TIMP3 and TIMP4. [149] The expression pattern of MMPs and TIMPs has been studied both in human and canine mitral valves (normal and myxomatous). However, only 6 MMPs (1, 2, 3, 9, 13, and 14) were covered in previous studies, and the results were variable probably due to use of a variety of methods (immunohistochemistry, PCR, and microarray) used to quantify expression level (mRNA and protein).

The latest canine microarray used in this study had the widest coverage of 22 MMPs (of a total 25 MMPs) and 4 TIMPs. While mRNA level does not necessarily equate to final protein concentration (post-translational modification and other proteasome mechanisms), generally speaking low or no genomic expression could mean low or no protein translated, but high genomic expression does not always mean high protein expression. Finally, the quantified signal intensity value for each MMP and TIMP can be an indicator for their genomic expression level, and this was not provided in the report by Oyama. [106] The signal intensity for MMPs and TIMPs in comparison to previous reports is summarized in Table 3-34. The expression of MMP1 was negligible, but most other studies identified up-regulation of MMP1 in myxomatous valves (PCR and IHC). The only consistent findings were expression for MMP9 and TIMP3, where MMP9 showed no expression and TIMP3 had higher expression. It is also important to note that MMP2 (gelatinase) was the highest MMP expressed in both diseased and normal mitral valves, suggesting an active remodelling status.

Table 3-34 Expression of MMPs and TIMPs, comparison data

	Lu (present study)		Aupperle [50]	Aupperle [150]	Disatian [104]	Obayashi [151]	Oyama [106]	Rabkin Human [56]
	Microarray		IHC	PCR	IHC	IHC	microarray	IHC
	MMVD	Control						
MMP1	62	61	ND	↑	↑	↑		↑
MMP2	3950	5139	↓	±		ND	±	↑
MMP3	145	323				↑		
MMP7	31	30						
MMP8	36	47						
MMP9	23	21	ND	±		ND	±	↑
MMP11	130	167						
MMP12	283↑	79						
MMP13	23	27			↑		±	↑
MMP14	702↓	1090	↑	↑				
MMP15	104	122						
MMP16	92↓	249						
MMP17	139	154						
MMP19	761	775						
MMP20	33	32						
MMP21	89	65						
MMP23B	337	321						
MMP24	59	61						
MMP25	52	54						
MMP26	18	17						
MMP27	16	18						
MMP28	324	355						
TIMP1	1362	1385					↑	
TIMP2	4614	6115	↑	↑				
TIMP3	8497	7665	↑	↑				
TIMP4	260	193	ND	↑				

ND: not detectable, ↑: higher expression, ↓:lower expression, ±: no change

Cathepsins

Cathepsins (CTS) are proteases (collagenases) and classification of cathepsins is based on their structure and catalytic activity. They are serine proteases: Cathepsin A (CTSA) and G (CTSG); cysteine proteases: Cathepsin B (CTSB), C (CTSC), F (CTSF), H (CTSH), K (CTSK), L1 (CTSL1), L2 (CTSL2), L3 (CTSL3), O (CTSO), S (CTSS), W (CTSW) and Z (CTSZ); aspartyl proteases: Cathepsin D (CTSD) and E (CTSE). [152] Probes against transcripts encoding all cathepsins (except CTSG) were screened in the canine microarray. The highly expressed cathepsins were CTSK (signal intensity > 6,000), CTSS (signal intensity > 3,000), CTSA (signal intensity >

3,000), CTSB (signal intensity > 3,000), CTSH (signal intensity > 1,000), and CTSC (signal intensity > 1000). The most potent collagenase is CTSK, and its expression was high in MMVD and controls. [152,153] Cathepsin S was another highly and differentially expressed cathepsin (2.27 fold-increased, $p<0.001$), and CTSS also has collagenolytic, elastinolytic and basement membrane cleavage (nidogen and laminin as substrates) activity. [152,154] Elevated CTSS expression in MMVD suggested a higher than normal enzymatic activity contributing to greater extracellular matrix degradation and basement membrane instability. Unlike the conflicting results for MMP expression, the findings on cathepsins (mRNA level) match the observation (protein level) in human myxomatous mitral valves, where CTSK and CTSS were also highly expressed in activated myofibroblasts. [56] The stimulatory factors and substrates of CTSS and CTSK are shown in Table 3-35.

Table 3-35 Stimulatory factors and substrates of cathepsin S and K [155]

Cathepsins	Stimulatory Factors	Substrates
Cathepsin K	Angiotensin II, IL-1β, TNF-α, IFN-γ	Elastin, collagen
Cathepsin S	Angiotensin II, IL-1β, IFN-γ, VEGF, bFGF, H_2O_2	Elastin, collagen, fibronectin, laminin, nidogen

Basement membrane components

The basement membrane is a continuous specialized protein sheet underlying endothelial cells throughout the cardiovascular system, and is mainly composed of intertwined networks of laminin, nidogen, collagen type IV and HSPG2. The main function of the basement membrane is to structurally support endothelial cells and separate them from tissue compartments. Disruption of basement membrane results in vascular bedding instability. It is also known that different combinations of isoforms of laminin, HSPG2, and nidogen in the basement membrane structure result in different functions. In fact, dynamic regulation of a single basement membrane molecule can have influence on endothelial cell proliferation, migration, and stability. [156,157]

In the gene network down-regulated genes associated with basement membrane, including laminin beta 1 (LAMB1), LAMA2, NID1, coupled with increased expression of Cathepsin S (CTSS) were identified in canine MMVD. Increased expression of cathepsin K and cathepsin S has been reported in human MMVD, and cyclic strain has been also shown to be associated cathepsin K expression in sheep mitral valves. [36,56] Since endothelial cells are suggested to be responsible for synthesis and deposition of basement membrane components, the current results might imply established endothelial damage and dysfunction due to mechanical stress and aging or valve endothelial cells locally dismantling basement membranes and acquiring a mesenchymal phenotype (EndoMT). [158,159]

In myxomatous mitral valves, marked endothelium denudation and exposure of basement membrane is found in severely affected mitral valves. [49] Collagen 6A3 (2.46-fold decreased) also serves as an anchorage between basement membrane and interstitial matrices, and both endothelial and interstitial cells are capable of collagen VI synthesis. Decreased production of collagen VI suggests detachment of endothelial and interstitial cells from the basement membrane. [157] In myxomatous mitral valves, breakdown of NID1, laminin, collagen and elastin by CTSS (2.27-fold increased) impairs basement membrane integrity and stability. [154] Instability of the basement membrane in MV allows endothelial cell migration or EndoMT.

Surprisingly, laminin expression in canine MMVD not only localized in the sub-endothelium, but also marginally presented at the periphery of myxomatous region. [48] The ectopic expression of basement membrane components may suggest an on-going re-organization of endothelial-interstitial matrix network.

Proteoglycan, HAS2, HAPLN1, CILP

Proteoglycans (PGs) are composed of a core protein with one or more covalently attached GAGs. Classification of PGs can be based on the nature of their GAG chains, HA (hyaluronan), CS (chondroitin sulfate), DS (dermatan sulfate), HS (heparan sulfate) and KS (keratan sulfate) or size. Certain members are considered as "small leucine-rich proteoglycan family" (SLRP) such as decorin, biglycan, fibromodulin, and lumican. PGs are a major component of the extracellular matrix and play a crucial role in many soft connective tissues, providing visco-elasticity and

resistance to compression and tension. PGs are also involved in many biological functions such as cell migration, differentiation, proliferation, and signalling. [160] In early atrioventricular valve development, PGs and GAGs are the main components. [70]

PGs (signal intensity) in normal and myxomatous mitral valves were the highest for any of the expressed transcripts. Lumican and versican were the top two PGs (signal intensity > 10,000), following by biglycan, decorin, and prolargin (signal intensity > 5,000). CHAD and KERA were the only significantly down-regulated PG genes. Chondroadherin is a leucine-rich repeat protein which mediates adhesion of isolated cells (mainly chondrocytes) using integrin α2β1 and interacts with extracellular matrix. [161] Degradation of CHAD has been observed in scoliotic intervertebral discs, and has been suggested to play role in cartilage homeostasis and degeneration. [162] Keratocan is a SLRP abundant in cornea and plays a pivotal role in organising extracelluar matrix assembly accounting for corneal transparency. [163] Grossly myxomatous mitral valves lose transparency as the disease develops, and down-regulation of KERA in MMVD might explain these findings. There is no information on CHAD and KERA expression in normal and myxomatous mitral valves, but in a proteomic study the SLRPs decorin and biglycan were found up-regulated in early-stage MMVD, but down-regulated in the late stage disease [164] In human MMVD, biglycan (protein), decorin (both mRNA and protein), and versican (protein) were found more abundantly expressed in myxomatous mitral valves compared with normal. [165,166] In the canine transcriptome there was no change in expression of the major PGs lumican, versican, decorin, and biglycan suggesting that cellular and structural changes in end-stage MMVD had no direct effect on PG genes expression. The variation of PG expression from different studies may suggest post-transcriptional and translational modification of PG mRNA and proteins.

Adhesion molecules

The expression of cell adhesion molecules (CAMs) such as ICAM-1, PECAM-1 (CD31), E-selectin (SELE), and VCAM-1 by endothelial cells has been shown to play important roles in immune cell trafficking and CAMs expression can also be

stimulated by inflammatory cytokines such as interleukins, TNF-α, and IFN-γ. [167,168] In MMVD there is no inflammatory cell infiltration reported and this has been confirmed in this study. [12] Interestingly, increased expression of inflammatory cytokines with absence of inflammatory cells in canine MMVD are likely to be canine-specific as these are not reported in any human MMVD transcriptomic studies. [106,114,115] In the signal intensity analysis, ICAM-1, PECAM-1, E-selectin and VCAM-1 were screened. The expression of PECAM-1 was the highest (signal intensity > 3,000), and there was higher expression of SELE in MMVD valves. One study has also shown strong expression of E-selectin as well as VCAM-1 in myxomatous mitral valve. [168]

There are two layers of endothelial cells covering the atrial and ventricular sides of mitral valves. Between every endothelial cell, vascular endothelial cadherin (VE-cadherin) is the major component of adherens junction, and it binds via its cytoplasmic domain to cytoskeletal proteins. Its functions include controlling closure and opening of the cell-cell endothelial adherens junctions, cell motility, and maintaining vascular permeability and integrity. VE-cadherin also plays a role in cell-cell signal transduction through intracellular partners such as p120, β-catenin, and plakoglobin. [167] The two major cadherins expressed by vascular endothelial cells are VE-cadherin (CDH5, CD144) and neuronal cadherin (N-cadherin, CDH2). [167] In the current microarray data, high expression of four cadherins was identified, including CDH13 (T-cadherin, heart, signal intensity > 3,000), CDH11 (OB-cadherin, osteoblast, signal intensity > 2,000), CDH5 (VE-cadherin, vascular endothelial, signal intensity > 1,000), and CDH2 (N-cadherin, neural, signal intensity > 500). Unlike VE-cadherin and N-cadherin, where their localization is limited to the cell junction controlling intercellular adhesion, T-cadherin is equally distributed over the entire cell surface or concentrated at the leading edges of migrating cells, and this lack of transmembrane domain may suggest its role as migratory molecules rather than a true adhesion molecule. [169] Experimentally overexpression of T-cadherin in endothelial cells and smooth muscle cells promotes spontaneous cell migration, formation of stress fibres, and phenotype alteration from quiescent to pro-migratory. [170] In cardiovascular disease, higher expression of H-cadherin has been found in atherosclerotic lesions in aorta, and it may be due to its identity as another LDL-

receptor, which signals through ERK1/2 and promotes cell proliferation and migration. [171]

Phosphorylation and partial internalization of VE-cadherin weakens the intercellular junctions, and reduces endothelium permeability. However, down-regulation of VE-cadherin through NOTCH-SNAI1 or TGF-β signalling permits endothelial migration and EndoMT (Figure 3-35). [86] In the current study, NOTCH1 was down-regulated, but the transcriptional factor RBPJK up-regulated in the transcriptome suggesting there may be a NOTCH-independent SNAI1 signalling pathway in MMVD.

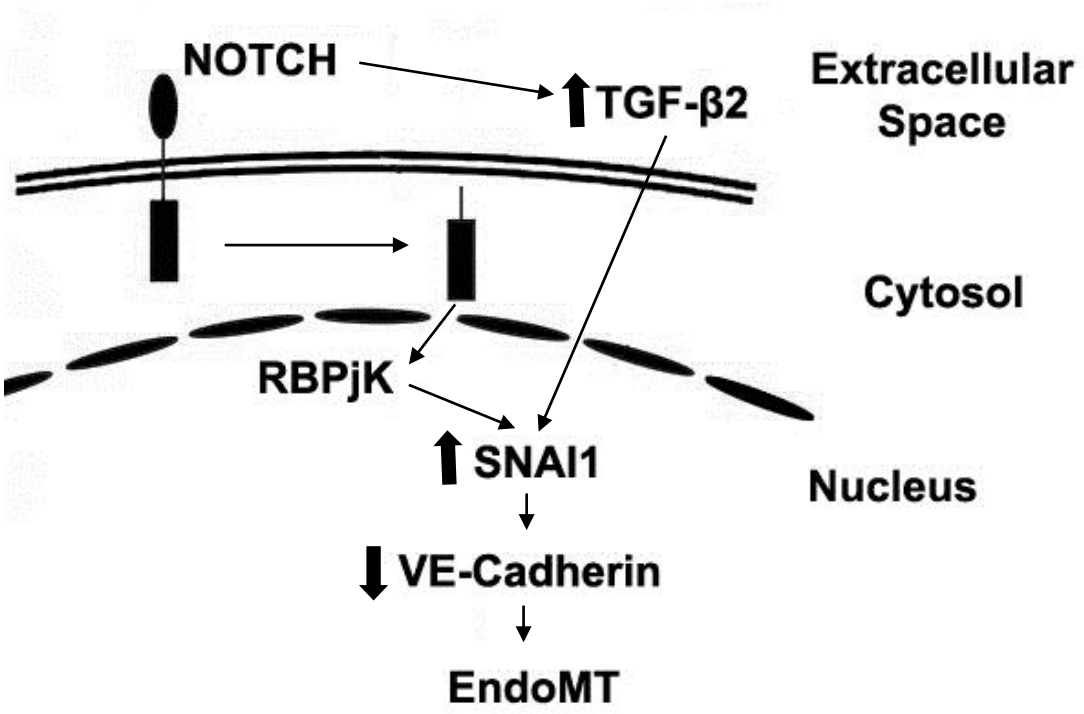

Figure 3-35 Model for NOTCH and TGF-β Superfamily Signalling in EndoMT. NOTCH signalling raises the level of TGF-β2. TGF-β2 also increases the activity of the transcription factor SNAI1. Increased SNAI1 expression results in down-regulation of VE-cadherin. Down-regulation of VE-cadherin may be the initial event in the activation of EndoMT. NOTCH signalling may also trigger SNAI1 independent of TGF-β signalling. Modified from [86].

Cadherin-11 (CDH11) is a cell-cell adhesion protein mainly expressed at the junction between the mesenchyme and the osteoblasts, and it also participates in mesenchymal-to-osteochondral differentiation. [172] CDH11 has been showed to be expressed in endocardial cushion (both endocardial and mesenchymal cells) during valve development, and the expression becomes more restricted to endothelial cells in late valve remodelling. [172] In an aortic valve interstitial cell model, Hutchson has demonstrated myofibroblastic differentiation (increased α-SMA expression) of aVIC along with up-regulation of CDH11 by TGF-β1. In the same study, calcified aortic valve leaflets also showed increased co-expression of α-SMA and CDH11 in lesion sites.[173] Compared with human aortic calcification, high but unchanged expression of CDH11 in canine MMVD may suggest an uninterrupted stimulation which maintains baseline osteochondral phenotype of valve interstitial cells.

Fibronectin is a multi-domain glycoprotein, and is found in extracellular matrix and basement membrane. Fibronectin binds to collagen I, II, and III, and interacts with hyaluronan and heparan sulphate, which strengthens the fibrillar adhesion to cells. In addition, fibronectin also plays an important role in cell adhesion and migration. [174–176] Functions of fibronectin in valve tissue remain largely unknown. In a wounding model (porcine mitral valve interstitial cells), there was expression of fibronectin at the wound edge by valve interstitial cells and this was associated with prominent fibrillar adhesions composed of α5β1 integrin (ITGA5 and ITGB1), suggesting its role in cell migration. [176] Realignment of extracellular fibronectin fibrils was also demonstrated to be associated with myofibroblast activation by TGF-β. [127] Expression of fibronectin has been reported in canine normal (sub-endothelium and fibrosa) and myxomatous mitral valves (sub-endothelium and periphery of myxomatous areas). [48] Fibronectin mRNA level was unchanged in the present study and its association with myofibroblast activation in myxomatous mitral valves remains to be elucidated.

EndoMT

In heart development, EMT (epithelial-to-mesenchymal transition) plays a key role in endocardial cushion formation (Type I), whereas in adulthood, EMT plays a role in fibrosis (Type II EMT) and tumour malignancy (Type II EMT). [1] EndoMT is a

subcategory of EMT, where cells switch from an endothelial to mesenchymal phenotype during the early stages of valvulogenesis and in myocardial fibrosis. In the transcriptomic profiling, an expression pattern suggestive of EndoMT was recognised, and this included differential expression of genes associated with basement membrane components, mesenchymal differentiation, and NOTCH signalling (Table 3-36). Briefly, there was a phenotypic transition into a mesenchymal phenotype in MMVD, which was represented as increased expression of mesenchymal markers, such as SM22 (TAGLN), and γ-SMA (ACTG2). The mesenchymal transition might be triggered by up-regulation of TGF-β superfamily members and their receptors (BMP6 and BMPR1). With the decreased expression of basement membrane components (NID1 and LAMA2) and increased expression of basement membrane lytic enzyme (CTSS), basement membrane disruption would permit migration of transitioned endothelial cells. The up-regulation of hyaluronic acid synthase 2 (HAS2) would allow production of the hyaluronic acid rich sub-endothelial matrix necessary for EndoMT. This process will be discussed more detail in Chapter 5.

Table 3-36. Differentially expressed genes associated with EndoMT.

Category	Gene	Fold-Change	p-value	Signal intensity	
				Control	MMVD
Basement membrane	Nidogen 1, NID1	-3.08	0.0004	1645	467
	Laminin 2, LAMA2	-5.15	0.0011	365	69
	Cathepsin S, CTSS	2.26	0.0001	1405	3310
Mesenchymal Differentiation	Myosin heavy chain 11, MYH11	4.93	0.0050	80	438
	Transgelin, TAGLN, SM22	2.39	0.0042	1635	3994
	Smooth muscle actin γ, ACTG2	15.35	0.0031	73	1473
TGF-β & superfamily Signalling	Bone morphogenic protein 6, BMP6	2.38	0.0006	293	755
	Bone morphogenic protein receptor 1 B, BMPR1B	2.20	0.0038	197	424
	β-catenin, CTNNB1	1.38	0.0037	1866	2642
	Hyaluronic acid synthase 2, HAS2	2.18	0.0001	417	934
NOTCH Signalling	NOTCH1	-2.33	0.0001	545	247
	RBPJ	1.60	0.0034	1401	2312
	NFATC1	-1.87	0.0036	908	517
	NFATC2	-2.13	0.0066	329	159

Study Limitations

There are several limitations to this study. Mitral valve tissues collected for diseased and control group have distinct age difference where MMVD valves were sampled from old dogs and control valves were sampled from young dogs. In addition, control mitral valves (Beagles) and diseased mitral valves (CKCSs) were collected from two breeds. Though breed-specific pathogenesis may exist, studies in Chapter 2 suggest that similar cellular changes and pathology could be found among different breeds. The total RNA was extracted from a heterogeneous population of cells from normal and myxomatous mitral valves, and the pooling of mRNA from cells with different phenotypes may decrease the expression variation of one gene; RNA profiling was a snapshot at two time points (normal and end-stage disease) and the genomic map and the discovered gene sets might be a reflection of difference in the tissue functioning over time, rather than initiators of myxomatous degeneration (cause or effect). *In silico* analysis of gene-gene interaction are based on databases derived from published literature (different experimental settings such as different cells and tissues used for modelling), and the gene networks may not necessarily represent the real relationship between genes in MMVD. Epigenetic control over gene expression such as microRNAs silencing mRNA could always be a factor for post-transcriptional modification, such that the transcriptional level will not completely represent the amount of protein translated, and will not always be representative of the end biological function. However, low or no expression of mRNA generally means low or no expression of the protein. The exception would be that some proteins have long half-lives, and they may be present when mRNAs are absent.

While this is the first breed-specific transcriptional profiling in canine MMVD, age-matched diseased-free control samples are nearly impossible to obtain. Aging itself is an important factor in canine MMVD, and it is impossible to tell MMVD valves from elderly CKCS are genetically similar. Thus, low grade (Whitney) and age-matched mitral valves from CKCS may serve a better control samples. Since ECM deposition and lamination in valve tissues are regulated by multiple genes in short time spans it would be necessary to investigate dynamic transcriptional control of ECM turnover and coordination with cellular events during the progression of

MMVD. [82] Lastly, there were a number of unannotated canine transcripts in the data sets, but seasonal updates for annotations can allow future re-analysis.

Microarray data can be influenced by the biological system of interest and technical artefacts. Traditional methodologies of microarray analysis focused on identifying statistical differences (FDR, fold-change, and p-value) between groups of samples, and manipulating the cutoff setting can greatly affect the final gene list for data mining. BioLayout *Express*^{3D} shows inter-individual variability which would influence averaged expression values and traditional fold-change values. This is consistent with the PCA result which placed one MMVD value sample close to control samples (3.3.2). Analysis through signal intensity value gave an impression of expression level, which allowed identification of a trend in genes of interest. However, there was no significant difference between normal and MMVD valves for some of the genes associated with EndoMT. This could be attributed to the variability of the samples which resulted in high standard deviation. The intragroup variability of the myxomatous valves could also be due to the different stages of degeneration, and these could not be identified grossly. Having evaluated the role of variability in reducing the power to detect significant differences, there were many differences that were not significant that warrant further investigation as they may be false negatives resulting from the lack of power.

In conclusion, the characterization of MMVD identified by transcriptomic profiling and analysis included inflammation, cell movement, development, extracellular matrix organization and EMT. LDL signalling was also identified as an un-expected upstream regulator of differentially expressed genes. Two canonical pathways associated with endothelial functions identified were alveolar-mediated endocytosis and endothelin signalling, supporting a role for the endothelium in MMVD. Signal intensity analysis identified genes involved in extracellular matrix components, EndoMT, and valve development. There were patterns of gene expression consistent with weakening of ECM networking, disruption of basement membranes, increased cell migration potential, active endothelial differentiation and myofibroblastic differentiation in MMVD compared with normal mitral valve.

4 Chapter 4 Analysis of Gene Expression in MMVD by Quantitative Polymerase Chain Reaction (Q-PCR)

4.1 Introduction

Q-PCR has been favourably used as a technique to validate microarray data for a decade in numerous high-throughput transcriptomic studies. [177] One study showed marked quantitative concordance between Q-PCR and microarray when the candidate genes are high in signal intensity (spot intensity) and with low variability. [178] This is considered as "high-quality" microarray data and rarely requires validation. However, a major drawback of microarrays is the narrow dynamic range for differentiating the genes with weak signals due to background noise interference, whereas Q-PCR has wider dynamic range and is capable of detecting differential expression in less abundant genes. [178] In the same study, it was also suggested that up to 21% of genes in this category may be false negatives determined by microarray. This could also vary from sample to sample such as RNAs extracted from cell culture and tissue.

In this study, the aim was to validate microarray data from different groups of signal intensities that had been determined as differentially expressed by microarray. Two groups of genes were selected for Q-PCR. Group A were genes selected based on their signal intensity for validation. Group B were genes known to be involved in EndoMT which showed a trend of expression pattern in their signal intensities, but there was no statistical support for differential expression. In group A, a total of 15 candidate genes, which were initially identified by microarray analysis (out of total possible list of 5397 genes) were selected for validation, and were sub-divided into three groups based on their signal strengths as shown in Table 4-1.

Table 4-1 Classification of candidate genes for Q-PCR assays

Group	Criteria	Gene
Group A1	signal intensity for MMVD and control both < 512	LAMA2, MYH11, MMP12, ANGPT1
Group A2	signal intensity for MMVD and control both ≥ 512	ENG, CHAD, KERA, SOX9
Group A3	signal intensity for MMVD and control; one ≥ 512 and one < 512	COL6A3, HTR2B, BMP6, ADAMTS19, ACTG2
Group B	EndoMT associated gene not identified as differentially expressed by microarray	NOTCH1, HAS2, ACTA2, CDH5, SNAI1

4.2 Material and Methods

4.2.1 First-strand cDNA synthesis for Q-PCR

For each sample (3 controls and 3 MMVD RNA samples used for microarray analysis), 4 to 5 µg of total RNA was used for first-strand cDNA synthesis for Q-PCR. Total RNA, 1 µl of oligo $(dT)_{20}$ (Invitrogen), 1µl of 10mM dNTP MIX (10 mM each dATP, dGTP, dCTP and dTTP at neutral pH) (Invitrogen) and distilled water (to 13µl total volume) were added to a nuclease-free micro-centrifuge tube. The sample was heated at 65˚C for 5 minutes and incubated on ice for 1 minute. The content then was collected by a short centrifugation, and mixed with 4µl of 5x first-strand buffer (Invitrogen), 1µl of 0.1 M DTT (Dithiothreitol) (Invitrogen), 1 µl of RNaseOUT Recombinant RNase Inhibitor (Invitrogen), and 1 µl of SuperScript III RT (200 units/µl) (Invitrogen) were added to the micro-centrifuge tube. The content was mixed by gentle pipetting and incubated at 50˚C for 45 minutes, followed by heat inactivation at 70˚C for 15 minutes. The cDNA was used as a template for amplification in PCR, or stored at -20˚C for up to 2 months.

4.2.2 Q-PCR

Roche Universal Probe Library system (Roche Applied Science) in combination with the Roche Probe Master (Roche Applied Science) was used for Q-PCR. Six RNA samples used for microarray were validated by Q-PCR. Assays for 15 differentially expressed genes, 3 genes of interest (ACTA2, CDH5, and SNAI1 which were not differentially expressed) and one reference gene (Table 4-2) were designed as previously reported. [179]

Table 4-2 Primer Sequences for Microarray Data Validation by Q-PCR

Gene Name	Forward Primer	Reverse Primer	Probe No.
Microarray validation			
LAMA2	5'ccgcattgagctgacagtag3'	5'caaactggttgaggccatct3'	38
ENG	5'ggtgctcaagaaagacctcatc3'	5'gcaggacaaactggtcatctc3'	30
COL6A3	5'aaggaagcttcagcacaaaga3'	5'tgaactagaagccaaccttgc3'	39
HTR2B	5'ggtctggattacaaacagaatcg3'	5'tccctgttgctcaccagtct3'	6
MYH11	5'atgcagctggccaagaag3'	5'tctgagcaatttcatcatcgag3'	81
MMP12	5'ccaatttgagttttgatgctgt3'	5'cactgttctttggactctctgga3'	22
BMP6	5'tctccagcgcctcagattac3'	5'tggaagctcacatacagctca3'	4
ANGPT1	5'aggaaacgaaaagcagaactaca3'	5'atcagcaccatgtaagatcagg3'	18
CHAD	5'ccagtctttcggcagatacc3'	5'acatgtttcagtgtggtcacg3'	20
ADAMTS19	5'tcaaccctgcaatgagaaga3'	5'cgtatcactcggcagtacaca3'	14
ACTG2	5'ggtcatcaccattggcaac3'	5'tgaatcccagcagactccat3'	11
SOX9	5' ccaacgccatcttcaagg3'	5' ggagtgcacctcgctcat3'	63
KERA	5' gactatgcatgactttgactgtcc3'	5'tttcacagtataaagcagtagggaaa3'	29
HAS2	5'aggtgtcgggggagatgt3'	5'aaaagccatccagtatctcaca3'c	12
NOTCH1	5'gccaacaaagacatgcagaa3'	5'cttggcggtctcatagctg3'	63
Genes of interest (EndoMT)			
ACTA2	5'cggctactcctttgtgacg3'	5'cgtggccatctcgttctc3'	81
CDH5	5'tgcatcctcaccatcacagt3'	5'agctgctcgtggatctcg3'	4
SNAI1	5'caagatgcacatccgaagc3'	5'agcaggaaaacggcttctc3'	66
Reference Gene			
MRPS25	5'tcttggggaagaacaaggaa3'	5'agtgggctgggtgagaaag3'	15

Probe and Primer Design

For the candidate genes, corresponding canine cDNA sequences of the transcripts were found at Ensembl. [180] Briefly, the sequence was copied into Word (Office. Microsoft). Parentheses ([]) were inserted to represent introns in the sequence. The modified sequence was then copied into Assay Design Centre (Roche Applied Science) and the function of intron spanning assay strategy was enabled. Since canine is not a specified species in the Roche system, "Other Organism" was selected. Once all the parameters were correctly indicated, the primers were designed. The rules for assay designing were 1) closer to 5' end, 2) intron crossing, 3) sequence double-checked (BLAST). [181] The primers designed for microarray validation were LAMA2, ENG, COL6A3, HTR2B, MYH11, MMP12, BMP-6, ANGPT1, CHAD, ADAMTS19, ACTG2, SOX9, KERA, HAS2, NOTCH1, ACTA2 , CDH5, SNAI1, and the endogenous control gene MRPS25 was used for normalization. Primers (MWG Biotech) and probes (Universal Probe Library, Roche Diagnostics) were synthesized using locked nucleic acids with the 5′-end labelled with a reporter fluorescein dye (FAM, 6-carboxy fluorescein) and 3′-end labelled with a dark quencher dye.

Q-PCR Assay Set-up

Primers were dissolved in the suggested volume of water to create a concentration of 100 pmol/µl. Q-PCR assays were performed in triplicate in 96-well plates with one no-template-control (RNase-free water) for each sample. Occasionally Q-PCR reactions were performed in duplicate with one no-template-control due to the limited sample volume. For each well, the reaction mix consisted of 0.1 µl sequence specific probe (Universal Probe Library, Roche), 0.2 µl primers (100 pmol/ µl), 5 µl of 2x master mix (Roche Diagnostics), and 4.7 µl of first strand cDNA (200 – 400 ng/ µl). After reaction mix and the cDNA were separately pipetted into the designated wells (Table 4-3) the plate was sealed with adhesive PCR film (Thermo Scientific) and wrapped with tin foil to protect it from light. The plate was then vortexed for sufficient mixing of the reagents and centrifuged at 15,000 rpm (Eppendorf Centrifuge 5810R with plate holder) for 5 minutes at 4℃. The plate then was unwrapped and placed into the PCR machine (LightCycler 480; Roche

Diagnostics). The amplification was programmed and performed according to a standard PCR cycle (Table 4-4).

Table 4-3 Plate design for Q-PCR

	Control				Diseased			
LAMA2	cDNA + RM	cDNA + RM	cDNA + RM	NTC	cDNA + RM	cDNA + RM	cDNA + RM	NTC
COL6A3	cDNA + RM	cDNA + RM	cDNA + RM	NTC	cDNA + RM	cDNA + RM	cDNA + RM	NTC
MRPS25	cDNA + RM	cDNA + RM	cDNA + RM	NTC	cDNA + RM	cDNA + RM	cDNA + RM	NTC

*For each well, 5.3µl reaction mix (RM) and 4.7 µl cDNA made up 10µl reaction volume. NTC, no template control.

Table 4-4 Standard protocol for Q-PCR

Action	Temperature	Time	Cycle
Pre-incubation	95℃	10 minute	
Amplification	95℃	10 second	45
	60℃	30 second	
	72℃	1 second	
Cooling	40℃	30 second	1

The result for each well was presented as crossing point (C) and threshold value at a constant level of fluorescent signal. Q-PCR data were analysed using LightCycler 480 Basic Software (Roche Diagnostics). The endogenous control (MRPS25) was used for normalization, and the relative expression level was calculated following the ΔCt Method (the comparative Ct). Mann–Whitney *U* test was used for statistical analysis on the ΔCt values between diseased group and control group.

The equation for calculating relative expression (R):

$$R = 2^{-[Ct\ sample - Ct\ control]}$$

$$R = 2^{-\Delta Ct}$$

Theoretically, for the comparative Ct method to be valid, the efficiency of the target amplification (genes of interest) and the efficiency of the endogenous control (reference gene) amplification should be approximately equal. Therefore, efficiency tests for all primers were performed. Briefly, cDNA samples were serially diluted to create a sequence of [1], [1:10], and [1:100] for the standard curve, and the plate for Q-PCR was allocated as shown in Table 4-5. In general, the acceptable value for efficiency rate should be within 90% to 110%. Examples of the efficiency rate (E) calculation for MRPS25 are shown in Table 4-6 and Figure 4-1.

Table 4-5 Plate design for primers efficiency rate test

Primer 1			Primer 2			Primer 3			Primer 4		
1	1	1	1	1	1	1	1	1	1	1	1
1:10	1:10	1:10	1:10	1:10	1:10	1:10	1:10	1:10	1:10	1:10	1:10
1:100	1:100	1:100	1:100	1:100	1:100	1:100	1:100	1:100	1:100	1:100	1:100

Table 4-6 Q-PCR Cp value and input concentration for MRPS25

Name	log(Con.)	Cp	Con.
MRPS25	0	23.88	1
MRPS25	0	23.91	1
MRPS25	0	23.98	1
MRPS25	-1	27.08	0.1
MRPS25	-1	27.20	0.1
MRPS25	-1	27.13	0.1
MRPS25	-2	30.52	0.01
MRPS25	-2	30.25	0.01
MRPS25	-2	30.31	0.01

*Con. = concentration

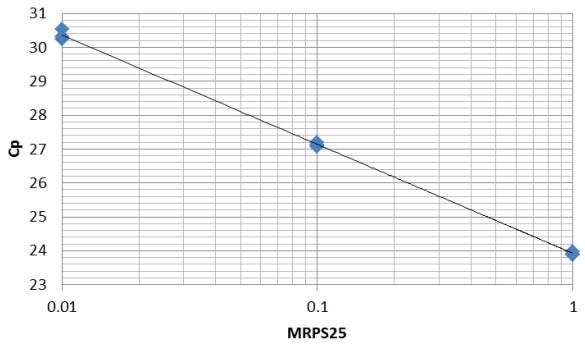

Y axis = Cp value

X axis = cDNA input (dilution)

SLOPE = -3.21833

POWER = (10,-1/SLOPE)) = 2.045

E = 100*(POWER-1) = 104.51

Figure 4-1 Example of Q-PCR efficiency rate calculation (MRPS25)

4.2.3 Statistical Analysis

Considering the very small sample size in this study (control n=3, disease n=3), normality testing was not conducted and non-parametric tests provided no power. Student's t-test was used to compare the relative expression (R) between the two groups. P-value less than 0.05 was considered significant.

4.3 Results

4.3.1 Primer Efficiency Rates

Efficiency rates for primers were determined prior to PCR reaction, and are summarized in Table 4-7. For 16 of 19 primers (including the house-keeping gene: MRPS25) efficiency rates were between 90% and 110%. However, there were three primers (MYH11 = 89.79%, KERA = 116.31%, and HAS2 = 128.48%) that were not within the ideal range (Figure 4-2).

Table 4-7 Efficiency rate for primers

Gene Name	Probe No.	Efficiency Rate	Gene Name	Probe No.	Efficiency Rate
LAMA2	38	96.45	ACTG2	11	93.92
ENG	30	95.36	SOX9	63	108.19
COL6A3	39	99.52	KERA	29	116.31
HTR2B	6	95.10	HAS2	12	128.48
MYH11	81	89.79	NOTCH1	63	103.76
MMP12	22	93.86	ACTA2	81	102.00
BMP6	4	96.06	CDH5	4	109.31
ANGPT1	18	97.10	SNAI1	66	93.06
CHAD	20	100.22	MRPS25	15	104.51
ADAMTS19	14	95.87			

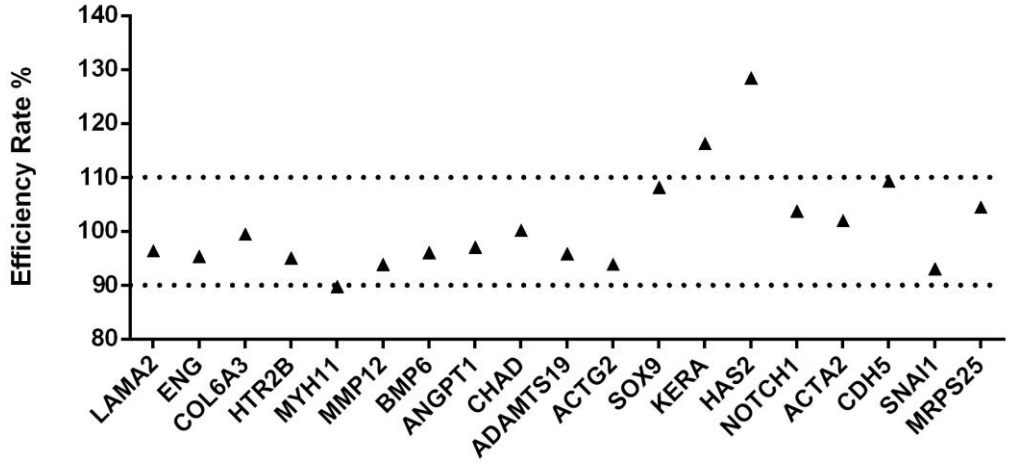

Figure 4-2 Primer efficiency rate for 19 designed primers. The primers for MYH11, KERA, and HAS2 are out of ideal range (90% - 110%)

4.3.2 Microarray Data Validation by Q-PCR

Microarray data validation was conducted by Q-PCR assays for 15 differentially expressed genes. Although there were differences in the magnitude of expression level, the trends of expression for each gene were generally in agreement with the microarray result (Figure 4-3). Thirteen genes (LAMA2, ENG, COL6A3, HTR2B, MYH11, MMP12, BMP6, ANGPT1, CHAD, ADAMTS19, ACTG2, KERA, and NOTCH1) were significantly and differentially expressed and did not conflict with the microarray result (Table 4-8). However, there was no difference for the expression of SOX9 ($p = 0.41$) and HAS2 ($p = 0.15$) in the Q-PCR assay, conflicting with the microarray results.

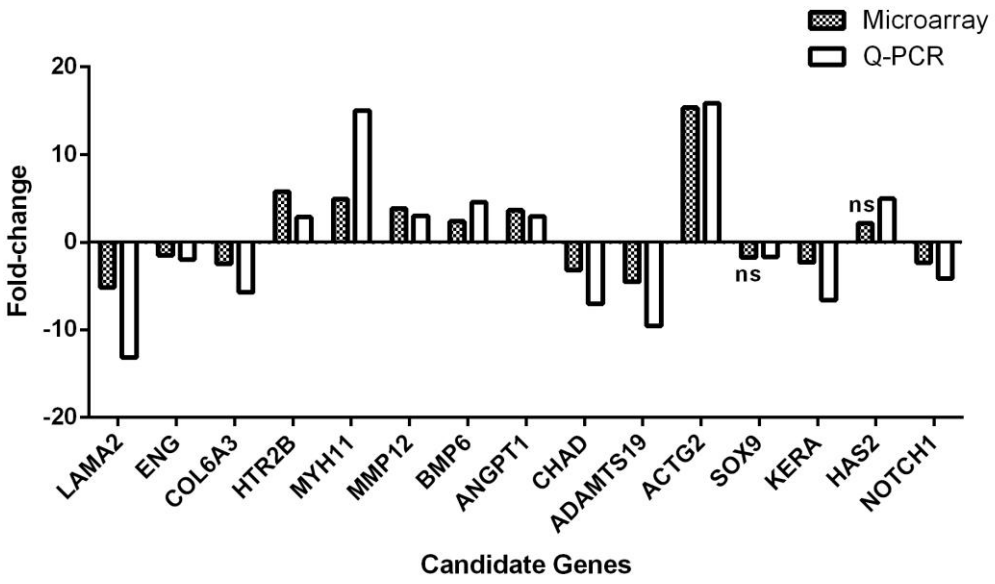

Figure 4-3 Fold changes for differentially expressed genes determined by microarray and validation by Q-PCR. ns = not significant.

Table 4-8 Microarray data compared with Q-PCR validation

Gene	**Microarray** Fold-Change	**Q-PCR** Fold-Change	**Q-PCR** p-value
LAMA2	-5.15	-13.18 ± 1.35	0.0005
ENG	-1.52	-1.98 ± 1.13	0.0033
COL6A3	-2.47	-5.72 ± 1.17	0.0004
HTR2B	5.78	2.87 ± 1.39	0.0170
MYH11	4.93	15.03 ± 2.62	0.0151
MMP12	3.82	3.01 ± 1.07	0.0021
BMP6	2.38	4.57 ± 1.50	0.0116
ANGPT1	3.65	2.93 ± 1.52	0.0218
CHAD	-3.17	-7.04 ± 1.81	0.0048
ADAMTS19	-4.52	-9.52 ± 1.76	0.0023
ACTG2	15.35	15.87 ± 2.25	0.0053
SOX9	-1.73	-1.66 ± 2.54	0.4186
KERA	-2.29	-6.61 ± 1.47	0.0012
HAS2	2.18	4.96 ± 2.14	0.1539
NOTCH1	-2.33	-4.12 ± 0.55	0.0001

Fold-change for Q-PCR = Mean ± S.D.

4.3.3 Q-PCR for Genes Related to EndoMT

Q-PCR assays for three genes (ACTA2, CDH5, and SNAI1) were found to be differentially expressed ($0.01 < p < 0.05$) between MMVD and control samples, with ACTA2 and SNAI1 up-regulated, and CDH5 down-regulated in myxomatous mitral valves (Table 4-9). The expression patterns for these 3 genes were also in agreement with their microarray signal strengths.

Table 4-9 Microarray validation by Q-PCR (ACTA2, CDH5, and SNAI1)

Gene	Fold-change	p-value	Signal Intensity (Median)	
			Control	MMVD
ACTA2	10.66 ± 1.23	0.027	329	1857
CDH5	-2.59 ± 0.70	0.029	1630	877
SNAI1	4.80 ± 0.31	0.045	162	419

Data presented as Mean ± standard deviation

4.4 Discussion

Overall, Q-PCR provided consistent result in the trend (up- or down-regulated) of gene expression in all candidate genes in Group A and Group B, but 2 genes (SOX9 and HAS2) in Group A showed no evidence of differential expression ($p > 0.05$).

In Group A, all the candidate genes belonging to A1 (low-low signal intensity) were in agreement with the microarray data, and this suggests robust data can be obtained even when genes have weak signal strengths (< 512) and high intragroup variability. However, SOX9 in Group A2 and HAS2 in Group A3 were found to have no difference in gene expression, and these findings were most likely due to primer efficiency issues, in which the primer for SOX9 was 108.19% (<110%, borderline) and HAS2 was 128.48% (>110%, overly exceeding optimal limit). No additional samples were available to allow further Q-PCR assays under better primers design. Because of these technical issues and because two genes were classified as Group A2

(high-high) and A3 (high-low or low-high) where the signal intensities between control and diseased groups were clear, it is reasonable to give priority to the microarray findings over the Q-PCR results.

In Group B, the trends for expression of 3 genes (ACTA2, CDH5, and SNAI1) associated with EndoMT were determined by looking at their individual signal intensities. However, they were not classified as differentially expressed genes by microarray due to their high intragroup signal strength variability (Figure 3-33, 3-24, 3-29 respectively). Q-PCR results suggested that the three genes were significantly differentially expressed (at $0.01 < p < 0.05$) comparing MMVD and control mitral valves. The reason why these genes were not discovered in the microarray may be due to the limited dynamic range of microarray analysis. Due to the large number of test conducted, it can be argued the p-value < 0.05 was not sufficiently stringent to claim significance using Q-PCR platform, and all three genes should have not be described as differentially expressed (Table 4-9). It is less biased to analyse the raw genomic expression profile (3.3.6 and 3.3.7) as a trend by platforms such as BioLayout *Express*^{3D} rather than on processed fold-change. To discover the accurate genomic expression of these genes, recruiting more samples in both groups and repeating Q-PCR assays with better designed primers is required.

The genomic expression at transcriptional level is not always equal to the translational level (protein) due to post-transcriptional modification mechanisms such as miRNAs silencing, and the fold-change difference on RNA expression does not necessarily represent true difference biological function in vivo. It is necessary to conduct protein quantification to validate if these mRNAs were translated into protein. Finally, since both microarray and Western Blotting are screening global mRNA and protein concentration from a heterogeneous cell population in mitral valves, performing immunohistochemistry (localization and qualitative study) would provide valuable information.

One challenge that limited the experimental design is the small sample size of the mitral valve tissues collect from small breed dogs. Generally, anterior mitral valve leaflet was mainly used for RNA extraction (microarray and Q-PCR), and posterior mitral valve leaflet was PFA-fixed for IHC. Though the myxomatous lesion could be

found all over the two leaflets, it would be ideal to collect tissues for RNA isolation, protein extraction, and PFA-fixed section from the same anatomical location.

5 Chapter 5 Reactivation of developmental pathways in Canine Myxomatous Mitral Valve Disease

5.1 Introduction

Johannes Holtfreter in the 1920s and Elizabeth Hay in the 1960s, and many others, identified epithelial-to-mesenchymal transition (EMT; Type 1) as being fundamental to embryo formation and differentiation. EMT, and its reverse MET, explains a process of cell phenotypic plasticity that not only allows organ development, but also may have a role in disease pathogenesis. [182] More recently the recognition of the role of EMT (Type 2 inflammatory) in conditions such as chronic fibrosis (renal, skin, cardiac, lung etc) and tumour malignancy (Type 3) not only helps to explain disease pathogenesis, but also identifies potential therapeutic targets. [1] The analogous process of EMT in heart valve development is EndoMT. The valve endothelium is a specialised form of squamous epithelium and can give rise to the analogous forms of the three types of EMT described above. In early valve development, endothelial cells lining the primitive heart tube at the sites close to where the atrio-ventricular (A-V) canal and outflow tract develop undergo EndoMT and invade the cardiac jelly and form the endocardial cushions. The A-V cushion eventually contributes to development of the mitral and tricuspid valves and is derived predominantly through EndoMT. The initiation of EndoMT is closely regulated by several growth factor-mediated signalling pathways including VEGF, TGF-β, BMP and NOTCH. [65] The mesenchymal cells that form VICs then contribute the extra-cellular matrix of the developing valve through to adulthood. In the adult valve it is presumed that VICs are predominantly quiescent or contributing to low level life-long valve remodelling, but during MMVD the VICs become activated, produce catabolic enzymes and contribute to matrix destruction and mechanical valve failure. [48,56,114,183] The exact mechanism by which these cellular changes occur is unknown, but one possible explanation is that it is a re-manifestation of EndoMT; a situation where developmental biology pathways designed to make the valve in the first place are now contributing to its destruction.

Important to valve formation from the endocardial cushion is the presence of cardiac jelly, which is mainly composed of the glycosaminoglycan hyaluronan (HA; hyaluronic acid) and is initially produced from the adjacent myocardium through the activity of HAS2. [80,83] The accumulation of HA causes expansion of the extracellular space and the HA-rich environment favours migration of transformed endothelial cells, and induces PI3K and ErbB2/3 signalling that promotes cell proliferation. In cultured embryos, disruption of HA synthesis prevents endocardial cushion formation. [85]

On the cellular level, endocardial endothelial cells undergo phenotypic transition by losing endothelial phenotype markers such as platelet endothelial cell adhesion molecule (PECAM-1, CD31), and VE-cadherin and begin to express the mesenchymal marker α-SMA. Their migratory ability is also obtained by losing cell-to-cell contact (loss of VE-cadherin) and secreting matrix metalloproteinases (MMPs, collagenases) which degrade the endocardial basal lamina. At the endocardial cushion, EndoMT contributes to the mesenchymal cells by the migration of the transformed endothelial cells into the underlying HA and chondroitin sulfate-rich cardiac jelly.

There is also evidence from other diseases that EMT can contribute to disease pathogenesis. Chronic fibrotic conditions and cancer are the best examples, and in the case of cardiovascular disease, at least in mouse models of myocardial fibrosis, EMT and EndoMT have both been implicated. This is not necessarily surprising considering 1/3 of cardiac fibroblasts in mouse myocardium are of endothelial origin. [2] In the case of myocardial fibrosis the process appears to be driven by the TGF-β signalling pathway, which is also up-regulated in human MMVD although this was not observed in the current study of canine MMVD (Chapter 3). [61,184]

Myxomatous degeneration results in destruction of the valve fibrosa and expansion of the spongiosa. In the advanced stages of the disease the distal leaflet lacks structure and the stroma primarily consists of glycosaminoglycans. [51] To that extent the valve structure somewhat resembles embryonic mesenchyme. At the same time there is evidence of endothelial cell loss and activation with accumulation of α-SMA and SMemb positive cells close to the endothelial surface. [38,49,52] The contribution of

complex developmental signalling pathways to MMVD pathogenesis has been recently suggested. [65] Since osteogenesis and chondrogenesis can be identified in aortic and mitral valves this would be further evidence that development signalling pathways are activated in different chronic valvulopathies. [65,185,186] Suggested possible candidate signalling pathways include BMP-Sox9, Wnt and NOTCH. [65]

In the chapter 3 and 4, differentially expressed genes indicating myofibroblastic differentiation, basement membrane disruption, and remodelling of endothelial adherens junctions were identified. The biological functions of these genes might suggest potential EndoMT in MMVD. However, data are limited to the transcriptional level and the cellular and tissue distributions of the encoded proteins are unknown. This study investigated evidence of EndoMT in MMVD by localizing expression of key EndoMT markers including α-SMA, CDH5, SNAI1, and HAS2.

5.2 Material and Methods

5.2.1 Tissue Sample

Myxomatous (n=14) and normal (n=12) mitral valves were collected from a population of mixed breed and age dogs, and Cavalier King Charles Spaniels presented to the Hospital for Small Animals, Royal (Dick) School of Veterinary Studies, the University of Edinburgh or from Beagles from Charles River Laboratories, Tranent, UK. The mitral valve tissue collection followed the same procedure described in **2.2.1.** Detail information of all samples is shown in Table 5-1.

Table 5-1 Detail information of mitral valve samples

ID	Breed	Age	Sex	MMVD Grade	MMVD Group
Myxomatous Mitral Valve n=14					
2010/01	CKCS	7y	Male	3	Severe
2009/59	CKCS	10y	Unknown	4	Severe
2009/51	CKCS	Unknown	Male	3	Severe
2009/50	CKCS	11y	Female	3	Severe
2009/41	CKCS	10y	Male	3	Severe
2009/33	CKCS	Unknown	Unknown	4	Severe
2011/01	CKCS	10y	Female	3	Severe
2009/07	CKCS	Unknown	Unknown	3	Severe
2011/02	CKCS	13y	Female	3	Severe
2010/07	Labrador Retriever	6y	Male	2	Mild
2010/10	Terrier X	9y	Male	2	Mild
2011/33	Border Collie	5y	Male	2	Mild
2012/17	Mongrel	3y	Female	3	Severe
2012/23	Mongrel	4y	Male	1	Mild
Control Mitral Valve n=12					
2013/02	Beagle	1y	Female	0	Normal
2013/01	Beagle	1y	Female	0	Normal
2013/03	Beagle	1y	Unknown	0	Normal
2012/03	Beagle	1y	Unknown	0	Normal
2012/07	Beagle	1y	Unknown	0	Normal
2013/04	Beagle	1y	Female	0	Normal
2013/08	Beagle	1y	Male	0	Normal
U82	Beagle	5y	Female	0	Normal
2011/29	Mongrel	5y	Male	0	Normal
2012/22	Mongrel	2y	Unknown	0	Normal
2011/15	Mongrel	1y	Female	0	Normal
2011/16	Mongrel	1y	Male	0	Normal

5.2.2 Immunohistochemistry

Please refer to 2.2.3. Antibodies used in this chapter are summarized in Table 5-2.

Table 5-2 Antibodies and working concentration used in this study

Name	Clonality	IHC	Made	Cat. No.
Primary Antibody				
α-SMA	Ms monoclonal	1:400	Sigma	A2547
CDH5	Rb polyclonal	1:50	Abcam	Ab33168
HAS2	Rb polyclonal	1:50	Abcam	Ab168816
SNAI1	Rb polyclonal	1:200	Santa Cruz	A1509
Secondary Antibody				
Alexafluor 488	Goat anti-Ms IgG (H+L)	1:100	Invitrogen	A10667
Alexafluor 568	Goat anti-Rb IgG (H+L)	1:100	Invitrogen	A11011
Biotinylated Antibody	Goat anti-Rb IgG (H+L)	1:1000	Vector	BA-1000

*Abbreviation: H+L, heavy and light chain. Ms, mouse. Rb, rabbit.

For each dog, a minimum of four sections were examined for each antibody. Positive controls included canine skin and duodenum, and for negative controls the primary antibody was omitted.

5.2.3 Image capture and Statistical analysis

Images were taken using a light microscope with fluorescent filters (Leica-DMLB). Tile-scanning was performed using a Zeiss LSM-710 confocal microscope. Semi-quantitative analysis of staining was graded as: 0, no staining; 1 mild <30% of cells; 2 marked between 30% and 60% of cells; 3 diffuse and strong >60%. MMVD valves and controls were blindly graded at distal and middle portion (negligible myxomatous changes) as shown in Figure 5-1. The Mann-Whitney test was used to compare the semi-quantitative value between the two groups. P-value less than 0.05 is considered significant. Qualitative and semi-quantitative assessment was carried out on the NovaRed stained (2.2.3) sections (HAS2). Fluorescent double-labelled sections (α-SMA/CDH5, α-SMA/HAS2, and α-SMA/SNAI1) were examined qualitatively.

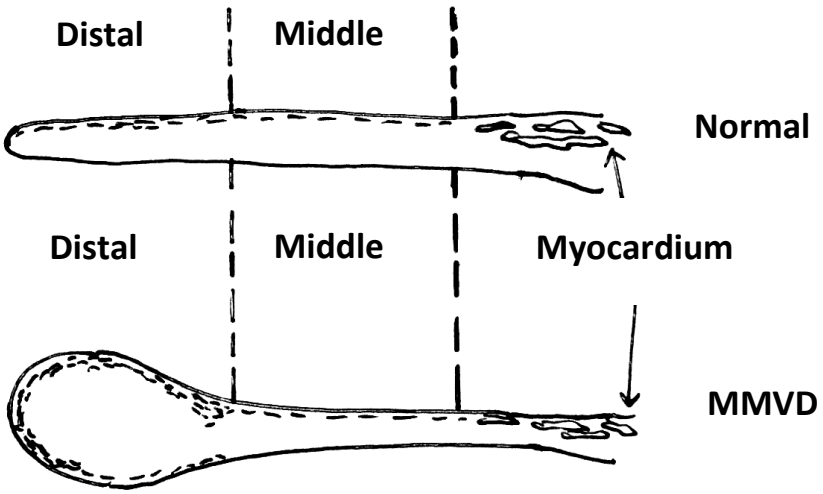

Figure 5-1 Representative image showing distal and middle portion of normal and MMVD valves.

5.3 Results

5.3.1 Spatial and Temporal Distribution of Activated Myofibroblasts in MMVD and Normal MV

All tile scanning images were orientated in a similar way, with atrial side upward and edge of the mitral valve leaflet towards left (Figure 5-2).

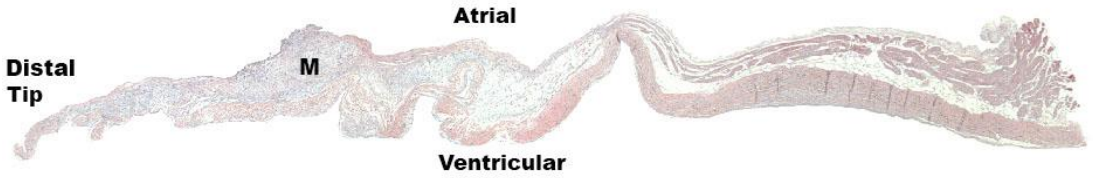

Figure 5-2 Orientation of the confocal microscopy images. M = myxomatous region

In the normal mitral valves no α-SMA positive cells were observed at the leaflet tip. However, in most normal mitral valves, there was a single layer of myofibroblasts in the mid-zone at the atrial side of the leaflet, and no α-SMA staining was noted on the surface of ventricular side (Figure 5-3).

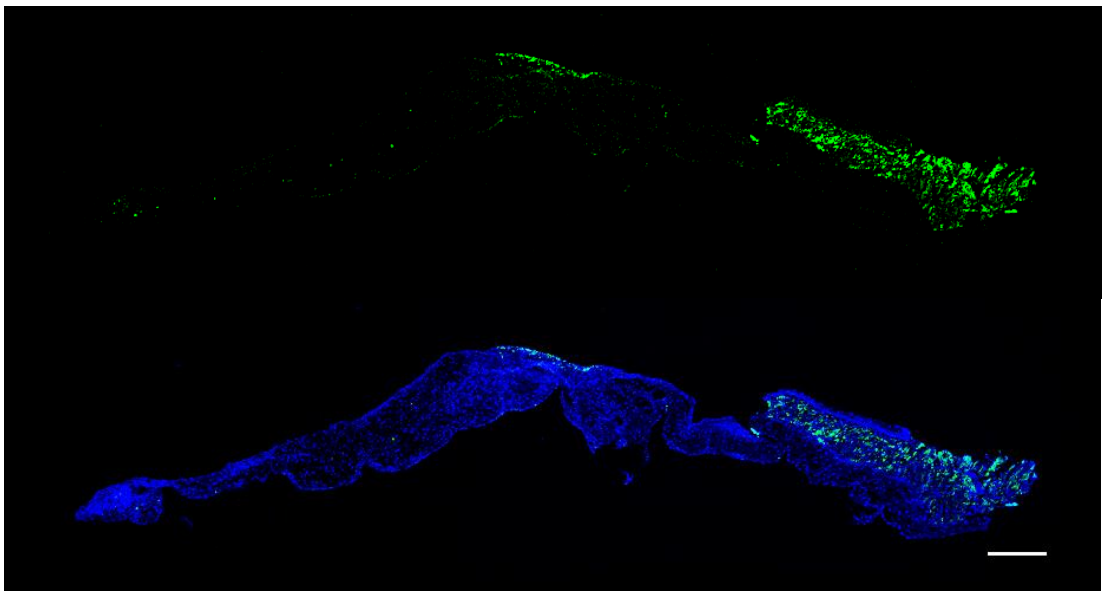

Figure 5-3 Photomicrograph of a full length mitral valve leaflet from a healthy dog. Tile scanning image from confocal microscopy. (Top) Immunofluorescence staining for α-SMA (green). (Bottom) Image merged with DAPI nucleic counterstaining (blue). Myocytes were positive for α-SMA, and there was a single layer of myofibroblasts at the mid atrial surface. Scale bar = 500µm

Bundles of myocytes at the basal part of the leaflet were also positive for α-SMA. Occasionally, there was a small number of α-SMA positive myocytes extending to the middle portion through spongiosa layer (Figure 5-4). Small linear clusters of myofibroblasts were also noted in two of twelve control mitral valves.

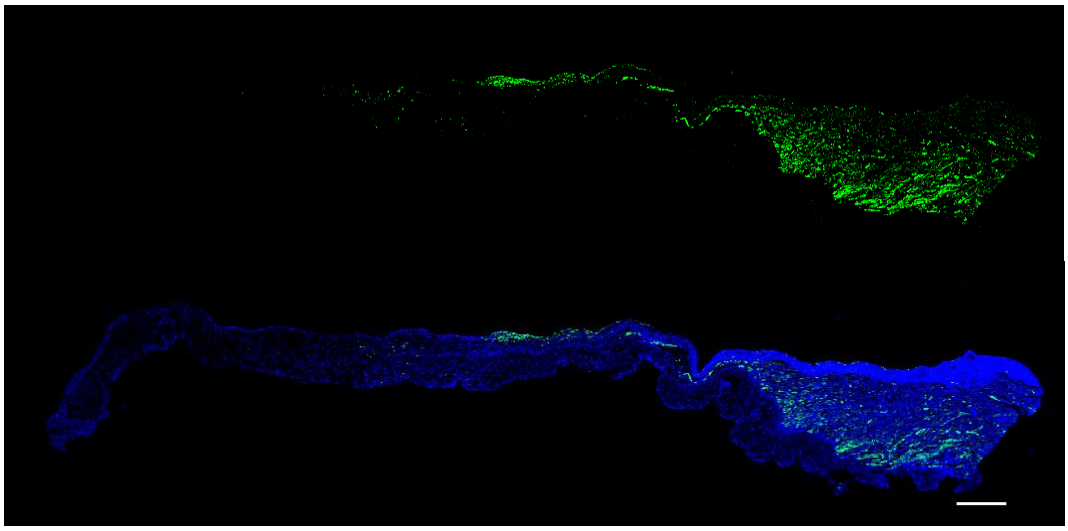

Figure 5-4 Tile scanning image of a normal mitral valve. (Top) Immunofluorescence staining for α-SMA (green). (Bottom) Image merged with DAPI (blue). Aggregation of myofibroblasts were seen in the mid portion at the atrial surface. Scale bar = 500µm.

In the mildly affected valves, nodular thickening changes were noted at the distal-zone with additional linear clusters of myofibroblasts aggregating adjacent to the sub-endothelium. In the distal myxomatous regions, the myofibroblast clusters were seen on both atrial and ventricular sides, and there was an extension (connection) between sub-endothelial myofibroblast clusters and stroma myofibroblast clusters (Figure 5-5 and Figure 5-6).

In the mid zone, where there was no obvious pathology, myofibroblast clusters were also seen at the atrial side as a single linear layer. Myocytes bundles at the proximal portion were also positive for α-SMA (see comment above). Due to section folding, occasionally antibody was trapped and resulted in artefact signal of α-SMA staining in the mid-portion of the leaflet (Figure 5-5).

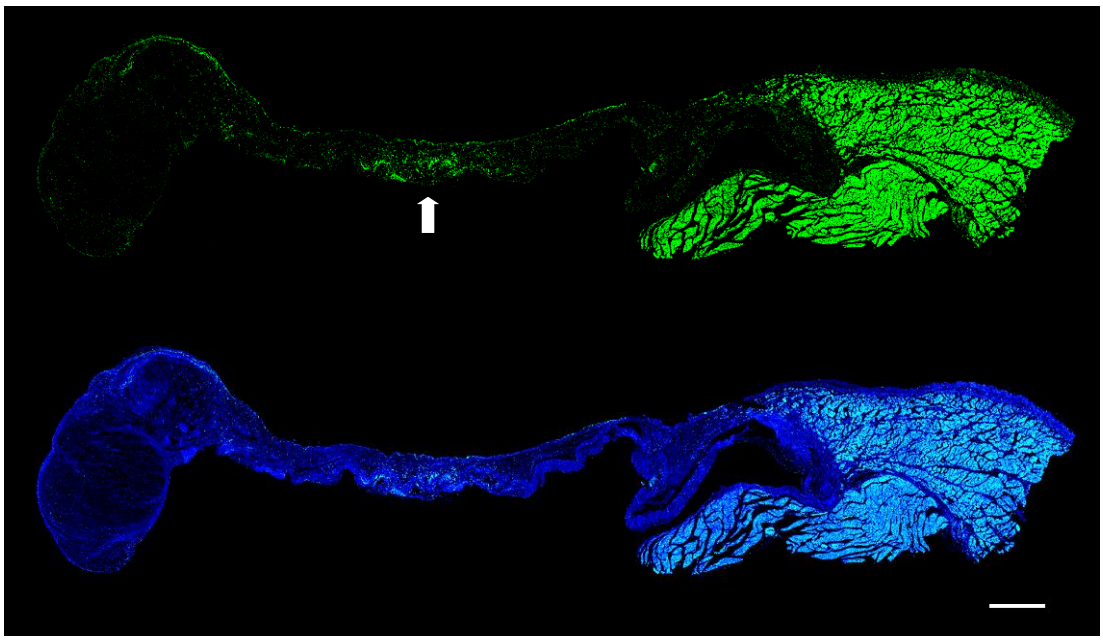

Figure 5-5 Tile scanning image of a mildly affected mitral valve. (Top) Immunofluorescence staining for α-SMA (green). (Bottom) Image merged with DAPI (blue). Single layer of myofibroblasts was observed in the mid portion at atrial surface. The artefact (antibody trapped owing to section folding) of α-SMA staining indicated by white arrow was found in the mid-portion. Scale bar = 500µm.

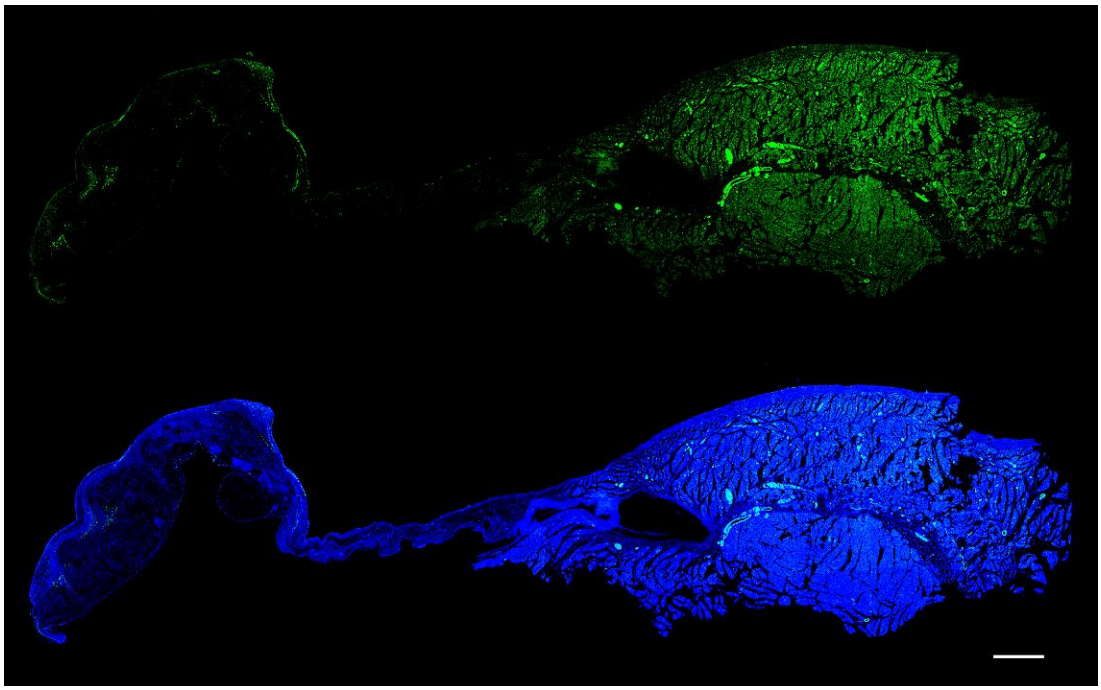

Figure 5-6 Tile scanning image of a mildly affected mitral valve. (Top) Immunofluorescence staining for α-SMA (green). (Bottom) Image merged with DAPI (blue). Single layer of

myofibroblasts was observed in the middle and distal portions at atrial surface. However, no pathological changes were observed in the middle portion. Small numbers of myofibroblast clusters were also noted in the distal myxomatous region. Scale bar = 500µm.

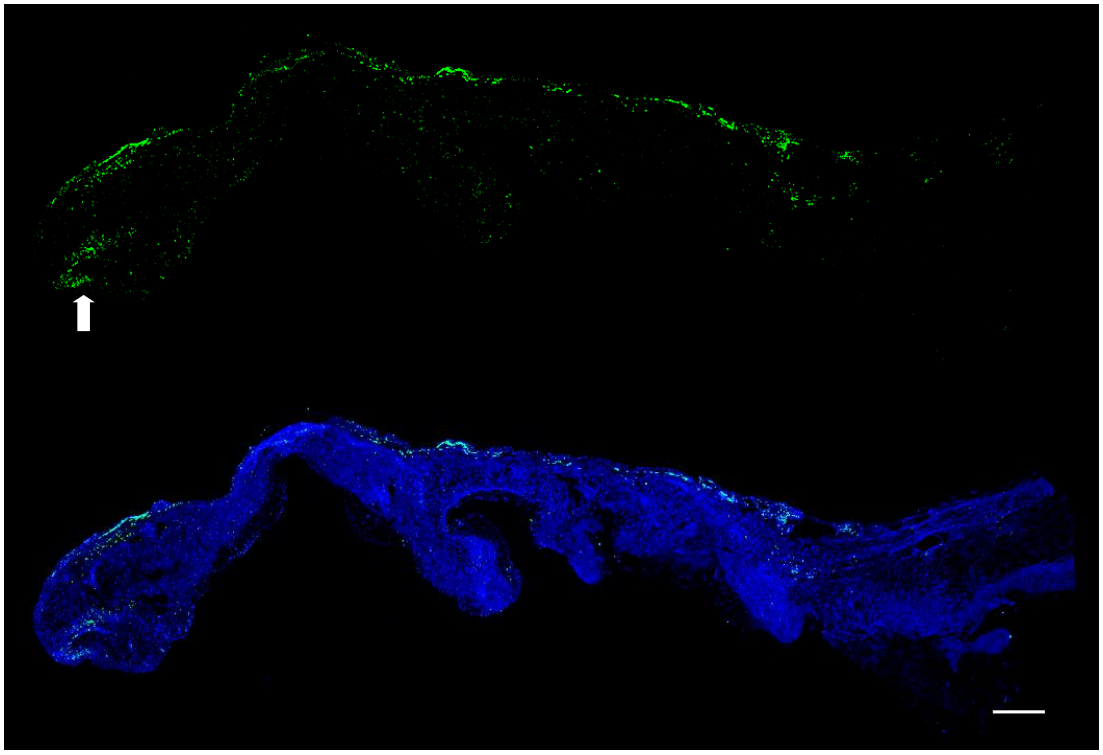

Figure 5-7 Tile scanning image of a mildly affected mitral valve. (Top) Immunofluorescence staining for α-SMA (green). (Bottom) Image merged with DAPI (blue). From basal to distal portion, linear clusters of myofibroblasts were evenly distributed along the atrial side of the leaflet. At the myxomatous region, whorl-like pattern of myofibroblast localization can be seen (white arrow). Scale bar = 500µm.

In one mildly affected MMVD valve, at the junction (neck) of myxomatous and normal MV structure, there were high numbers of myofibroblasts aggregating in the stroma (spongiosa layer) (Figure 5-8).

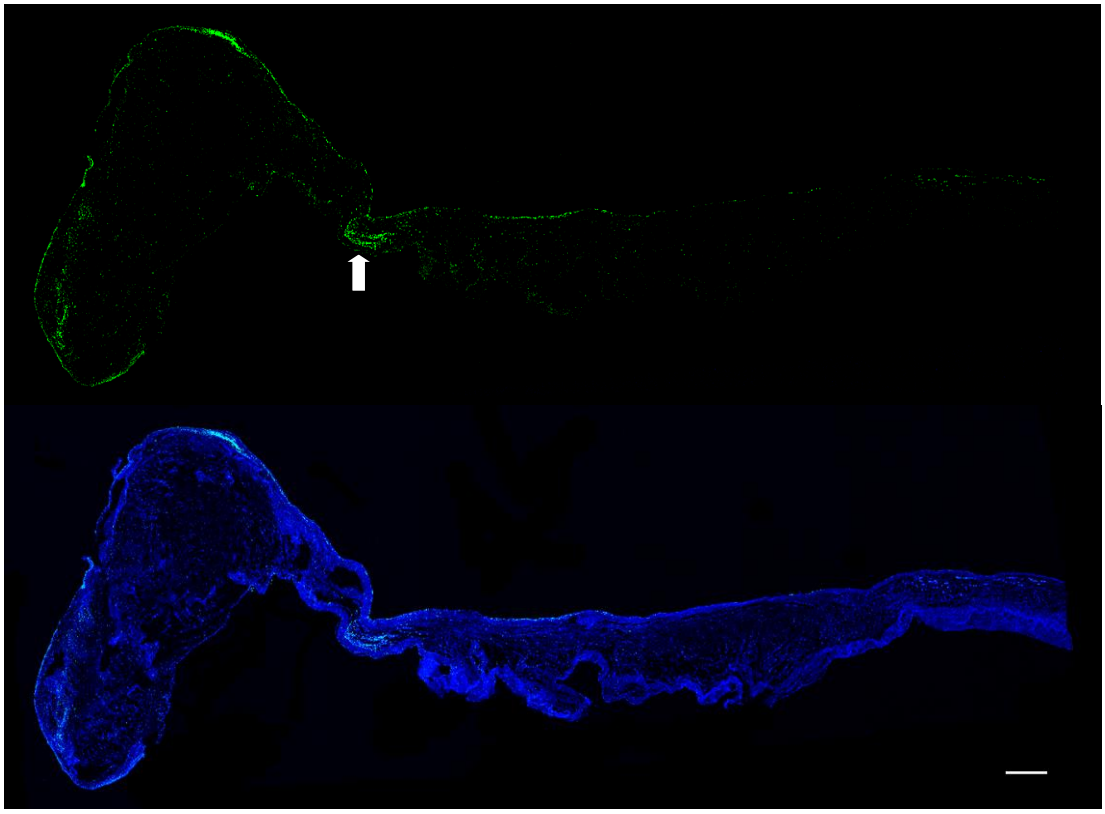

Figure 5-8 Tile scanning image of a mildly affected mitral valve. (Top) Immunofluorescence staining for α-SMA (green). (Bottom) Image merged with DAPI (blue). At the mid portion, single layer of myofibroblasts was found in the mid atrial surface of the leaflet (no myxomatous pathology). At the distal end, linear clusters of myofibroblasts were found at the sub-endothelium and myxomatous stroma. In this mitral valve, higher cellularity of myofibroblasts were noted at the distal end atrial surface. Interestingly, at the junction (neck) of myxomatous and normal MV structure, there were high numbers of myofibroblasts aggregating (white arrow) in the stroma (spongiosa layer). Scale bar = 500µm.

In the severely affected valves, whorl-like aggregations of myofibroblasts were seen in the expanded distal-zone stroma (Figure 5-9), and a marked increase in cell numbers was also noted. Furthermore, myofibroblast clusters were found localized at atrial and ventricular sides and they were restricted to the edge of the leaflet and myxomatous stroma. Surprisingly, there were no noticeable changes in the structure and cellularity in the mid-zone (Figure 5-10).

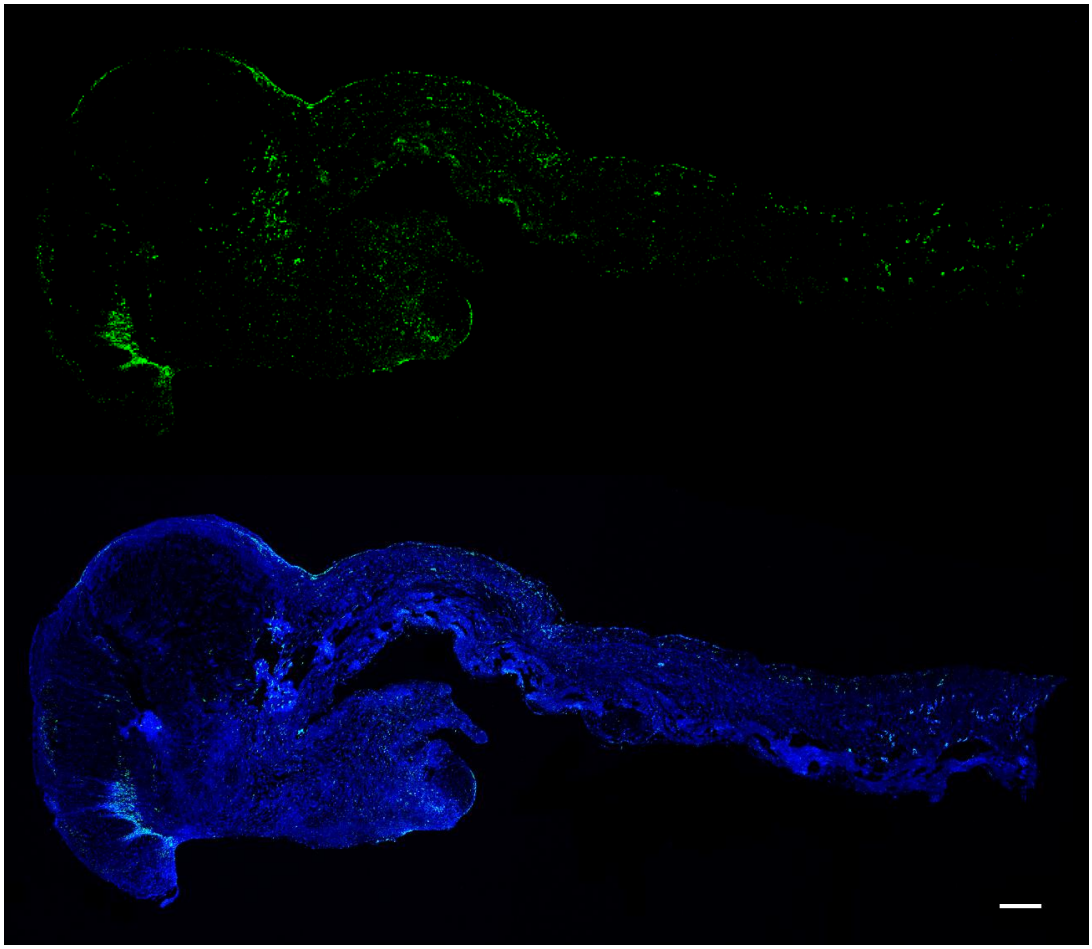

Figure 5-9 Tile scanning image of a severely affected mitral valve. (Top) Immunofluorescence staining for α-SMA (green). (Bottom) Image merged with DAPI (blue). Large numbers of myofibroblasts were found in the myxomatous stroma in a whorl-like pattern. At the junction of myxomatous and normal mitral valve structure, linear clusters of myofibroblasts were noted at the sub-endothelium near atrial surface. Scale bar = 500μm

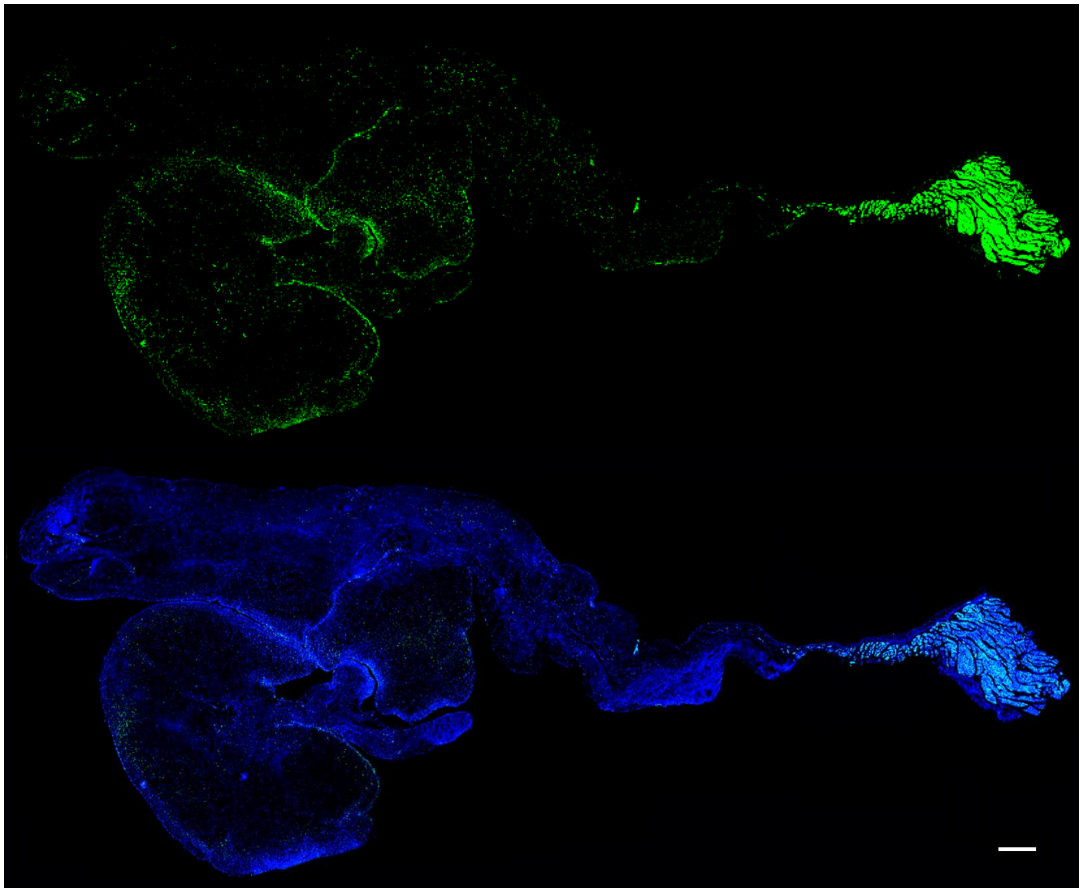

Figure 5-10 Tile scanning image of a severely affected mitral valve. (Top) Immunofluorescence staining for α-SMA (green). (Bottom) Image merged with DAPI (blue). Large numbers of myofibroblasts were mainly localized at the tip of the leaflet surface. Scale bar = 500μm.

5.3.2 HAS2 Expression in Normal and Myxomatous Mitral Valves

In normal mitral valves, there was a clear and continuous expression of HAS2 in endothelial cells predominantly at the atrialis side. Sparse expression of HAS2 was present in the spongiosa (Figure 5-11A and C). In contrast, HAS2 expression in the myxomatous mitral valve free edge was diffuse and a similar expression pattern of HAS2 was seen in the mid-zone (Figure 5-11B and D). Semi-quantitative analysis showed that expression of HAS2 at the free edge of the myxomatous mitral valves was significantly higher than the normal mitral valves, but there was no difference in the mid-zone of normal and myxomatous mitral valves (Figure 5-12).

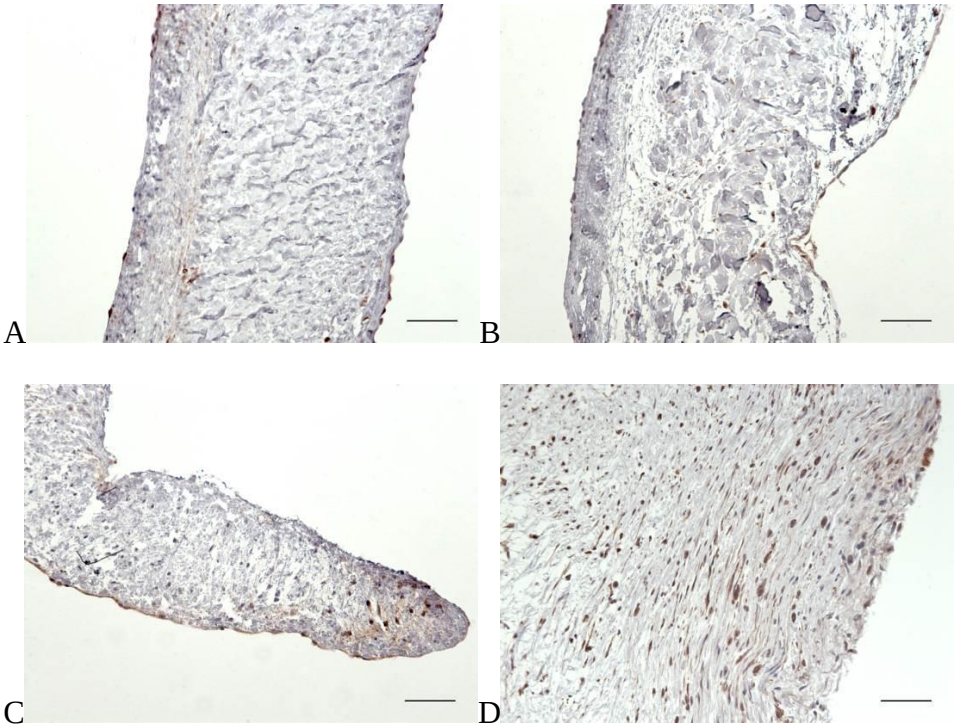

Figure 5-11(A)(C) Normal mitral valve. (B)(D) Myxomatous mitral valve. (A) In normal mitral valve mid-portion, HAS2 was expressed by interstitial cells in the spongiosa and endothelial cells at atrial and ventricular surface. Minimum amount of HAS2 was expressed in fibrosa layer. (B) In myxomatous mitral valve mid-portion, HAS2 expression was similar to normal mitral valve. Loose collagen bundles were seen in the fibrosa layer. (C) In the distal end of normal mitral valve, HAS2 was also expressed by endothelial cells at the valve surface, and a few interstitial cells were also positive for HAS2. (D) In the distal end of myxomatous mitral valve, HAS2 was strongly expressed by most interstitial cells. Scale bar = 50µm.

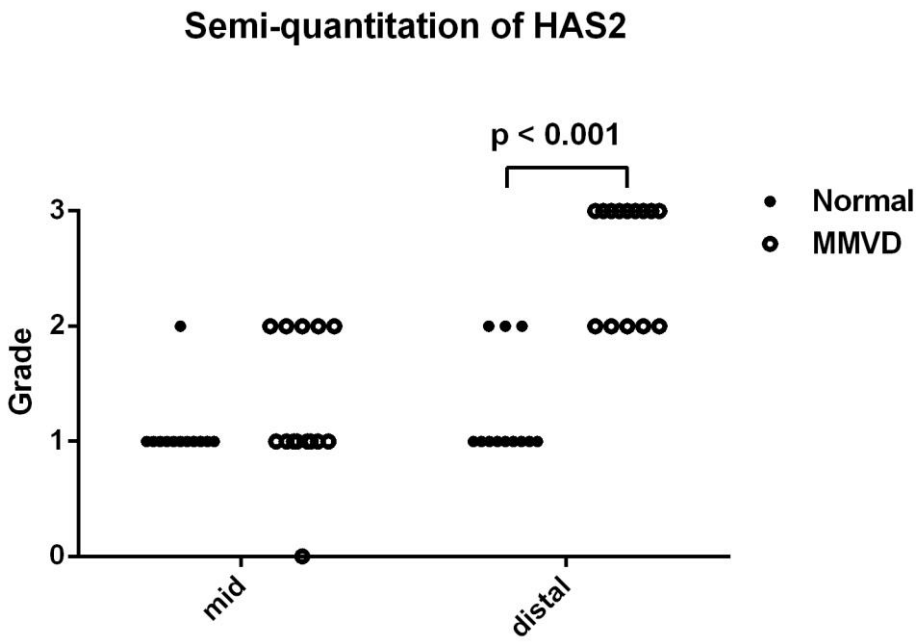

Figure 5-12 Semi-quantitative analysis of HAS2 immunohistochemistry. The expression of HAS2 was higher in the distal portion of the myxomatous mitral valves compared with normal mitral valves. There was no difference in HAS2 expression in the middle portion of the myxomatous and normal mitral valves. Difference were assessed using the Mann-Whitney test.

5.3.3 Myofibroblastic Expression of HAS2 in Myxomatous Mitral Valve

In normal mitral valves, localized expression of HAS2 was observed in the endothelium and spongiosa. Most HAS2 positive interstitial and endothelial cells were not associated with α-SMA stained cells, but a few HAS2 positive endothelial cells did co-express α-SMA (Figure 5-13, Figure 5-14, Figure 5-15, and Figure 5-16).

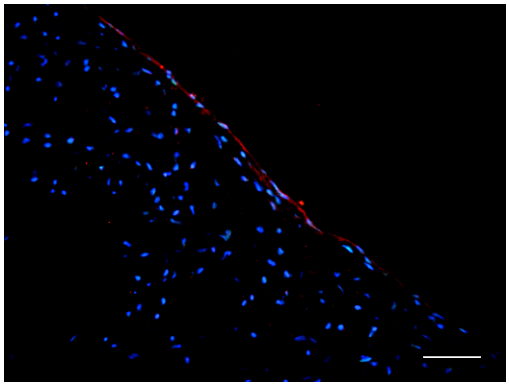

Figure 5-13 Photomicrograph of immunofluorescence staining for HAS2 (red). Atrial endothelial cells were expressing HAS2. Canine normal mitral valve. Scale bar = 50µm.

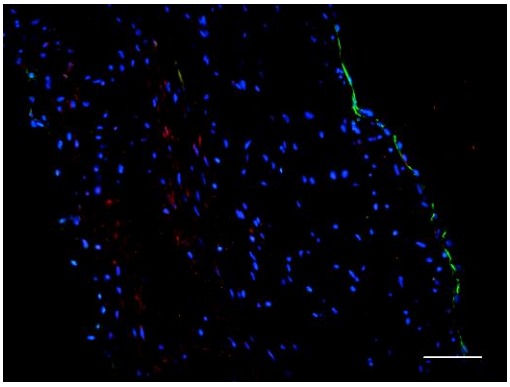

Figure 5-14 Photomicrograph of double-immunofluorescence staining for HAS2 (red) and α-SMA (green). Atrial sub-endothelial cells were positive for α-SMA. Interstitial cells in the spongiosa layer were also positive for HAS2. Canine normal mitral valve. Scale bar = 50µm.

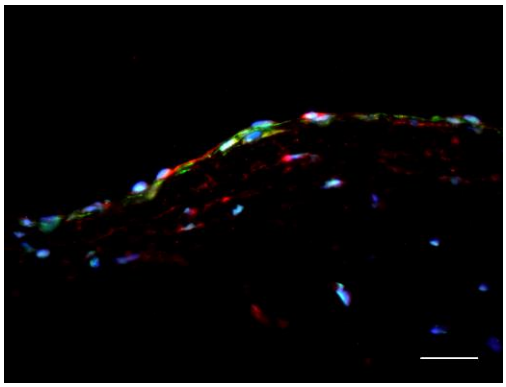

Figure 5-15 Photomicrograph of double-immunofluorescence staining for HAS2 (red) and α-SMA (green). The mitral valve atrial endothelial cells were co-expressing HAS2 and α-SMA. Canine normal mitral valve. Scale bar = 25 µm.

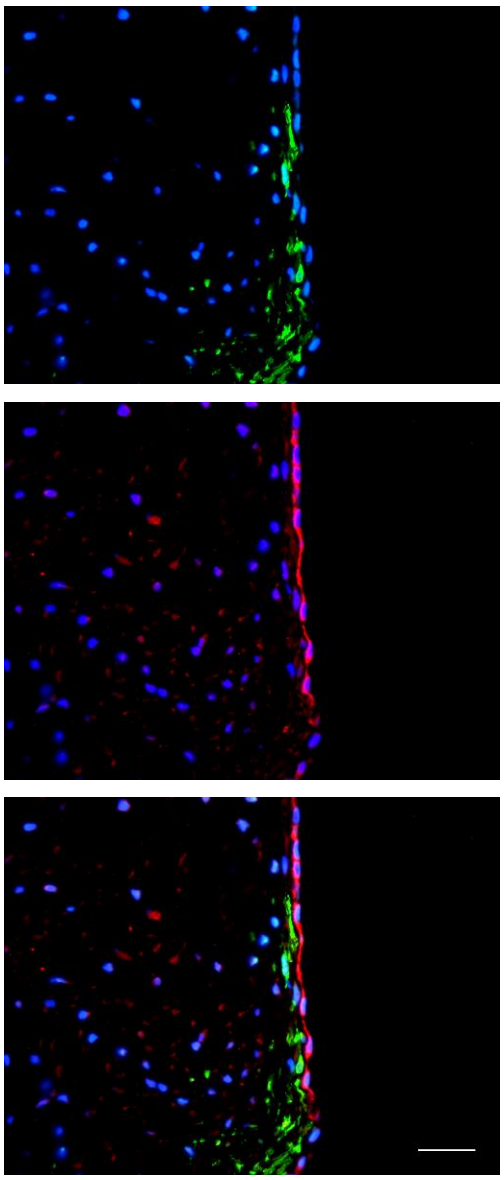

Figure 5-16 Photomicrograph of double-immunofluorescence staining for HAS2 (red) and α-SMA (green), and nuclei counterstained with DAPI. Mitral valve endothelial cells at the atrial surface were positive for HAS2 but negative for α-SMA. Myofibroblasts (α-SMA positive cells) adjacent to the atrial endothelial cells were not associated with HAS2 expression. Canine normal mitral valve. Scale bar = 25 µm.

In myxomatous mitral valves, there was a close correlation between HAS2 expression and myofibroblasts as confirmed by double-staining for HAS2 and α-SMA (Figure 5-17, Figure 5-18, Figure 5-19, and Figure 5-20). Furthermore, co-expression of HAS2 and α-SMA in endothelial cells was also noted in the region without sub-endothelial myofibroblast accumulation (Figure 5-21).

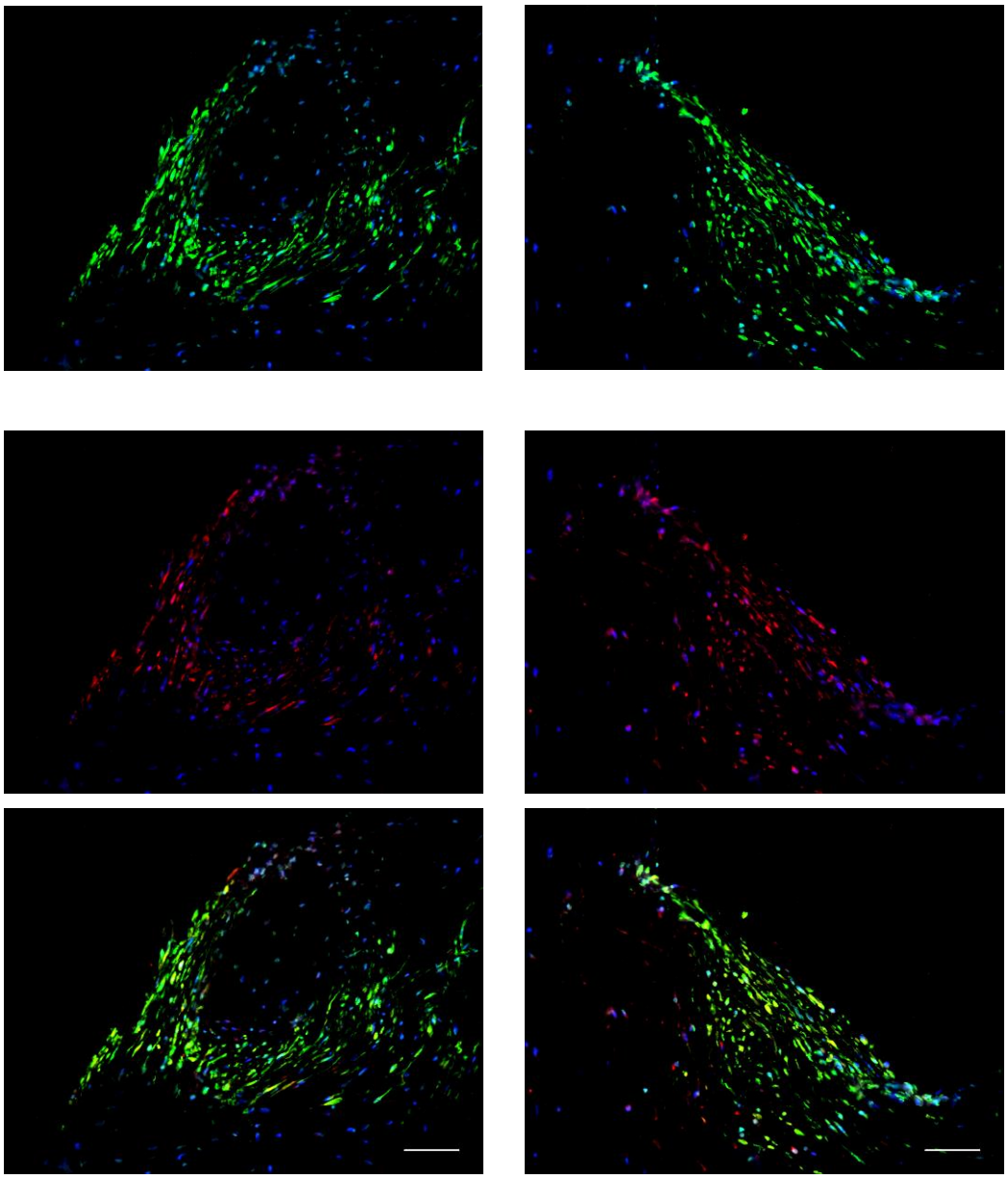

Figure 5-17 Photomicrograph of double-immunofluorescence staining for HAS2 (red) and α-SMA (green), and nuclei counterstained with DAPI. At distal end, there was whorl-like aggregation of myofibroblasts (α-SMA staining) in the overtly myxomatous region, and the expression pattern of HAS2 was closely associated with α-SMA expression. Canine myxomatous mitral valve. Scale bar = 50µm.

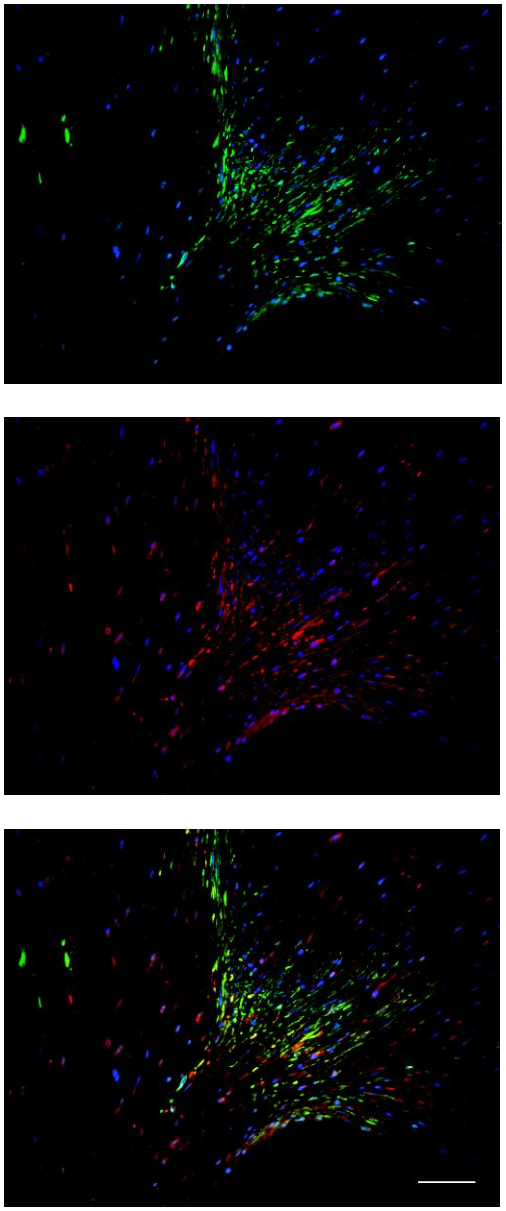

Figure 5-18 Photomicrograph of double-immunofluorescence staining for HAS2 (red) and α-SMA (green), and nuclei counterstained with DAPI. At distal end, co-expression of HAS2 and α-SMA in myofibroblasts clusters was also noted. Canine myxomatous mitral valve. Scale bar = 50µm.

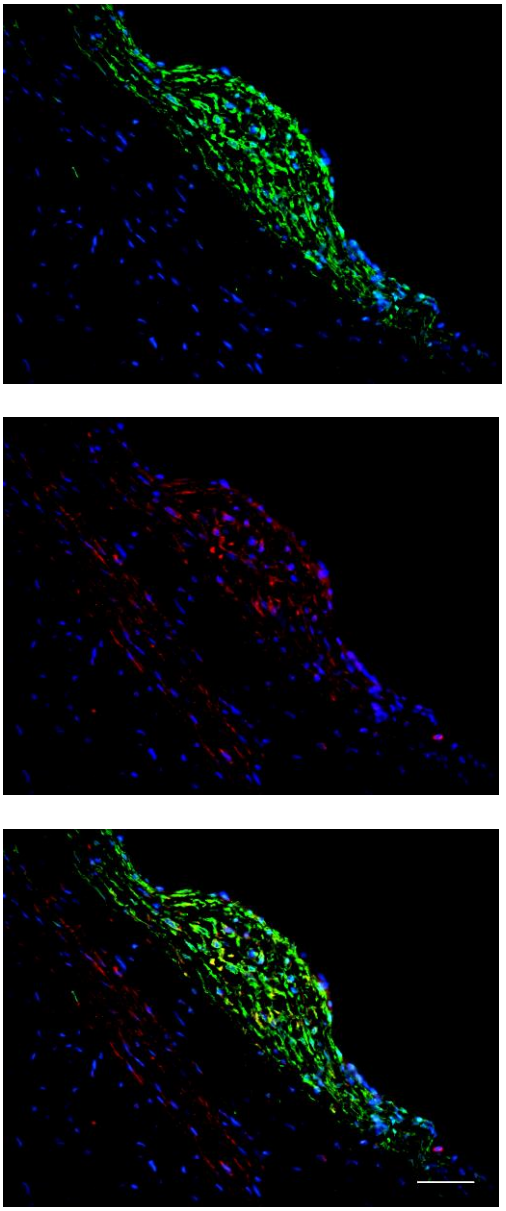

Figure 5-19 Photomicrograph of double-immunofluorescence staining for HAS2 (red) and α-SMA (green), and nuclei counterstained with DAPI. HAS2 was expressed by the interstitial cells in the spongiosa and myofibroblasts clusters. Canine myxomatous mitral valve. Scale bar = 50µm.

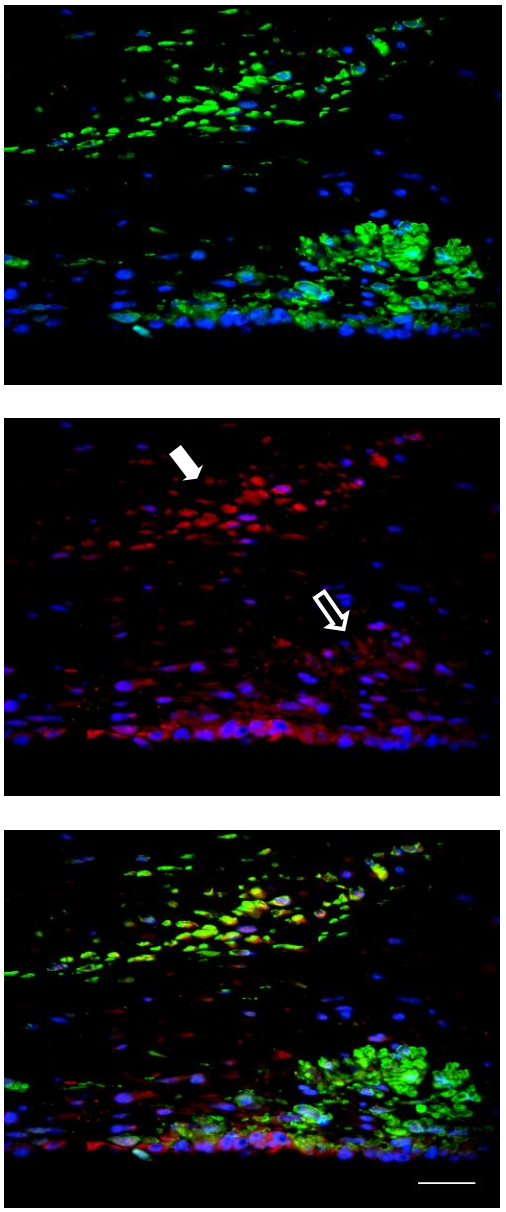

Figure 5-20 Photomicrograph of double-immunofluorescence staining for HAS2 (red) and α-SMA (green), and nuclei counterstained with DAPI. Endothelial cells at the mitral valve surface were positive for HAS2, and few of them were also expressing α-SMA. Two clusters of myofibroblasts were found in these regions, and they are morphologically different. The myofibroblast cluster deep in the stroma was highly associated HAS2 expression (white arrow), whereas the myofibroblasts cluster adjacent to the endothelial layer was partially positive for HAS2 (white hollow arrow). Canine myxomatous mitral valve. Scale bar = 25µm.

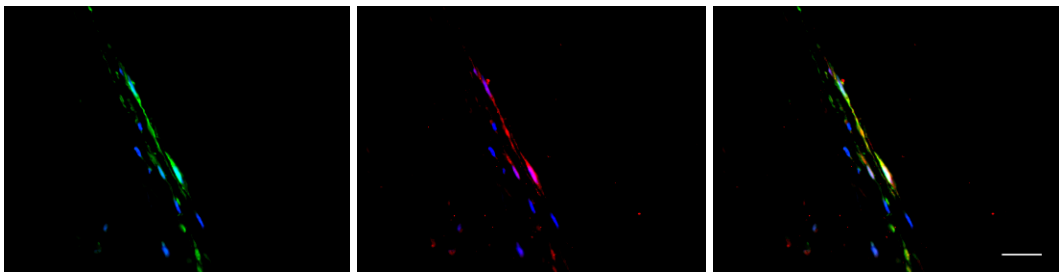

Figure 5-21 Photomicrograph of double-immunofluorescence staining for HAS2 (red) and α-SMA (green), and nuclei counterstained with DAPI. This image was taken from a myxomatous-free and non-myofibroblasts dominated area. Co-expression of HAS2 and α-SMA was observed in the elongated and spindle-shape cells near the mitral valve surface. Canine myxomatous mitral valve. Scale bar = 25µm.

5.3.4 SNAI1 Expression Pattern in Myofibroblast Clusters in Myxomatous Mitral Valves

In the normal mitral valve, expression of SNAI1 was minimal and localized to the endothelium (Figure 5-22).

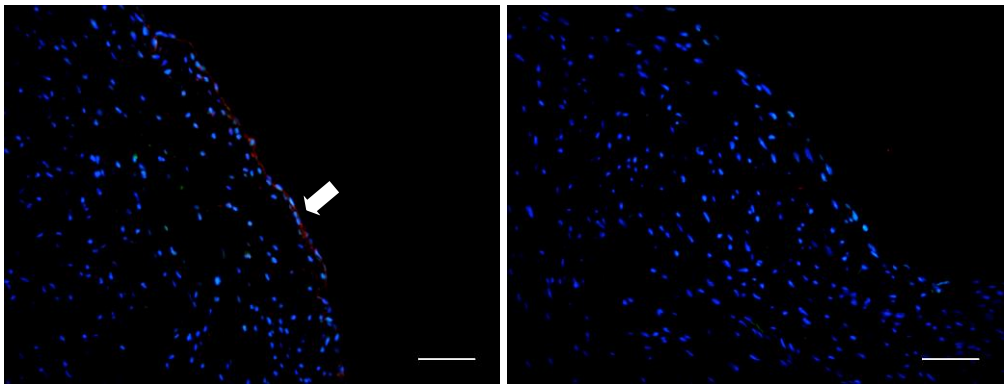

Figure 5-22 Photomicrograph of double-immunofluorescence staining for SNAI1 (red) and α-SMA (green), and nuclei counterstained with DAPI. In a myofibroblast-free area, SNAI1 was only mildly expressed by few endothelial cells (white arrow). (Left) SNAI1 expression was noted in the endothelium, but (Right) not all endothelial cells were expressing SNAI1. Canine normal mitral valve. Scale bar = 50µm.

In contrast, in myxomatous mitral valves, cells expressing SNAI1 were identified in the hyperplastic endothelium at the tip of the leaflet and the stroma of myxomatous regions (Figure 5-24, Figure 5-25, and Figure 5-26). Furthermore, SNAI1 positive cells found in myofibroblast clusters in myxomatous mitral valves were mainly α-SMA negative (Figure 5-23, Figure 5-24, and Figure 5-25).

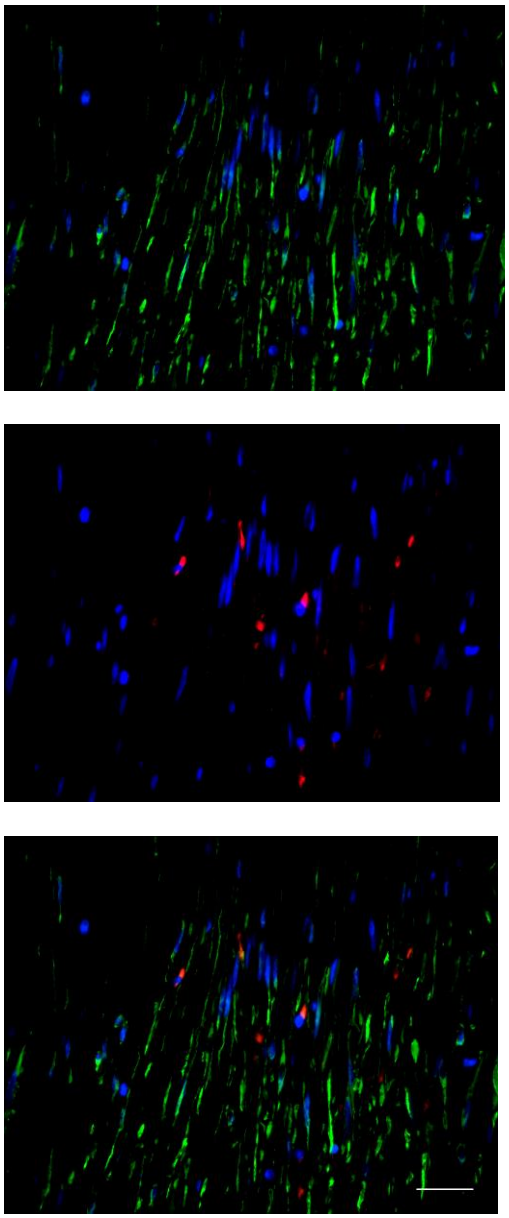

Figure 5-23 Photomicrograph of double-immunofluorescence staining for SNAI1 (red) and α-SMA (green), and nuclei counterstained with DAPI. In the myxomatous area, myofibroblasts (α-SMA positive) were elongated and spindle shape with polarity. However, SNAI1 positive cells in the myxomatous stroma were round shape, and they were mildly or not co-expressing α-SMA. Canine myxomatous mitral valve. Scale bar = 25µm.

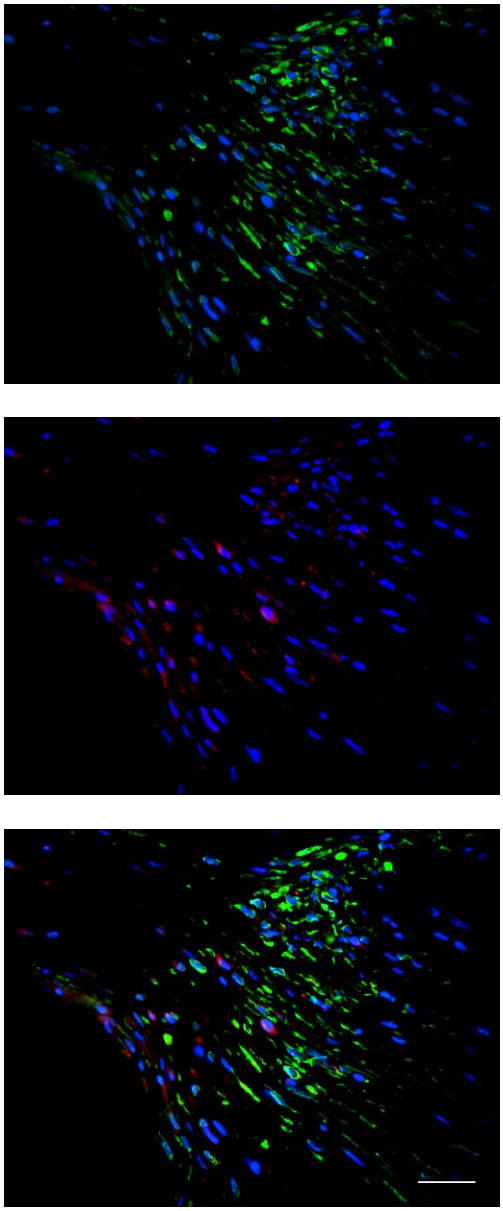

Figure 5-24 Photomicrograph of double-immunofluorescence staining for SNAI1 (red), α-SMA (green), and nuclei counterstained with DAPI. In the myofibroblasts cluster, SNAI1 positive cells were also expressing α-SMA. These were mainly distributed along the endothelium, but a few SNAI1 positive cells were found in the stroma. Canine myxomatous mitral valve. Scale bar = 25µm.

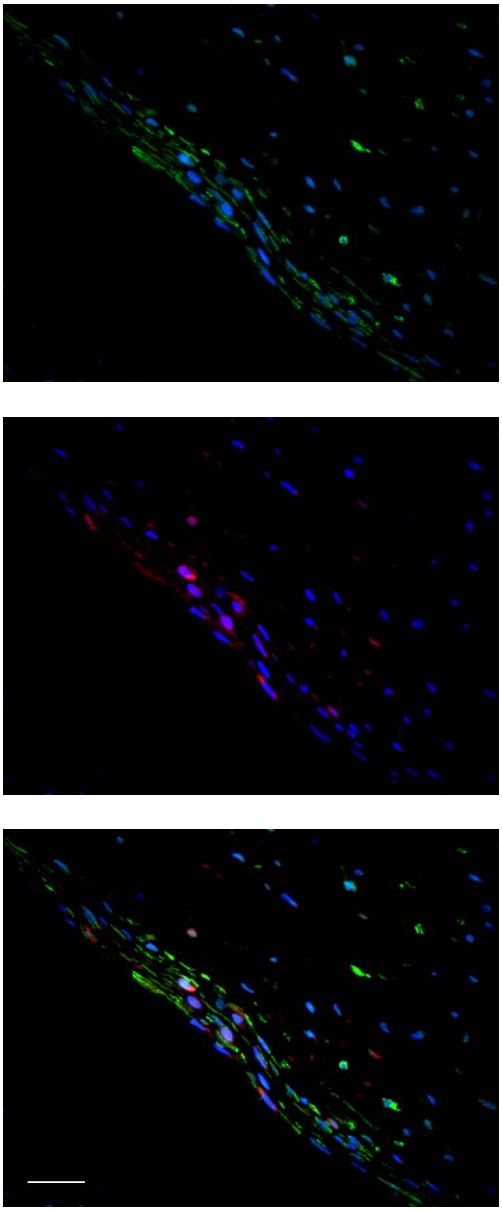

Figure 5-25 Photomicrograph of double-immunofluorescence staining for SNAI1 (red), and α-SMA (green), and nuclei counterstained with DAPI. Myofibroblasts were elongated in the linear clusters along the endothelial surface, but SNAI1 positive cells were polymorphic (mainly round shape, but few elongated shape). Co-expression of α-SMA and SNAI1 was only seen in few cells. Canine myxomatous mitral valve. Scale bar = 25µm.

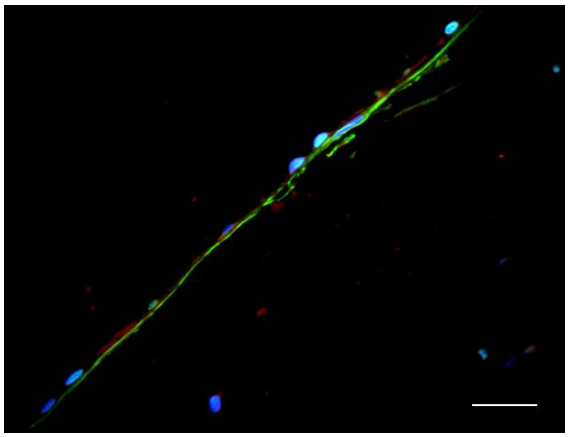

Figure 5-26 Photomicrograph of double-immunofluorescence staining for SNAI1 (red) and α-SMA (green), and nuclei counterstained with DAPI. Underneath the SNAI1 positive endothelial cells, there was an elongated and spindle shape myofibroblast. Canine myxomatous mitral valve. Scale bar = 25µm.

5.3.5 Co-expression of VE-Cadherin (CD144, CDH5) and α-SMA in Normal and Diseased Mitral Valve

CDH5 was highly expressed in the endothelium of both normal and myxomatous mitral valves, and a few of these cells co-expressed CDH5 and α-SMA. However, low level expression of CDH5 by interstitial cells was also noted in the spongiosa layer in the normal mitral valve and in the overtly myxomatous region (Figure 5-27 to Figure 5-32).

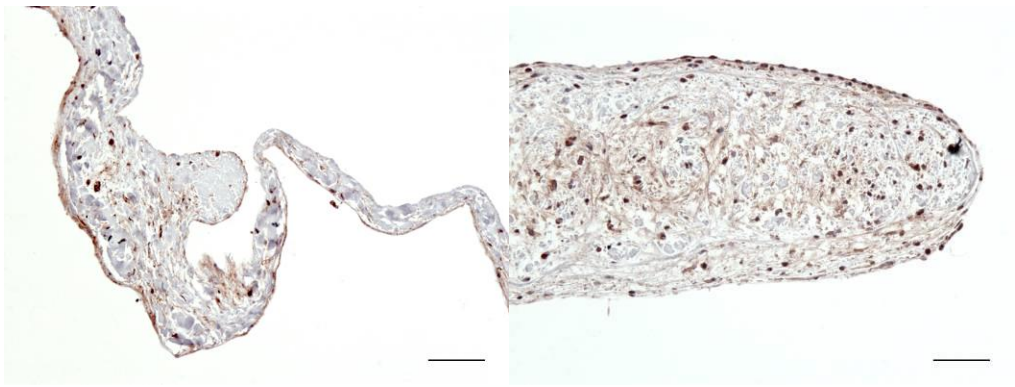

Figure 5-27 Immuno-staining images of CDH5, canine normal mitral valve. The expression of CDH5 was mainly in endothelium, with a few interstitial cells in the spongiosa and dense collagen bundles also positive for CDH5 (left). In another normal mitral valve (right), expression of CDH5 was found in spindle shape interstitial in the stroma at the distal end of the valve. Scale bar = 50 µm

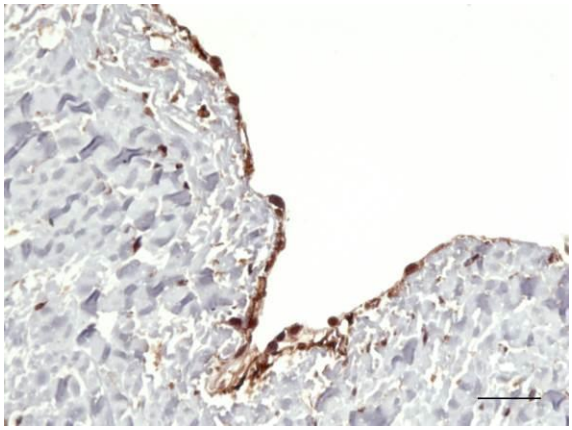

Figure 5-28 Photomicrograph of a normal mitral valve with immuno-staining for CDH5. Endothelial cells were positively stained for CDH5. Only few CDH5 positive cells were noted in the dense collagen bundles. Scale bar = 25 µm

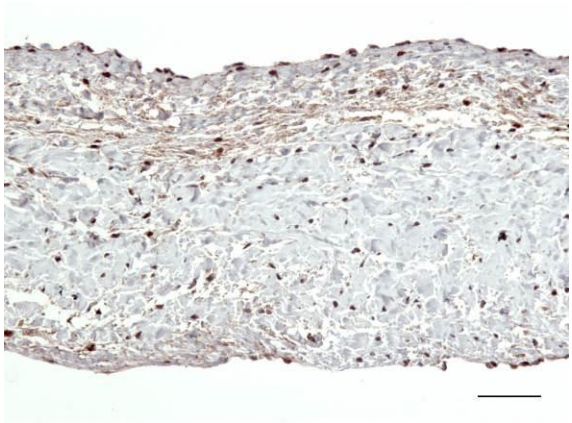

Figure 5-29 Photomicrograph of a normal mitral valve with immuno-staining for CDH5. Spindle shape interstitial cells in the spongiosa and endothelium showed positive staining for CDH5. Scale bar = 50 µm

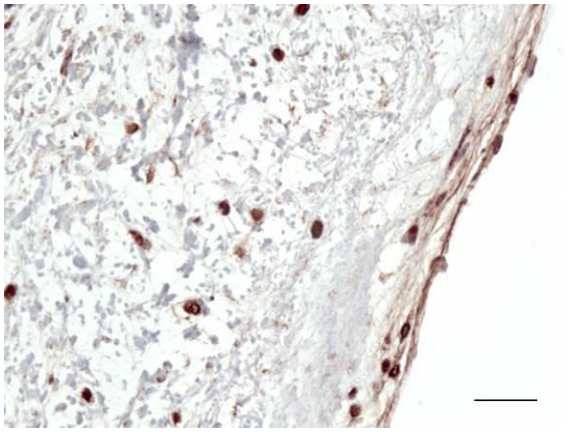

Figure 5-30 Photomicrograph of a myxomatous mitral valve with immuno-staining for CDH5. Endothelial cells in the myxomatous mitral valve were also expressing CDH5. In the stroma with myxoid deposition, interstitial cells were also positive for CDH5. Scale bar = 25 µm

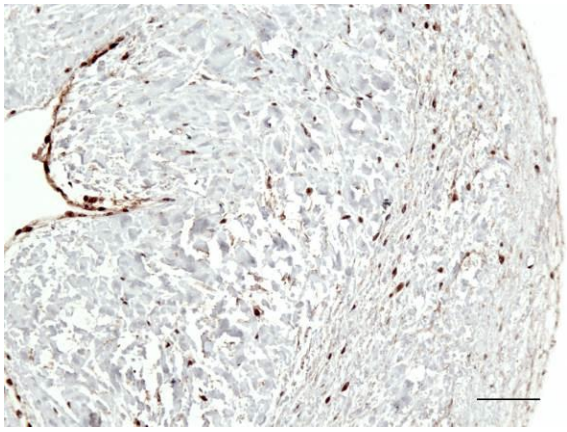

Figure 5-31 Photomicrograph of a myxomatous mitral valve with immuno-staining for CDH5. There was a strong CDH5 staining at the endothelium. Mild expression of CDH5 was also seen in interstitial cells at spongiosa layer. Scale bar = 50 µm

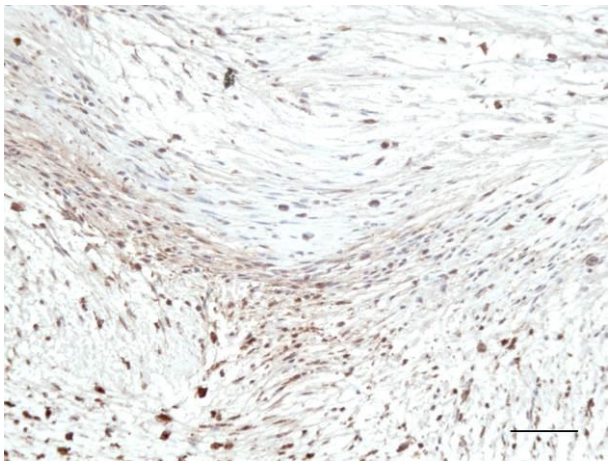

Figure 5-32 Photomicrograph of a myxomatous mitral valve with immuno-staining for CDH5. Whorl-like clusters of spindle shape interstitial cells were partially CDH5 positive. Scale bar = 50 µm

α-SMA+ cells in normal mitral valves were always identified to lie underneath the CDH5+ endothelial cells, with some also co-expressing CDH5. In myxomatous mitral valves, α-SMA+ cells aggregated in a multiple layered pattern, and most of the these cells were also CDH5+.

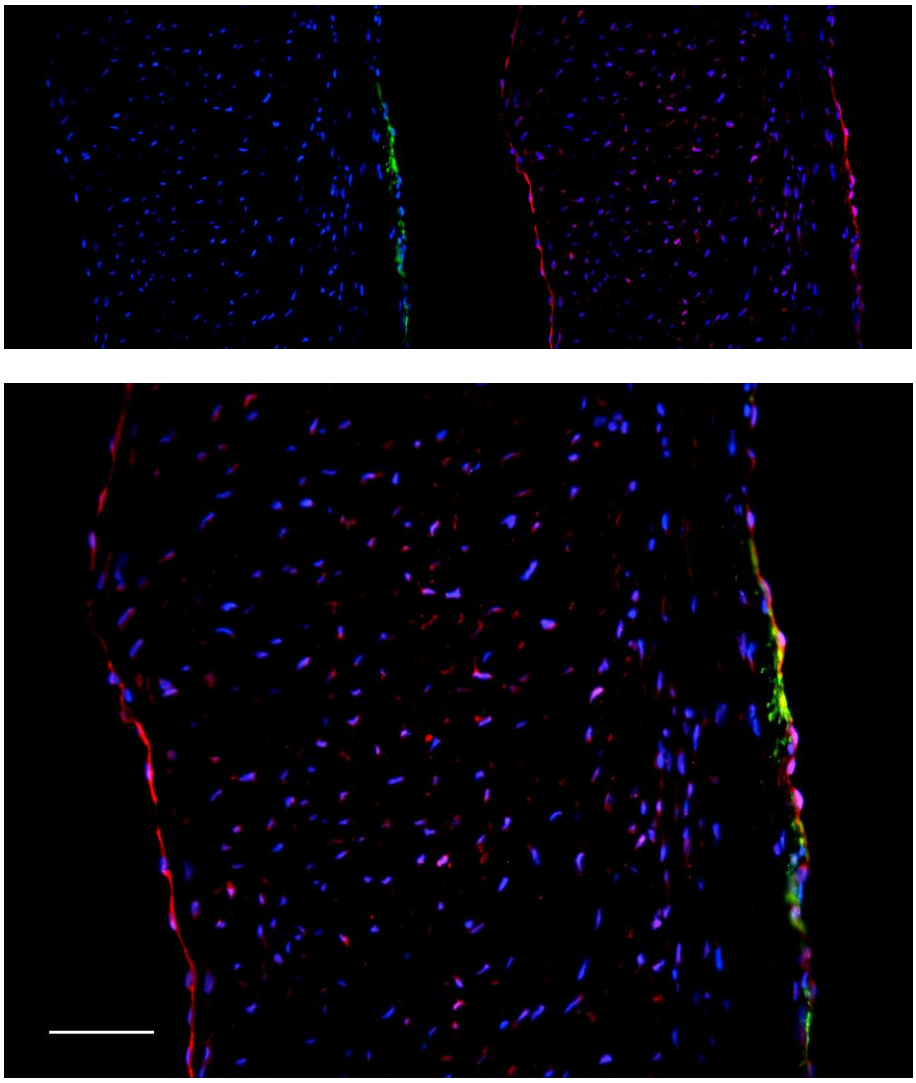

Figure 5-33 Photomicrograph of immunofluorescence images for CDH5 (red) and α-SMA (green), and nuclei counterstained with DAPI. Normal canine mitral valve, middle portion. (Top left) α-SMA with DAPI. (Top Right) CDH5 with DAPI. (Bottom) Merged image of α-SMA, CDH5, and DAPI. Endothelial cells on both atrial and ventricular side were CDH5 positive, and α-SMA positive myofibroblasts were only seen on the atrial sub-endothelium or sub-endothelial stroma. A few atrial endothelial cells were also co-expressing α-SMA. Scale bar = 50 µm

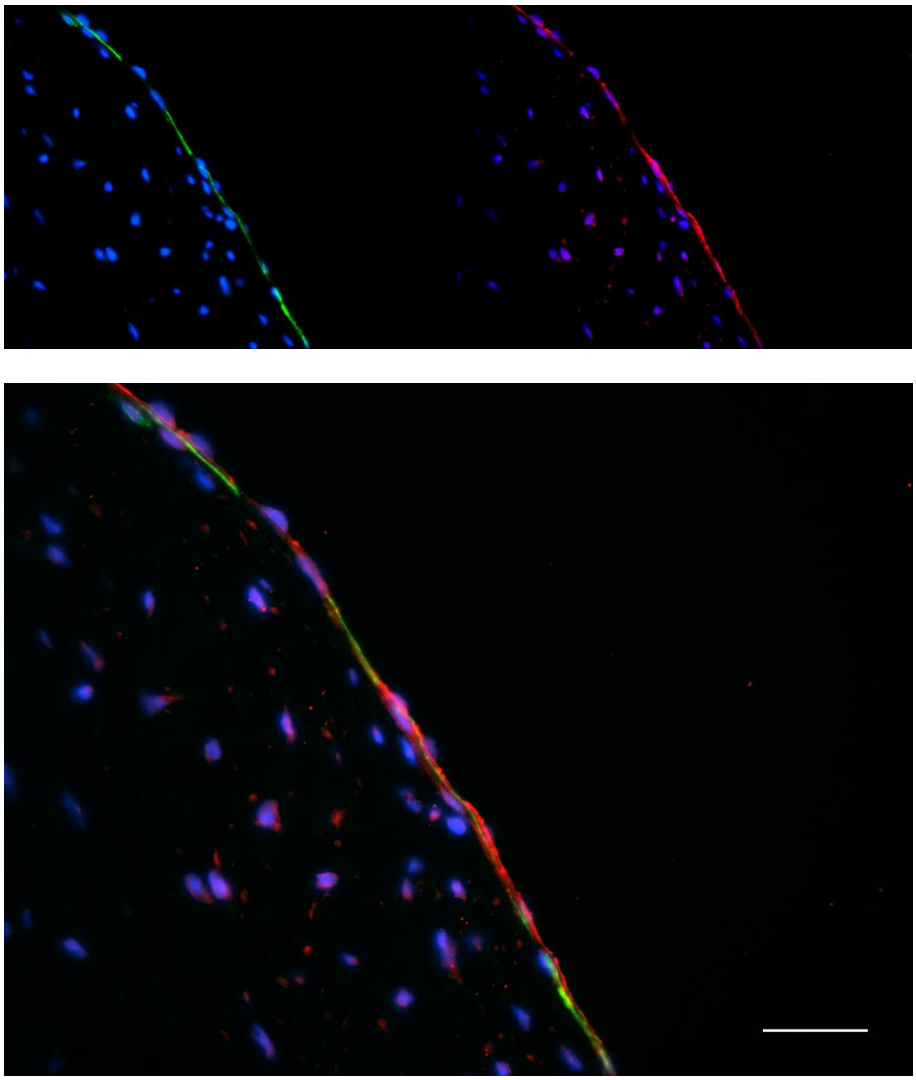

Figure 5-34 Photomicrograph of immunofluorescence images for CDH5 (red) and α-SMA (green), and nuclei counterstained with DAPI. Normal canine mitral valve, middle portion. (Top left) α-SMA with DAPI. (Top Right) CDH5 with DAPI. (Bottom) Merged image of α-SMA, CDH5, and DAPI. Endothelial cells on atrial side were CDH5 positive. A monolayer of myofibroblasts was closely sub-adjacent to the endothelial cells with one cell co-expressing CDH5 and α-SMA. Scale bar = 25 µm.

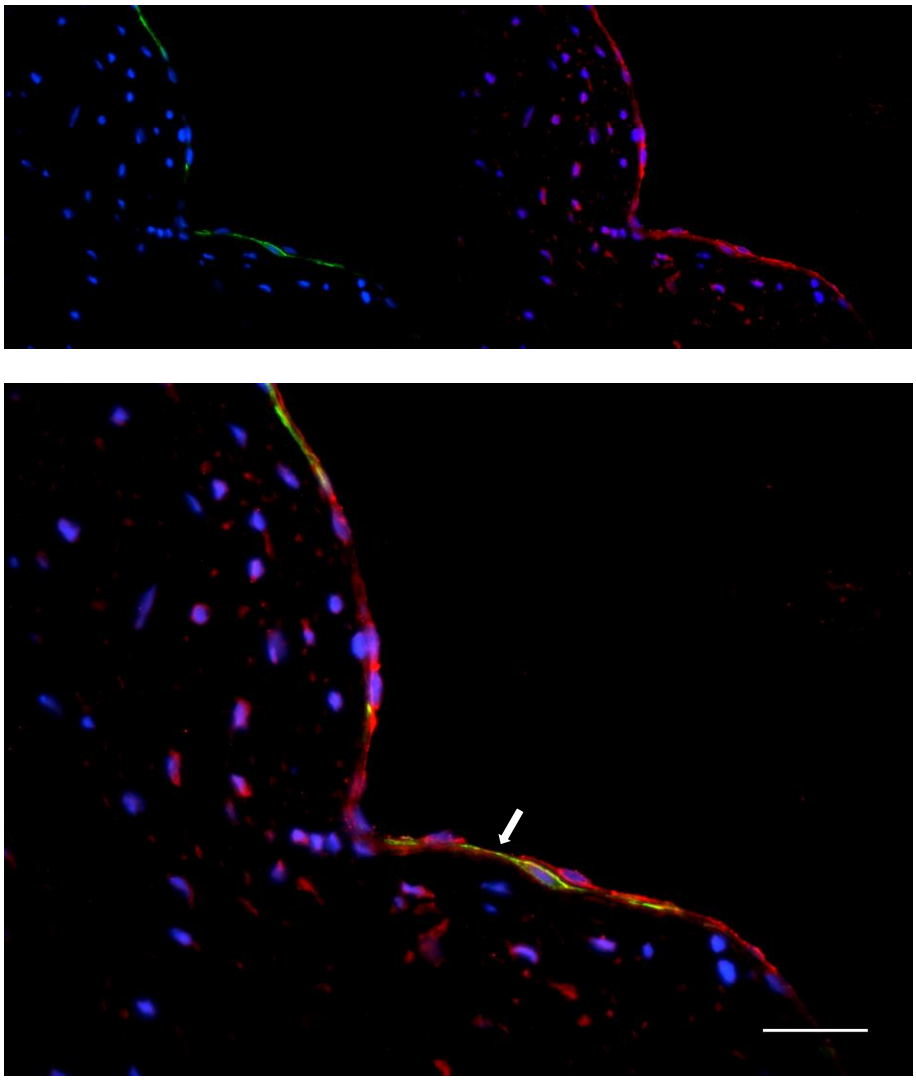

Figure 5-35 Photomicrograph of immunofluorescence images for CDH5 (red) and α-SMA (green), and nuclei counterstained with DAPI. Normal canine mitral valve, middle portion. (Top left) α-SMA with DAPI. (Top Right) CDH5 with DAPI. (Bottom) Merged image of α-SMA, CDH5, and DAPI. Endothelial cells on atrial side were CDH5 positive. A single myofibroblast was closely sub-adjacent to the endothelial cells, and there was a protrusion of cytoplasmic α-SMA (white arrow), suggesting migration (differentiation) of the atrial endothelial cells. Scale bar = 25 µm.

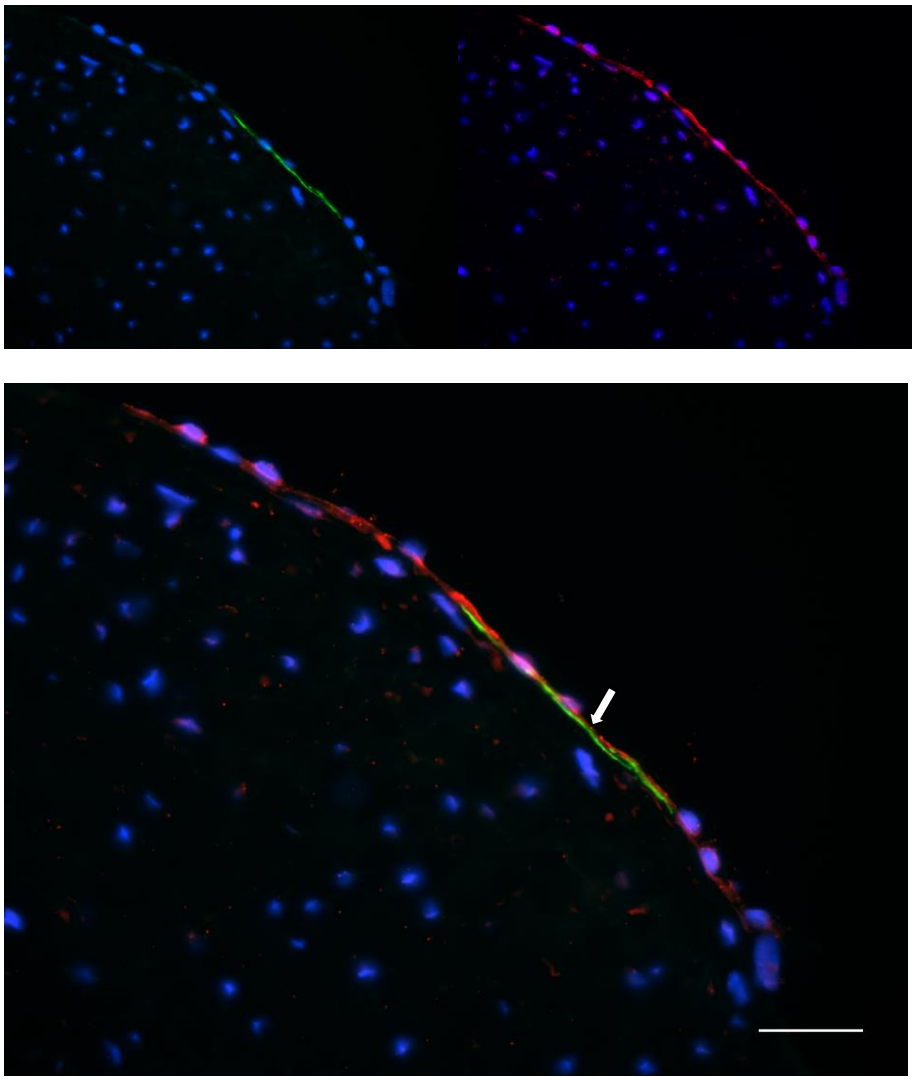

Figure 5-36 Photomicrograph of immunofluorescence images for CDH5 (red) and α-SMA (green), and nuclei counterstained with DAPI. Normal canine mitral valve, middle portion. (Top left) α-SMA with DAPI. (Top Right) CDH5 with DAPI. (Bottom) Merged image of α-SMA, CDH5, and DAPI. Endothelial cells on atrial side were CDH5 positive. A single myofibroblast was closely sub-adjacent to the endothelial cells, and there was a protrusion of cytoplasmic α-SMA (white arrow), suggesting migration (differentiation) of the atrial endothelial cells. Scale bar = 25 µm.

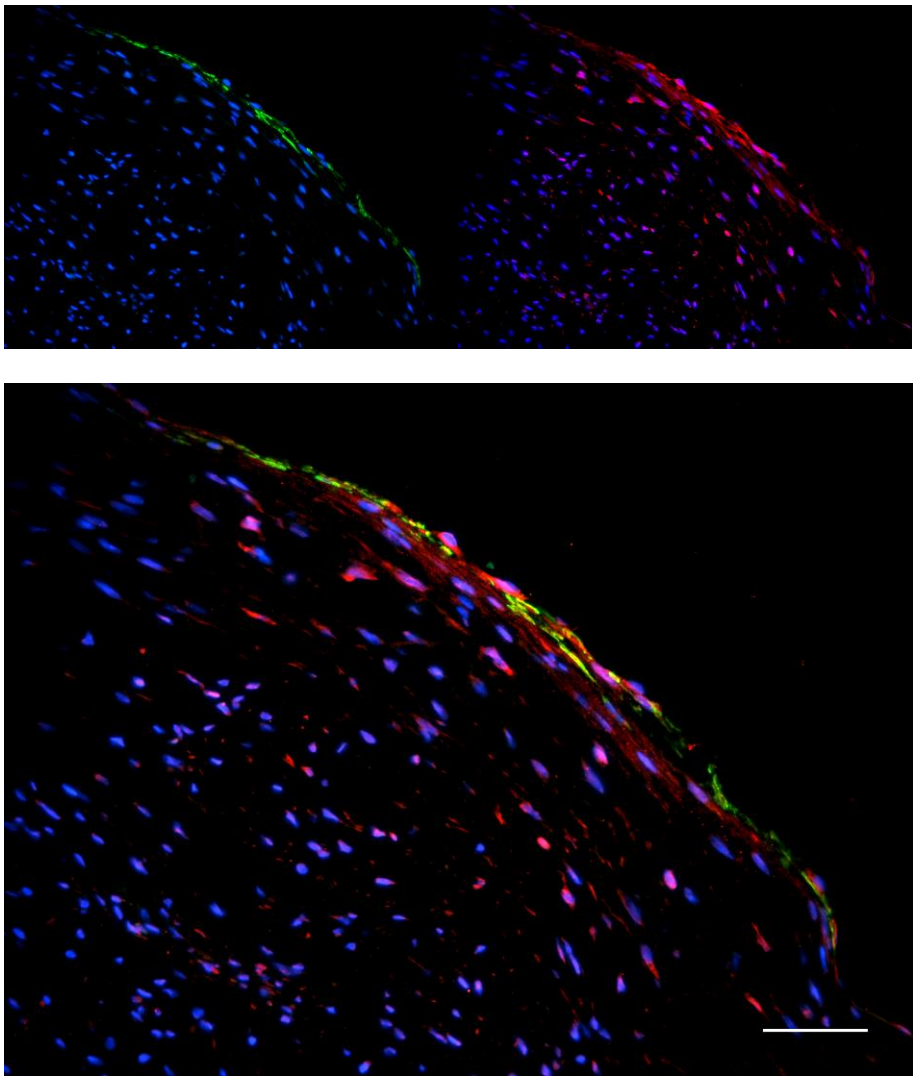

Figure 5-37 Photomicrograph of immunofluorescence images for CDH5 (red) and α-SMA (green), and nuclei counterstained with DAPI. Normal canine mitral valve, middle portion. (Top left) α-SMA with DAPI. (Top Right) CDH5 with DAPI. (Bottom) Merged image of α-SMA, CDH5, and DAPI. Atrial endothelial cells were CDH5 positive, and there were more CDH5 (+) spindle shape interstitial cells aggregating underneath the myofibroblast cluster. Myofibroblasts (α-SMA positive) were localized linearly sub-adjacent to the atrial endothelial cells with some endothelial expression of α-SMA. Scale bar = 50 µm.

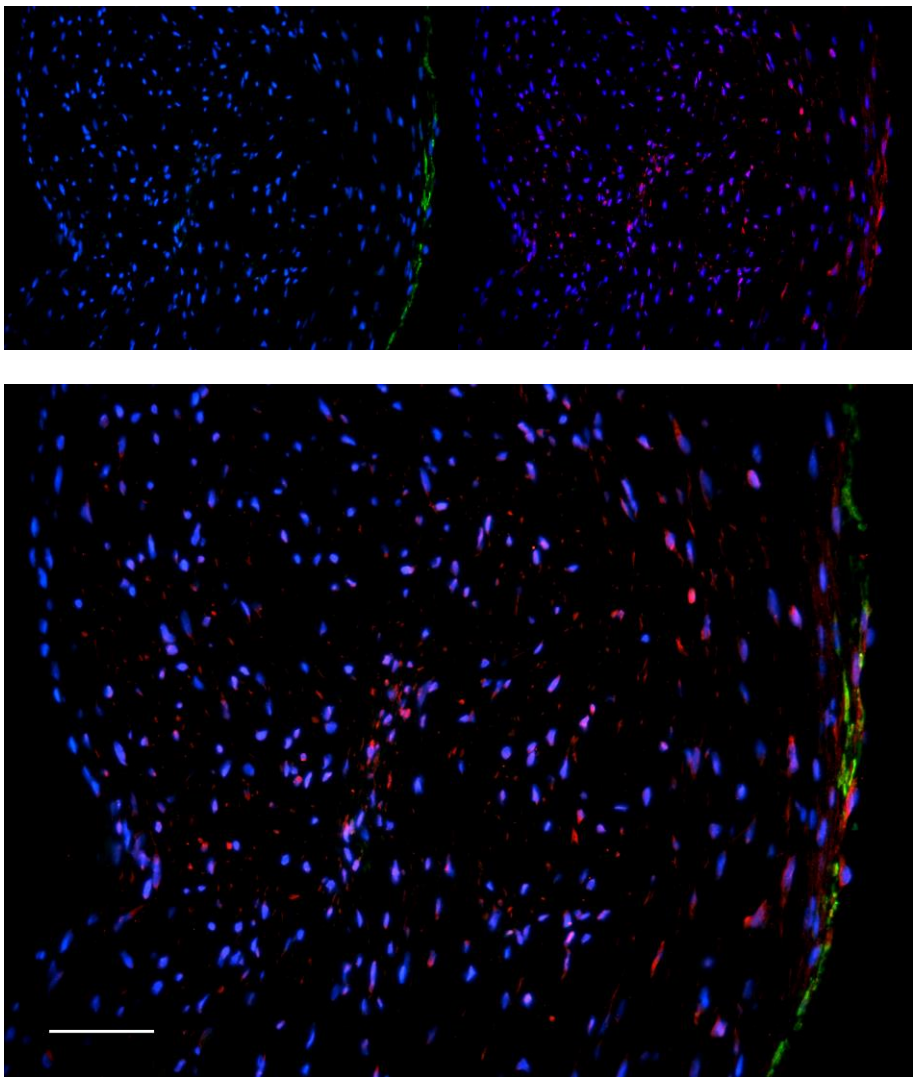

Figure 5-38 Photomicrograph of immunofluorescence images for CDH5 (red) and α-SMA (green), and nuclei counterstained with DAPI. Normal canine mitral valve, middle portion. (Top left) α-SMA with DAPI. (Top Right) CDH5 with DAPI. (Bottom) Merged image of α-SMA, CDH5, and DAPI. Atrial endothelial cells were CDH5 positive, and there were more CDH5 (+) spindle shape interstitial cells aggregating underneath the myofibroblast cluster. Myofibroblasts (α-SMA positive) were localized linearly sub-adjacent to the atrial endothelial cells with some endothelial expression of α-SMA. Scale bar = 50 µm.

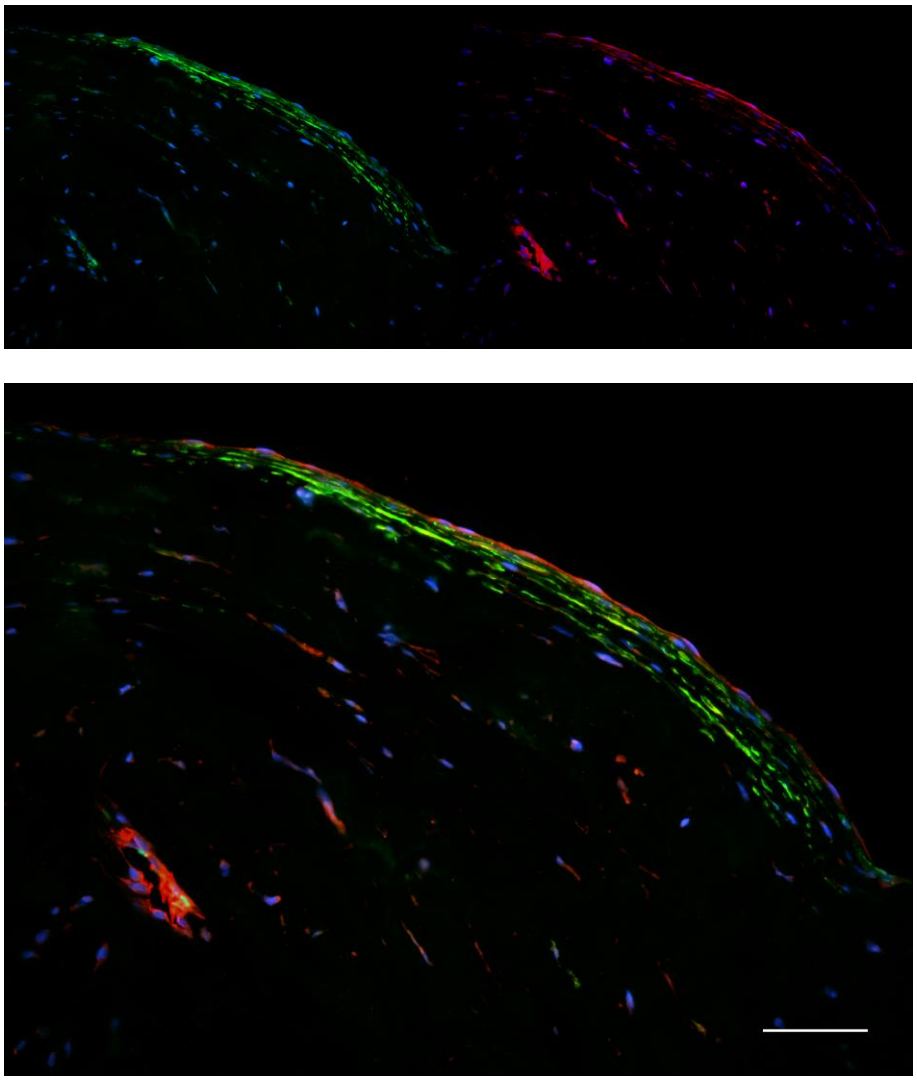

Figure 5-39 Photomicrograph of immunofluorescence images for CDH5 (red) and α-SMA (green), and nuclei counterstained with DAPI. Myxomatous canine mitral valve, mid portion. (Top left) α-SMA with DAPI (Top Right) CDH5 with DAPI (Bottom) Merged image of α-SMA, CDH5, and DAPI. Atrial endothelial cells and vessel endothelial cells were CDH5 positive, and a few endothelial cells were also co-expressing α-SMA. Linear clusters of myofibroblasts (α-SMA positive) were sub-adjacent to the endothelial cells, and the majority of the cells in the myofibroblast clusters were α-SMA+/CDH5-, with few cells that were positive for both CDH5 and α-SMA. Scale bar = 50 µm.

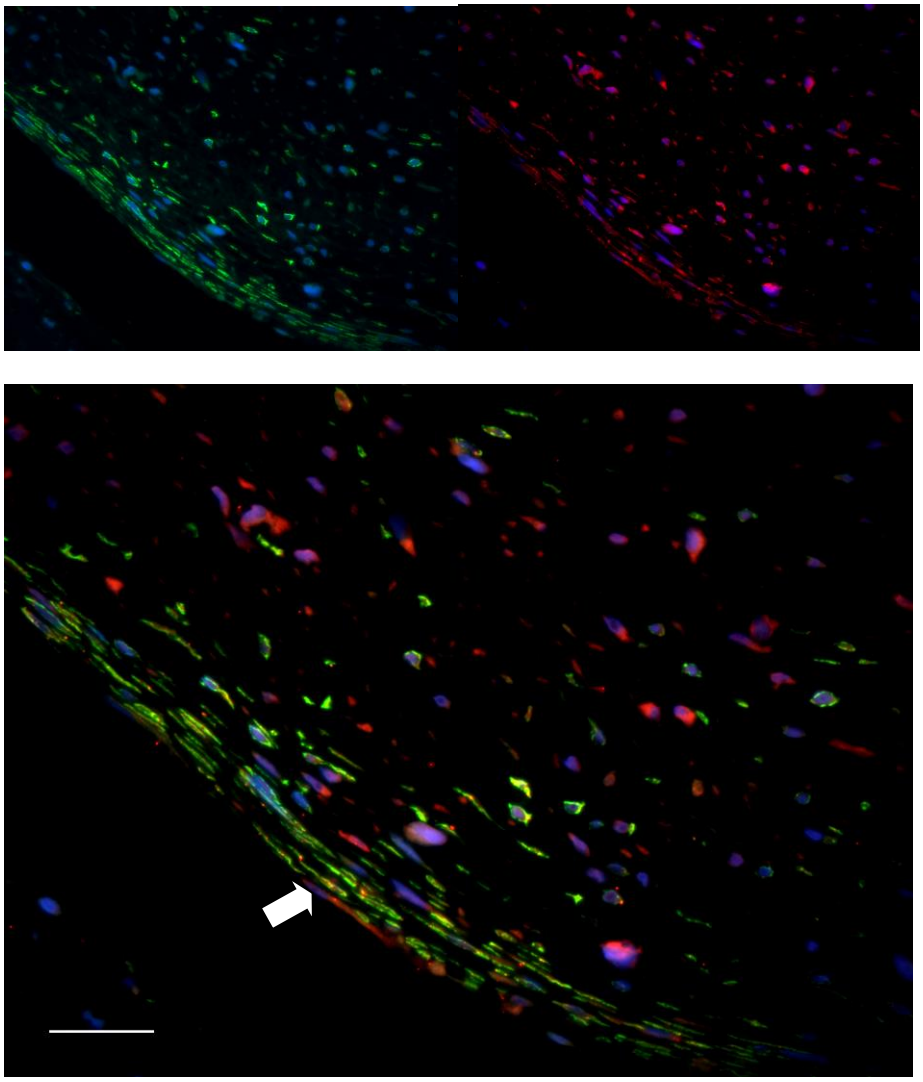

Figure 5-40 Photomicrograph of immunofluorescence images for CDH5 (red) and α-SMA (green), and nuclei counterstained with DAPI. Myxomatous canine mitral valve, distal-end. (Top left) α-SMA with DAPI. (Top Right) CDH5 with DAPI. (Bottom) Merged image of α-SMA, CDH5, and DAPI. There were no distinct CDH5+/α-SMA- endothelial cells at the surface of overtly myxomatous region, and only one CDH5+/ α-SMA- cell was noted in this field (white arrow). All sub-endothelial myofibroblasts (α-SMA+) clusters were spindle and elongated in shape with expression of CDH5. However, stroma myofibroblasts were not distributed in a linear cluster pattern, but also show co-expression of α-SMA and CDH5. Scale bar = 25 µm.

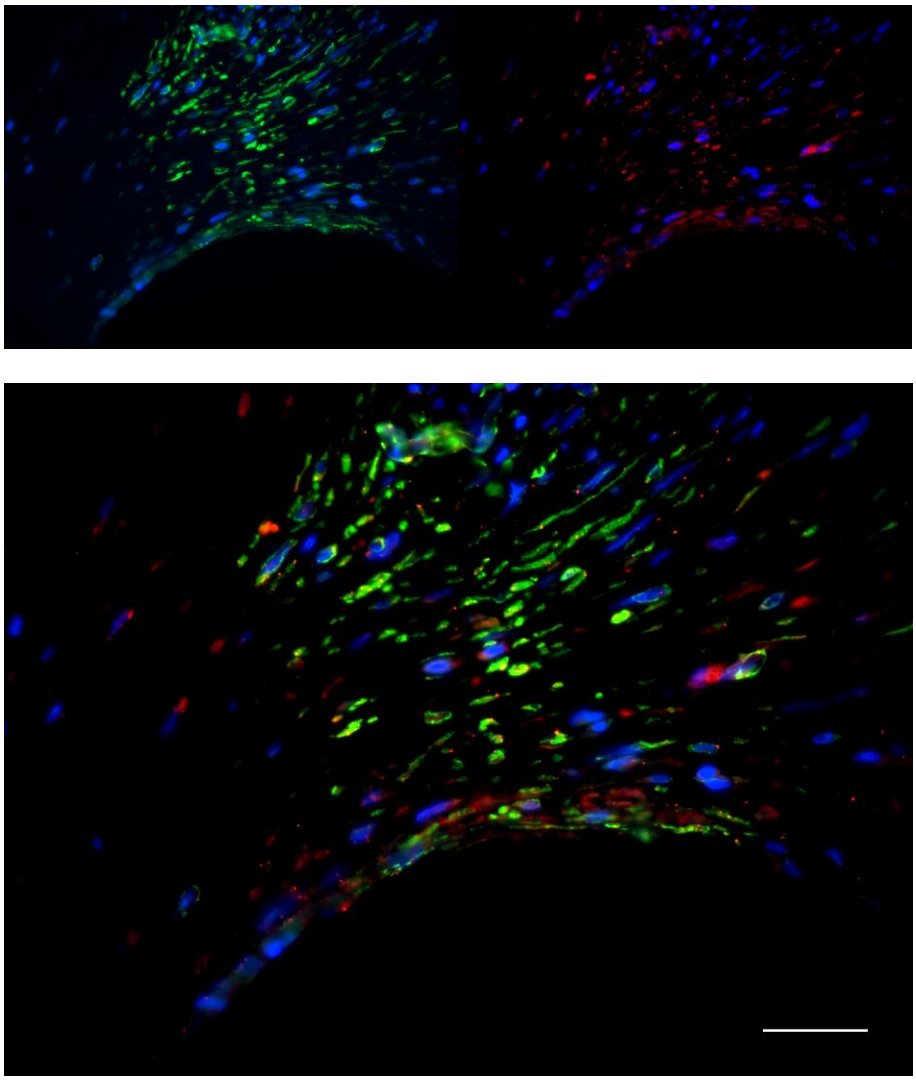

Figure 5-41 Photomicrograph of immunofluorescence images for CDH5 (red) and α-SMA (green), and nuclei counterstained with DAPI. Myxomatous canine mitral valve, distal-end. (Top left) α-SMA with DAPI. (Top Right) CDH5 with DAPI. (Bottom) Merged image of α-SMA, CDH5, and DAPI. There were no distinct CDH5+/α-SMA- endothelial cells at the surface of overtly myxomatous region. The myofibroblasts clusters were evenly distributed in this field. Though the majority of myofibroblasts were the classic spindle shape, there were also round cells. Interestingly, there were more round shape α-SMA-/CDH5+ cells in the myofibroblast clusters. Scale bar = 25 µm.

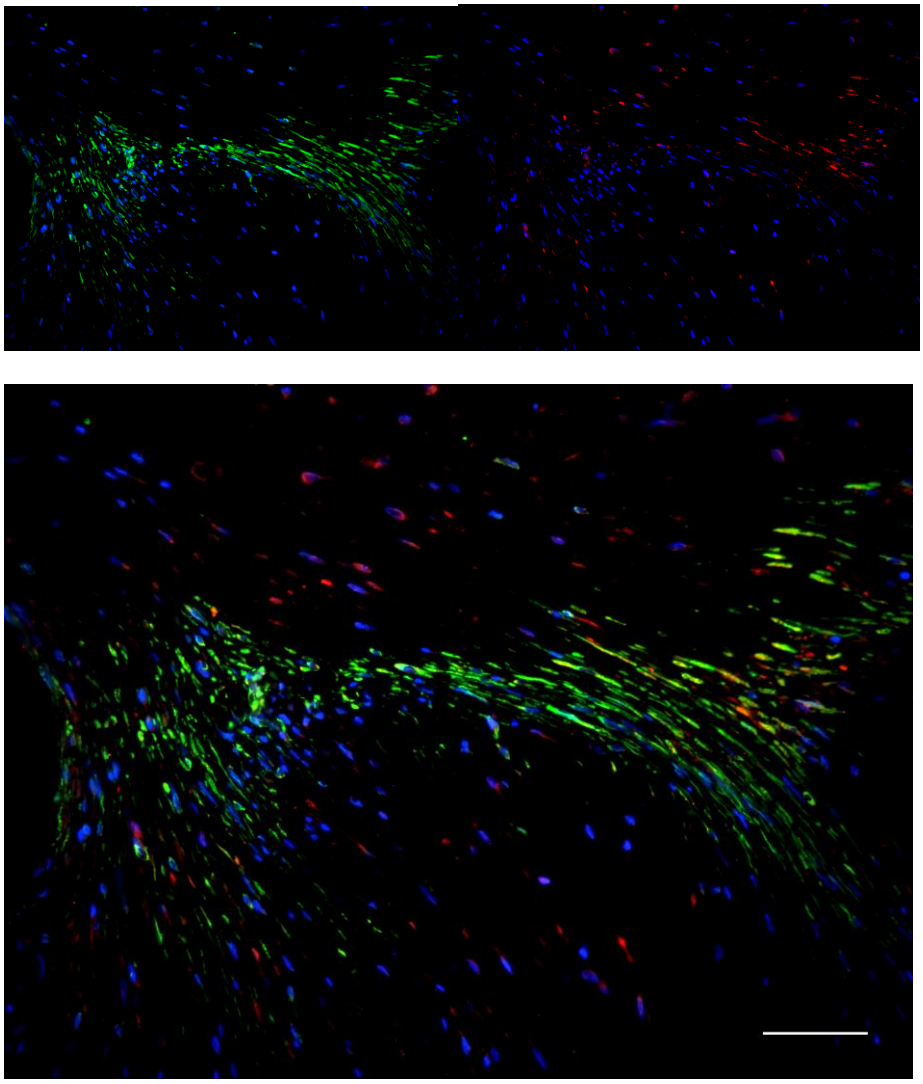

Figure 5-42 Photomicrograph of immunofluorescence images for CDH5 (red) and α-SMA (green), and nuclei counterstained with DAPI. Myxomatous canine mitral valve, distal-end. (Top left) α-SMA with DAPI. (Top Right) CDH5 with DAPI. (Bottom) Merged image of α-SMA, CDH5, and DAPI. Whorl-like pattern of myofibroblast clusters were seen at the overtly myxomatous area. In this section, most myofibroblasts were of spindle and elongated shape, and the differences in myofibroblasts direction between clusters at the surface (left) and stroma (right) may represent a difference in cell orientation. Scale bar = 50 µm.

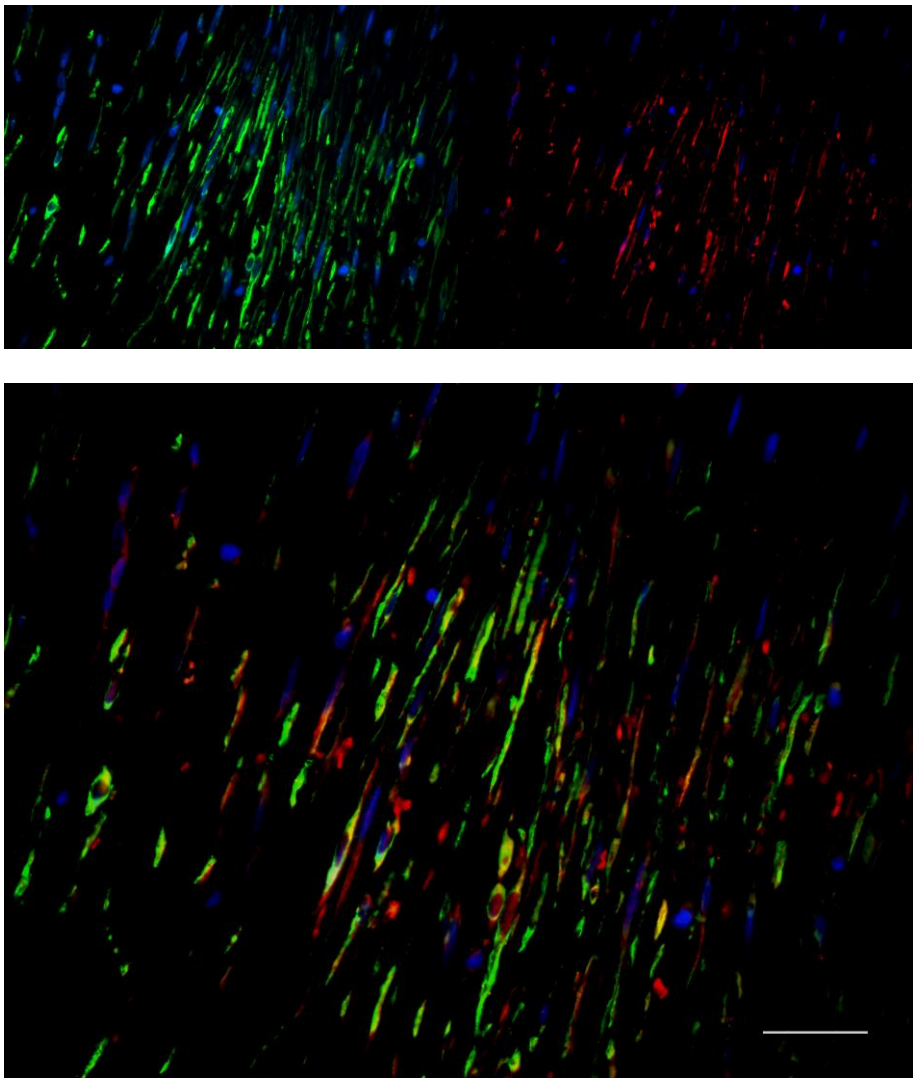

Figure 5-43 Photomicrograph of immunofluorescence images for CDH5 (red) and α-SMA (green), and nuclei counterstained with DAPI. Myxomatous canine mitral valve, distal-end. (Top left) α-SMA with DAPI. (Top Right) CDH5 with DAPI. (Bottom) Merged image of α-SMA, CDH5, and DAPI. In the myxomatous stroma, clusters of spindle shaped cells were a mixture of mainly α-SMA+/CDH5+ and α-SMA-/CDH5+ cells. Scale bar = 25 µm.

A summary of immunohistochemistry studies is presented in Table 5-3.

Table 5-3 Summary of the findings by IHC.

Markers	MMVD	Normal
HAS2	Increased expression at the edge of the leaflet, but no change in middle portion. Diffusely expressed in VECs and VICs.	Expressed strongly at VECs and some VICs.
HAS2 / α-SMA	HAS2 co-expressed with α-SMA in myofibroblast clusters (activated VICs) and some α-SMA(-) VICs.	HAS2 co-expressed only with small amount of activated VICs. α-SMA(+) cells were found adjacent to HAS2(+) VECs
SNAI1 / α-SMA	SNAI1 expression mainly found in round-shaped VICs in myofibroblast clusters, and not co-expressed with α-SMA	No co-expression. SNAI1 expression occasionally found in VECs.
CDH5 / α-SMA	CDH5 co-expressed with α-SMA both in VICs and VECs.	Strong CDH5 expression in VECs, but also found in VICs in spongiosa. Only a small amount of VECs co-expressed CDH5 and α-SMA.

5.4 Discussion

EndoMT in Mitral valve

During valvulogenesis in the embryonic heart, growth factors such as TGF-βs, BMPs, epidermal growth factor, vascular endothelial growth factors, and NOTCH-SNAI1 signalling trigger endocardial cushion endothelial cells to lose their cell-to-cell adhesion molecules. At the same time increased expression of catabolic enzymes which dismantle the basement membrane allows migration of transformed endothelial cells into the hyaluronan-rich cardiac jelly. The transition of endothelial cells through losing endothelial cell phenotype and acquiring mesenchymal phenotype by expression of α-SMA is the process of EndoMT, a sub-class of EMT. [1,86] In the previous chapters, transcriptomic profiling identified the key biological functions which suggest EndoMT is on-going in MMVD, and these included the inflammatory response, basement membrane disruption, and mesenchymal differentiation. [139]

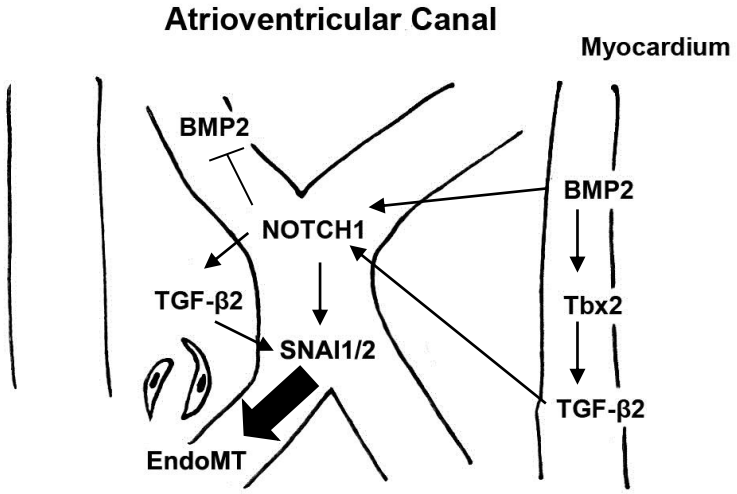

Figure 5-44 NOTCH1 orchestrates a network of signalling pathways for EndoMT and heart valve formation. The figure was modified from [187].

Figure 5-44 demonstrates the signalling pathways involved in EndoMT and their co-ordination by NOTCH during valve development. In the atrioventricular canal endocardium NOTCH normally represses BMP2. Interestingly, expression of

NOTCH is able to promote non-invasive EndoMT in a Snail1 and TGF-β2–dependent manner alone, but cannot initiate a complete invasive EndoMT. For complete invasion, BMP2 secreted from the adjacent myocardium is required to act in concert with NOTCH. BMP2 from the myocardium can induce EndoMT by maintaining SNAI1/2 activity in conjunction with NOTCH. [59,187] Surprisingly in the current study (Chapter 3) NOTCH expression was higher in normal mitral valves compared to myxomatous mitral valves, and this finding may suggest normal NOTCH expression may play a role in maintaining healthy mitral valve structure without of triggering EndoMT. The NOTCH-SNAI1 signalling pathway is described in more detail below.

HAS2 Expression in Normal Mitral Valves

In cardiac jelly biosynthesis of hyaluronan occurs at the plasma membrane by alternating addition of glucuronic acid and N-acetylglucosamine resulting in a polymer. This polymer may vary in length from 2000 to 25,000 disaccharides. There are three hyaluronan synthesizing enzymes found in vertebrates; Has1, 2 and 3, and HAS2 is highly expressed during heart development. [188] HAS2 has also been shown to be involved in endocardial cushion expansion and is considered the main source of hyaluronan production during valve formation and tissue regeneration. [98,189,190] The biological functions of hyaluronan have been comprehensively reviewed by Toole. [191] The chains of hyaluronan are negatively charged and osmotically active, which attracts large amounts of salt and water. Once hyaluronan is deposited in the cardiac jelly or connective tissues it links to extracellular matrix and forms a strong meshwork that is resistant to biomechanical forces. [191] In the adult heart hyaluronan is mainly found in aortic and mitral valve leaflets. Alterations in hyaluronan and its localization are linked to aortic valve calcification and down-regulation of hyaluronan receptor for endocytosis (HARE), without change in hyaluronan-binding protein (HABP). This was discovered in human myxomatous mitral valves confirming an important role for hyaluronic acid during normal cardiac valve function and a role in disease. [166,192,193]

In the present study, in normal canine mitral valves HAS2 expression was mainly seen in the endothelium at atrial and ventricular sides. However, a few HAS2

positive cells were found in the spongiosa layer (Figure 5-20). Endothelial expression of HAS2 in normal mitral valve may be due to mechanisms of valve homeostasis, remodelling and repair, and mechanical protection. Increased synthesis of hyaluronan forming along the leaflet surface acts as a cushion protecting underlying tissues against the shear stress created by blood flow. In atherosclerosis, hyaluronan is suggested to be atheroprotective and increased expression of HAS2 under shear stress conditions has also been demonstrated in an arterial pulsatile laminar flow model using human umbilical vein endothelial cells (HUVECs) which supports this hypothesis.[194] In addition to being a structural component of the cardiac jelly, exogenous hyaluronan is able to induce EndoMT in endocardial cushion explants derived from HAS2-null hearts. [195] In ovarian tumour cells hyaluronan-induced ErbB2 phosphorylation leads to β-catenin nuclear translocation, transcriptional activation, and increased cell migration. [188,196] In the spongiosa of normal mitral valves, a few spindle shape interstitial cells (α-SMA-) expressed HAS2 (Figure 5-16), possibly indicating the presence of a pro-migratory phenotype of valve interstitial cells. If that is the case, this is likely to be triggered by TGF-β/BMP signalling through a MEKK3/ERK1/2/5-dependent cascade pathway. [93,197,198]

HAS2 Expression in Myofibroblasts

In myxomatous mitral valves prominent myofibroblast (α-SMA+) clusters were identified at the edge of the mitral valves and in the stroma of the overtly myxomatous area (Figure 5-18). Myofibroblast clusters were generally co-expressing HAS2 with α-SMA. In lung fibrosis models myofibroblast accumulation is also found at sites of tissue remodelling with associated increased collagen and hyaluronan production and over-expression of HAS2 by myofibroblast produces a more aggressive phenotype leading to severe lung fibrosis and death. [199] Therefore up-regulation of HAS2 with myofibroblastic differentiation in myxomatous mitral valves also suggests that an aggressive (productive) phenotype of interstitial cells with invasiveness exists. The identification of HAS2+/α-SMA- spongiosa interstitial cells in normal and myxomatous mitral valves might suggest myofibroblastic differentiation begins with HAS2 overexpression which facilitates TGF-β1 signalling and is followed by acquisition of a migratory phenotype (α-SMA expression). [200]

Interestingly, α-SMA was also expressed by a few HAS2+ endothelial cells at the atrial side (Figure 5-15) of the normal mitral valves, indicating on-going EndoMT.

SNAI1 Expression

During embryonic development, members of the Snail family of zinc-finger transcription factors play essential roles in valvulogenesis. Induction of EndoMT is one of their best-known functions. From recent experimental findings SNAI1 has been suggested as a survival factor and inducer of cell movement, rather than solely as an inducer of EndoMT or cell fate (Figure 5-45). Many up-stream regulators of SNAI1 gene such as TGF-β, BMP, NOTCH, and WNT have been identified (Figure 5-45). [201]

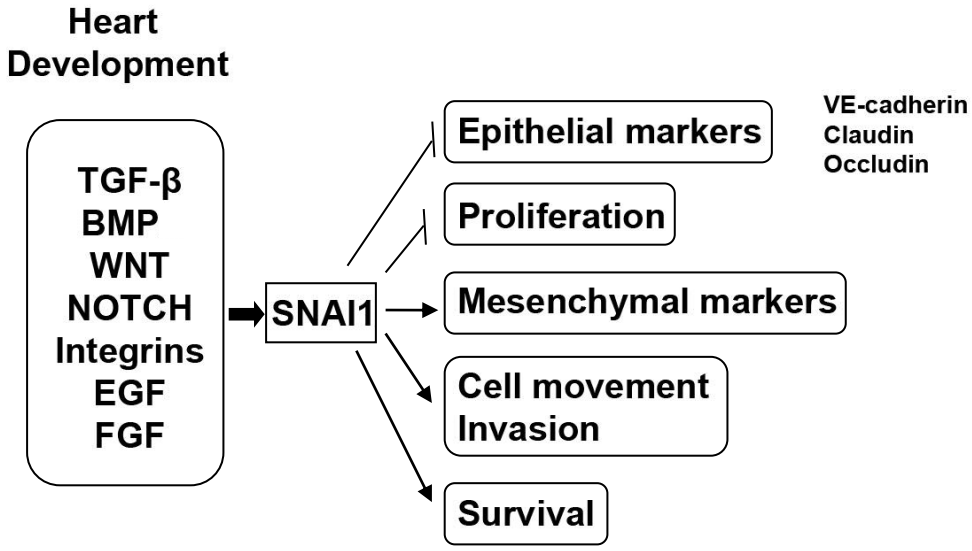

Figure 5-45 SNAI1 expression is associated with down-regulation of epithelial or endothelial markers and inhibition of proliferation, but promoting mesenchymal markers, cell survival and cell movement. Up-stream regulators of SNAI1. Modified from [201].

In normal canine mitral valves there was a strong expression of Snail, but only seen in the endothelial cells and not interstitial cells. A possible explanation is that this may be associated with endothelial cell survival. [201] In myxomatous mitral valves SNAI1+ cells were found within the myofibroblast cluster towards the leaflet surface and in the stroma (Figure 5-23, 5-24, and 5-25). These SNAI1+ cells were mostly α-SMA- and had a distinctive round shaped morphology compared with the adjacent

spindle shape myofibroblasts. These SNAI1+/α-SMA- cells might be trans-differentiated cells through partial EndoMT (acquiring migratory phenotype without expressing α-SMA) and originating from surface endothelial cells. [201]

Due to the SNAI1 expression, these differentiated cells not only obtain migratory phenotype, but show minimum proliferative activity. [201] SNAI1+ cells then trigger differentiation of surrounding VICs into aVIC through a paracrine mechanism, which was shown in a myocardium fibrosis model. [202] Interestingly, SNAI1+ transformed cells triggered the adjacent cardiac fibroblast activation through paracrine secretion of connective tissue growth factor (CTGF), and activated cardiac fibroblasts showed higher extracellular matrix synthetic activity. [202] In canine myxomatous mitral valve disease, this paracrine mechanism could play a key role in VIC activation.

Experimental studies in kidney fibrosis, myocardial infarction, and myxomatous mitral valve disease suggest myofibroblasts play a key role in extracellular matrix synthesis and deposition. [108–110] Myofibroblasts are identified as cells that are capable of tissue repair after damage by secreting extracellular matrix and can contract through α-SMA possibly contributing to valve mechanics. [58,203] The orchestration of secreted cytokines, such as TGF-β, by myofibroblasts plays a major role in tissue remodelling. [159] Several studies have examined myofibroblasts in MMVD but the origin of these cells remains unknown. In a kidney fibrosis model, it was predicted that 50% of the myofibroblasts are derived through proliferation from resident fibroblasts, 35 % differentiate from bone marrow-derived cells, 10 % arise from EndoMT, and 5 % through EMT. [204] In the mitral valve, whether or not there is similar proportion of myofibroblasts derived from EndoMT to that seen in kidney requires further investigation.

In the high-resolution confocal microscopy tile-scanning there was a small number of myofibroblasts close to the atrial endothelium in the pathology-free mid portion of the normal valve (Figure 5-3 and 5-4). In contrast, a few myofibroblasts were present in the mid portion of myxomatous mitral valves, but present as numerous linear clusters along the surface, and at the edge of the myxomatous regions (Figure 5-7). Since Ki-67 expression was demonstrated in myxomatous mitral valve but absent from normal valves, (Chapter 2) there are three likely sources of myofibroblasts; proliferation, EndoMT and resident fibroblast activation. Considering the potential

different sources of VICs, the accumulation of activated myofibroblasts in MMVD might occur in response to a variety of unrelated stimuli, such as inflammatory cytokines, growth factors (e.g. TGF-β) and mechanical stress. [55,139,205]

In conclusion, immunohistochemistry was able to identify evidence of EndoMT in normal and myxomatous mitral valves. Expression (genes and proteins) of ACTA2 (α-SMA), CDH5 (VE-cadherin), SNAI1 and HAS2 was investigated in MMVD and normal valves. Although both microarray and Q-PCR results showed no evidence (marginal p-value) of change in CDH5, ACTA2, SNAI1 expression, some evidence of EndoMT derived from IHC may support the hypothesis of EndoMT and the capacity for endothelial migration in MMVD pathogenesis. Of particular interest is the expression of HAS2 in myxoid stroma and close to the endothelium of diseased valves. It is the presence of HA that drives embryonic valve development and allows EndoMT to progress. Furthermore, there is co-expression of HAS2 with α-SMA in endothelial and interstitial cells, and this phenotype may suggest a more aggressive (productive) behaviour of myofibroblasts. VE-cadherin is clearly expressed in both normal and diseased valve endothelium, suggesting cell-to-cell contact has not been completely lost. Co-expression of VE-cadherin and α-SMA in normal (endothelial cells) and myxomatous mitral valves (stroma cells) also suggest that one source of origin of myofibroblasts is through EndoMT.

Studies of MMVD have tended to examine the cellular and molecular events where there is end-stage disease and the series of events that have led to that situation are difficult to elucidate. One hypothesis derived from the present study as well as the literature, is that unidentified processes result in activation of a quiescent VIC population in the valve stroma to an activated phenotype and these cells then contribute to inappropriate remodelling of the valve. The trigger might be endothelial activation and/or damage which then results in activation of the TGF-β/5HT signalling pathway enabling VIC phenotypic transformation. EndoMT suggests an additional disease pathogenesis hypothesis whereby the α-SMA positive cells seen in MMVD partially originate from the resident VIC population (activation) or are differentiated endothelial cells (EndoMT). EndoMT events could be a consequence of endothelial damage and dysfunction of endothelial-interstitial signalling. [55] Understanding the role of EndoMT might allow identification of novel therapeutic

targets, such as normalization of genomic expression (NOTCH-SNAI1-TGF-β signalling).

6 Chapter 6 MicroRNA Expression in Canine Myxomatous Mitral Valves

6.1 Introduction

MicroRNAs (miRNA) are short (19-22 nucleotides), single-stranded, non-coding RNAs that specifically anneal with complementary sequences in mRNAs. Binding the designated mRNA, the microRNA silences the mRNA and suppresses protein expression. In general, one miRNA has multiple targets, and depending on its abundance, a miRNA can act as a fine-tuner of gene expression (orchestrating various pathways) or as an on/off switch. [206,207] These features highlight the great potential of miRNAs as therapeutic targets in many diseases. The most widely studied applications of miRNAs to date are predominantly cancer and cardiovascular disease, and this is based on miRNA expression profiling in animal models or samples from patients with cardiac disease. As examples of therapeutic possibilities, anti-miR-21 (chemically engineered oligonucleotides) which inhibit activity of miR-21 have been shown to have potential anti-fibrotic effects in lung and kidney fibrosis, a clinical trial of miRNA has been reported in treatment of hepatitis C infection and fibrosis- and hypertrophy-associated miR-29a has been recognized as a biomarker for hypertrophic cardiomyopathy (HCM) in human. [208,209,210,211] Nevertheless, more studies are needed to understand the biological function of miRNA.

One of the challenges in miRNA research is target prediction, which is generally based on bioinformatics methods and databases such as Targetscan or DIANA-micro-T-CDS, and the data is sometimes overwhelming and requiring further and repeated data mining[212,213,214]. To date, there have been several miRNA profile data reports for canine cancer, but there is no miRNA profiling data available for myxomatous mitral valve in any species. This study aims to investigate the miRNA transcriptomic expression pattern and identify potential functions in canine MMVD using miRNA target prediction platforms mentioned above along with the bioinformatics tool BioLayout *Express*[3D]. This will allow the expression profiling of miRNA based on the use of a correlation measure to define similarities between groups. [123]

6.2 Material and Methods

6.2.1 Microarray

A list of differentially expressed miRNAs was manually separated from the total differentially expressed gene list initially generated in Chapter 3. For cutoff setting, fold-change ≥ 2 or ≤ -2, FDR < 0.05, and p-value < 0.05 were considered significant.

6.2.2 miRNA Expression Validation

Reverse Transcription (RT) PCR

The cDNAs for TaqMan microRNA assays (cfa-miR-218-1, cfa-miR29c-1, and cfa-miR-23b) were synthesized from the same RNA samples as used for microarray analysis (Chapter3) using the TaqMan MicroRNA Reverse Transcription primers and universal reverse transcription kit (Roche). Briefly, 1 µl of miRNA specific RT-primer, 1 µl of dNTPs (Roche), and 100 ng to 2 µg of total RNA (1 – 5 µl) was added to a clean Eppendorf tube. Nuclease-free water was added to make up to 13 µl of final reaction volume. The sample was heated at 65˚C for 5 minutes followed by 1 minute incubation on ice, after which 4 µl of 5x first-strand buffer (Roche), 1 µl of 0.1M DTT, 1 µl RNase inhibitor (Roche), and 1 µl of SuperScript III (Roche) were added. The sample was incubated at 50˚C for 45 minutes. Inactivation of the reaction was achieved by incubation at 75˚C for 15 minutes. Final 20 µl of cDNA samples were stored at -20˚C prior to use.

Q-PCR

The MicroRNA Q-PCR assays were performed in duplicate in 96-well plates with one no-template-control (RNase-free water) for each sample. For each well, the reaction mix consisted of 1µl ready-made mixture of miRNA-specific forward PCR primer, specific reverse PCR primer, and miRNA-specific MGB probe (Life technologies), 0.5 µl of 2x master mix (Roche Diagnostics), 0.75 µl of first strand cDNA, 5 µl of 2x universal PCR master mix (Roche), and 3.75 µl of nuclease-free water. After reaction mix and the cDNA were separately pippeted into the designated wells, the plate was sealed with PCR film (Thermo Scientific) and wrapped with tin foil to protect from light. The plate was then vortexed and centrifuged down at 15,000 rpm for 5 minutes at 4℃. The plate was unwrapped and placed into the PCR

machine (LightCycler 480; Roche Diagnostics). The amplification was programmed and performed according to a standard PCR cycle (Table 6-2). Since cfa-miR-218 is encoded in intron12 and 15 of SLIT2, the SLIT2 gene was also assayed by the same Q-PCR method as described in 4.2.2. MRPS25 was also used as a reference gene in this study. Detail of the miRNA assays can be found in Table 6-1.

Test for primer efficiency rate and calculation for relative gene expression were performed following same method described in 4.2.2.

Table 6-1 Information for the miRNAs assays and the primers for SLIT2

Assay ID	miRNA	Gene family ID	Sequence
008281_mat	cfa-miR-23b	MIPF0000027	AUCACAUUGCCAGGGAUUA
000587	cfa-miR-29c	MIPF0000009	UAGCACCAUUUGAAAUCGGUUA
000521	cfa-miR-218	MIPF0000026	UUGUGCUUGAUCUAACCAUGU
Gene Name	Probe No.	Forward Primer	Reverse Primer
SLIT2	37	5’ cgcttctgccatttacagc 3’	5’ cggagagggacaggctct 3’
MRPS25	15	5’tcttggggaagaacaaggaa3’	5’agtgggctgggtgagaaag3’

Table 6-2 Programmed PCR cycles for miRNA assays

Action	Temperature	Time	Cycle
Pre-incubation	95℃	10 minute	
Amplification	95℃	10 second	45
	60℃	30 second	
	72℃	1 second	
Cooling	40℃	30 second	1

6.2.3 miRNA Target and Pathway prediction

TargetScan 6.2

The targets of individual differentially expressed miRNAs were analyzed in TargetScan 6.2. [212] The top 200 predicted targets were retrieved irrespective of site conservation (within primitive creature and preserved through evolution). For each predicted target of each miRNA, the sum of the context+ score for the sites to that miRNA was calculated as the total context+ score. Predicted targets of each miRNA family are sorted by total context+ score. The representative miRNA is the miRNA in its family with the most favorable (lowest) total context+ score. If more than one miRNA has the most favorable context+ score, the miRNA with the lowest number and/or letter is shown. Poorly conserved sites are given the same weight as conserved sites. Although only one miRNA is chosen as the representative miRNA, all the other miRNAs of the miRNA family are also predicted to target the same target gene at the same target site(s). Since overlapping sites cannot be occupied at the same time, some are removed to create a set of non-overlapping sites while maximizing the total context score. These non-overlapping sites are used to calculate the total context score. [215]

The six contributors to the context+ score were; site-type contribution, 3' pairing contribution, local AU contribution, position contribution, TA (target site abundance) contribution, and SPS (see-pairing stability) contribution.

DIANA-TOOLs

DNA Intelligent Analysis (DIANA) DIANA-miRPath 2.0 is a miRNA pathway analysis web-server, and was used to predict the targets of miRNA clusters identified by BioLayout *Express*^{3D}. Briefly, it utilized miRNA predicted targets and experimentally verified targets and combined these results with merging and meta-analysis algorithms, performing hierarchical clustering of miRNAs and pathways based on their interaction. [216,217]

6.2.4 BioLayout *Express*^{3D}

Network analysis and visualization was conducted using BioLayout *Express*^{3D} version 3.3. Briefly, signal intensity value for all miRNAs for all samples were

formatted in an excel file following the software manual instructions. [123] The network graph was then illustrated using a correlation threshold of $r \geq 0.9$. Markov clustering algorithm (MCL) analysis was conducted at an inflation value 2.2 (controlling granularity of clustering) according to recommendations. [123] Clusters of miRNA were exported and mined in DIANA-micro-T-CDS for miRNA pathway prediction.

6.3 Results

6.3.1 Overview of miRNA Expression

In total, 302 miRNAs were profiled by the microarray (Affymetrix Canine Gene 1.0 ST Array). There were only 29 miRNAs that were differentially expressed and all of them were down-regulated in MMVD (Table 6-3).

Table 6-3 Differentially expressed miRNAs

Transcript ID	miRNA	Fold-Change	p-value	Overlapping transcripts
14273759	cfa-miR-340	-8.49	1.78E-05	ENSCAFT00000038586; **RNF130-201**; intron 2
14384476	cfa-let-7c	-7.85	0.00149098	ENSCAFT00000032603; exon 1
14404220	cfa-miR-218-1	-6.82	0.000110552	ENSCAFT00000044488; **SLIT2-201**; intron 12 ENSCAFT00000026343; **SLIT2-202**; intron 15
14337772	cfa-miR-708	-6.70	1.33E-05	ENSCAFT00000048242; intron 1
14296611	cfa-miR-30e	-4.89	2.17E-06	ENSCAFT00000004517; **NFYC-201**; intron 5
14430582	cfa-miR-214	-4.82	1.34E-08	ENSCAFT00000023557; **DNM3-201**; intron 13
14341700	cfa-miR-15a	-4.55	0.00303761	ENSCAFT00000032594; exon 1
14409053	cfa-miR-125b	-4.39	0.000297807	ENSCAFT00000032610; exon 1
14294874	cfa-miR-2414	-4.39	3.30E-05	n/a
14455304	cfa-miR-181b	-4.28	9.06E-05	intergenic
14458526	cfa-miR-532	-4.24	0.00139701	ENSCAFT00000025340; **CLCN5-201**; intron 3
14262641	cfa-miR-23b	-4.14	1.41E-06	ENSCAFT00000032742; exon 1 ENSCAFT00000001991; **FANCC-202**; intron 12
14433552	cfa-miR-29b	-4.02	0.00317446	ENSCAFT00000032570; exon 1

14433550	cfa-miR-29c	-3.56	0.000169906	ENSCAFT00000032614; exon 1 ENSCAFT00000048008; intron 15
14263997	cfa-miR-let7e	-3.39	4.31E-05	ENSCAFT00000032552; exon 1
14369956	cfa-miR-107	-3.14	0.00021131	ENSCAFT00000032573; exon 1 ENSCAFT00000039603; intron 5 ENSCAFT00000011488; intron 5
14455306	cfa-miR-181a	-3.05	0.000567175	Intergenic
14384474	cfa-miR-99a	-3.04	8.63E-05	Intergenic
14278575	cfa-miR-32	-2.81	0.000116053	ENSCAFT00000004537; **TMEM245-201**; intron 14
14407894	cfa-miR-145	-2.69	0.00133843	Intergenic
14452361	cfa-miR-454	-2.60	0.000893899	ENSCAFT00000042908; **SKA2-201**; intron 1
14430433	cfa-miR-1843	-2.56	0.00227232	ENSCAFT00000042380; exon 1 ENSCAFT00000022674; **RFWD2-201**; intron 18
14328621	cfa-let-7g	-2.53	0.00166027	ENSCAFT00000032716; exon 1 ENSCAFT00000015643; **WDR82-201**; intron 2
14427963	cfa-miR-197	-2.45	0.001507	ENSCAFT00000032599; exon 1
14284320	cfa-miR-30c	-2.41	0.000218963	ENSCAFT00000004517; NFYC-201; intron 5
14407896	cfa-miR-143	-2.40	0.00306725	Intergenic
14275110	cfa-miR-872	-2.39	4.03E-05	ENSCAFT00000002673; **IFT74-201**; intron 13
14462818	cfa-miR-545	-2.05	0.00656767	Intergenic
14409051	cfa-let-7a	-2.02	0.00290226	Intergenic

Signal intensity for miRNA

The expression of all 29 miRNAs was generally low (signal intensity < 300) in myxomatous mitral valves, but comparatively high in normal mitral valves (signal intensity between 300 and 1,000). Again, when the signal intensity was lower than 100, it was considered as no expression or background noise. The only highly expressed miRNA was cfa-miR-218, for which the signal intensity was around 1,000 in normal mitral valves (Figure 6-1).

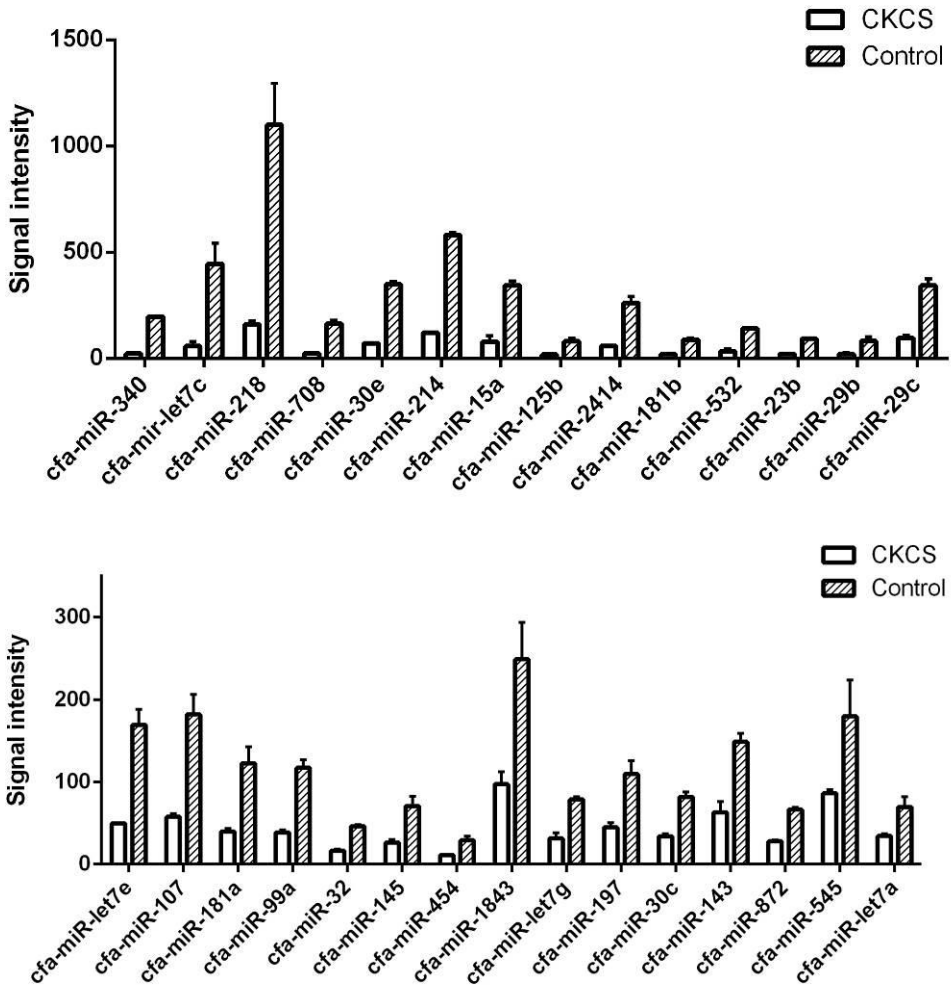

Figure 6-1 Signal intensity for 29 differentially expressed miRNAs

6.3.2 Efficiency Rate for Primers

The efficiency rates for miRNA specific primers, SLIT2, and MRPS25 are shown in Table 6-4.

Table 6-4 Efficiency rate for miRNA specific primers, SLIT2, and MRPS25

Assay	Efficiency Rate %	Assay	Probe No	Efficiency Rate
cfa-miR-23b	89.17	SLIT2	37	130
cfa-miR-29c	93.68	MRPS25	15	104.51
cfa-miR-218	96.06			

The efficiency rate of primers for cfa-miR-29c (93.68%), cfa-miR-218 (96.06%), and MRPS25 (104.51%) were within acceptable range (90-110%). The efficiency rate of the primer for cfa-miR-23b (89.17%) was borderline. The only value outside the acceptable range was the efficiency rate for SLIT2 (130%). (Figure 6-2)

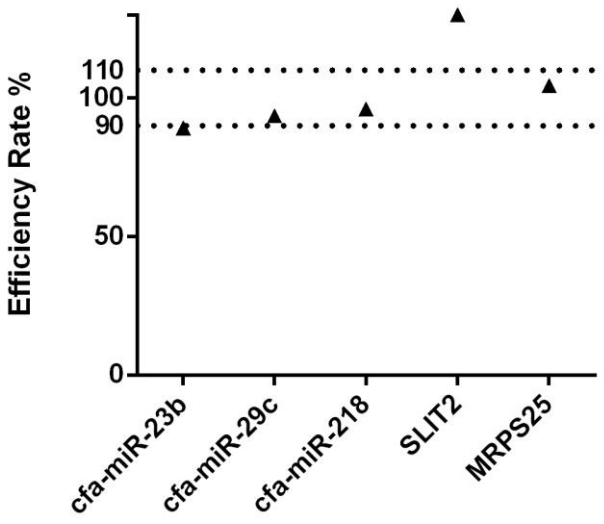

Figure 6-2 Efficiency rate for miRNA specific primers, SLIT2, and MRPS25

6.3.3 miRNA Microarray Validation

In general, the expression pattern of miRNAs and SLIT2 determined by Q-PCR was in agreement with the microarray findings, all of which were down-regulated in myxomatous mitral valves. Interestingly, very large fold-changes were noted for cfa-miR-29c (46.26-fold decrease) and cfa-miR-218 (170.07-fold decrease) compared with results from the microarray. (Table 6-5 and Figure 6-3)

Table 6-5 Result of Q-PCR validation for miRNA and SLIT2

miRNA & Gene	Fold-Change (microarray)	Fold-Change (Q-PCR)	p-value (Q-PCR)	Signal Intensity (microarray)	
				Control	MMVD
cfa-miR-23b	-4.14	-4.88 ± 1.70	0.043	92	22
cfa-miR-29c	-3.56	-46.26 ± 1.31	0.004	335	96
cfa-miR-218	-6.82	-170.07 ± 1.62	0.002	1211	167
SLIT2	unchanged	-3.82 ± 2.23	0.057	4201	2019

Fold-change for Q-PCR is presented as Mean±S.D.

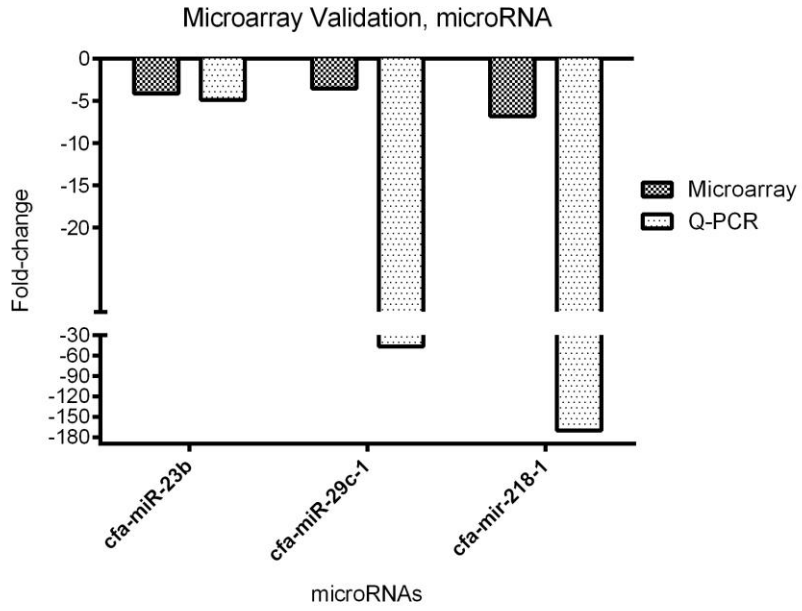

Figure 6-3 miRNA microarray data validation

The signal intensity (from the microarray) of cfa-miR-23b, cfa-miR-29c, cfa-miR-218, and SLIT2 are shown in Figure 6-4. Although SLIT2 expression was lower in MMVD it was not statistically significant.

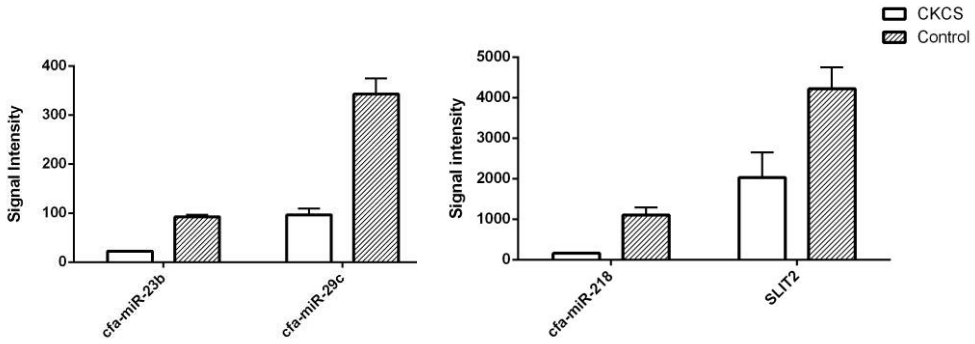

Figure 6-4 Signal intensity for cfa-miR-23b, cfa-miR-29c, cfa-miR-218, and SLIT2

6.3.4 miRNA Target Prediction

The targets of miRNAs were arranged according to the total context+ score (lower the score, stronger the target prediction) and are summarized in Table 6-6 and Table

6-7. The complete targets of differentially expressed microRNAs are present in the Appendix 9.3.

Table 6-6 Selected microRNA targets predicted by TargetScan. (Total context+ score <-0.5)

Target Gene	Total context+ score	Representative miRNA	Target Gene	Total context+ score	Representative miRNA
FGF2	-1.42	cfa-miR-195	BMP8A	-0.6	cfa-miR-99a
ADAMTS17	-1.06	cfa-miR-29b	COL1A1	-0.59	cfa-miR-29a
COL4A4	-0.99	cfa-miR-29a	NOS1	-0.58	cfa-miR-15b
SRGAP2	-0.95	cfa-miR-145	COL1A2	-0.58	cfa-miR-29a
COL3A1	-0.93	cfa-miR-29b	HS3ST2	-0.58	cfa-miR-99a
COL4A5	-0.85	cfa-miR-29b	ITGB8	-0.58	cfa-miR-145
COL11A1	-0.85	cfa-miR-29a	HTR7	-0.58	cfa-miR-197
FBN1	-0.82	cfa-miR-29a	COL7A1	-0.57	cfa-miR-29b
ADAMTS2	-0.8	cfa-miR-29a	SRGAP1	-0.57	cfa-miR-145
GLCE	-0.79	cfa-miR-218	HTR4	-0.56	cfa-miR-497
ADAMTS5	-0.79	cfa-miR-197	COL4A1	-0.56	cfa-miR-29c
ELN	-0.78	cfa-miR-29b	CSGALNACT2	-0.56	cfa-miR-29a
COL9A1	-0.74	cfa-miR-29a	HS3ST3B1	-0.56	cfa-miR-99a
FNDC7	-0.69	cfa-miR-143	ACTC1	-0.55	cfa-miR-218
COL5A3	-0.68	cfa-miR-29b	HAS3	-0.55	cfa-miR-29b
COL12A1	-0.65	cfa-miR-15a	LRP6	-0.54	cfa-miR-15a
CTSE	-0.65	cfa-miR-29b	MMP13	-0.54	cfa-miR-99a
AFAP1L2	-0.65	cfa-miR-197	COL5A1	-0.53	cfa-miR-29a
PCDH7	-0.64	cfa-miR-1843	VEGFA	-0.53	cfa-miR-29a
CRTAP	-0.63	cfa-miR-125b	CTSB	-0.52	cfa-miR-214
COL1A1	-0.61	cfa-miR-218	ITGAM	-0.5	cfa-miR-197

Table 6-7 Selected microRNA targets predicted by TargetScan. (Total context+ score > -0.5 ,<-0.3)

Target Gene	Total context+ score	Representative miRNA	Target Gene	Total context+ score	Representative miRNA
NOS1	-0.49	cfa-miR-761	COL14A1	-0.41	cfa-let-7g
NF1	-0.49	cfa-miR-16	COL1A2	-0.41	cfa-let-7g
ADAMTS14	-0.49	cfa-miR-29a	ITGA4	-0.41	cfa-miR-708
FGF12	-0.48	cfa-miR-218	FGF7	-0.41	cfa-miR-16
IL16	-0.47	cfa-miR-214	CLDN12	-0.41	cfa-miR-15b
ROBO1	-0.47	cfa-miR-29a	ADAM21	-0.41	cfa-miR-32
LAMA2	-0.47	cfa-miR-29a	COL19A1	-0.4	cfa-miR-218
VCAN	-0.47	cfa-miR-103	MMP11	-0.4	cfa-miR-761

ADAMTS15	-0.46	cfa-let-7j	HTR1F	-0.4	cfa-miR-532
TNC	-0.46	cfa-miR-218	ADAM12	-0.4	cfa-miR-301a
CLDN12	-0.46	cfa-miR-23a	CTNND1	-0.4	cfa-miR-197
COL15A1	-0.46	cfa-miR-29b	HTR2C	-0.4	cfa-miR-197
NOS1	-0.46	cfa-miR-103	HS6ST3	-0.39	cfa-miR-218
COL3A1	-0.46	cfa-miR-1843	HSPA4	-0.39	cfa-miR-708
HSPG2	-0.45	cfa-miR-497	ECE2	-0.39	cfa-miR-214
HTR4	-0.45	cfa-miR-125b	LDLR	-0.39	cfa-miR-130b
COL2A1	-0.44	cfa-miR-29b	ACTC1	-0.39	cfa-miR-872
ADAMTS18	-0.44	cfa-miR-29b	IL6R	-0.38	cfa-miR-218
FGFR3	-0.44	cfa-miR-99a	HAPLN1	-0.38	cfa-miR-218
IL15	-0.44	cfa-miR-130a	NOS3	-0.38	cfa-miR-214
VEGFA	-0.43	cfa-miR-16	VCAN	-0.38	cfa-miR-23a
COL6A3	-0.43	cfa-miR-29a	HAS2	-0.38	cfa-miR-23a
COL22A1	-0.43	cfa-miR-29a	ADAMTSL3	-0.38	cfa-miR-32
ITGA2	-0.43	cfa-miR-145	BGN	-0.38	cfa-miR-25
ECEL1	-0.42	cfa-miR-195	ITFG1	-0.38	cfa-miR-145
IL12A	-0.42	cfa-miR-23a	ACTG1	-0.38	cfa-miR-145
LRP6	-0.42	cfa-miR-29b	ADAM28	-0.38	cfa-miR-454
ITGAV	-0.42	cfa-miR-32	ESAM	-0.38	cfa-miR-1843
ADAM23	-0.42	cfa-miR-25	ITGAL	-0.38	cfa-miR-143
LRP8	-0.42	cfa-miR-130a	FGF9	-0.38	cfa-miR-143
ADAMTS8	-0.41	cfa-let-7f			

6.3.5 BioLayout *Express*^{3D} & DIANA miRPath Analysis

Nodes representing miRNAs (probesets), with edges representing correlations between individual expression profiles above $r \geq 0.95$, and the colour of the nodes representing the cluster to which they have been assigned are shown in Figure 5-8. The figure shows 106 nodes and 11 major clusters. Most clusters to the left side of the figure were representing lower expression of miRNA in MMVD, and cluster 3 is the only cluster showing higher expression of miRNA in MMVD.

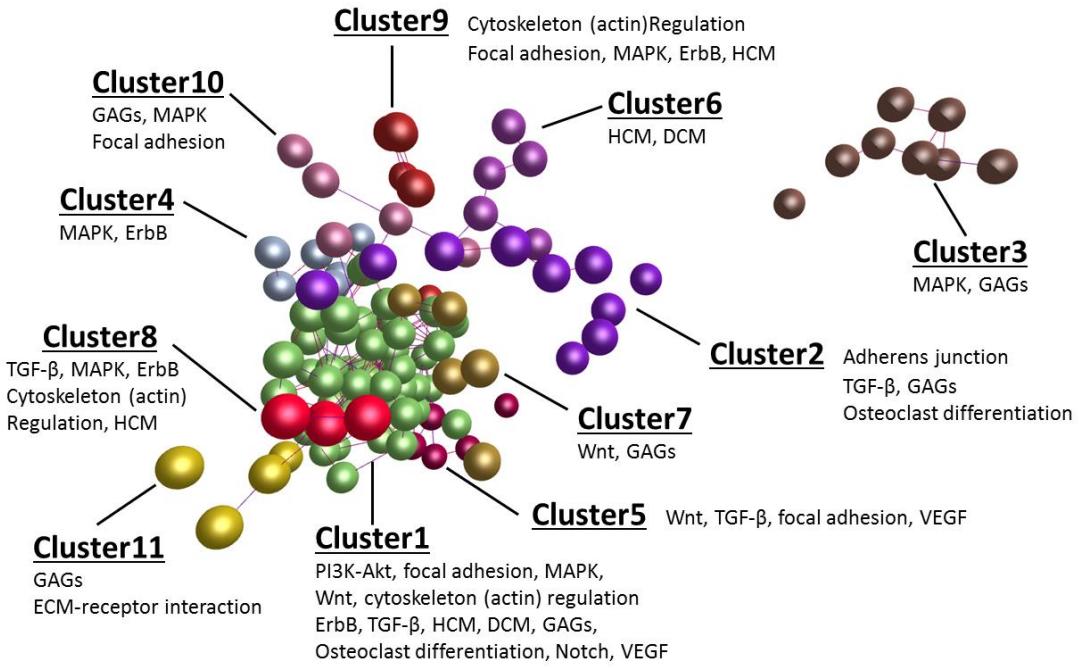

Figure 6-5 Clustering of miRNAs based on their expression profiles, and KEGG pathways associated with each cluster.

miRNAs in each cluster were imported into DIANA miRPath web-server for further data mining. The most significant and biological relevant KEGG (Kyoto Encyclopedia of Genes and Genomes) pathways were attributed to each cluster. [218] Briefly, cluster 1 contained the highest number of miRNAs that were down-regulated in MMVD, and the significant KEGG pathways were associated with PI3K-Akt, focal adhesion, MAPK, Wnt, cytoskeleton regulation, ErbB, TGF-β, hypertrophic cardiomyopathy (HCM), dilated cardiomyopathy (DCM), GAGs biosynthesis, osteoclast differentiation, NOTCH, and VEGF. The satellite clusters (2, 4, 5, 6, 7, 8, 9, 10, and 11) contained similar KEGG pathways, such as TGF- β, focal adhesion, and GAGs biosynthesis.

6.4 Discussion

In general, all 29 differentially expressed miRNAs were down-regulated. However, there were differences in signal intensities for each miRNA. miRNA-218 (>1,000) had the highest signal intensity, followed by miR-let-7c and miR-214 (>500).

Moderate signal intensities (>300) could be seen for miR-30, miR-15, miR-29, miR-2414, and miR-1843. Finally, two thirds of the miRNAs had low signal intensities (of < 150). Overall low signal intensity of miRNAs found in MMVD tissue may be due to the background noise or alternatively a truly low miRNA level, suggesting an inactive epigenetic control over genomic expression. On the other hand, higher miRNA expression in normal mitral valves may indicate a more stringent epigenetic regulation of genome activity. Active cellular changes and increased ECM biosynthesis in MMVD may be the result of dampened inhibitory activity of miRNAs, whereas in normal mitral valves higher level of miRNAs may play a critical role in silencing valve interstitial cells. The best example of such processes is where miR-29, which regulates numerous ECM-related transcripts, is a direct cause of fibrotic lesions in numerous tissues in knockout animal models. [207,211]

There are two genome-wide association studies (GWAS) for CKCS, but they present conflicting results[18,19]. However, one study identified 2 loci on chromosome 13 (1.58 Mb region, Figure 6-6) and chromosome 14 (1.68 Mb region, Figure 6-7) [18,19] Interestingly VPS13B (vacuolar protein sorting 13 homolog B) is the only protein-coding transcript in the 1.58Mb region and cfa-mir-599 (unchanged) and cfa-mir-875 (unchanged), are encoded by the VPS13B sequence in dogs, but not in humans. Mutations of VPS13B cause Cohen syndrome in humans (mental retardation, facial dysmorphism, microcephaly, early onset and progressive myopia, retinal dystrophy, truncal obesity with slender extremities, and joint laxity). This phenotype does not entirely resemble the global heritable diseases (MMVD, syringomyelia, fibrotic pancreatitis) seen in CKCSs. [219] Furthermore, critical transcription factors are targeted by these two miRNAs (Table 6-8), suggesting a potential epigenetic disorder might contribute to the heritable diseases of CKCSs.

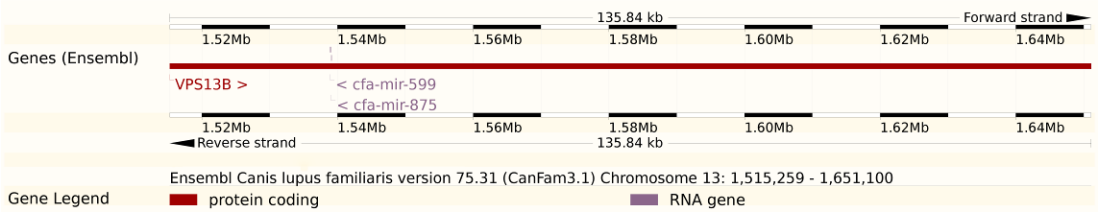

Figure 6-6 Chromosome 13, region between 1.52Mb and 1.64Mb. VPS13B is the only protein-coding transcript covering the 1.58Mb region and mutation of VPS13 is associated with Cohen

syndrome in humans. However, cfa-mir-599 and cfa-mir-875 are also transcribed from the VPS13B region, off the reverse strand.

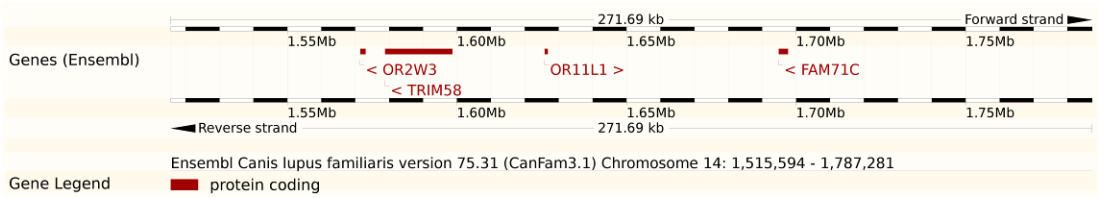

Figure 6-7 Chromosome 14, region between 1.55Mb and 1.75Mb. FAM71C is encoded near the susceptible 1.68Mb region, but there is no disease associated with FAM71C mutation.

Table 6-8 Target prediction for cfa-miR-875 and cfa-miR-599

cfa-miR-875		cfa-miR-599	
Target Gene	Gene Description	Target Gene	Gene Description
TGFB3	Transforming growth factor, beta 3	PAFAH1B1	Platelet-activating factor acetylhydrolase 1b, regulatory subunit 1
TOB2	Transducer of ErBb2	ANGPTL2	Angiopoietin-like 2
MAP3K2	Mitogen-activated protein kinase 2		

In terms of cardiovascular biology, some miRNAs are associated with angiogenesis, metabolism, and inflammation, and pathophysiology of heart diseases. For example miR-29 acts as an anti-fibrotic regulator in myocardial fibrosis. [207,211,220] To date, there are nearly 2,000 human miRNAs (hsa-miR) and 502 canine miRNAs (cfa-miR) catalogued, and the numbers are constantly being added to. [221] The functions of these miRNAs remain largely unknown. In the canine microarray chip, the coverage of the cfa-miRNAs is around 60% (302/502), and only 29 cfa-miRNAs (all down-regulated) passed the statistical cutoff. In the 1395 (non-coding and uncharacterized RNA, ncRNA) differentially expressed probe-sets, 10% (139/1395) were manually identified to be cfa-miRNAs (59) or transcript homologs (80) to other species, and the rest 90% (1256/1395) of the probe-sets were ncRNAs. Whether or not these ncRNAs also play roles in MMVD pathogenesis is uncertain, but understanding epigenetic regulation of genes provides a new perspective when considering the heritability of complex disease such as MMVD.

EndoMT is a complex phenomenon in which endothelial cells acquire a mesenchymal phenotype by expressing mesenchymal markers (α-SMA and Collagen I) instead of VE-cadherin. [222] In valvulogenesis, the formation of the atrioventricular endocardial cushion is dependent on the differentiation of endocardial cushion endothelial cells into mesenchymal cells that invade the cardiac jelly[82,100]. MiR-21 has been implicated in cancer metastasis and is also involved in TGF-β–induced EndoMT via a PTEN/Akt-dependent pathway. [223] In endothelial cells, exposure to TGF-β directly up-regulates miR-21. [224] In the microarray results, both TGF-β and miR-21 were not differentially expressed in canine myxomatous mitral valves compared with normal valves, suggesting TGF-β and its down-stream miR-21 are not affected under diseased condition. However, in the previous chapter, evidence of EndoMT in normal and myxomatous mitral valves was found and this may indicate a constant effect of TGF-β maintaining cellular phenotype and valve homeostasis. In prostate, breast, lung, and colorectal cancer, miR-29 and miR-30 have been identified to be associated with metastatic progression, and both microRNAs have the same target, SNAI1, which is a key transcriptional factor that inhibits expression of E-cadherin in EMT (or VE-cadherin in EndoMT). [225] Interestingly, miR-29 (-3.56 fold-change) and miR-30 (-4.89 fold-change) were both found to be down-regulated in myxomatous mitral valves. The unchanged but high expression of TGF-β in mitral valves is likely a contributor to normal valve homeostasis and the control of EndoMT may be through epigenetic modifiers such as miR-29 and miR-30.

In myxomatous mitral valves, one of the most striking findings in the miRNA screening was the down-regulation of miR-29b (-4.02 fold-change) considering its well-characterised role in inhibition of ECM deposition. The expression of miR-29 tends to be high in fibroblasts (equivalent to VICs in mitral valves), and there are at least 16 confirmed ECM genes regulated by miR-29.[226] The miR-29 family, including miR-29a, miR-29b, and miR-29c, are mainly homologous in sequence and expressed as two bicistronic (two short RNA sequence) clusters, and their critical role in cardiac fibrosis has been demonstrated using a myocardial infarction model. [227] In the miRNA target prediction analysis, more than 20 miR-29-targeted genes were identified (canine specific) which were are highly relevant to MMVD. The majority of the targets were transcripts involved in ECM protein synthesis, such as

collagens, ADAMTS family members, FBN1, ELN, CTSE, HAS3, proteoglycan (CSGALNACT2), and a basement membrane component (LAMA2). The other targets of miR-29 were VEGFA and ROBO, which regulate endothelial cell function and migration (Table 6-9).

Table 6-9 Predicted Target Genes for cfa-miR-29

cfa-miR-29 Target Genes	
ADAMTS Family	**COLLAGEN**
ADAMTS17	COL4A4
ADAMTS2	COL3A1
ADAMTS14	COL4A5
ADAMTS18	COL11A1
Other ECM	COL9A1
FBN1	COL5A3
ELN	COL1A1
CTSE	COL1A2
CSGALNACT2	COL7A1
HAS3	COL4A1
LAMA2	COL5A1
VEC Signalling	COL15A1
ROBO1	COL2A1
VEGFA	COL6A3
	COL22A1

In the myocardial infarction model, down-regulation of miR-29 was identified with up-regulation of ECM-associated genes near the lesion sites, suggesting a healing or remodelling mechanism controlled by miR-29. [227] ECM-related genes were down-regulated after introducing anti-miR-29 in the same study. [227] A recognised feature of MMVD pathology is loss of a laminated structure and excessive deposition of disorganized ECM making the weakened mitral valves unable to withstand mechanical forces under normal haemodynamic challenges. Lower levels of miR-29 found in canine myxomatous mitral valves might suggest a higher level of ECM protein production and greater degree of tissue remodelling compared to normal mitral valves. A further interesting observation is that inhibition of miR-29 enhances the vascular integrity during aneurysm formation in a mouse Marfan syndrome model. [228] Taken together, the data suggests multi-faceted roles for miR-29 which might make it a therapeutic target for ECM-associated disorders, such as MMVD. In

MMVD, down-regulation of miR-29 may suggest a decreased inhibition of ECM production and enhanced remodelling. However, to what degree miR-29 can trigger structural repair and remodelling without causing fibrosis in MMVD would need investigation.

For all the differentially expressed miRNAs, cfa-miR-218-1 had the highest signal intensity with the marked differences between control (mean = 1211) and MMVD (mean = 167). Furthermore, the level of SLIT2 (sequence encoding cfa-miR-218) also showed the same expression pattern (control mean = 4201 and MMVD mean = 2019) confirming its important role as a post-transcriptional regulator in MMVD. Roundabout (ROBO) receptors (ROBO1 and ROBO2) and their ligands (SLIT) are key regulators of axon guidance and vascular sprouting, and Slit-Robo signalling also controls endothelial cell migration. [229] Since blood vessels and nerves are organized in identical patterns during embryonic development, it has been suggested that vessels and nerves share a similar set of pathways controlling cell migration and pathfinding. [230] MiR-218 is encoded within introns in the Slit genes (SLIT2 and Slit3) and directly represses the expression of Robo receptors (ROBO1 and ROBO2) and multiple proteoglycan biosynthetic components such as GLCE (glucuronic acid epimerase), HS3ST3B1, and HS6ST3. (Table 6-10) [229] Knockdown of miR-218 results in deregulation of Slit-Robo signalling, abnormal endothelial cell migration, and retinal vasculature deformation. (Figure 6-8) [229]

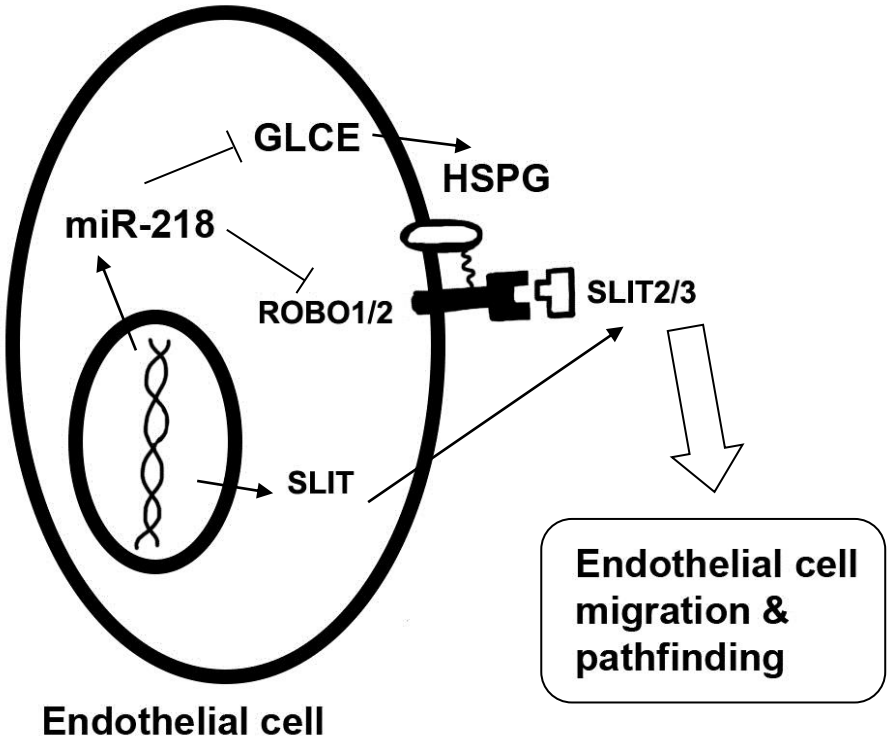

Figure 6-8 The SLIT2/3 genes give rise to both SLIT2/3 and miR-218. Slit proteins interact with the Robo1/2 receptors and miR-218 inhibits GLCE, which reduces production of HSPG leading to endothelial cell migration and patterning. The figure was modified from [229,231].

In the target prediction analysis for cfa-miR-218 there were many ECM related targets such as COL1A1, COL19A1, TNC, and HAPLN1. The fibroblast growth factor (FGF12) and cardiac muscle actin (ACTC1) were also targeted by cfa-miR-218. (Table 6-10)

Table 6-10 cfa-miR-218 target prediction.

Target Gene	Gene Description	Signal Intensity (Microarray)	
		CKCS	Control
GLCE	Heparan sulphate modification (C5 epimerization)	1169	1274
COL1A1	Collagen, type I, alpha 1	1588	3423
ACTC1	Actin, alpha, cardiac muscle 1	108	5786
FGF12	Fibroblast growth factor 12	689	537
TNC	Tenascin C	666	1135
COL19A1	Collagen, type XIX, alpha 1	24*	30*
HS6ST3	Heparan sulphate modification (3-O and 6-O sulfation)	n/a	n/a
HAPLN1	Hyaluronan and proteoglycan link protein 1	2007	3284
SRGAP2	Interacts with Robo (regulation of actin dynamics)	260	407
HS3ST3B1	Heparan sulphate modification (3-O sulfation)	79*	109*
Robo1	Slit receptor	1521	1438
Robo2	Slit receptor	53*	81*

*Background noise, signal intensity < 100.

Tenascin C is a glycoprotein mainly expressed in ligaments and tendons, and TNC modulates adhesion of cells to fibronectin and can be classified as an anti-adhesive or adhesion-modulating extracellular matrix protein. [232] The expression of TNC is highly up-regulated during embryonic development (valvulogenesis) and in the adult, and TNC is transiently expressed during organogenesis, and is mostly absent or down-regulated in fully developed organs. However, under pathological conditions such as infection, inflammation, or tumourogenesis, expression of TNC reappears. [233,234] In one unpublished study of normal porcine aortic and pulmonic valves, there was higher expression of TNC in the aortic valve and TNC was localized more on the aortic side of the valve compared to the ventricular side. [235] These differences in TNC distribution may suggest that TNC expression is associated with mechanical stress and remodelling status. In the canine microarray result, there was no difference of TNC expression between MMVD and control. However, post-transcriptional control of miR-218 may have effects on translation of TNC in tissue, and it is worth further investigation.

Lastly, the main functions of cfa-miR-218 can be broadly summarized as Slit-Robo signalling, collagen and PG biosynthesis, matrix networking and fibroblast differentiation. Applying these biological functions to MMVD pathogenesis, down-regulation of cfa-miR-218 (-6.82 fold-change) in MMVD may suggest there are aberrant SLIT-ROBO signalling and tenascin expression leading to endothelial dysfunction and cell migration, excessive and disorganized extracellular matrix production and enhanced myofibroblastic differentiation.

During heart valve development, the formation of the endocardial cushion arises from swelling of cardiac endothelium due to increased production of extracellular matrix (cardiac jelly). [80] The glycosaminoglycan hyaluronan is the major ECM component secreted by endocardial endothelial cells. Depletion of hyaluronan synthesis also leads to absence of endocardial cushions and a loss of endocardial cushion cellularization through EndoMT due to lack of a hyaluronan-augmented activation of ErbB2-ErbB3 receptor. [97,188,195,236] Hyaluronan production also results in expansion of the extracellular space by binding salt and water and induces PI3K and ErbB signalling. [191] The hyaluronic acid synthase 2 is the major hyaluronan

synthase in cardiovascular tissues and is positively and negatively controlled by regulators such as BMP (+) and miR-23 (-). [189,197] In MMVD, cfa-miR-23 was significantly down-regulated (-4.14 fold-change) which would reduce degradation of HAS2 mRNA. This finding was consistent with the results in the previous chapter, where increased HAS2 expression was found co-localized with myofibroblast clusters at the myxomatous valve edge. Moreover, miR-23 also targets transcripts related to ECM (versican and HGSNAT), endothelial signalling (EDNRB), basement membrane (LAMC3) and fibroblast proliferation (FGF12) (Table 6-11). Whether or not miR-23 has effects on the final production of hyaluronan, migration of VICs (and VECs), and remodelling in MMVD requires further investigation.

Table 6-11 cfa-miR-23 target prediction

Target Gene	Gene Description	Signal Intensity (Microarray)	
		CKCS	Control
CLDN12	Claudin 12	815	988
VCAN	Versican	9183	9023
HAS2	Hyaluronic acid synthase 2	934	417
EDNRB	Endothelin receptor type B	402	206
HGSNAT	Heparan-alpha-glucosaminide N-acetyltransferase	670	801
LAMC3	Laminin, gamma 3	258	319
FGF12	Fibroblast growth factor 12	689	537

In canine mitral valve tissues, the most dramatic difference between MMVD and controls was the expression of miR-218, with -6.82-fold (microarray) and -170-fold (Q-PCR) down-regulation in myxomatous mitral valves. Several heart specific miRNAs such as miR-208 have been identified to be positively associated with circulating and tissue miR-208 levels in acute myocardial infarction, and some (miR-223 and miR-197) show negative association. [220,237] Therefore, it is especially important to understand whether the circulating miR-218 is also associated with the tissue level and disease severity. It is possible that miR-218 could be used as a biomarker, prognostic indicator or therapeutic target for canine MMVD.

7 Chapter 7 Discussion

MMVD is the single most common cardiac disease in veterinary medicine, and understanding the temporal and dynamic changes on a cellular and genomic level is important. In this project, myxomatous mitral valves from CKCSs were histologically assessed and compared with mixed breed myxomatous mitral valves using standard cellular markers for VECs, VICs, and inflammatory cells. No difference could be identified in the end-stage myxomatous mitral valves of CKCS and other dogs, suggesting that regardless of the cause, end-stage myxomatous mitral valves present the same cellular changes in CKCS and non-CKCS. However, it is not known if these cellular changes are linked to ECM component turnover.

A global transcriptomic profiling was conducted to investigate gene regulation in the end-stage myxomatous mitral valves from CKCSs and healthy adult beagles. With advanced bioinformatics and the latest gene network analysis platforms and using the updated canine microarray, the current study of myxomatous mitral valve transcriptome confirmed the key biological functions, such as serotonin signalling and inflammation, reported in a previous study [106], but also led to two novel findings; possible reactivation of developmental pathways associated with EndoMT and miRNA down-regulation. Furthermore, using BioLayout *Express*^{3D} to analyse gene signal strength allowed identification of the expression trend irrespective of what was found using the fold-change method. Although there were some inconsistent findings comparing microarray analysis and Q-PCR assays, microarray raw data was valuable and informative.

Following on from the microarray analysis tissue sections of mitral valves were probed with specific antibodies of interest to examine their expression pattern. This identified the novel finding of increased expression of HAS2, potentially mediated by developmental pathways (BMP and SNAI1) and EndoMT. Investigation of temporal and spatial distribution of aVICs provided further evidence of life-long valve remodelling (repair), presumably in response to changes of mechanical force such as fluid shear stress created by normal valve movement and accentuated by mitral regurgitation.

Considering data from the published literature and the current transcriptomic data, a mechanistic pathophysiology of canine myxomatous mitral valve degeneration can be hypothesized. The conventional view is that changes and damage to the leaflet are restricted to the distal zone, but the current study found changes occurring in the mid-zone of normal valves, suggesting a more complex story with ongoing valve repair.

7.1 A Model of MMVD:

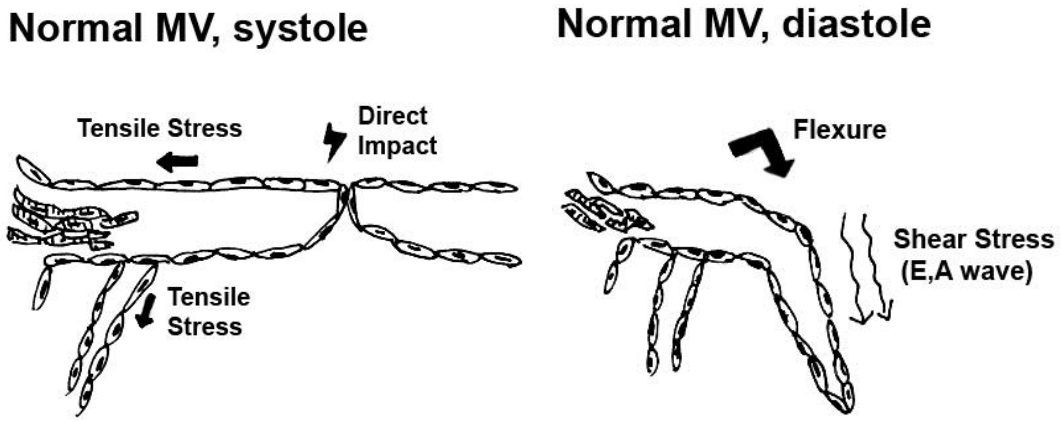

Figure 7-1 A normal working mitral valve with various mechanical forces during systole and diastole.

Under normal loading conditions mitral valve leaflets and the subvalvular apparatus together function synergistically to maintain leak-free mitral coaptation during systole. The interface of the valve commissures receives direct shock at the closure of the two leaflets during systole. Tensile stress (stretch of chordae tendineae and annulus), flexure, and fluid shear stress during cardiac cycle also may contribute to valve damage. (Figure 7-1) [85]

Healthy endothelium forms tight surface junctions under SLIT2-Robo-miR218 signalling, and HAS2 expression by VECs also provides cushioning against physiological shear stress. [188,189,194,195,236] Mechanical damage to mitral valve structure and denudation of VECs might be the result of long-term wear. [49,51,101,107,138,238] This is hypothesised to be repaired by repopulation of residential

endothelial progenitor cells (EPCs) or bone-marrow-derived EPC. [60,102,239,240] Repair and remodelling of stromal damage is thought to be mediated by EndoMT and paracrine VICs-activation mechanism. (Figure 7-2) [202] Based on evidence from the current transcriptomic study ECM residual products from ECM breakdown could serve as endogenous ligands for toll-like receptors (TLR), and TLR signalling triggers inflammation and inflammatory-mediated EndoMT. [137,241] However, the cellular changes in normal mitral valves are restricted to the middle-atrial portion based on histological findings. Nevertheless, structural changes have been noted in the mid-zone using SEM and while speculative it may be that mid-zone damage altering valve mechanics could contribute to development of the more readily observable and characteristic distal-zone changes. [242] The excessive production of disorganized ECM and initiation of nodular lesion formation at the valve tip may be due to onset of regurgitation as a consequence of structural changes deeper in the valve. (Figure 7-3)

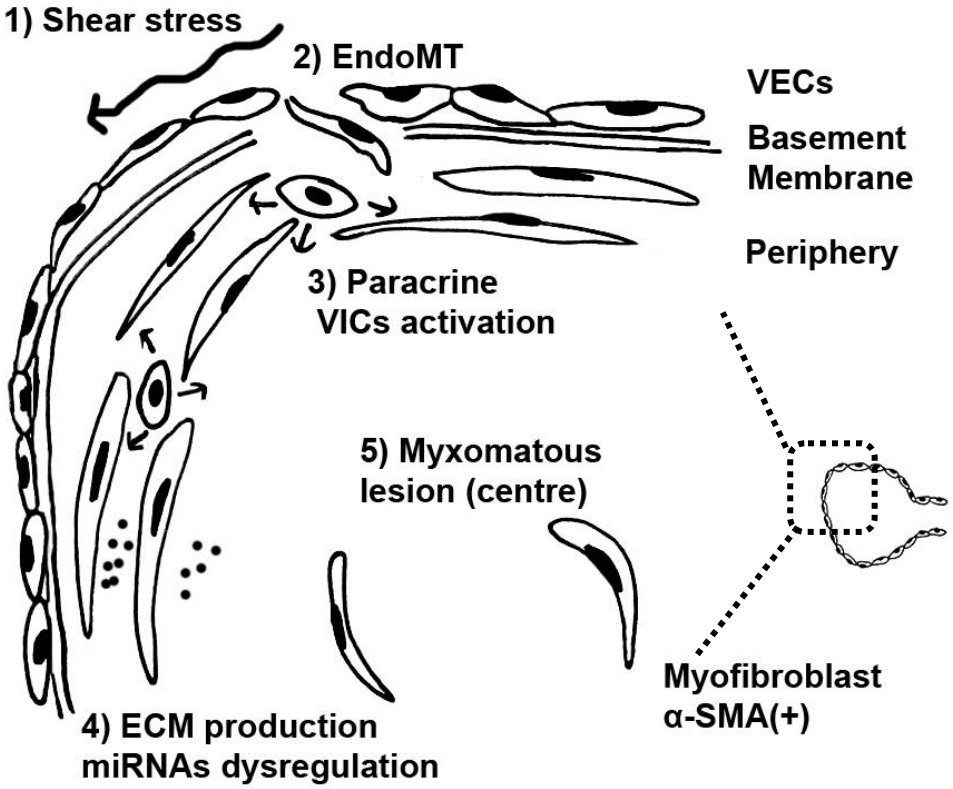

Figure 7-2 Paracrine mechanism of transformed VECs and activation of surrounding VICs.

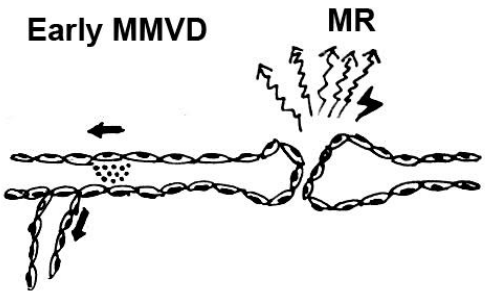

Figure 7-3 Mitral regurgitant jets in early MMVD.

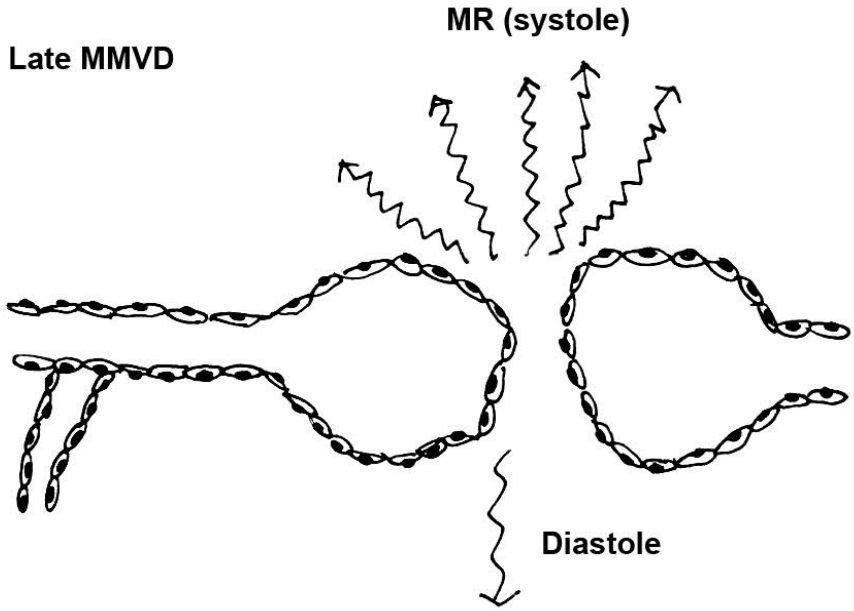

Figure 7-4 Severe mitral regurgitation in late MMVD.

In late stage MMVD, VEC denudation at valve tip is evident, and there is likely to be endothelial dysfunction (Figure 7-4). [57] This is consistent with the findings in the transcriptomic study such as down-regulation of basement membrane and collagen anchorage genes (NID1, LAMA2, and COL6A3) and miRNA dysregulation (cfa-miR-218, miR-23, and miR-29).With loss of miR-23 and miR-29 secretion by VECs this would trigger excessive production of ECM by sub-endothelial VICs. Increased HAS2 gene expression at the valve tip and down-regulation of endothelial specific miR-218 causes aberrant proteoglycan production and instability of endothelial cell-to-cell junctions.

7.2 Limitations of the Study

In this project, end-stage myxomatous mitral valves from CKCSs were used to screen global genomic expression and to model general canine MMVD pathogenesis. It is possible that there were genetic factors contributing to the development of MMVD in the four CKCS valves, with unidentified mutations contributing to aberrant genomic regulation.

What is not known is what determines the onset of MMVD. Several possible contributing factors such as platelet abnormality unique to CKCS and ECM genes associated with structural integrity have been identified, but there are likely to be more factors associated with canine MMVD such as abnormal epigenetic control of genes (for example, through miRNAs). This study demonstrates the major genomic profile differences between young healthy mitral valves from beagles and severely diseased valves from CKCSs. Since mitral valves are constantly challenged by continuous and dynamic biomechanical forces under complex haemodynamic conditions, it is important to better understand the most significant force (regurgitant shear stress) that contributes to mitral valve degeneration and how this might affect gene expression.

Additional limitations of this study include the lack of age- and breed-matched controls, and restrictive information derived from a single-shot profile at a small sample size (n=4). Due to the diverse phenotype and uncharacterized genetic components associated with canine MMVD, it will be necessary to better differentiate MMVD phenotype between breeds and for different ages. Genomic profiling of mitral valves from all stages of MMVD with consistent age correlation is required in order to build up a temporal picture of changes of gene activity associated with disease progression. This topic will be covered by a further study building on the data already derived for aged dogs.

The microarray analysis using different platforms of software provides diverse data mining methods and results. Because most databases of bioinformatic platforms are based on the published literature or experimental settings varying between different tissues, cell lines, and species, the exact biological functions discovered by gene network analysis are not necessarily completely representative of degenerative

processes found in canine MMVD. Q-PCR assays did show good agreement with the microarray analysis in terms of the gene expression pattern, but it is necessary to recruit a large number of samples in order to confirm significance.

To overcome some of the limitations, parallel to this PhD project, canine MVEC clones and primary mitral VIC cultures have been expanded from healthy mitral valve and phenotypically characterised (not included in this thesis). Pure canine MVEC clones and MVIC culture will provide a species-specific *in vitro* model for cfa-miRNA examination and gene regulation for future studies.

7.3 Summary

1. Regardless of the early onset and rapid progression of MMVD seen in CKCS, there are no differences in general pathology and cellular changes (myofibroblastic differentiation) comparing CKCSs and non-CKCS MMVD. This still needs to be confirmed to be the same for extra-cellular matrix changes. This suggests that MMVD in CKCS might be representative of all canine breeds affected by MMVD and that CKCS MMVD can be regarded as a model for the disease in dogs. Furthermore, the heritable component of CKCS MMVD might be related to the age of onset and rapidity of progression not the eventual pathology outcome.
2. The updated transcriptional profile of canine MMVD, with tissues from a single breed (CKCS) and using stringent thresholds, greatly improves insight into gene regulation of MMVD. The study confirmed that serotonin signalling (up-regulation of 5HTR2B) is present in MMVD pathogenesis as first reported by Oyama et al [106], and supports the application of efforts by other research groups investigating this signalling pathway in MMVD
3. The top five biologically relevant functions identified by transcriptomics analysis to be altered were inflammatory response, cellular movement, cardiovascular development, extracellular matrix organization, and epithelial-to-mesenchymal transition.

4. Developmental genes and pathways governing EndoMT, such as NOTCH, and SNAI1 may be contributing factors to MMVD. This was detected by the combination of transcriptomics and in silico gene network analysis.
5. Analysing signal intensities for each probe-set associated with ECM biosynthesis (Collagens, ADAMTS, MMPs, TIMPs, and PGs), there was strong evidence for decreased ECM turnover rate under diseased conditions, and this might be associated with the prominent myofibroblastic differentiation seen with the disease.
6. Evidence of EndoMT was identified in normal and myxomatous mitral valves by examining co-expression of mesenchymal (α-SMA) and endothelial (CDH5) cell markers in the myxoid stroma and close to the endothelium. This suggests EndoMT is a primary contributor to disease pathogenesis or a confounding factor.
7. Increased myofibroblastic expression of HAS2 in myxomatous mitral valves suggested an elevation in hyaluronan synthesis (not confirmed), and this is reminiscent of what is found in embryonic mesenchyme (cardiac jelly production) producing conditions that favour cell migration.
8. The EndoMT and aberrant expression of NOTCH found in MMVD could be a consequence of endothelial damage and dysfunction of endothelial-interstitial interaction.
9. Around 60% (302/502) of cfa-miRNAs were profiled in the canine array, and all 29 differentially expressed cfa-miRNAs were down-regulated. Within these miRNAs, miR-218, miR-23, and miR-29 were the key post-transcriptional regulators that could be implicated in MMVD considering their ECM-related targets.

7.4 Future Plans

1. The transcriptomic study was conducted on normal dogs and dogs with end-stage in MMVD with a lack of intermediate stage samples. Larger age-

matched mitral valve sample cohorts with different grades of myxomatous lesions should be investigated to generate a dynamic map of gene expression throughout the natural history of MMVD.

2. The ADAMTS family genes have important functions controlling collagen formation and ECM turnover, and their expression has not been studied in canine MMVD. Several genes of the ADAMTS family were differentially expressed, and their expression pattern needs to be investigated in greater detail in normal and diseased valves.
3. Surprisingly LDLR was identified as a positive up-stream regulator in canine MMVD. Since LDLR is considered a risk factor for human cardiovascular disease, it would be worth investigating LDLR function in a large cohort of MMVD (CKCS and non-CKCS) and normal dogs, and as a potential biomarker of disease.
4. Although evidence of EndoMT has been identified in normal and myxomatous mitral valves, more work is needed to understand what is the role in MMVD and the factors that initiate and control EndoMT in both normal and diseased valves.
5. Considering the large difference in cfa-miR-218 expression in myxomatous mitral valves and its high signal intensity in normal mitral valves, it would be interesting to look at circulating cfa-miR-218 in serum samples of a large cohort of MMVD and normal dogs to see if it might be a useful biomarker or prognostic indicator for canine MMVD.
6. Full-spectrum cfa-miRNAs profiling on myxomatous mitral valves using RNA-seq (RNA sequencing, next generation sequencing) should be conducted.
7. Localization of miRNAs (cfa-miR-218, cfa-miR-23, cfa-miR-29) by using *in situ* hybridization in normal and myxomatous mitral valves aids understanding their expression patterns and origins.
8. The role of increased production of hyaluronan, as suggested by increased expression of HAS2, and subsequent enhancement of cell migration (CDH5),

myofibroblastic differentiation (ACTA2) and valve remodelling (catabolic enzyme and ECM-related transcripts) requires further investigation, and this might be best achieved in a dynamic bioreactor maintained cell culture system.

In summary the present study has revealed a potential role for EndoMT in MMVD. Further investigation of changes in mitral valves throughout the life course and understanding of the regulators and modulators that bring about the disease state will assist in both treating the disease and breeding away from key genetic factors, with improvement to the health of all dogs.

7.5 Publications & Abstracts

7.5.1 Published

1. Yang C.H., Culshaw G.J., Liu M.M., **Lu C-C**., French A.T., Clements D.N., Corcoran B.M. Canine Tissue-Specific Expression of Multiple Small Leucine Rich Proteoglycans. The Veterinary Journal. 2012 Aug;193(2):374-80.
2. Liu M-M., T.C. Flanagan, **Lu C-C.**, A.T. French, D.J. Argyle, B.M. Corcoran. Cultured and Characterisation of Canine Mitral Valve Interstitial and Endothelial Cells. The Veterinary Journal. 2015. In Press.
3. **Lu C-C.**, Liu M-M., French A.T., Clinton M., Culshaw G., Argyle D.A, Corcoran B.M.. Gene Network and Canonical Pathway Analysis in Canine Myxomatous Mitral Valve Disease: a Microarray Study. The Veterinary Journal. 2015. In Press.

7.5.2 Preparing for Submission

1. **Lu C-C**., Liu M-M., French A.T., Culshaw G.J., Corcoran B.M. Cellular Changes in Cavalier King Charles Spaniel Myxomatous Mitral Valves. **Being revised**.
2. **Lu C-C.**, Liu M-M., Clinton M., Culshaw G.J., Argyle D.A, Corcoran B.M.. Evidence for Endothelial to Mesenchymal transition (EndoMT) in the Pathogenesis of Canine Myxomatous Mitral Valve Disease. **Being revised**.

7.5.3 Abstract (Oral Presentation)

1. Lu C-C., Liu M-M., French AT., Culshaw G., Corcoran B.M. Cellular changes in the Mitral Valve of Cavalier King Charles Spaniel with Late-stage Myxomatous Mitral Valve Disease. Association for Veterinary Teaching and Research Work (AVTRW) 68th Annual Conference, Nottingham, UK (2011).
2. Lu C-C., Liu M-M., Argyle D., French AT., Culshaw G., Corcoran B.M. Expression of Cadherin-5 (CD144) in Canine Myxomatous Mitral Valve Degeneration (MMVD). The Society for Heart Valve Disease 7th Biennial Congress, Venice, Italy (2012).

3. Lu C-C., Liu M-M., Clinton M., Culshaw G., Argyle D.A, Corcoran B.M.. The Role of Development in Degeneration – Canine Myxomatous Mitral Valve. Royal (Dick) School of Veterinary Studies Research Student (RDSVS) Day, Edinburgh, UK (2014).

4. Lu C-C., Liu M-M., Clinton M., Culshaw G., Argyle D.A, Corcoran B.M.. Spatial and Temporal Distribution of Myofibroblasts in Canine Myxomatous Mitral Valve Disease. American College of Veterinary Internal Medicine (ACVIM) Forum, Nashville, USA (2014).

5. Lu C-C., Liu M-M., Clinton M., Culshaw G., Argyle D.A, Corcoran B.M.. Endothelial to Mesenchymal Trans-differentiation in Canine Myxomatous Mitral Valve Disease. American College of Veterinary Internal Medicine (ACVIM) Forum, Nashville, USA (2014).

6. Lu C-C., Clinton M., Argyle D.A, Corcoran B.M.. MicroRNAs Expression in Canine Myxomatous Mitral Valve Disease. Congress of the European College of Veterinary Internal Medicine – Companion Animals (ECVIM-CA), Mainz, Germany (2014).

7.5.4 Abstracts (Posters for RDSVS Research Student Day)

1. Lu C-C., Liu M-M., French AT., Culshaw G., Corcoran B.M. Cellular Changes in the Mitral Valve of Cavalier King Charles Spaniel with Late-stage Myxomatous Mitral Valve Disease (2012).

2. Lu C-C., Liu M-M., Argyle D., French AT., Culshaw G., Corcoran B.M. Expression of CD144 in Canine Myxomatous Mitral Valve (2013).

8 References

1. Kovacic JC, Mercader N, Torres M, Boehm M, Fuster V. Epithelial-to-mesenchymal and endothelial-to-mesenchymal transition: from cardiovascular development to disease. *Circulation*. 2012;125(14):1795-808.

2. Piera-Velazquez S, Li Z, Jimenez S. Role of endothelial-mesenchymal transition (EndoMT) in the pathogenesis of fibrotic disorders. *Am J Pathol*. 2011;179(3):1074-80.

3. Zeisberg EM, Tarnavski O, Zeisberg M, et al. Endothelial-to-mesenchymal transition contributes to cardiac fibrosis. *Nat Med*. 2007;13(8):952-61.

4. Blaine DP. *Canine Pathology or A Full Description of the Diseases of Dogs*. London: T. Boosey; 1817.

5. Anyanwu AC, Adams DH. Etiologic classification of degenerative mitral valve disease: Barlow's disease and fibroelastic deficiency. *Semin Thorac Cardiovasc Surg*. 2007;19(2):90-96.

6. Whitney JG. Observations on the effect of age on the severity of heart valve lesions in the dog. *J Small Anim Pract*. 1974;15(8):511-22.

7. Borgarelli M, Buchanan JW. Historical review, epidemiology and natural history of degenerative mitral valve disease. *J Vet Cardiol*. 2012;14(1):93-101.

8. Borgarelli M, Savarino P, Crosara S, et al. Survival Characteristics and Prognostic Variables of Dogs with Mitral Regurgitation Attributable to Myxomatous Valve Disease. *J Vet Intern Med*. 2008;22(1):120-8.

9. Fox PR, Sisson D, Moïse NS. *Textbook of Canine and Feline Cardiology: Principles and Clinical Practice*. Philadelphia: W.B. Saunders Company; 1999.

10. Tilley LP, Smith FWK. *Manual of Canine and Feline Cardiology*. St Louis: Elsevier Science Health Science Division; 2007.

11. Kittleson MD, Kienle RD. *Small Animal Cardiovascular Medicine*. St Louis: Mosby, Incorporated; 1998.

12. Buchanan JW. Chronic valvular disease (endocardiosis) in dogs. *Adv Vet Sci Comp Med*. 1977;21:75-106.

13. Borgarelli M, Haggstrom J. Canine Degenerative Myxomatous Mitral Valve Disease: Natural History, Clinical Presentation and Therapy. *Vet Clin North Am Small Anim Pract*. 2010;40(4):651-63.

14. Borgarelli M, Zini E, D'Agnolo G, et al. Comparison of primary mitral valve disease in German Shepherd dogs and in small breeds. *J Vet Cardiol*. 2004;6(2):27-34.

15. Beardow AW, Buchanan JW. Chronic mitral valve disease in cavalier King Charles spaniels: 95 cases (1987-1991). *J Am Vet Med Assoc*. 1993;203(7):1023-29.

16. Coile DC. *Cavalier King Charles Spaniels*. Hauppauge: Barron's Educational Series; 2008.

17. Moffat N. *Cavalier King Charles Spaniel: Your Happy Healthy Pet*. Hoboken: Wiley; 2006.

18. French AT, Ogden R, Eland C, et al. Genome-wide analysis of mitral valve disease in Cavalier King Charles Spaniels. *Vet J*. 2012;193(1):283-6.

19. Madsen MB, Olsen LH, Häggström J, et al. Identification of 2 loci associated with development of myxomatous mitral valve disease in Cavalier King Charles Spaniels. *J Hered*. 2011;102(S1):S62-7.

20. Lewis T, Swift S, Woolliams JA, Blott S. Heritability of premature mitral valve disease in Cavalier King Charles spaniels. *Vet J*. 2011;188(1):73-6.

21. Tarnow I, Kristensen AT, Texel H, Olsen LH, Pedersen HD. Decreased platelet function in Cavalier King Charles Spaniels with mitral valve regurgitation. *J Vet Intern Med*. 2003;17(5):680-6.

22. Olsen LH, Kristensen T, Häggström J, et al. Increased platelet aggregation response in Cavalier King Charles Spaniels with mitral valve prolapse. *J Vet Intern Med*. 2001;15(3):209-16.

23. Cowan SM, Bartges JW, Gompf RE, et al. Giant platelet disorder in the Cavalier King Charles Spaniel. *Exp Hematol*. 2004;32(4):344-50.

24. Davis B, Toivio-Kinnucan M, Schuller S, Boudreaux MK. Mutation in beta1-tubulin correlates with macrothrombocytopenia in Cavalier King Charles Spaniels. *J Vet Intern Med*. 2008;22(3):540-5.

25. Pedersen HD, Mow T. Hypomagnesemia and Mitral Valve Prolapse in Cavalier King Charles Spaniels. *J Vet Med Ser A*. 1998;45(1-10):607-14.

26. Tarnow I, Olsen LH, Kvart C, et al. Predictive value of natriuretic peptides in dogs with mitral valve disease. *Vet J*. 2009;180(2):195-201.

27. Arndt JW, Reynolds C, Singletary GE, Connolly JM, Levy RJ, Oyama M a. Serum serotonin concentrations in dogs with degenerative mitral valve disease. *J Vet Intern Med*. 2009;23(6):1208-13.

28. Ljungvall I, Höglund K, Lilliehöök I, et al. Serum serotonin concentration is associated with severity of myxomatous mitral valve disease in dogs. *J Vet Intern Med*. 2013;27(5):1105-12.

29. Pedersen HD, Häggstrom J, Olsen LH, et al. Idiopathic asymptomatic thrombocytopenia in Cavalier King Charles Spaniels is an autosomal recessive trait. *J Vet Intern Med*. 2002;16(2):169-73.

30. Connolly JM, Bakay M, Fulmer JT, et al. Fenfluramine disrupts the mitral valve interstitial cell response to serotonin. *Am J Pathol*. 2009;175(3):988-97.

31. Volmar KE, Hutchins GM. Aortic and Mitral Fenfluramine-Phentermine Valvulopathy in 64 Patients Treated With Anorectic Agents. *Arch Pathol Lab Med*. 2001;125(12):1555-61.

32. Shively BK, Roldan CA, Gill EA, Najarian T, Loar SB. Prevalence and Determinants of Valvulopathy in Patients Treated With Dexfenfluramine. *Circ* . 1999;100 (21):2161-7.

33. Connolly HM, Crary JL, McGoon MD, et al. Valvular Heart Disease Associated with Fenfluramine–Phentermine. *N Engl J Med*. 1997;337(9):581-8.

34. Oyama MA. Insights into Serotonin Signalling Mechanisms Associated with Canine Degenerative Mitral Valve Disease. *J Vet Intern Med*. 2010;24(1):457-36.

35. Jian B, Xu J, Connolly J, et al. Serotonin Mechanisms in Heart Valve Disease I Serotonin-Induced Up-Regulation of Transforming Growth. 2002;161(6):2111-21.

36. Lacerda CMR, Kisiday J, Johnson B, Orton EC. Local serotonin mediates cyclic strain-induced phenotype transformation, matrix degradation, and glycosaminoglycan synthesis in cultured sheep mitral valves. *Am J Physiol Heart Circ Physiol*. 2012;302(10):H1983-90.

37. Disatian S, Orton EC. Autocrine serotonin and transforming growth factor beta 1 signalling mediates spontaneous myxomatous mitral valve disease. *J Heart Valve Dis*. 2009;18(1):44-51.

38. Disatian S, Lacerda C, Orton EC. Tryptophan hydroxylase 1 expression is increased in phenotype-altered canine and human degenerative myxomatous mitral valves. *J Heart Valve Dis*. 2010;19(1):71-8.

39. Perloff JK, Roberts WC. The mitral apparatus: functional anatomy of mitral regurgitation . *Circulation*. 1972;46 (2):227-39.

40. Dasi LP, Sucosky P, De Zelicourt D, Sundareswaran K, Jimenez J, Yoganathan AP. Advances in cardiovascular fluid mechanics: bench to bedside. *Ann N Y Acad Sci*. 2009;1161(1):1-25.

41. Fox PR. Pathology of myxomatous mitral valve disease in the dog. *J Vet Cardiol*. 2012;14(1):103-26.

42. Fenoglio JJ, Pham TD, Wit AL, Bassett AL, Wagner BM. Canine mitral complex: ultrastructure and electromechanical properties. *Circ Res*. 1972;31 (3):417-30.

43. Schneider RJ, Perrin DP, Vasilyev NV, Marx GR, del Nido PJ, Howe RD. Mitral annulus segmentation from 3D ultrasound using graph cuts. *Med Imaging, IEEE Trans*. 2010;29(9):1676-87.

44. Berdajs D, Zünd G, Camenisch C, Schurr U, Turina MI, Genoni M. Annulus Fibrosus of the Mitral Valve: Reality or Myth. *J Card Surg*. 2007;22(5):406-9.

45. Grewal J, Suri R, Mankad S, et al. Mitral annular dynamics in myxomatous valve disease: new insights with real-time 3-dimensional echocardiography. *Circulation*. 2010;121(12):1423-31.

46. Rodriguez F, Langer F, Harrington KB, et al. Importance of mitral valve second-order chordae for left ventricular geometry, wall thickening mechanics, and global systolic function. *Circulation* . 2004;110(11S1):II115-22.

47. Silbiger JJ, Bazaz R. Contemporary insights into the functional anatomy of the mitral valve. *Am Heart J*. 2009;158(6):887-95.

48. Aupperle H, März I, Thielebein J, Kiefer B, Kappe A, Schoon H-A. Immunohistochemical characterization of the extracellular matrix in normal mitral valves and in chronic valve disease (endocardiosis) in dogs. *Res Vet Sci*. 2009;87(2):277-83.

49. Corcoran BM, Black A, Anderson H, et al. Identification of surface morphologic changes in the mitral valve leaflets and chordae tendineae of dogs with myxomatous degeneration. *Am J Vet Res*. 2004;65(2):198-206.

50. Aupperle H, Thielebein J, Kiefer B, März I, Dinges G, Schoon H. An immunohistochemical study of the role of matrix metalloproteinases and their tissue inhibitors in chronic mitral valvular disease (valvular endocardiosis) in dogs. *Vet J*. 2009;180(1):88-94.

51. Han RI, Black A, Culshaw G, French AT, Corcoran BM. Structural and cellular changes in canine myxomatous mitral valve disease: an image analysis study. *J Heart Valve Dis*. 2010;19(1):60-70.

52. Han RI, Black A, Culshaw GJ, French AT, Else RW, Corcoran BM. Distribution of myofibroblasts, smooth muscle-like cells, mcrophages, and mast cells in mitral valve leaflets of dogs with myxomatous mitral valve disease. *J Vet Res*. 2008;69(6):763-9.

53. Aupperle H, März I, Thielebein J, Kiefer B, Dinges G, Schoon H. Distribution of extracellular matrix components in normal and degenerated canine tricuspid valve leaflets. *J Comp Pathol*. 2009;141(1):41-51.

54. Flanagan TC, Black A, O'Brien M, Smith TJ, Pandit a. S. Reference models for mitral valve tissue engineering based on valve cell phenotype and extracellular matrix analysis. *Cells Tissues Organs*. 2006;183(1):12-23.

55. Butcher JT, Nerem RM. Valvular endothelial cells regulate the phenotype of interstitial cells in co-culture: effects of steady shear stress. *Tissue Eng*. 2006;12(4):905-15.

56. Rabkin E, Aikawa M, Stone JR, Fukumoto Y, Libby P, Schoen FJ. Activated interstitial myofibroblasts express catabolic enzymes and mediate matrix remodelling in myxomatous heart valves. *Circulation*. 2001;104(21):2525-32.

57. Black A, French AT, Dukes-McEwan J, Corcoran BM. Ultrastructural morphologic evaluation of the phenotype of valvular interstitial cells in dogs with myxomatous degeneration of the mitral valve. *Am J Vet Res*. 2005;66(8):1408-14.

58. Sousa AM, Liu T, Guevara O, et al. Smooth muscle alpha-actin expression and myofibroblast differentiation by TGFbeta are dependent upon MK2. *J Cell Biochem*. 2007;100(6):1581-92.

59. Garside VC, Chang AC, Karsan A, Hoodless PA. Co-ordinating NOTCH, BMP, and TGF-β signalling during heart valve development. *Cell Mol Life Sci*. 2013;70(16):2899-917.

60. Sales VL, Engelmayr GC, Mettler BA, Johnson JA, Sacks MS, Mayer JE. Transforming growth factor-beta1 modulates extracellular matrix production, proliferation, and apoptosis of endothelial progenitor cells in tissue-engineering scaffolds. *Circulation*. 2006;114(1S):I193-9.

61. Aupperle H, März I, Thielebein J, Schoon H-A. Expression of transforming growth factor-beta1, -beta2 and -beta3 in normal and diseased canine mitral valves. *J Comp Pathol*. 2008;139(2-3):97-107.

62. Cushing MC, Liao J-T, Anseth KS. Activation of valvular interstitial cells is mediated by transforming growth factor-beta1 interactions with matrix molecules. *Matrix Biol*. 2005;24(6):428-37.

63. Liu AC, Gotlieb AI. Transforming growth factor-beta regulates in vitro heart valve repair by activated valve interstitial cells. *Am J Pathol*. 2008;173(5):1275-85.

64. Liu AC, Joag VR, Gotlieb AI. The emerging role of valve interstitial cell phenotypes in regulating heart valve pathobiology. *Am J Pathol*. 2007;171(5):1407-18.

65. Orton EC, Lacerda CMR, Maclea HB. Signalling pathways in mitral valve degeneration. *J Vet Cardiol*. 2012;14(1):7-17.

66. Schoen FJ. Evolving concepts of cardiac valve dynamics: the continuum of development, functional structure, pathobiology, and tissue engineering. *Circulation*. 2008;118(18):1864-80.

67. Hadian M, Corcoran BM, Bradshaw JP. Molecular changes in fibrillar collagen in myxomatous mitral valve disease. *Cardiovasc Pathol*. 2010;19(5):e141-8.

68. Stein PD, Wang C-H, Riddle JM, Sabbah HN, Magilligan Jr. DJ, Hawkins ET. Scanning electron microscopy of operatively excised severely regurgitant floppy mitral valves. *Am J Cardiol*. 1989;64(5):392-4.

69. Mow T, Pedersen HD. Increased endothelin-receptor density in myxomatous canine mitral valve leaflets. *J Cardiovasc Pharmacol*. 1999;34(2):254-60.

70. Aikawa E, Whittaker P, Farber M, et al. Human semilunar cardiac valve remodelling by activated cells from fetus to adult: implications for postnatal adaptation, pathology, and tissue engineering. *Circulation*. 2006;113(10):1344-52.

71. Swenson L, Häggström J, Kvart C, Juneja RK. Relationship between parental cardiac status in Cavalier King Charles spaniels and prevalence and severity of chronic valvular disease in offspring. *J Am Vet Med Assoc*. 1996;208(12):2009-12.

72. Nasuti JF, Zhang PJ, Feldman MD, et al. Fibrillin and other matrix proteins in mitral valve prolapse syndrome. *Ann Thorac Surg*. 2004;77(2):532-6.

73. Olsen LH, Fredholm M, Pedersen HD. Epidemiology and Inheritance of Mitral Valve Prolapse in Dachshunds. *J Vet Intern Med*. 1999;13(5):448-56.

74. Mcdonald PC, Wilson JE, Mcneill S, et al. The challenge of defining normality for human mitral and aortic valves Geometrical and compositional analysis. 2002;11:193-209.

75. Hayek E, Gring CN, Griffin BP. Mitral valve prolapse. *Lancet*. 2005;365(9458):507-18.

76. Griffiths LG, Orton EC, Boon JA. Evaluation of techniques and outcomes of mitral valve repair in dogs. *J Am Vet Med Assoc*. 2004;224(12):1941-5.

77. Uechi M, Mizukoshi T, Mizuno T, et al. Mitral valve repair under cardiopulmonary bypass in small-breed dogs: 48 cases (2006-2009). *J Am Vet Med Assoc*. 2012;240(10):1194-201.

78. King AS. *The Cardiorespiratory System: Integration of Normal and Pathological Structure and Function*. Hoboken: Wiley; 1999.

79. Noden DM, DeLahunta A. *The Embryology of Domestic Animals: Developmental Mechanisms and Malformations*. Baltimore: Williams & Wilkins; 1985.

80. Hinton RB, Yutzey KE. Heart valve structure and function in development and disease. *Annu Rev Physiol*. 2011;73:29-46.

81. Chakraborty S, Combs MD, Yutzey KE. Transcriptional regulation of heart valve progenitor cells. *Pediatr Cardiol*. 2010;31(3):414-21.

82. Combs MD, Yutzey KE. Heart valve development: regulatory networks in development and disease. *Circ Res*. 2009;105(5):408-21.

83. Butcher JT, Markwald RR. Valvulogenesis: the moving target. *Philos Trans R Soc Lond B Biol Sci*. 2007;362(1484):1489-503.

84. Pucéat M. Embryological origin of the endocardium and derived valve progenitor cells: from developmental biology to stem cell-based valve repair. *Biochim Biophys Acta*. 2013;1833(4):917-22.

85. De Vlaming A, Sauls K, Hajdu Z, et al. Atrioventricular valve development: new perspectives on an old theme. *Differentiation*. 2012;84(1):103-16.

86. Armstrong EJ, Bischoff J. Heart valve development: endothelial cell signalling and differentiation. *Circ Res*. 2004;95(5):459-70.

87. Timmerman LA, Grego-Bessa J, Raya A, et al. NOTCH promotes epithelial-mesenchymal transition during cardiac development and oncogenic transformation. *Genes Dev*. 2004;18(1):99-115.

88. Boyer AS, Ayerinskas II, Vincent EB, McKinney LA, Weeks DL, Runyan RB. TGFbeta2 and TGFbeta3 have separate and sequential activities during epithelial-mesenchymal cell transformation in the embryonic heart. *Dev Biol*. 1999;208(2):530-45.

89. Song W, Jackson K, McGuire PG. Degradation of type IV collagen by matrix metalloproteinases is an important step in the epithelial-mesenchymal transformation of the endocardial cushions. *Dev Biol*. 2000;227(2):606-17.

90. Brown CB, Boyer AS, Runyan RB, Barnett J V. Antibodies to the type II TGFbeta receptor block cell activation and migration during atrioventricular cushion transformation in the heart. *Dev Biol*. 1996;174(2):248-57.

91. Brown CB, Boyer AS, Runyan RB, Barnett J V. Requirement of type III TGF-β receptor for endocardial cell transformation in the heart. *Sci*. 1999;283 (5410):2080-2.

92. Chen Y-G, Massagué J. Smad1 recognition and activation by the ALK1 group of transforming growth factor-β family receptors. *J Biol Chem*. 1999;274 (6):3672-7.

93. Ma L, Lu M-F, Schwartz RJ, Martin JF. Bmp2 is essential for cardiac cushion epithelial-mesenchymal transition and myocardial patterning. *Dev*. 2005;132 (24):5601-11.

94. Wang J, Sridurongrit S, Dudas M, et al. Atrioventricular cushion transformation is mediated by ALK2 in the developing mouse heart. *Dev Biol*. 2005;286(1):299-310.

95. Sugi Y, Yamamura H, Okagawa H, Markwald RR. Bone morphogenetic protein-2 can mediate myocardial regulation of atrioventricular cushion mesenchymal cell formation in mice. *Dev Biol*. 2004;269(2):505-18.

96. Walsh EC, Stainier DYR. UDP-Glucose dehydrogenase required for cardiac valve formation in zebrafish. *Science*. 2001;293 (5535):1670-3.

97. Clinic M, City SL. Heart-valve mesenchyme formation is dependent on hyaluronan-augmented activation of ErbB2 – ErbB3 receptors. *Nat Med*. 2002;8(8):850-5.

98. Camenisch TD, Spicer AP, Brehm-Gibson T, et al. Disruption of hyaluronan synthase-2 abrogates normal cardiac morphogenesis and hyaluronan-mediated transformation of epithelium to mesenchyme. *J Clin Invest*. 2000;106(3):349-60.

99. Mjaatvedt CH, Yamamura H, Capehart AA, Turner D, Markwald RR. The Cspg2 gene, disrupted in the hdf tutant, is required for right cardiac chamber and endocardial cushion formation. *Dev Biol*. 1998;202(1):56-66.

100. Lockhart M, Wirrig E, Phelps A, Wessels A. Extracellular matrix and heart development. *Birth Defects Res A Clin Mol Teratol*. 2011;91(6):535-50.

101. Sacks MS, Yoganathan AP. Heart valve function: a biomechanical perspective. *Philos Trans R Soc B Biol Sci* . 2008;363 (1502):2481.

102. Dal-Bianco JP, Aikawa E, Bischoff J, et al. Active adaptation of the tethered mitral valve: insights into a compensatory mechanism for functional mitral regurgitation. *Circulation*. 2009;120(4):334-42.

103. Pedersen HD, Häggström J. Mitral valve prolapse in the dog: a model of mitral valve prolapse in man. *Cardiovasc Res*. 2000;47(2):234-43.

104. Disatian S, Ehrhart EJ, Zimmerman S, Orton EC. Interstitial cells from dogs with naturally occurring myxomatous mitral valve disease undergo phenotype transformation. *J Heart Valve Dis*. 2008;17(4):402-11.

105. Winter JCF De. Using the Student's t -test with extremely small sample sizes. *Prat assessment, Res Eval*. 2013;18(10).

106. Oyama MA, Chittur S V. Genomic expression patterns of mitral valve tissues from dogs with degenerative mitral valve disease. *Am J Vet Res*. 2006;67(8):1307-18.

107. Grande-Allen KJ, Liao J. The heterogeneous biomechanics and mechanobiology of the mitral valve: implications for tissue engineering. *Curr Cardiol Rep*. 2011;13(2):113-20.

108. Frangogiannis NG, Michael LH, Entman ML. Myofibroblasts in reperfused myocardial infarcts express the embryonic form of smooth muscle myosin heavy chain (SMemb). *Cardiovasc Res*. 2000;48(1):89-100.

109. Hinz B, Phan SH, Thannickal VJ, Galli A, Bochaton-Piallat M-L, Gabbiani G. The myofibroblast: one function, multiple origins. *Am J Pathol*. 2007;170(6):1807-16.

110. Virag JI, Murry CE. Myofibroblast and endothelial cell proliferation during murine myocardial infarct repair. *Am J Pathol*. 2003;163(6):2433-40.

111. Aikawa E, Whittaker P, Farber M, et al. Human semilunar cardiac valve remodelling by activated cells from fetus to adult: implications for postnatal adaptation, pathology, and tissue engineering. *Circulation*. 2006;113 (10):1344-52.

112. Balaoing LR, Post AD, Liu H, Minn KT, Grande-Allen KJ. Age-related changes in aortic valve hemostatic protein regulation. *Arterioscler Thromb Vasc Biol*. 2013;34(1):72-80.

113. Kalia A, Gupta RP. Proteomics: a paradigm shift. *Crit Rev Biotechnol*. 2005;25(4):173-198.

114. Sainger R, Grau JB, Branchetti E, et al. Human myxomatous mitral valve prolapse: role of bone morphogenetic protein 4 in valvular interstitial cell activation. *J Cell Physiol*. 2012;227(6):2595-604.

115. Hulin A, Deroanne CF, Lambert CA, et al. Metallothionein-dependent up-regulation of TGF-β2 participates in the remodelling of the myxomatous mitral valve. *Cardiovasc Res*. 2012;93(3):480-89.

116. Genovese CR, Lazar NA, Nichols T. Thresholding of Statistical Maps in Functional Neuroimaging Using the False Discovery Rate. *Neuroimage*. 2002;15(4):870-8.

117. Reiner A, Yekutieli D, Benjamini Y. Identifying differentially expressed genes using false discovery rate controlling procedures. *Bioinforma* . 2003;19 (3):368-75.

118. Fleige S, Pfaffl MW. RNA integrity and the effect on the real-time qRT-PCR performance. *Mol Aspects Med*. 2006;27(2-3):126-39.

119. Imbeaud S, Graudens E, Boulanger V, et al. Towards standardization of RNA quality assessment using user-independent classifiers of microcapillary electrophoresis traces. *Nucleic Acids Res*. 2005;33(6):e56.

120. Bolstad BM, Irizarry RA, Å strand M, Speed TP. A comparison of normalization methods for high density oligonucleotide array data based on variance and bias. *Bioinforma* . 2003;19 (2):185-93.

121. Chen J, Bardes EE, Aronow BJ, Jegga AG. ToppGene Suite for gene list enrichment analysis and candidate gene prioritization. *Nucleic Acids Res* . 2009;37(S2):W305-11.

122. Huang DW, Sherman BT, Lempicki RA. Bioinformatics enrichment tools: paths toward the comprehensive functional analysis of large gene lists. *Nucleic Acids Res*. 2009;37 (1):1-13.

123. Theocharidis A, van Dongen S, Enright AJ, Freeman TC. Network visualization and analysis of gene expression data using BioLayout Express(3D). *Nat Protoc*. 2009;4(10):1535-50.

124. Liebert MA, Zhang Z, Schwartz S, Wagner L, Miller W. A greedy algorithm for aligning DNA sequences. 2000;7:203-14.

125. Geirsson A, Singh M, Ali R, et al. Modulation of transforming growth factor-β signalling and extracellular matrix production in myxomatous mitral valves by angiotensin II receptor blockers. *Circulation*. 2012;126(2S1):S189-97.

126. Verrecchia F, Chu M-L, Mauviel A. Identification of novel TGF-β/Smad gene targets in dermal fibroblasts using a combined cDNA microarray/promoter transactivation approach. *J Biol Chem*. 2001;276 (20):17058-62.

127. Walker GA, Masters KS, Shah DN, Anseth KS, Leinwand LA. Valvular myofibroblast activation by transforming growth factor-beta: implications for pathological extracellular matrix remodelling in heart valve disease. *Circ Res*. 2004;95(3):253-60.

128. Osorio JH. The variability in the canine lipid profile values and its possible relationship with the measurement method used. *Vet zootec.* 2009;3(1):70-7.

129. Watson P. Chronic Pancreatitis in Dogs. *Top Companion Anim Med*. 2012;27(3):133-9.

130. Watson PJ, Roulois AJA, Scase T, Johnston PEJ, Thompson H, Herrtage ME. Prevalence and breed distribution of chronic pancreatitis at post-mortem examination in first-opinion dogs. *J Small Anim Pract*. 2007;48(11):609-18.

131. Demer LL. Cholesterol in Vascular and Valvular Calcification. *Circulation*. 2001;104 (16):1881-3.

132. Sowa G. Caveolae, caveolins, cavins, and endothelial cell function: new insights. *Front Physiol*. 2012;2:120.

133. Galdo F Del, Lisanti MP. Caveolin-1, TGF-β receptor internalization, and the pathogenesis of systemic sclerosis. *Curr Opin Rheumatol*. 2008;20(6):713-9.

134. Salanueva IJ, Cerezo A, Guadamillas MC, del Pozo MA. Integrin regulation of caveolin function. *J Cell Mol Med*. 2007;11(5):969-80.

135. Pedersen LG, Offenberg H, Moesgaard SG, Thomsen PD, Pedersen HD, Olsen LH. Transcription levels of endothelin-1 and endothelin receptors are associated with age and leaflet location in porcine mitral valves. *J Vet Med Ser A*. 2007;54(3):113-8.

136. Hirata Y, Emori T, Eguchi S, et al. Endothelin receptor subtype B mediates synthesis of nitric oxide by cultured bovine endothelial cells. *J Clin Invest*. 1993;91(4):1367-73.

137. Chao W. Toll-like receptor signalling : a critical modulator of cell survival and ischemic injury in the heart. *Am J Physiol Heart Circ Physiol*. 2009;296(1):H1-12.

138. Stephens EH, Nguyen TC, Itoh A, Ingels NB, Miller DC, Grande-Allen KJ. The effects of mitral regurgitation alone are sufficient for leaflet remodelling. *Circulation*. 2008;118(14S):S243-9.

139. Mahler GJ, Farrar EJ, Butcher JT. Inflammatory cytokines promote mesenchymal transformation in embryonic and adult valve endothelial cells. *Arterioscler Thromb Vasc Biol*. 2013;33(1):121-30.

140. Gordon M, Hahn R. Collagens. *Cell Tissue Res*. 2010;339(1):247-57.

141. Klewer SE, Krob SL, Kolker SJ, Kitten GT. Expression of type VI collagen in the developing mouse heart. *Dev Dyn*. 1998;211(3):248-55.

142. Kruithof BPT, Krawitz SA, Gaussin V. Atrioventricular valve development during late embryonic and postnatal stages involves condensation and extracellular matrix remodelling. *Dev Biol*. 2007;302(1):208-17.

143. Kern CB, Twal WO, Mjaatvedt CH, et al. Proteolytic cleavage of versican during cardiac cushion morphogenesis. *Dev Dyn*. 2006;235(8):2238-47.

144. Stankunas K, Hang CT, Tsun Z-Y, et al. Endocardial Brg1 represses ADAMTS1 to maintain the microenvironment for myocardial morphogenesis. *Dev Cell*. 2008;14(2):298-311.

145. Chandra A, D'Cruz L, Aragon-Martin JA, et al. Focus on molecules: ADAMTSL4. *Exp Eye Res*. 2012;104(0):95-6.

146. Le Goff C, Cormier-Daire V. The ADAMTS(L) family and human genetic disorders. *Hum Mol Genet* . 2011;20 (R2):R163-7.

147. Kern CB, Wessels A, McGarity J, et al. Reduced versican cleavage due to Adamts9 haploinsufficiency is associated with cardiac and aortic anomalies. *Matrix Biol*. 2010;29(4):304-16.

148. Jungers KA, Le Goff C, Somerville RPT, Apte SS. Adamts9 is widely expressed during mouse embryo development. *Gene Expr Patterns*. 2005;5(5):609-17.

149. Aupperle H, Disatian S. Pathology, protein expression and signalling in myxomatous mitral valve degeneration: comparison of dogs and humans. *J Vet Cardiol*. 2012;14(1):59-71.

150. Aupperle H, Thielebein J, Kiefer B, et al. Expression of genes encoding matrix metalloproteinases (MMPs) and their tissue Inhibitors (TIMPs) in normal and diseased canine mitral valves. *J Comp Pathol*. 2009;140:271-7.

151. Obayashi K, Miyagawa-Tomita S, Matsumoto H, Koyama H, Nakanishi T, Hirose H. Effects of transforming growth factor-β3 and matrix metalloproteinase-3 on the pathogenesis of chronic mitral valvular disease in dogs. *Am J Vet Res*. 2011;72(2):194-202.

152. Turk V, Stoka V, Vasiljeva O, et al. Cysteine cathepsins: from structure, function and regulation to new frontiers. *Biochim Biophys Acta - Proteins Proteomics*. 2012;1824(1):68-88.

153. Fonović M, Turk B. Cysteine cathepsins and their potential in clinical therapy and biomarker discovery. *Proteomics Clin Appl*. 2014:8(5-6):416-26.

154. Sage J, Leblanc-Noblesse E, Nizard C, et al. Cleavage of nidogen-1 by cathepsin S impairs its binding to basement membrane partners. *PLoS One*. 2012;7(8):e43494.

155. Question R. Basic science for clinicians role for cysteine protease cathepsins in heart disease. *Circulation*. 2012;125(12):1551-62.

156. Hallmann R, Horn N, Selg M, Wendler O, Pausch F, Sorokin LM. Expression and function of laminins in the embryonic and mature vasculature. 2005;10:979-1000.

157. Davis GE, Senger DR. Endothelial extracellular matrix: biosynthesis, remodelling, and functions during vascular morphogenesis and neovessel stabilization. *Circ Res*. 2005;97(11):1093-107.

158. Lakatta EG, Levy D. Arterial and cardiac aging: major shareholders in cardiovascular disease enterprises: part I: aging arteries: a "set up" for vascular disease . *Circulation* . 2003;107(1):139-146.

159. Li J, Bertram JF. Review: Endothelial-myofibroblast transition, a new player in diabetic renal fibrosis. *Nephrology*. 2010;15(5):507-12.

160. Stephens EH, Chu C-K, Grande-Allen KJ. Valve proteoglycan content and glycosaminoglycan fine structure are unique to microstructure, mechanical load and age: Relevance to an age-specific tissue-engineered heart valve. *Acta Biomater*. 2008;4(5):1148-60.

161. Haglund L, Tillgren V, Addis L, Wenglén C, Recklies A, Heinegård D. Identification and characterization of the integrin α2β1 binding motif in chondroadherin mediating cell attachment. *J Biol Chem*. 2011;286 (5):3925-34.

162. Haglund L, Ouellet J, Roughley P. Variation in chondroadherin abundance and fragmentation in the human scoliotic disc. *Spine*. 2009;34(14):1513-8.

163. Liu C-Y, Birk DE, Hassell JR, Kane B, Kao WW-Y. Keratocan-deficient mice display alterations in corneal structure. *J Biol Chem* . 2003;278(24):21672-7.

164. Lacerda CMR, Disatian S, Orton EC. Differential protein expression between normal, early-stage, and late-stage myxomatous mitral valves from dogs. *Proteomics Clin Appl*. 2009;3(12):1422-29.

165. Radermecker M, Limet R, Lapiere C, Nusgens B. Increased mRNA expression of decorin in the prolapsing posterior leaflet of the mitral valve. *Interact Cardiovasc Thorac Surg*. 2003;2(3):389-94.

166. Gupta V, Barzilla JE, Mendez JS, et al. Abundance and location of proteoglycans and hyaluronan within normal and myxomatous mitral valves. *Cardiovasc Pathol*. 2009;18(4):191-7.

167. Dejana E, Orsenigo F. Endothelial adherens junctions at a glance. *J Cell Sci*. 2013;126(Pt12):2545-9.

168. Müller AM, Cronen C, Kupferwasser LI, Oelert H, Müller K-M, Kirkpatrick CJ. Expression of endothelial cell adhesion molecules on heart valves: up-regulation in degeneration as well as acute endocarditis. *J Pathol*. 2000;191(1):54-60.

169. Philippova M, Ivanov D, Tkachuk V, Erne P, Resink T. Polarisation of T-cadherin to the leading edge of migrating vascular cells in vitro: a function in vascular cell motility? *Histochem Cell Biol*. 2003;120(5):353-60.

170. Ivanov D, Philippova M, Tkachuk V, Erne P, Resink T. Cell adhesion molecule T-cadherin regulates vascular cell adhesion, phenotype and motility. *Exp Cell Res*. 2004;293(2):207-18.

171. Philippova M, Joshi MB, Pfaff D, et al. T-cadherin attenuates insulin-dependent signalling, eNOS activation, and angiogenesis in vascular endothelial cells. *Cardiovasc Res* . 2012;93 (3):498-507.

172. Zhou J, Bowen C, Lu G, et al. Cadherin-11 expression patterns in heart valves associate with key functions during embryonic cushion formation, valve maturation and calcification. *Cells Tissues Organs*. 2013;198(4):300-10.

173. Hutcheson JD, Chen J, Sewell-Loftin MK, et al. Cadherin-11 regulates cell–cell tension necessary for calcific nodule formation by valvular myofibroblasts. *Arterioscler Thromb Vasc Biol* . 2013;33(1):114-20.

174. Saito S, Yamaji N, Yasunaga K, et al. The fibronectin extra domain A activates matrix metalloproteinase gene expression by an interleukin-1-dependent mechanism. *J Biol Chem*. 1999;274(43):30756-63.

175. Akhtar S, Meek KM, James V. Immunolocalization of Elastin, Collagen Type I and Type III, Fibronectin, and Vitronectin in Extracellular Matrix Components of Normal and Myxomatous Mitral Heart Valve Chordae Tendineae. *Cardiovasc Pathol*. 1999;8(4):203-11.

176. Fayet C, Bendeck MP, Gotlieb AI. Cardiac valve interstitial cells secrete fibronectin and form fibrillar adhesions in response to injury. *Cardiovasc Pathol*. 2007;16(4):203-11.

177. Chuaqui RF, Bonner RF, Best CJM, et al. Post-analysis follow-up and validation of microarray experiments. *Nat Genet*. 2002;32 Suppl(december):509-14.

178. Beckman KB, Lee KY, Golden T, Melov S. Gene expression profiling in mitochondrial disease: sssessment of microarray accuracy by high-throughput Q-PCR. *Mitochondrion*. 2004;4:453-70.

179. Yang C-H, Culshaw GJ, Liu M-M, et al. Canine tissue-specific expression of multiple small leucine rich proteoglycans. *Vet J*. 2012;193(2):374-80.

180. Flicek P, Amode MR, Barrell D, et al. Ensembl 2014. *Nucleic Acids Res*. 2014;42(D1):D749-55.

181. Camacho C, Coulouris G, Avagyan V, et al. BLAST+: architecture and applications. *BMC Bioinformatics*. 2009;10:421.

182. Hamburger V. Introduction: Johannes Holtfreter, pioneer in experimental embryology. *Dev Dyn*. 1996;205(3):214-16.

183. Aupperle H, März I, Thielebein J, Dinges G, Schoon H. Histomorphological findings and expression of matrix metalloproteinases and their tissue specific inhibitors (TIMPs) in normal tricuspid valves and in chronic tricuspid valvular disease in dogs. *Vet J*. 2010;183(2):176-183.

184. Ng CM, Cheng A, Myers LA, et al. TGF- β – dependent pathogenesis of mitral valve prolapse in a mouse model of Marfan syndrome. 2004;114(11):1586-92.

185. Chakraborty S, Cheek J, Sakthivel B, Aronow BJ, Yutzey KE. Shared gene expression profiles in developing heart valves and osteoblast progenitor cells. *Physiol Genomics*. 2008;35(1):75-85.

186. Cheek JD, Wirrig EE, Alfieri CM, James JF, Yutzey KE. Differential activation of valvulogenic, chondrogenic, and osteogenic pathways in mouse models of myxomatous and calcific aortic valve disease. *J Mol Cell Cardiol*. 2012;52(3):689-700.

187. MacGrogan D, Luna-Zurita L, de la Pompa JL. NOTCH signalling in cardiac valve development and disease. *Birth Defects Res A Clin Mol Teratol*. 2011;91(6):449-59.

188. Lagendijk AK, Szabó A, Merks RMH, Bakkers J. Hyaluronan: a critical regulator of endothelial-to-mesenchymal transition during cardiac valve formation. *Trends Cardiovasc Med*. 2013;23(5):135-42.

189. Lagendijk AK, Goumans MJ, Burkhard SB, Bakkers J. MicroRNA-23 restricts cardiac valve formation by inhibiting HAS2 and extracellular hyaluronic acid production. *Circ Res*. 2011;109(6):649-57.

190. Bakkers J, Kramer C, Pothof J, Quaedvlieg NEM, Spaink HP, Hammerschmidt M. HAS2 is required upstream of Rac1 to govern dorsal migration of lateral cells during zebrafish gastrulation. *Development*. 2004;131(3):525-37.

191. Toole BP. Hyaluronan: from extracellular glue to pericellular cue. *Nat Rev Cancer*. 2004;4(7):528-39.

192. Johansson B, Holmgren A, Hedström M, Engström-Laurent A, Engström KG. Evaluation of hyaluronan and calcifications in stenotic and regurgitant aortic valves. *Eur J Cardio-Thoracic Surg*. 2011;39(1):27-32.

193. Rodriguez KJ, Piechura LM, Masters KS. Regulation of valvular interstitial cell phenotype and function by hyaluronic acid in 2-D and 3-D culture environments. *Matrix Biol*. 2011;30(1):70-82.

194. Maroski J, Vorderwülbecke BJ, Fiedorowicz K, et al. Shear stress increases endothelial hyaluronan synthase 2 and hyaluronan synthesis especially in regard to an atheroprotective flow profile. *Exp Physiol*. 2011;96(9):977-86.

195. Camenisch TD, Biesterfeldt J, Brehm-Gibson T, Bradley J, McDonald JA. Regulation of cardiac cushion development by hyaluronan. *Exp Clin Cardiol*. 2001;6(1):4-10.

196. Bourguignon LYW, Peyrollier K, Gilad E, Brightman A. Hyaluronan-CD44 interaction with neural Wiskott-Aldrich Syndrome protein (N-WASP) promotes actin polymerization and ErbB2 activation leading to β-Catenin nuclear translocation, transcriptional up-regulation, and cell migration in ovarian tumor cells. *J Biol Chem* . 2007;282(2):1265-80.

197. Klewer SE, Yatskievych T, Pogreba K, Stevens M V, Antin PB, Camenisch TD. HAS2 expression in heart forming regions is independent of BMP signalling. *Gene Expr Patterns*. 2006;6(5):462-70.

198. Craig E a, Austin AF, Vaillancourt RR, Barnett J V, Camenisch TD. TGFβ2-mediated production of hyaluronan is important for the induction of epicardial cell differentiation and invasion. *Exp Cell Res*. 2010;316(20):3397-405.

199. Li Y, Jiang D, Liang J, et al. Severe lung fibrosis requires an invasive fibroblast phenotype regulated by hyaluronan and CD44. *J Exp Med*. 2011;208(7):1459-71.

200. Midgley AC, Rogers M, Hallett MB, et al. Transforming Growth Factor-β1 (TGF-β1)-stimulated fibroblast to myofibroblast differentiation is mediated by hyaluronan (HA)-facilitated epidermal growth factor receptor (EGFR) and CD44 co-localization in lipid rafts. *J Biol Chem* . 2013;288(21):14824-38.

201. Barrallo-Gimeno A, Nieto MA. The Snail genes as inducers of cell movement and survival: implications in development and cancer. *Development*. 2005;132(14):3151-61.

202. Lee S-W, Won J-Y, Kim WJ, et al. Snail as a potential target molecule in cardiac fibrosis: paracrine action of endothelial cells on fibroblasts through snail and CTGF axis. *Mol Ther*. 2013;21(9):1767-7.

203. Hinz B, Dugina V, Ballestrem C, Wehrle-haller B, Chaponnier C. Smooth muscle actin is crucial for focal adhesion maturation in Myofibroblasts. *Mol Biol Cell*. 2003;14(6):2508-19.

204. LeBleu VS, Taduri G, O'Connell J, et al. Origin and function of myofibroblasts in kidney fibrosis. *Nat Med*. 2013;19(8):1047-53.

205. Kokudo T, Suzuki Y, Yoshimatsu Y, Yamazaki T, Watabe T, Miyazono K. Snail is required for TGFbeta-induced endothelial-mesenchymal transition of embryonic stem cell-derived endothelial cells. *J Cell Sci*. 2008;121(20):3317-24.

206. Fiedler J, Batkai S, Thum T. MicroRNA-based therapy in cardiology. *Herz*. 2014;39(2):194-200.

207. Van Rooij E, Olson EN. MicroRNA therapeutics for cardiovascular disease: opportunities and obstacles. *Nat Rev Drug Discov*. 2012;11(11):860-72.

208. Chau BN, Xin C, Hartner J, et al. MicroRNA-21 Promotes Fibrosis of the Kidney by Silencing Metabolic Pathways. *Sci Transl Med* . 2012;4(121):121ra18.

209. Liu G, Friggeri A, Yang Y, et al. miR-21 mediates fibrogenic activation of pulmonary fibroblasts and lung fibrosis. *J Exp Med* . 2010;207(8):1589-97.

210. Janssen HLA, Reesink HW, Lawitz EJ, et al. Treatment of HCV Infection by Targeting MicroRNA. *N Engl J Med*. 2013;368(18):1685-94.

211. Roncarati R, Viviani Anselmi C, Losi MA, et al. Circulating miR-29a, among other up-regulated microRNAs, is the only biomarker for both hypertrophy and fibrosis in patients with hypertrophic cardiomyopathy. *J Am Coll Cardiol*. 2014;63(9):920-7.

212. Friedman RC, Farh KK-H, Burge CB, Bartel DP. Most mammalian mRNAs are conserved targets of microRNAs. *Genome Res*. 2009;19(1):92-105.

213. Maragkakis M, Reczko M, Simossis VA, et al. DIANA-microT web server: elucidating microRNA functions through target prediction. *Nucleic Acids Res* . 2009;37 (suppl 2):W273-6.

214. Maragkakis M, Alexiou P, Papadopoulos G, et al. Accurate microRNA target prediction correlates with protein repression levels. *BMC Bioinformatics*. 2009;10(1):295.

215. Garcia DM, Baek D, Shin C, Bell GW, Grimson A, Bartel DP. Weak seed-pairing stability and high target-site abundance decrease the proficiency of lsy-6 and other microRNAs. *Nat Struct Mol Biol*. 2011;18(10):1139–46.

216. Vergoulis T, Vlachos IS, Alexiou P, et al. TarBase 6.0: capturing the exponential growth of miRNA targets with experimental support. *Nucleic Acids Res* . 2012;40(1):D222-9.

217. Vlachos IS, Kostoulas N, Vergoulis T, et al. DIANA miRPath v.2.0: investigating the combinatorial effect of microRNAs in pathways. *Nucleic Acids Res* . 2012;40(1):W498-504.

218. Kanehisa M, Goto S, Sato Y, Furumichi M, Tanabe M. KEGG for integration and interpretation of large-scale molecular data sets. *Nucleic Acids Res*. 2012;40:D109-14.

219. Balikova I, Lehesjoki A-E, de Ravel TJL, et al. Deletions in the VPS13B (COH1) gene as a cause of Cohen syndrome. *Hum Mutat*. 2009;30(9):E845-54.

220. Condorelli G, Latronico MVG, Cavarretta E. microRNAs in cardiovascular diseases: current knowledge and the road ahead. *J Am Coll Cardiol*. 2014;63(21)2177-87.

221. Kozomara A, Griffiths-Jones S. miRBase: annotating high confidence microRNAs using deep sequencing data. *Nucleic Acids Res*. 2014;42(D1):D68-73.

222. Kaneko K, Li X, Zhang X, Lamberti JJ, Jamieson SW, Thistlethwaite PA. Endothelial expression of bone morphogenetic protein receptor type 1a is required for atrioventricular valve formation. *Ann Thorac Surg*. 2008;85(6):2090-8.

223. Kakkar R, Lee RT. Intramyocardial Fibroblast Myocyte Communication. *Circ Res* . 2010;106(1):47-57.

224. Cavarretta E, Latronico MVG, Condorelli G. Endothelial-to-mesenchymal transition and microRNA-21: The game is on again . *Arterioscler Thromb Vasc Biol* . 2012;32(2):165-6.

225. Díaz-López A, Moreno-Bueno G, Cano A. Role of microRNA in epithelial to mesenchymal transition and metastasis and clinical perspectives. *Cancer Manag Res*. 2014;6:205-16.

226. Kriegel AJ, Liu Y, Fang Y, Ding X, Liang M. The miR-29 family: genomics, cell biology, and relevance to renal and cardiovascular injury. *Physiol Genomics*. 2012;44(4):237-44.

227. Van Rooij E, Sutherland LB, Thatcher JE, et al. Dysregulation of microRNAs after myocardial infarction reveals a role of miR-29 in cardiac fibrosis. *Proc Natl Acad Sci U S A*. 2008;105(35):13027-32.

228. Merk DR, Chin JT, Dake B a, et al. miR-29b participates in early aneurysm development in Marfan syndrome. *Circ Res*. 2012;110(2):312-24.

229. Small EM, Sutherland LB, Rajagopalan KN, Wang S, Olson EN. MicroRNA-218 regulates vascular patterning by modulation of Slit-Robo signalling. *Circ Res*. 2010;107(11):1336-44.

230. Carmeliet P, Tessier-Lavigne M. Common mechanisms of nerve and blood vessel wiring. *Nature*. 2005;436(7048):193-200.

231. Fish JE, Wythe JD, Xiao T, et al. A Slit/miR-218/Robo regulatory loop is required during heart tube formation in zebrafish. *Development*. 2011;138(7):1409-19.

232. Orend G, Chiquet-ehrismann R. Adhesion modulation by antiadhesive molecules of the extracellular matrix. *Exp Cell Res*. 2000;261(1):104-10.

233. Chiquet-Ehrismann R, Chiquet M. Tenascins: regulation and putative functions during pathological stress. *J Pathol*. 2003;200(4):488-99.

234. Lloyd P, Jones FS. Tenascin-C in development and disease : gene regulation and cell function. *Matrix Biol*. 2000;19(7):581-96.

235. Kalola A. Regulation and Function of Tenascin-C in Heart Valve Homeostasis Regulation and Function of Tenascin-C in Heart Valve Homeostasis. *PennScience*. 2006;5(1):30-3.

236. Camenisch TD, Spicer AP, Brehm-Gibson T, et al. Disruption of hyaluronan synthase-2 abrogates normal cardiac morphogenesis and hyaluronan-mediated transformation of epithelium to mesenchyme. *J Clin Invest*. 2000;106(3):349-60.

237. Udali S, Guarini P, Moruzzi S, Choi S-W, Friso S. Cardiovascular epigenetics: from DNA methylation to microRNAs. *Mol Aspects Med*. 2013;34(4):883-901.

238. Skallerud B, Prot V, Nordrum IS. Modelling active muscle contraction in mitral valve leaflets during systole: a first approach. *Biomech Model Mechanobiol*. 2011;10(1):11-26.

239. Boilson BA, Larsen K, Harbuzariu A, et al. Regulation of circulating progenitor cells in left ventricular dysfunction. *Circ Heart Fail*. 2010;3(5):635-42.

240. Sen S, McDonald SP, Coates PTH, Bonder CS. Endothelial progenitor cells: novel biomarker and promising cell therapy for cardiovascular disease. *Clin Sci (Lond)*. 2011;120(7):263-83.

241. Rieder F, Kessler SP, West G a, et al. Inflammation-induced endothelial-to-mesenchymal transition: a novel mechanism of intestinal fibrosis. *Am J Pathol*. 2011;179(5):2660-73.

242. Han RI, Impoco G, Culshaw G, French AT, Black A, Corcoran BM. Cell maceration scanning electron microscopy and computer-derived porosity measurements in assessment of connective tissue microstructure changes in the canine myxomatous mitral valve. *Vet J*. 2013;197(2):502-5.

9 Appendix

9.1 Up-regulated Genes

Transcript ID	Gene Symbol	Gene name	Fold-Change	p-value
14356140	ADAMDEC1	ADAM-like, decysin 1	16.43	0.0023638
14279513	HSP70	Heat shock protein 70	15.76	2.20E-06
14308629	ACTG2	Actin, gamma 2, smooth muscle, enteric	15.35	0.0030887
14430334	ANGPTL1	Angiopoietin-like 1	7.93	0.0001341
14291033	IL6	Interleukin 6	7.87	0.0048311
14277604	CDKN2A	p14ARF protein	7.53	0.0003567
14298902	SFRP2	Secreted frizzled-related protein 2	7.11	0.0018832
14409533	IL18	Interleukin 18	6.93	0.0029053
14429457	C4BPA	Complement component 4 binding protein, alpha	6.74	0.0052239
14452716	CCL13	Chemokine ligand 13	6.40	0.0036236
14305101	IGKC	Immunoglobulin kappa constant	5.87	0.0080731
14401712	RGS2	Regulator of G-protein signalling 2	5.81	0.0012611
14356695	HTR2B	5-hydroxytryptamine receptor 2B	5.78	0.0048892
14409039	SNORD14B	pSNORD14B-a snoRNA	5.75	0.003647
14387651	CXCL10	chemokine ligand 10	5.40	0.0004294
14324892	CD180	CD180	5.39	0.0050902
14339519	MS4A7	Membrane-spanning 4-domains, subfamily A, member 7	5.29	0.0004264
14402028	RGS4	Regulator of G-protein signalling 4	5.25	0.0037782
14395863	HOXD8	Homeobox D8	4.95	0.00021
14277060	CXCL14	Chemokine ligand 14	4.94	0.0013862
14421671	MYH11	Myosin heavy chain 11	4.94	0.0050241
14330446	DNAJB1	DnaJ (Hsp40) homolog, subfamily B, member 1	4.87	0.0011413
14276379	IRGM	Immunity-related GTPase family, M	4.76	0.0015678
14389567	CSTA	Cystatin A (stefin A)	4.66	0.0044598
14364302	OLR1	Oxidized low density lipoprotein (lectin-like) receptor 1	4.64	0.0069276
14346717	CPNE4	Copine IV	4.63	0.000963
14399010	KCNE4	Potassium voltage-gated channel, Isk-related family	4.31	0.0004064
14296316	LOC100855494	Relaxin receptor 1-like	4.24	0.0077952
14441121	MDGA2	MAM domain containing glycosylphosphatidylinositol anchor 2	4.19	0.0004333
14404932	PLCXD3	Phosphatidylinositol-specific phospholipase C, X domain containing 3	4.16	0.0049998
14259926	BLVRB	Biliverdin reductase B	4.04	0.0012035
14418564	CLEC3A	C-type lectin domain family 3, member	4.00	0.0073173

		A		
14433991	PTGS2	Prostaglandin-endoperoxide synthase 2	3.98	0.0013685
14306037	FCGR1A	Fc fragment of IgG, high affinity Ia, receptor, CD64	3.87	0.0026072
14409809	MMP12	Matrix metallopeptidase 12 (macrophage elastase)	3.82	0.0005609
14378900	UCHL1	Ubiquitin carboxyl-terminal esterase L1 (ubiquitin thiolesterase)	3.73	0.0019072
14337646	CTSC	Cathepsin C	3.69	0.0036112
14387161	DAPP1	Dual adaptor of phosphotyrosine and 3-phosphoinositides	3.68	0.0020442
14265296	MIA	Melanoma inhibitory activity	3.67	0.000295
14298963	FGG	Fibrinogen gamma chain	3.66	0.0033911
14415876	C5H17orf61	Chromosome 5 open reading frame, human C17orf61	3.66	0.0008839
14287764	ANGPT1	Angiopoietin 1	3.65	9.78E-05
14308417	DNAH6	Dynein, axonemal, heavy chain 6	3.64	0.0014576
14447242	EVI2B	Ecotropic viral integration site 2B	3.61	0.0027801
14301010	ENPP6	Ectonucleotide phosphodiesterase 6	3.59	0.0008702
14457347	TLR8	Toll-like receptor 8	3.56	0.000581
14335858	LOC100856456	Transcription factor jun-B-like	3.56	0.0062055
14427829	LOC100855953	Leukocyte surface antigen CD53-like	3.55	0.0006372
14376000	ARAP2	ArfGAP with RhoGAP domain, ankyrin repeat and PH domain 2	3.51	4.32E-05
14397988	CASP8	Caspase 8, apoptosis-related cysteine peptidase	3.51	0.000147
14390098	ZBTB11	Zinc finger and BTB domain containing 11	3.46	0.0011206
14306097	LOC100855873	uncharacterized	3.38	9.18E-05
14315779	RAB1B	Member RAS oncogene family	3.36	0.0007053
14297194	CYP4B1	Cytochrome P450, family 4, subfamily B, polypeptide 1	3.35	0.0070399
14384937	KCNJ15	Potassium inwardly-rectifying channel, subfamily J, member 15	3.35	0.0012843
14388813	EPHA3	EPH receptor A3	3.34	0.0016206
14400997	FCGR3A	Fc fragment of IgG, low affinity IIIa, receptor, CD16a	3.32	0.0019346
14279408	LST1	Leukocyte specific transcript 1	3.22	5.69E-05
14302908	MSR1	Macrophage scavenger receptor 1	3.22	0.0030312
14387182	BANK1	B-cell scaffold protein with ankyrin repeats 1	3.19	0.0004135
14408542	CDH6	Cadherin 6, type 2, K-cadherin (foetal kidney)	3.16	0.0030894
14384410	LOC478384	Multidrug resistance-associated protein 1-like	3.15	0.0001173
14269496	RPS27A	Ribosomal protein S27a	3.12	0.0057618
14393246	CLDN1	Claudin 1	3.07	0.0062876
14257671	PDCD1LG2	Programmed cell death 1 ligand 2	3.04	0.0023886
14430646	SELE	Selectin E	3.02	0.0035648

14461642	CXHXorf21	Chromosome X open reading frame, human CXorf21	2.98	0.0010594
14260050	GMFG	Glia maturation factor, gamma	2.97	9.31E-05
14432035	S100A4	S100 calcium binding protein A4	2.96	0.0011562
14366798	C3AR1	Complement component 3a receptor 1	2.95	0.0035321
14289740	IGJ	Immunoglobulin J polypeptide, linker protein for immunoglobulin alpha and mu polypeptides	2.94	0.0051636
14255312	ATP8B1	ATPase, aminophospholipid transporter, class I, type 8B, member 1	2.92	0.0016777
14375983	TLR1	Toll-like receptor 1	2.92	0.0015849
14316910	SLC7A11	Solute carrier family 7 (anionic amino acid transporter light chain, xc- system), member 11	2.90	0.0003853
14395737	LOC100669834	3-ketoacyl-CoA thiolase	2.90	0.0082638
14458099	GPR34	G protein-coupled receptor 34	2.86	0.0012531
14399254	STK17B	Serine/threonine kinase 17b	2.84	0.0040246
14336520	EMR1	Egf-like module containing, mucin-like, hormone receptor-like 1	2.83	0.0066345
14266174	SCN1B	Sodium channel, voltage-gated, type I, beta subunit	2.83	0.0010587
14459404	HNRNPH2	heterogeneous nuclear ribonucleoprotein H2 (H')	2.82	0.0001491
14305354	TACR1	Tachykinin receptor 1	2.81	0.005963
14401130	CD48	CD48 molecule	2.79	0.0001312
14376548	ARSK	Arylsulfatase family, member K	2.76	0.0004966
14395111	LOC100856186	Histone H2B type 1-like	2.71	0.0069714
14415921	LSMD1	LSM domain containing 1	2.71	0.0015234
14330808	ACP5	Acid phosphatase 5, tartrate resistant	2.71	0.0032024
14388619	CFI	Complement factor I	2.67	0.0004298
14430287	PLA2G4A	Phospholipase A2, group IVA (cytosolic, calcium-dependent)	2.67	6.15E-05
14293112	SKAP2	Src kinase associated phosphoprotein 2	2.66	0.0033201
14285991	NOV	Nephroblastoma overexpressed gene	2.64	0.0001948
14295395	PLXNC1	Plexin C1	2.64	0.0001755
14417953	SLC2A5	Solute carrier family 2 (facilitated glucose/fructose transporter), member 5	2.64	0.0003722
14438172	AKAP5	A kinase (PRKA) anchor protein 5	2.64	0.004823
14277492	BNC2	Basonuclin 2	2.63	0.0005092
14423410	GCLM	Glutamate-cysteine ligase, modifier subunit	2.62	0.0011236
14367425	CECR1	Cat eye syndrome chromosome region, candidate 1	2.61	0.0028325
14444226	CD300C	CD300c molecule	2.60	0.0061729
14455870	MUSTN1	Musculoskeletal, embryonic nuclear protein 1	2.60	0.0026978
14369941	SLC16A12	Solute carrier family 16, member 12	2.58	0.0030007
14394611	F13A1	Coagulation factor XIII, A1 polypeptide	2.58	0.00097
14461264	PIR	Pirin (iron-binding nuclear protein)	2.58	0.0048184

14307331	CGREF1	Cell growth regulator with EF-hand domain 1	2.58	0.0027185
14355262	ALOX5AP	Arachidonate 5-lipoxygenase-activating protein	2.58	0.0014917
14364714	MRPL51	Mitochondrial ribosomal protein L51	2.56	0.000589
14260868	SERPINB8	Serpin peptidase inhibitor, clade B (ovalbumin), member 8	2.56	0.0006415
14306915	OSR1	Odd-skipped related 1 (Drosophila)	2.50	0.0027473
14376453	FAM174A	Family with sequence similarity 174, member A	2.50	0.0001622
14316336	FKBP2	FK506 binding protein 2	2.50	0.0007302
14290617	LOC100855806	Guanine nucleotide-binding protein G(I)/G(S)/G(O) subunit gamma-11-like	2.50	5.55E-06
14290717	DYNC1I1	Dynein, cytoplasmic 1, intermediate chain 1	2.49	0.0009569
14347154	PCOLCE2	Procollagen C-endopeptidase enhancer 2	2.48	0.0050051
14295006	RNASE8	Ribonuclease, RNase A family, 8	2.48	0.0001736
14293512	LOC100856330	Transcription factor EC-like	2.48	0.0028158
14311075	LPXN	Leupaxin	2.47	0.0002508
14404160	KCNMB1	Potassium large conductance calcium-activated channel, subfamily M, beta member 1	2.47	0.0007783
14326462	C1QC	Complement component 1, q subcomponent, C chain	2.45	0.0034431
14393476	PDCD10	Programmed cell death 10	2.45	0.0001784
14300558	LSM1	LSM1 homolog, U6 small nuclear RNA associated (S. cerevisiae)	2.45	7.82E-05
14260509	PEPD	Peptidase D	2.44	0.0012788
14457934	CYBB	Cytochrome b-245, beta polypeptide	2.44	0.0005148
14262002	SOD2	Superoxide dismutase 2, mitochondrial	2.44	0.0055162
14329923	LRRC25	Leucine rich repeat containing 25	2.43	0.0064751
14282827	HLA-DMB	Major histocompatibility complex, class II, DM beta	2.42	0.0006325
14409755	CASP4	Caspase 4, apoptosis-related cysteine peptidase	2.42	0.00462
14414808	TAGLN	Transgelin, smooth muscle protein 22-α	2.40	0.0042533
14341081	LOC100855439	Lymphatic vessel endothelial hyaluronan receptor 1	2.40	0.0024844
14360356	P2RX7	Purinergic receptor P2X, ligand-gated ion channel, 7	2.40	0.0080105
14279411	AIF1	Allograft inflammatory factor 1	2.39	6.21E-05
14423570	GBP7	Guanylate binding protein 7	2.39	0.0010409
14463411	ACSL4	Acyl-CoA synthetase long-chain family member 4	2.38	0.0001702
14393925	BMP6	Bone morphogenetic protein 6	2.38	0.0006752
14293421	THAP5	THAP domain containing 5	2.38	0.0049522
14388251	EIF4E	Eukaryotic translation initiation factor 4E, transcript variant 1	2.38	3.06E-05
14420727	LOC100856347	Apoptosis-associated speck-like protein containing a CARD-like	2.37	1.64E-05

14394786	CCDC90A	Coiled-coil domain containing 90A	2.37	0.0002194
14397810	PLCL1	Phospholipase C-like 1	2.37	0.0011644
14281184	PTP4A1	Protein tyrosine phosphatase type IVA, member 1	2.36	0.0027559
14378086	LOC488754	UPF0235 protein C15orf40 homolog	2.36	0.0007535
14368831	ACSL5	Acyl-CoA synthetase long-chain family member 5	2.36	0.0025964
14349723	LOC100855575	Prefoldin subunit 4-like	2.35	0.0002414
14276284	TLR4	Toll-like receptor 4	2.35	0.0007263
14405830	KCNK1	Potassium channel, subfamily K, member 1	2.34	7.61E-06
14282689	PBX2	Pre-B-cell leukemia homeobox 2	2.34	0.0006961
14306306	PSMD4	Proteasome (prosome, macropain) 26S subunit, non-ATPase, 4	2.34	0.0010403
14390084	SENP7	SUMO1/sentrin specific peptidase 7	2.33	0.0005753
14424895	BUD31	BUD31 homolog (S. cerevisiae)	2.32	0.0001206
14389549	CD86	CD86	2.31	0.0061988
14339560	LOC100688295	HIG1 domain family member 1A-like	2.30	0.0009726
14282987	MNF1	Mitochondrial nucleoid factor 1	2.30	0.0004498
14425484	LOC607096	Integrin alpha-D-like	2.29	0.0082467
14289182	COMMD8	COMM domain containing 8	2.29	0.0014787
14455843	YKT6	Synaptobrevin homolog YKT6-like	2.29	0.0001039
14370194	BLNK	B-cell linker	2.29	0.007452
14324913	TAF9	TAF9 RNA polymerase II, TATA box binding protein (TBP)-associated factor	2.28	0.0007525
14310860	LMO2	LIM domain only 2 (rhombotin-like 1)	2.28	0.0003799
14366241	ARNTL2	Aryl hydrocarbon receptor nuclear translocator-like 2	2.28	0.0053733
14437194	COCH	Coagulation factor C homolog, cochlin	2.28	0.0033649
14269495	LOC481020	Ribosomal protein S27a pseudogene	2.28	0.0002827
14384036	HEXA	Hexosaminidase A (alpha polypeptide)	2.27	8.53E-05
14316455	RARRES3	Retinoic acid receptor responder	2.27	0.001159
14309451	CTSS	Cathepsin S	2.27	0.0001155
14272857	PIGF	Phosphatidylinositol glycan anchor biosynthesis, class F	2.27	2.42E-05
14268697	SLC41A2	Solute carrier family 41, member 2	2.26	0.0007109
14452113	TMEM100	Transmembrane protein 100-like	2.26	0.0002165
14424902	ARPC1B	Actin related protein 2/3 complex, subunit 1B	2.25	0.0003128
14355340	LOC100856417	Ras-like protein family member 11A-like	2.24	0.0043578
14464562	CLIC2	Chloride intracellular channel 2	2.24	0.0004549
14261042	SEC11C	SEC11 homolog C (S. cerevisiae)	2.23	0.0006212
14324259	SRA1	Steroid receptor RNA activator 1	2.23	0.000316
14459417	ARMCX3	Armadillo repeat containing, X-linked 3	2.22	0.0004459
14380316	PLDN	Pallidin homolog (mouse)	2.22	0.0007458
14330676	DNASE2	Deoxyribonuclease II, lysosomal	2.22	0.0007203

14257638	JAK2	Janus kinase 2	2.21	8.78E-05
14372222	TMEM70	Transmembrane protein 70	2.21	1.44E-05
14435696	GALNT1	UDP-N-acetyl-alpha-D-galactosamine:polypeptide N-acetylgalactosaminyltransferase 1	2.21	0.0003822
14304046	EMILIN1	Elastin microfibril interfacer 1	2.20	0.0044554
14269753	PLEK	Pleckstrin	2.20	0.0009991
14272109	CHST11	Carbohydrate (chondroitin 4) sulfotransferase 11	2.20	0.0041996
14366663	GABARAPL1	GABA(A) receptor-associated protein like 1	2.20	0.0005529
14387085	BMPR1B	Bone morphogenetic protein receptor, type IB	2.20	0.0038141
14297852	HNRNPC	Heterogeneous nuclear ribonucleoprotein C (C1/C2), transcript variant 4	2.20	0.0003674
14333765	PDE12	Phosphodiesterase 12	2.20	0.0001047
14430268	C7H1orf27	Chromosome 7 open reading frame, human	2.19	0.0079821
14364180	HEBP1	Heme binding protein 1	2.19	0.0016488
14458636	TSR2	TSR2, 20S rRNA accumulation, homolog (S. cerevisiae)	2.19	0.0001605
14288059	HAS2	Hyaluronan synthase 2	2.18	0.0009851
14274424	UQCRQ	Ubiquinol-cytochrome c reductase, complex III subunit VII	2.18	0.0031511
14387277	AIMP1	Aminoacyl tRNA synthetase complex-interacting multifunctional protein 1	2.18	0.0006014
14296247	GUCY1B3	Guanylate cyclase 1, soluble, beta 3	2.17	0.000957
14408225	CARD6	Caspase recruitment domain family, member 6	2.17	0.0029127
14435335	CKS1B	CDC28 protein kinase regulatory subunit 1B	2.17	0.0010044
14316453	LOC100855614	39S ribosomal protein L33, mitochondrial-like	2.17	0.0010788
14383296	GTF2A2	General transcription factor IIA, 2, 12kDa	2.16	1.95E-05
14434952	FBXO28	F-box protein 28	2.16	8.51E-06
14309398	LOC100855771	Acidic leucine-rich nuclear phosphoprotein 32 family	2.15	7.47E-06
14363362	TWF1	Twinfilin, actin-binding protein, homolog 1 (Drosophila)	2.14	8.38E-05
14437560	LOC100856165	Abhydrolase domain-containing protein 12B-like	2.14	0.0003549
14255611	ABRACL	ABRA C-terminal like	2.14	0.0004002
14261673	NUP43	Nucleoporin	2.14	1.81E-05
14439109	C8H14orf109	Chromosome 8 open reading frame, human C14orf109	2.14	0.0011247
14279522	CFB	Complement factor B	2.14	0.0028465
14329619	CCR1	Chemokine receptor 1	2.14	0.0077394
14314380	C18H11orf46	Chromosome 18 open reading frame, human C11orf46	2.14	0.000794
14406768	C4H10orf57	Chromosome 4 open reading frame,	2.14	0.0004043

		human C10orf57		
14317409	C19H2orf76	Chromosome 19 open reading frame, human C2orf76	2.13	0.0005309
14388654	TIFA	TRAF-interacting protein with forkhead-associated domain	2.13	0.0006229
14423819	TTLL7	Tubulin tyrosine ligase-like family, member 7	2.13	0.0005671
14370250	PIK3AP1	Phosphoinositide-3-kinase adaptor protein 1	2.13	0.0056387
14447044	CCL5	Chemokine ligand 5	2.12	0.00276
14375538	HAUS3	HAUS augmin-like complex, subunit 3	2.12	0.0003076
14452355	LOC100856241	Spindle and kinetochore-associated protein 2-like	2.12	0.0008738
14344008	TMEM90B	Synapse differentiation-inducing gene protein 1-like	2.11	0.0001278
14341803	LCP1	Lymphocyte cytosolic protein 1 (L-plastin)	2.11	0.0054745
14280111	CDKN1A	Cyclin-dependent kinase inhibitor 1A	2.11	0.0064265
14295451	SNRPF	Small nuclear ribonucleoprotein polypeptide F	2.11	2.02E-05
14404409	HAVCR1	Hepatitis A virus cellular receptor 1	2.10	0.0075884
14291509	DNAJB9	DnaJ (Hsp40) homolog, subfamily B, member 9	2.10	0.000596
14255007	TXNL4A	Thioredoxin-like 4A	2.10	0.0001545
14387790	RASGEF1B	RasGEF domain family, member 1B	2.10	0.0068825
14457994	MID1IP1	MID1 interacting protein 1	2.09	0.0005058
14290397	ADAM22	ADAM metallopeptidase domain 22	2.09	0.0031606
14334256	LOC100855747	Mesencephalic astrocyte-derived neurotrophic factor-like	2.09	0.0055892
14294722	PRDX1	Peroxiredoxin 1	2.09	0.0008154
14347364	P2RY12	Purinergic receptor P2Y, G-protein coupled, 12	2.09	0.0054882
14326966	PDPN	Podoplanin	2.09	0.000746
14457450	LOC100856271	Carbonic anhydrase 5B, mitochondrial-like	2.09	0.0008696
14456401	LOC100855962	1,2-dihydroxy-3-keto-5-methylthiopentene dioxygenase-like	2.09	0.0020511
14311483	SPI1	Spleen focus forming virus (SFFV) proviral integration oncogene	2.08	0.0041846
14367224	LOC100682990	uncharacterized	2.08	0.0081128
14302847	ERI1	Exoribonuclease 1	2.08	0.0003779
14447759	LSM5	LSM5 homolog, U6 small nuclear RNA associated	2.07	0.0039929
14339931	C21H11orf73	Chromosome 21 open reading frame, human C11orf73	2.07	0.0003094
14321596	ITFG1	Integrin alpha FG-GAP repeat containing 1	2.07	0.0021643
14312979	C18H11orf48	Chromosome 18 open reading frame, human C11orf48	2.07	0.0013839
14375926	UGDH	UDP-glucose 6-dehydrogenase	2.07	0.002583
14271865	NCF4	Neutrophil cytosolic factor 4	2.07	0.0003315

14320343	KCTD16	Potassium channel tetramerisation domain containing 16	2.07	0.0019304
14326126	RPS6KA1	Ribosomal protein S6 kinase	2.07	0.0039676
14342436	ITGBL1	Integrin, beta-like 1 (with EGF-like repeat domains)	2.06	0.001201
14393763	NQO2	NADPH dehydrogenase, quinone 2	2.06	9.50E-05
14291222	CHN2	Chimerin 2	2.05	0.0017276
14309855	C1orf162	Chromosome 1 open reading frame 162	2.05	0.0037296
14343523	UGGT2	UDP-glucose glycoprotein glucosyltransferase 2	2.05	9.49E-05
14388094	HSD17B11	Hydroxysteroid dehydrogenase 11	2.05	0.0017765
14374668	CHSY1	Chondroitin sulfate synthase 1	2.04	0.000203
14437248	NPAS3	Neuronal PAS domain protein 3	2.04	0.0050785
14326622	LOC612968	UPF0327 protein C1orf151-like	2.04	2.36E-07
14376263	MFSD7	Major facilitator superfamily domain containing 7	2.04	0.0010188
14323171	CREM	cAMP responsive element modulator	2.03	0.0024523
14460399	HTATSF1	HIV-1 Tat specific factor 1	2.03	2.65E-05
14415665	PSMB6	Proteasome (prosome, macropain) subunit, beta type, 6	2.03	3.38E-05
14457364	RAB9A	RAB9A, member RAS oncogene family	2.03	8.25E-05
14390880	LOC100856388	Oxysterol-binding protein-related protein 11-like	2.03	6.57E-05
14264356	FLT3LG	Fms-related tyrosine kinase 3 ligand	2.02	0.0038599
14282545	HSPA1L	Heat shock 70kDa protein 1-like	2.02	0.0005714
14459962	SLC25A5	Solute carrier family 25 (mitochondrial carrier; adenine nucleotide translocator), member 5	2.02	0.0013401
14310009	C18H7orf25	Chromosome 18 open reading frame, human C7orf25	2.02	0.0044332
14353865	REEP4	Receptor accessory protein 4	2.02	0.001033
14303184	CDKN2AIP	CDKN2A interacting protein	2.02	0.0022166
14373072	CYP7B1	Cytochrome P450, family 7, subfamily B, polypeptide 1	2.02	0.0070221
14432045	S100A6	S100 calcium binding protein A6	2.01	0.0060007
14434527	ATP1B1	ATPase, Na+/K+ transporting, beta 1 polypeptide	2.01	0.0072442
14444221	LOC100686047	CMRF35-like molecule-like	2.01	0.0018697
14278898	POLE3	Polymerase (DNA directed), epsilon 3, accessory subunit	2.01	0.0025687
14276770	HINT1	Histidine triad nucleotide binding protein 1	2.01	0.0030206
14255629	GPR126	G protein-coupled receptor 126	2.00	0.0016917
14260025	EID2	EP300-interacting inhibitor of differentiation 2-like	2.00	0.0011167
14366159	FAR2	Fatty acyl CoA reductase 2	2.00	0.0012864
14402106	DUSP12	Dual specificity phosphatase 12	1.91	0.0038568
14265178	RPS19	Ribosomal protein S19	1.90	5.11E-05

14407201	ATP6V0E1	ATPase, H+ transporting, lysosomal 9kDa, V0 subunit e1	1.88	0.0002092
14447839	GNG10	Guanine nucleotide binding protein (G protein), gamma 10	1.88	9.96E-05
14442139	NPC2	Niemann-Pick disease, type C2	1.83	3.27E-05
14350497	DSTN	Destrin	1.82	0.0009115
14340701	PRKCDBP	Protein kinase C, delta binding protein	1.77	0.0003068
14400410	SERPINE2	Serpin peptidase inhibitor, clade E (nexin, plasminogen activator inhibitor type 1), member 2	1.75	0.0008742
14272245	SULT1C4	Sulfotransferase family, cytosolic, 1C, member 4	1.74	0.0004385
14307327	OST4	Oligosaccharyltransferase 4 homolog (S. cerevisiae)	1.73	0.0006299
14432911	LOC100686444	Ribosomal protein L23 pseudogene on chromosome 7	1.73	0.0004456
14432910	PLXDC1	Plexin domain containing 1	1.73	0.0004456
14397472	FRZB	Frizzled-related protein	1.72	0.0027688
14260028	RPS16	Ribosomal protein S16	1.71	0.0076111
14390307	ATG3	Autophagy related 3	1.70	0.0002805
14388746	SEC24D	SEC24 family, member D (S. cerevisiae)	1.68	0.0032373
14437994	HIF1A	Hypoxia inducible factor 1, alpha subunit (basic helix-loop-helix transcription factor)	1.67	0.0008835
14342163	CLN5	Ceroid-lipofuscinosis, neuronal 5	1.66	0.0001417
14343958	GAS6	Growth arrest-specific 6	1.66	0.0024621
14445842	MIEN1	Migration and invasion enhancer 1	1.65	0.0038984
14461000	VAMP7	Vesicle-associated membrane protein 7	1.65	0.0012581
14445369	RAB5C	RAB5C, member RAS oncogene family	1.64	0.0002226
14275171	DNAJA1	DnaJ (Hsp40) homolog, subfamily A, member 1	1.62	0.0040381
14458010	LOC100682978	Renin receptor-like	1.61	0.00107
14292191	ATP6V1F	ATPase, H+ transporting, lysosomal 14kDa, V1 subunit F	1.61	0.0029837
14328550	LOC100855678	5'-nucleotidase domain-containing protein 2-like	1.60	0.0033803
14344504	RPSA	Ribosomal protein SA	1.60	0.0020778
14379164	RBPJ	Recombination signal binding protein for immunoglobulin kappa J region	1.60	0.0034678
14261577	FUCA2	Fucosidase, alpha-L- 2, plasma	1.58	0.0010007
14350033	RPS21	Ribosomal protein S21	1.58	0.0041851
14412087	RER1	RER1 retention in endoplasmic reticulum 1 homolog (S. cerevisiae)	1.58	0.0033288
14303909	RAB10	RAB10, member RAS oncogene family	1.58	0.0003814
14271471	RBX1	Ring-box 1, E3 ubiquitin protein ligase	1.57	0.0001233
14446749	CLTC	Clathrin, heavy chain (Hc)	1.57	0.0029127
14333938	SPCS1	Signal peptidase complex subunit 1 homolog (S. cerevisiae)	1.56	0.0010232
14401955	AIDA	Axin interactor, dorsalization associated	1.56	0.0010192

14340406	FOLR2	Folate receptor 2 (foetal)	1.56	0.0031528
14303474	RPS7	Ribosomal protein S7	1.55	0.0017809
14398657	ARPC2	Actin related protein 2/3 complex, subunit 2	1.55	6.05E-05
14379076	PGM2	Phosphoglucomutase 2	1.55	0.0027705
14440227	LGMN	Legumain	1.55	0.0012816
14279695	DLA-DRA	MHC class II DR alpha chain	1.54	0.007323
14269713	ACTR2	ARP2 actin-related protein 2 homolog (yeast)	1.53	0.0036564
14388140	PIGY	Phosphatidylinositol glycan anchor biosynthesis, class Y	1.53	0.0045689
14414061	STT3A	STT3, subunit of the oligosaccharyltransferase complex, homolog A	1.52	0.0001464
14330142	C20H19orf42	Chromosome 20 open reading frame, human C19orf42	1.52	0.000737
14387670	SCARB2	Scavenger receptor class B, member 2	1.52	0.005629
14319137	ITGB1	Integrin beta-1 (fibronectin receptor, beta polypeptide, CD29)	1.52	0.0010731
14360089	TMED2	Transmembrane emp24 domain trafficking protein 2	1.52	6.32E-05
14440261	DAD1	Defender against cell death 1	1.52	0.0034178
14321748	PTP4A2	Protein tyrosine phosphatase type IVA, member 2	1.52	0.0001996
14427965	GNAI3	Guanine nucleotide binding protein (G protein), alpha inhibiting activity polypeptide 3	1.51	0.0011621
14262925	ANXA1	Annexin A1	1.50	0.0045024
14442936	HSP90AA1	Heat shock protein 90kDa alpha	1.50	0.006474

9.2 Down-Regulated Genes

Transcript ID	Gene Symbol	Gene name	Fold-Change	p-value
14317987	RNU6-21	U6 small nuclear 21 (RNU6-21), small nuclear RNA	-9.41	0.0023737
14274311	KIAA1024L	KIAA1024-like	-8.55	0.0017609
14383643	CILP	Cartilage intermediate layer protein,	-6.20	0.0015588
14459309	TNMD	Tenomodulin	-5.48	0.0045327
14353342	GJB6	Gap junction protein, beta 6	-5.27	0.0033142
14432404	DSC2	Desmocollin 2	-5.18	0.0056081
14256801	LAMA2	Laminin, alpha 2	-5.16	0.0010771
14293892	SNORA55	H/ACA box 55 (SNORA55), small nucleolar RNA	-4.98	0.0033681
14404304	CCNJL	Cyclin J-like	-4.64	0.0006434
14274287	ADAMTS19	A disintegrin and metalloproteinase with thrombospondin motif 19	-4.52	0.0046562
14347367	IGSF10	Immunoglobulin superfamily, member 10	-4.43	0.0039529
14263948	ZNF267	Zinc finger protein 267	-4.36	0.0012417
14404821	HCN1	Potassium/sodium hyperpolarization-activated cyclic nucleotide-gated channel 1	-4.30	0.0042065
14423291	LOC479934	Lipid phosphate phosphatase-related protein type 5-l	-4.23	0.0003116
14456802	RN5-8S	5.8S ribosomal RNA	-4.11	0.0003119
14440266	LOC606860	Cytochrome c oxidase subunit 6C-like variant 2	-3.84	0.0011047
14351625	NNAT	neuronatin, transcript variant 2	-3.77	0.0009186
14384782	CBR1	Carbonyl reductase 1	-3.61	0.0003973
14276971	FSTL4	Follistatin-like 4	-3.53	0.0022076
14316083	CDC42EP2	CDC42 effector protein (Rho GTPase binding) 2	-3.35	0.0003867
14289271	EIF1	Eukaryotic translation initiation factor 1 (EIF1)	-3.33	0.0022232
14416005	VAMP2	Vesicle-associated membrane protein 2	-3.32	5.29E-06
14409018	SCN3B	Sodium channel, voltage-gated, type III, beta subunit	-3.26	0.0035518
14279273	ATAT1	Alpha tubulin acetyltransferase 1	-3.24	0.0001465
14408526	PDZD2	PDZ domain containing 2	-3.22	0.0020964
14452015	CHAD	Chondroadherin	-3.17	0.0070053
14334891	CILP2	cartilage intermediate layer protein 2	-3.11	0.0002831
14266793	KIF5A	Kinesin family member 5A	-3.10	3.89E-05
14330901	DOCK6	Dedicator of cytokinesis 6	-3.10	0.0001512
14402587	NID1	Nidogen 1	-3.09	0.0004765
14440633	ADCY4	Adenylate cyclase 4	-3.01	0.0009372
14311489	MYBPC3	Myosin binding protein C, cardiac	-3.00	0.0035104
14399182	TMEFF2	Transmembrane protein with EGF-like	-2.97	0.0001874

		and two follistatin-like domains 2		
14328977	NICN1	Nicolin 1	-2.95	0.0008845
14421559	SYT17	Synaptotagmin XVII	-2.91	0.0020807
14442940	MOK	MOK protein kinase	-2.90	9.29E-06
14316459	LGALS12	Lectin, galactoside-binding, soluble, 12	-2.88	0.0026561
14409246	MPZL2	Myelin protein zero-like 2	-2.88	0.0058972
14464011	LOC100683463	Protein FAM127-like	-2.87	0.0002329
14392321	CLDN11	Claudin 11	-2.87	0.0026389
14313855	PCLO	Presynaptic cytomatrix protein	-2.87	0.0027832
14263819	LENG8	Leukocyte receptor cluster member 8	-2.87	0.0014422
14457986	TSPAN7	Tetraspanin 7	-2.85	0.0011349
14360243	MLXIP	MLX interacting protein	-2.85	0.0008552
14441890	ZFP36L1	Zinc finger protein 36, C3H type-like 1	-2.84	0.0002014
14403626	ZMIZ1	Zinc finger, MIZ-type containing 1	-2.84	0.0036372
14325844	LOC100855498	Serine incorporator 2-like	-2.82	0.0001817
14450321	MAPT	Microtubule-associated protein tau	-2.81	0.0026711
14424200	AUTS2	Autism susceptibility candidate 2	-2.78	0.0001845
14277414	FREM1	FRAS1 related extracellular matrix 1	-2.69	0.0003133
14264759	HIF3A	Hypoxia inducible factor 3, alpha subunit	-2.67	0.0012752
14265052	ZNF283	Zinc finger protein 283	-2.67	0.0021741
14415096	LOC100686634	uncharacterized	-2.67	0.0004244
14400025	IGFBP5	Insulin-like growth factor binding protein 5	-2.65	0.0002239
14381604	RYR3	Ryanodine receptor 3	-2.64	0.0028378
14455066	LOC100855805	Cyclin-dependent kinase 9-like	-2.64	0.0003616
14259800	ATP1A3	ATPase, Na+/K+ transporting, alpha 3 polypeptide	-2.64	0.0073086
14376198	LOC100856492	DDB1- and CUL4-associated factor 16-like	-2.63	0.0008798
14344644	CCBP2	Chemokine binding protein 2	-2.63	0.0006024
14453155	FAM222B	Family with sequence similarity 222, member B	-2.63	5.18E-05
14277894	CNTFR	Ciliary neurotrophic factor receptor	-2.60	0.0016514
14460473	LOC100855971	Protein LDOC1-like	-2.59	0.001504
14378505	GRK4	G protein-coupled receptor kinase 4	-2.58	0.0011628
14373535	MMP16	Matrix metallopeptidase 16	-2.58	0.0040699
14460548	MAMLD1	Mastermind-like domain containing 1	-2.56	0.0004072
14287635	LOC100684029	Ubiquitin-conjugating enzyme E2 N-like	-2.55	0.0046652
14336439	PRAM1	PML-RARA regulated adaptor molecule 1	-2.54	0.0020339
14417429	MXRA8	Matrix-remodelling associated 8	-2.53	0.0011745
14293539	CTTNBP2	Cortactin binding protein 2	-2.52	0.0069934
14306182	ADAMTSL4	ADAMTS-like 4	-2.52	0.0001809
14294468	TTC39A	Tetratricopeptide repeat domain 39A	-2.49	0.0008643

14277190	GFRA3	GDNF family receptor alpha 3	-2.47	0.0083011
14444488	TANC2	Tetratricopeptide repeat, ankyrin repeat and coiled-coil containing 2	-2.47	0.0013202
14329816	SUGP2	SURP and G patch domain containing 2	-2.47	0.0005754
14356848	COL6A3	Collagen, type VI, alpha 3	-2.47	0.0002998
14321931	SRSF4	Serine/arginine-rich splicing factor 4	-2.46	0.0004164
14263835	TTYH1	Tweety homolog 1 (Drosophila)	-2.44	0.0003127
14419301	FAM65A	Family with sequence similarity 65, member A	-2.44	0.0015519
14305406	DQX1	DEAQ box RNA-dependent ATPase 1	-2.44	0.0004586
14272457	NPAS2	Neuronal PAS domain protein 2	-2.44	0.0015415
14398770	TTLL4	Tubulin tyrosine ligase-like family, member 4	-2.43	0.0036999
14401442	PIK3C2B	Phosphoinositide-3-kinase, class 2, beta polypeptide	-2.42	0.0022057
14409363	SIK3	SIK family kinase 3	-2.42	2.16E-05
14297622	SZT2	Seizure threshold 2 homolog (mouse)	-2.42	0.0004458
14367455	MICAL3	Microtubule associated monooxygenase, calponin and LIM domain containing 3	-2.41	1.11E-05
14373768	TMEM232	Transmembrane protein 232	-2.41	0.001817
14329911	ISYNA1	Inositol-3-phosphate synthase 1	-2.41	0.0003538
14331738	RFX2	Regulatory factor X, 2	-2.40	0.0013869
14403871	FAM193B	Family with sequence similarity 193, member B	-2.39	0.000138
14282609	TNXB	Tenascin XB	-2.38	0.0009905
14353345	GJB2	Gap junction protein, beta 2	-2.37	0.0052903
14438313	PLEKHH1	Pleckstrin homology domain containing, family H (with MyTH4 domain) member 1	-2.37	0.0018726
14453076	SGK494	Serine/threonine-protein kinase SgK494	-2.37	0.0001657
14419748	NSUN5	NOP2/Sun domain family, member 5	-2.36	0.0007726
14377933	CRTC3	CREB regulated transcription coactivator 3	-2.33	0.0004378
14448168	NOTCH1	NOTCH 1	-2.33	0.0001854
14272455	LOC100855789	60S ribosomal protein L31-like	-2.33	0.0003392
14415042	SIK2	Salt-inducible kinase 2	-2.32	0.0002157
14358930	LOC612180	Lambda chain V-I region BL2-like	-2.32	4.61E-05
14299531	HIPK2	Homeodomain interacting protein kinase 2	-2.32	0.0029422
14356909	PER2	Period homolog 2 (Drosophila)	-2.31	0.0001976
14286551	KIAA1875	uncharacterized	-2.31	0.0027602
14298252	KERA	Keratocan	-2.29	0.0044131
14403272	EIF4EBP2	Eukaryotic translation initiation factor 4E binding protein 2	-2.28	0.0064816
14368859	TCF7L2	Transcription factor 7-like 2 (T-cell specific, HMG-box)	-2.28	0.0047273
14363340	NELL2	NEL-like 2 (chicken)	-2.28	0.0034098

14320231	PCDHB6	Protocadherin beta 6	-2.27	0.0002363
14400879	LOC100855882	Melanoma inhibitory activity protein 3-like	-2.27	5.40E-05
14451257	RAMP2	Receptor (G protein-coupled) activity modifying protein 2	-2.27	0.002994
14375245	MTHFS	5,10-methenyltetrahydrofolate synthetase (5-formyltetrahydrofolate cyclo-ligase)	-2.26	0.0053607
14330891	TMEM205	Transmembrane protein 205	-2.26	0.0057389
14270169	BAZ2A	Bromodomain adjacent to zinc finger domain, 2A	-2.25	0.0015751
14304824	TMEM127	Transmembrane protein 127	-2.25	0.0011494
14383583	RBPMS2	RNA binding protein with multiple splicing 2	-2.25	0.0014787
14367330	RAD52	RAD52 homolog (S. cerevisiae)	-2.24	0.0001395
14444903	DCAKD	Dephospho-CoA kinase domain containing	-2.24	0.0020062
14443984	WBP2	WW domain binding protein 2	-2.23	2.34E-05
14279460	CSNK2B	Casein kinase 2, beta polypeptide	-2.23	0.0003457
14449897	ITGB4	Integrin, beta 4	-2.23	0.0015219
14458986	ITGB1BP2	Integrin beta 1 binding protein (melusin) 2	-2.23	8.74E-05
14286396	PTP4A3	Protein tyrosine phosphatase type IVA, member 3	-2.22	0.0030047
14336449	ZNF414	Zinc finger protein 414	-2.22	0.0047063
14281354	KCNQ5	Potassium voltage-gated channel, KQT-like subfamily, member 5	-2.22	0.0014712
14327169	PEX14	Peroxisomal biogenesis factor 14	-2.22	0.0005239
14287353	SLC4A4	Solute carrier family 4 (sodium bicarbonate cotransporter), member 4	-2.21	0.000228
14425883	CCDC101	Coiled-coil domain containing 101	-2.20	0.0051057
14356360	FAM160B2	Family with sequence similarity 160, member B2	-2.20	0.0032004
14259044	RASIP1	Ras interacting protein 1	-2.19	4.02E-05
14360655	SLC24A6	Solute carrier family 24 (sodium/potassium/calcium exchanger), member 6	-2.18	0.0002015
14334149	ALAS1	Aminolevulinate, delta-, synthase 1	-2.18	8.27E-05
14312916	NXF1	Nuclear RNA export factor 1	-2.17	0.0012885
14428916	RABGGTB	Rab geranylgeranyltransferase, beta subunit	-2.17	0.0061676
14433201	PPP1R12B	Protein phosphatase 1, regulatory subunit 12B	-2.17	0.0002056
14280756	TMEM63B	Transmembrane protein 63B	-2.17	0.0008502
14380057	STARD9	StAR-related lipid transfer (START) domain containing 9	-2.16	0.0003973
14309367	MTMR11	Myotubularin related protein 11	-2.16	0.0014399
14257931	MZF1	Myeloid zinc finger 1	-2.16	0.0014903
14328985	AMT	Aminomethyltransferase	-2.16	0.0059803
14455291	OLFML2A	Olfactomedin-like 2A	-2.15	0.0020429

14283991	TRAM2	Translocation associated membrane protein 2	-2.14	0.0007098
14373705	C29H8orf37	Chromosome 29 open reading frame, human C8orf37	-2.13	0.0032976
14352215	NFATC2	Nuclear factor of activated T-cells, cytoplasmic, calcineurin-dependent 2	-2.13	0.0065708
14263990	LOC611704	uncharacterized	-2.13	0.001024
14310307	ATXN7L1	Ataxin 7-like 1	-2.13	0.0011088
14380678	LIPC	Lipase, hepatic	-2.13	0.0021006
14406539	ZMYND17	Zinc finger, MYND-type containing 17	-2.12	0.0035858
14339306	NAV2	Neuron navigator 2	-2.12	0.0052866
14422144	SRL	Sarcalumenin	-2.12	0.0028729
14403912	PDLIM7	PDZ and LIM domain 7 (enigma)	-2.12	0.000384
14281639	NT5E	5'-nucleotidase, ecto (CD73)	-2.12	0.0068563
14459376	DRP2	DRP2 // dystrophin related protein 2	-2.12	0.0004183
14416031	CTC1	CTS telomere maintenance complex component 1	-2.12	0.0012763
14374950	SEMA4B	Sema domain, immunoglobulin domain (Ig), transmembrane domain (TM) and short cytoplasmic domain	-2.12	0.0046086
14422322	SRRM2	Serine/arginine repetitive matrix 2	-2.11	0.0016852
14387683	CCDC158	Coiled-coil domain containing 158, transcript variant 1	-2.11	0.0043208
14401528	ELK4	ELK4, ETS-domain protein (SRF accessory protein 1)	-2.11	0.0014438
14362060	SMPD4	Sphingomyelin phosphodiesterase 4, neutral membrane (neutral sphingomyelinase-3)	-2.10	0.0007038
14321532	N4BP1	NEDD4 binding protein 1	-2.10	0.0001242
14379465	LPCAT4	Lysophosphatidylcholine acyltransferase 4	-2.10	0.000707
14357744	ATP2A2	ATPase, Ca++ transporting, cardiac muscle, slow twitch 2	-2.10	0.0040478
14368535	AS3MT	Arsenic (+3 oxidation state) methyltransferase	-2.09	0.004156
14306498	LOC483226	Methylosome protein 50-like	-2.09	0.0010908
14322014	WASF2	WAS protein family, member 2	-2.08	0.0019819
14441993	MAP3K9	Mitogen-activated protein kinase 9	-2.08	0.0048941
14321743	TMEM234	Transmembrane protein 234	-2.08	0.0009542
14335775	NFIX	Nuclear factor I/X (CCAAT-binding transcription factor)	-2.08	0.0043217
14307431	IFT172	Intraflagellar transport 172 homolog (Chlamydomonas)	-2.08	0.0005102
14362408	ATF7	Activating transcription factor 7	-2.07	0.0049196
14420251	LOC608835	Proline-rich protein 3-like	-2.07	0.0001469
14365377	TENC1	Tensin like C1 domain containing phosphatase	-2.07	0.0030479
14300209	LOC611426	uncharacterized	-2.06	0.0001624
14410241	BCL6B	B-cell CLL/lymphoma 6, member B	-2.06	0.0001833
14269730	MEIS1	Meis homeobox 1	-2.06	0.0076083

14319305	NEBL	Nebulette	-2.06	0.0008921
14355659	CBR4	Carbonyl reductase 4	-2.05	0.0039953
14418313	CRISPLD2	Cysteine-rich secretory protein LCCL domain containing 2	-2.04	0.0005238
14453163	LOC100856195	Flotillin-2-like	-2.04	0.0019161
14453266	GIT1	G protein-coupled receptor kinase interacting ArfGAP 1	-2.03	0.0021455
14421037	ATXN2L	Ataxin 2-like	-2.03	0.0017541
14315712	BBS1	Bardet-Biedl syndrome 1	-2.01	7.08E-05
14282289	LOC100856242	Nurim-like	-2.01	0.0026293
14399678	INO80D	INO80 complex subunit D	-2.01	0.0001585
14319630	FAM171A1	Family with sequence similarity 171, member A1	-2.01	0.0032473
14303678	GREB1	Growth regulation by estrogen in breast cancer 1	-2.01	0.000169
14422165	CREBBP	CREB binding protein	-2.01	0.0041639
14356674	SP110	SP110 nuclear body protein	-2.01	0.0023131
14305965	BCL9	B-cell CLL/lymphoma 9	-2.01	0.0062644
14294098	LSM10	U7 small nuclear RNA associated	-2.00	0.0001365
14360531	C26H12orf51	Chromosome 26 open reading frame, human C12orf51	-2.00	0.0008397
14386568	FRAS1	Fraser syndrome 1	-2.00	0.0070327
14300868	SORBS2	Sorbin and SH3 domain containing 2	-1.99	0.0043209
14419763	RHBDD2	Rhomboid domain containing 2	-1.99	0.0015067
14429473	CD55	CD55	-1.98	0.0017287
14379046	KLF3	Kruppel-like factor 3 (basic)	-1.98	1.23E-05
14426693	MKL2	MKL/myocardin-like 2	-1.94	0.0016282
14422375	RNPS1	RNA binding protein S1, serine-rich domain	-1.92	0.0006026
14331498	CERS4	Ceramide synthase 4	-1.91	0.0029483
14282384	DDX39B	DEAD (Asp-Glu-Ala-Asp) box polypeptide 39B	-1.89	0.0028996
14361544	SF3A1	Splicing factor 3a, subunit 1	-1.89	0.0010373
14312690	SF1	Splicing factor 1	-1.87	0.0006843
14260690	NFATC1	Nuclear factor of activated T-cells, cytoplasmic, calcineurin-dependent 1	-1.87	0.0036493
14312494	SYVN1	Synovial apoptosis inhibitor 1, synoviolin	-1.86	0.0010776
14433723	PTPN14	Protein tyrosine phosphatase, non-receptor type 14	-1.86	0.0008193
14358363	SSH1	slingshot homolog 1 (Drosophila)	-1.85	0.0008985
14333287	LOC100856259	SET domain-containing protein 5-like	-1.85	0.000861
14256190	TULP4	Tubby like protein 4	-1.85	0.0055682
14311164	SLC43A3	Solute carrier family 43, member 3	-1.85	0.0008504
14431996	GATAD2B	GATA zinc finger domain containing 2B	-1.81	0.0027215
14310205	LAMB1	Laminin, beta 1	-1.80	0.0044402
14360447	ATXN2	Ataxin 2	-1.79	0.0003399

14269237	EPAS1	Endothelial PAS domain protein 1	-1.78	0.006405
14406378	C10orf54	Chromosome 10 open reading frame 54	-1.76	0.0041549
14264607	EMP3	Epithelial membrane protein 3	-1.76	0.0069596
14437668	SAMD4A	Sterile alpha motif domain containing 4A	-1.75	0.0067634
14309603	LOC100856450	Pogo transposable element with ZNF domain-like	-1.74	0.0016606
14352781	PROSER1	Proline and serine rich 1	-1.74	0.0020732
14458281	USP11	Ubiquitin specific peptidase 11	-1.74	0.0002903
14390820	HEG1	HEG homolog 1 (zebrafish)	-1.74	0.0013119
14444308	SOX9	SRY (sex determining region Y)-box 9	-1.73	0.0048806
14337814	GAB2	GRB2-associated binding protein 2	-1.72	0.0019492
14288043	SNTB1	Syntrophin, beta 1	-1.72	0.0039552
14431823	KCNN3	Potassium intermediate/small conductance calcium-activated channel, subfamily N, member 3	-1.72	0.0006795
14335617	TECR	Trans-2,3-enoyl-CoA reductase	-1.71	0.0005928
14383275	MYO1E	Myosin IE	-1.70	0.0069968
14306172	ECM1	Extracellular matrix protein 1	-1.70	0.0011319
14329375	MAP4	Microtubule-associated protein 4	-1.69	0.0007358
14456137	LRRC37A2	Leucine rich repeat containing 37, member A2	-1.69	0.0071945
14425853	YPEL3	Yippee-like 3 (Drosophila)	-1.68	0.0009338
14370464	GOT1	Glutamic-oxaloacetic transaminase 1	-1.67	0.007637
14364247	CSDA	Cold shock domain protein A	-1.66	0.0021388
14446155	NFE2L1	Nuclear factor (erythroid-derived 2)-like 1	-1.66	0.0010265
14283733	RCAN2	Regulator of calcineurin 2	-1.65	0.0057276
14460279	HPRT1	Hypoxanthine phosphoribosyltransferase 1	-1.65	4.66E-05
14271370	ACO2	Aconitase 2, mitochondrial	-1.65	0.003443
14287965	ENPP2	Ectonucleotide phosphodiesterase 2	-1.64	0.0071504
14295467	ELK3	ETS-domain protein (SRF accessory protein 2)	-1.63	0.0002033
14435712	MAPRE2	Microtubule-associated protein, RP/EB family, member 2	-1.63	0.0030262
14319243	ARHGAP21	Rho GTPase activating protein 21	-1.62	0.0001376
14360729	MED13L	Mediator complex subunit 13-like	-1.61	0.0080276
14267946	CYB5R3	Cytochrome b5 reductase 3	-1.61	0.0013967
14345683	TSC22D2	TSC22 domain family, member 2	-1.60	0.0065129
14447314	TNFAIP1	Tumor necrosis factor, alpha-induced protein 1 (endothelial)	-1.60	0.0015703
14322498	ECE1	Endothelin converting enzyme 1	-1.60	0.0070936
14351034	PSMF1	Proteasome (prosome, macropain) inhibitor subunit 1	-1.60	0.0010511
14261067	ZNF532	Zinc finger protein 532	-1.59	0.0052136
14349213	SRSF6	Serine/arginine-rich splicing factor 6	-1.59	0.0006142
14331518	RAB11B	Member RAS oncogene family	-1.59	0.004916

14356006	DPYSL2	Dihydropyrimidinase-like 2	-1.58	0.0024522
14434363	PRRC2C	Proline-rich coiled-coil 2C	-1.58	0.0013934
14374483	ATP10A	ATPase, class V, type 10A	-1.56	0.0021843
14401056	DEDD	Death effector domain containing	-1.56	0.0012595
14318073	FAT4	FAT tumor suppressor homolog 4 (Drosophila)	-1.56	0.0055227
14361056	SPPL3	Signal peptide peptidase like 3	-1.56	0.0013294
14299705	PTN	Pleiotrophin	-1.56	5.54E-05
14435451	INTS3	Integrator complex subunit 3	-1.56	0.0047204
14364103	LOC488929	WW domain-binding protein 11-like	-1.56	1.34E-05
14327602	VGLL4	Vestigial like 4 (Drosophila)	-1.55	0.0006058
14421705	KIAA0430	KIAA0430 ortholog	-1.55	0.0033955
14275482	LOC100856258	Golgi-associated plant pathogenesis-related protein 1-like	-1.55	0.0075174
14402043	DDR2	Discoidin domain receptor tyrosine kinase 2	-1.54	0.0024805
14357902	TRAFD1	TRAF-type zinc finger domain containing 1	-1.54	2.87E-06
14436816	MMP14	Matrix metallopeptidase 14	-1.53	0.0003635
14285019	PNISR	PNN-interacting serine/arginine-rich protein	-1.52	0.0003459
14449024	ENG	Endoglin	-1.52	0.0031292
14265772	CAPNS1	Calpain, small subunit 1	-1.51	0.0052279
14462353	HUWE1	UBA and WWE domain containing 1, E3 ubiquitin protein ligase	-1.51	0.0008192
14278691	LPAR1	Lysophosphatidic acid receptor 1	-1.51	0.0001846
14390433	ZBTB20	Zinc finger and BTB domain containing 20	-1.51	0.0016855
14455642	TMED4	Transmembrane emp24 protein transport domain containing 4	-1.50	0.0001022

9.3 miRNAs Target Prediction

9.3.1 miR-340

Target Gene	Conserved sites				Poorly conserved sites				Total context+ score	Representative miRNA
	Total	8mer	7mer-m8	7mer-1A	Total	8mer	7mer-m8	7mer-1A		
LRP1B	**3**	2	0	1	**0**	0	0	0	-0.26	cfa-miR-340
ADAMTS18	**1**	0	0	1	**6**	1	1	4	-0.2	cfa-miR-340
ADAM2	**0**	0	0	0	**1**	1	0	0	-0.19	cfa-miR-340
CDH9	**0**	0	0	0	**3**	1	0	2	-0.15	cfa-miR-340

9.3.2 miR-let-7

Target Gene	Conserved sites				Poorly conserved sites				Total context+ score	Representative miRNA
	Total	8mer	7mer-m8	7mer-1A	Total	8mer	7mer-m8	7mer-1A		
ADAMTS15	**2**	2	0	0	**0**	0	0	0	-0.46	cfa-let-7j
ADAMTS8	**1**	1	0	0	**0**	0	0	0	-0.41	cfa-let-7f
COL14A1	**1**	0	1	0	**1**	0	0	1	-0.41	cfa-let-7g
COL1A2	**1**	1	0	0	**0**	0	0	0	-0.41	cfa-let-7g
COL3A1	**1**	1	0	0	**0**	0	0	0	-0.34	cfa-let-7a
CLDN12	**1**	1	0	0	**0**	0	0	0	-0.34	cfa-let-7f

9.3.3 miR-218

Target Gene	Conserved sites				Poorly conserved sites				Total context+ score	Representative miRNA
	Total	8mer	7mer-m8	7mer-1A	Total	8mer	7mer-m8	7mer-1A		
GLCE	**3**	3	0	0	**0**	0	0	0	-0.79	cfa-miR-218
COL1A1	**1**	1	0	0	**2**	0	1	1	-0.61	cfa-miR-218
ACTC1	**0**	0	0	0	**3**	1	2	0	-0.55	cfa-miR-218
FGF12	**3**	1	2	0	**1**	0	0	1	-0.48	cfa-miR-218
TNC	**1**	1	0	0	**0**	0	0	0	-0.46	cfa-miR-218
COL19A1	**0**	0	0	0	**1**	1	0	0	-0.4	cfa-miR-218
HS6ST3	**1**	1	0	0	**1**	0	1	0	-0.39	cfa-miR-218
HAPLN1	**2**	1	1	0	**0**	0	0	0	-0.38	cfa-miR-218
SRGAP2	**1**	1	0	0	**0**	0	0	0	-0.34	cfa-miR-218
HS3ST3B1	**1**	1	0	0	**0**	0	0	0	-0.33	cfa-miR-218

9.3.4 miR-708

Target Gene	Conserved sites				Poorly conserved sites				Total context+ score	Representative miRNA
	Total	8mer	7mer-m8	7mer-1A	Total	8mer	7mer-m8	7mer-1A		
ITGA4	**0**	0	0	0	**1**	1	0	0	-0.41	cfa-miR-708
HSPA4	**0**	0	0	0	**2**	0	2	0	-0.39	cfa-miR-708

9.3.5 miR-30

Target Gene	Conserved sites				Poorly conserved sites				Total context+ score	Representative miRNA
	Total	8mer	7mer-m8	7mer-1A	Total	8mer	7mer-m8	7mer-1A		
FGF23	**0**	0	0	0	**2**	1	0	1	-0.35	cfa-miR-30e
SNAI2	**0**	0	0	0	**2**	2	0	0	-0.33	cfa-miR-30e
COL12A1	**1**	1	0	0	**0**	0	0	0	-0.32	cfa-miR-30e
CAV1	**1**	1	0	0	**0**	0	0	0	-0.29	cfa-miR-30e
HAS2	**0**	0	0	0	**2**	1	0	1	-0.29	cfa-miR-30e
COL9A1	**0**	0	0	0	**1**	1	0	0	-0.27	cfa-miR-30e
CLDN16	**0**	0	0	0	**2**	1	1	0	-0.26	cfa-miR-30e

9.3.6 miR-214 / 761

Target Gene	Conserved sites				Poorly conserved sites				Total context+ score	Representative miRNA
	Total	8mer	7mer-m8	7mer-1A	Total	8mer	7mer-m8	7mer-1A		
CTSB	**0**	0	0	0	**3**	1	1	1	-0.52	cfa-miR-214
NOS1	**2**	0	1	1	**2**	0	0	2	-0.49	cfa-miR-761
IL16	**0**	0	0	0	**3**	1	1	1	-0.47	cfa-miR-214
MMP11	**0**	0	0	0	**3**	0	3	0	-0.4	cfa-miR-761
ECE2	**0**	0	0	0	**3**	0	3	0	-0.39	cfa-miR-214
NOS3	**0**	0	0	0	**1**	1	0	0	-0.38	cfa-miR-214

9.3.7 miR-15 / 16 / 195 / 497

Target Gene	Conserved sites				Poorly conserved sites				Total context+ score	Representative miRNA
	Total	8mer	7mer-m8	7mer-1A	Total	8mer	7mer-m8	7mer-1A		
FGF2	**2**	2	0	0	**3**	1	1	1	-1.42	cfa-miR-195
COL12A1	**3**	0	3	0	**0**	0	0	0	-0.65	cfa-miR-15a
NOS1	**1**	1	0	0	**2**	0	2	0	-0.58	cfa-miR-15b
HTR4	**1**	1	0	0	**2**	0	2	0	-0.56	cfa-miR-497
LRP6	**2**	0	2	0	**2**	0	1	1	-0.54	cfa-miR-15a
NF1	**1**	1	0	0	**1**	0	1	0	-0.49	cfa-miR-16
HSPG2	**1**	1	0	0	**1**	0	0	1	-0.45	cfa-miR-497
VEGFA	**1**	1	0	0	**0**	0	0	0	-0.43	cfa-miR-16
ECEL1	**1**	1	0	0	**0**	0	0	0	-0.42	cfa-miR-195
FGF7	**2**	0	1	1	**0**	0	0	0	-0.41	cfa-miR-16
CLDN12	**1**	1	0	0	**0**	0	0	0	-0.41	cfa-miR-15b

9.3.8 miR-125

Target Gene	Conserved sites				Poorly conserved sites				Total context+ score	Representative miRNA
	Total	8mer	7mer-m8	7mer-1A	Total	8mer	7mer-m8	7mer-1A		
CRTAP	**0**	0	0	0	**3**	2	0	1	-0.63	cfa-miR-125b
HTR4	**0**	0	0	0	**2**	1	0	1	-0.45	cfa-miR-125b

9.3.9 miR-532

Target Gene	Conserved sites				Poorly conserved sites				Total context+ score	Representative miRNA
	Total	8mer	7mer-m8	7mer-1A	Total	8mer	7mer-m8	7mer-1A		
HTR1F	**0**	0	0	0	**2**	1	1	0	-0.4	cfa-miR-532
CDH10	**0**	0	0	0	**1**	1	0	0	-0.37	cfa-miR-532
ADAMTS5	**0**	0	0	0	**4**	1	2	1	-0.37	cfa-miR-532
TNN	**0**	0	0	0	**1**	1	0	0	-0.37	cfa-miR-532
MMP13	**0**	0	0	0	**1**	1	0	0	-0.36	cfa-miR-532
LRP6	**1**	0	1	0	**1**	0	1	0	-0.33	cfa-miR-532
CAV2	**0**	0	0	0	**2**	0	0	2	-0.32	cfa-miR-532

9.3.10 miR-23

Target Gene	Conserved sites				Poorly conserved sites				Total context+ score	Representative miRNA
	Total	8mer	7mer-m8	7mer-1A	Total	8mer	7mer-m8	7mer-1A		
CLDN12	**1**	1	0	0	**1**	1	0	0	-0.46	cfa-miR-23a
IL12A	**0**	0	0	0	**2**	1	0	1	-0.42	cfa-miR-23a
VCAN	**1**	1	0	0	**1**	0	1	0	-0.38	cfa-miR-23a
HAS2	**1**	1	0	0	**1**	1	0	0	-0.38	cfa-miR-23a
EDNRB	**0**	0	0	0	**2**	2	0	0	-0.36	cfa-miR-23a
HGSNAT	**0**	0	0	0	**2**	0	1	1	-0.33	cfa-miR-23a
LAMC3	**0**	0	0	0	**1**	1	0	0	-0.3	cfa-miR-23a
FGF12	**0**	0	0	0	**1**	1	0	0	-0.3	cfa-miR-23a

9.3.11 miR-29

Target Gene	Conserved sites				Poorly conserved sites				Total context+ score	Representative miRNA
	Total	8mer	7mer-m8	7mer-1A	Total	8mer	7mer-m8	7mer-1A		
ADAMTS17	**3**	1	2	0	**1**	0	1	0	-1.06	cfa-miR-29b
COL4A4	**2**	0	2	0	**2**	1	1	0	-0.99	cfa-miR-29a
COL3A1	**2**	2	0	0	**0**	0	0	0	-0.93	cfa-miR-29b
COL4A5	**2**	2	0	0	**0**	0	0	0	-0.85	cfa-miR-29b
COL11A1	**2**	0	2	0	**1**	0	1	0	-0.85	cfa-miR-29a
FBN1	**2**	1	1	0	**1**	0	0	1	-0.82	cfa-miR-29a
ADAMTS2	**2**	1	1	0	**3**	0	2	1	-0.8	cfa-miR-29a
ELN	**3**	2	1	0	**0**	0	0	0	-0.78	cfa-miR-29b
COL9A1	**1**	1	0	0	**1**	0	1	0	-0.74	cfa-miR-29a
COL5A3	**3**	1	2	0	**0**	0	0	0	-0.68	cfa-miR-29b
CTSE	**0**	0	0	0	**2**	1	0	1	-0.65	cfa-miR-29b
COL1A1	**3**	1	0	2	**0**	0	0	0	-0.59	cfa-miR-29a
COL1A2	**2**	1	0	1	**0**	0	0	0	-0.58	cfa-miR-29a
PCDHA9	**1**	1	0	0	**0**	0	0	0	-0.58	cfa-miR-29a
PCDHAC2	**1**	1	0	0	**0**	0	0	0	-0.58	cfa-miR-29a
PCDHAC1	**1**	1	0	0	**0**	0	0	0	-0.58	cfa-miR-29a
PCDHA13	**1**	1	0	0	**0**	0	0	0	-0.58	cfa-miR-29a
PCDHA12	**1**	1	0	0	**0**	0	0	0	-0.58	cfa-miR-29a
PCDHA11	**1**	1	0	0	**0**	0	0	0	-0.58	cfa-miR-29a
PCDHA10	**1**	1	0	0	**0**	0	0	0	-0.58	cfa-miR-29a
PCDHA8	**1**	1	0	0	**0**	0	0	0	-0.58	cfa-miR-29a
PCDHA7	**1**	1	0	0	**0**	0	0	0	-0.58	cfa-miR-29a
PCDHA6	**1**	1	0	0	**0**	0	0	0	-0.58	cfa-miR-29a

PCDHA5	**1**	1	0	0	**0**	0	0	0	-0.58	cfa-miR-29a
PCDHA4	**1**	1	0	0	**0**	0	0	0	-0.58	cfa-miR-29a
PCDHA3	**1**	1	0	0	**0**	0	0	0	-0.58	cfa-miR-29a
PCDHA2	**1**	1	0	0	**0**	0	0	0	-0.58	cfa-miR-29a
PCDHA1	**1**	1	0	0	**0**	0	0	0	-0.58	cfa-miR-29a
COL7A1	**2**	1	1	0	**0**	0	0	0	-0.57	cfa-miR-29b
COL4A1	**2**	1	0	1	**0**	0	0	0	-0.56	cfa-miR-29c
CSGALNACT2	**0**	0	0	0	**3**	0	2	1	-0.56	cfa-miR-29a
HAS3	**3**	1	2	0	**1**	0	1	0	-0.55	cfa-miR-29b
COL5A1	**3**	2	1	0	**0**	0	0	0	-0.53	cfa-miR-29a
VEGFA	**1**	1	0	0	**0**	0	0	0	-0.53	cfa-miR-29a
ADAMTS14	**2**	2	0	0	**1**	0	1	0	-0.49	cfa-miR-29a
ROBO1	**1**	1	0	0	**0**	0	0	0	-0.47	cfa-miR-29a
LAMA2	**1**	1	0	0	**0**	0	0	0	-0.47	cfa-miR-29a
COL15A1	**1**	1	0	0	**0**	0	0	0	-0.46	cfa-miR-29b
COL2A1	**1**	1	0	0	**0**	0	0	0	-0.44	cfa-miR-29b
ADAMTS18	**2**	1	1	0	**0**	0	0	0	-0.44	cfa-miR-29b
COL6A3	**1**	1	0	0	**0**	0	0	0	-0.43	cfa-miR-29a
COL22A1	**1**	1	0	0	**1**	0	0	1	-0.43	cfa-miR-29a
LRP6	**2**	0	2	0	**0**	0	0	0	-0.42	cfa-miR-29b

9.3.12 miR-103 / 107

Target Gene	Conserved sites				Poorly conserved sites				Total context+ score	Representative miRNA
	Total	8mer	7mer-m8	7mer-1A	Total	8mer	7mer-m8	7mer-1A		
VCAN	**1**	1	0	0	**2**	0	0	2	-0.47	cfa-miR-103
NOS1	**2**	0	2	0	**2**	0	1	1	-0.46	cfa-miR-103

9.3.13 miR-181

Target Gene	Conserved sites				Poorly conserved sites				Total context+ score	Representative miRNA
	Total	8mer	7mer-m8	7mer-1A	Total	8mer	7mer-m8	7mer-1A		
IL16	**0**	0	0	0	**1**	1	0	0	-0.32	cfa-miR-181a
HTR1F	**0**	0	0	0	**3**	0	2	1	-0.3	cfa-miR-181c

9.3.14 miR-99

Target Gene	Conserved sites				Poorly conserved sites				Total context+ score	Representative miRNA
	Total	8mer	7mer-m8	7mer-1A	Total	8mer	7mer-m8	7mer-1A		
BMP8A	**0**	0	0	0	**1**	1	0	0	-0.6	cfa-miR-99a
HS3ST2	**1**	1	0	0	**0**	0	0	0	-0.58	cfa-miR-99a
HS3ST3B1	**1**	1	0	0	**0**	0	0	0	-0.56	cfa-miR-99a
MMP13	**0**	0	0	0	**1**	1	0	0	-0.54	cfa-miR-99a
FGFR3	**1**	1	0	0	**0**	0	0	0	-0.44	cfa-miR-99a
ITFG2	**0**	0	0	0	**1**	0	1	0	-0.36	cfa-miR-99a
CDH6	**0**	0	0	0	**1**	0	1	0	-0.32	cfa-miR-99b
ITGA2	**0**	0	0	0	**1**	0	0	1	-0.3	cfa-miR-99a
CLDN11	**1**	0	1	0	**0**	0	0	0	-0.28	cfa-miR-99a
BMPR2	**1**	0	0	1	**0**	0	0	0	-0.27	cfa-miR-99a
COL17A1	**0**	0	0	0	**1**	0	0	1	-0.25	cfa-miR-99a

LAMC1	**0**	0	0	0	**1**	0	0	1	-0.21	cfa-miR-99a

9.3.15 miR-25 / 32 / 363

Target Gene	Conserved sites				Poorly conserved sites				Total context+ score	Representative miRNA
	Total	8mer	7mer-m8	7mer-1A	Total	8mer	7mer-m8	7mer-1A		
ITGAV	**1**	1	0	0	**3**	0	1	2	-0.42	cfa-miR-32
ADAM23	**1**	1	0	0	**0**	0	0	0	-0.42	cfa-miR-25
ADAM21	**0**	0	0	0	**1**	1	0	0	-0.41	cfa-miR-32
ADAMTSL3	**1**	1	0	0	**0**	0	0	0	-0.38	cfa-miR-32
BGN	**1**	1	0	0	**0**	0	0	0	-0.38	cfa-miR-25
KERA	**0**	0	0	0	**2**	0	1	1	-0.37	cfa-miR-32
PCDH9	**1**	0	0	1	**1**	0	1	0	-0.36	cfa-miR-363
ADAM19	**1**	1	0	0	**1**	0	0	1	-0.36	cfa-miR-32

9.3.16 miR-145

Target Gene	Conserved sites				Poorly conserved sites				Total context+ score	Representative miRNA
	Total	8mer	7mer-m8	7mer-1A	Total	8mer	7mer-m8	7mer-1A		
SRGAP2	**3**	3	0	0	**2**	0	1	1	-0.95	cfa-miR-145
ITGB8	**3**	1	2	0	**0**	0	0	0	-0.58	cfa-miR-145
SRGAP1	**3**	1	2	0	**1**	1	0	0	-0.57	cfa-miR-145
ITGA2	**0**	0	0	0	**2**	2	0	0	-0.43	cfa-miR-145
ITFG1	**0**	0	0	0	**1**	1	0	0	-0.38	cfa-miR-145
ACTG1	**1**	1	0	0	**0**	0	0	0	-0.38	cfa-miR-145
CTSL2	**0**	0	0	0	**2**	1	1	0	-0.36	cfa-miR-145

9.3.17 miR-130 / 301 / 454

Target Gene	Conserved sites				Poorly conserved sites				Total context+ score	Representative miRNA
	Total	8mer	7mer-m8	7mer-1A	Total	8mer	7mer-m8	7mer-1A		
IL15	**0**	0	0	0	**2**	0	2	0	-0.44	cfa-miR-130a
LRP8	**1**	1	0	0	**1**	0	0	1	-0.42	cfa-miR-130a
ADAM12	**1**	1	0	0	**0**	0	0	0	-0.4	cfa-miR-301a
LDLR	**3**	0	3	0	**0**	0	0	0	-0.39	cfa-miR-130b
ADAM28	**0**	0	0	0	**1**	1	0	0	-0.38	cfa-miR-454
CTNNA3	**0**	0	0	0	**1**	0	1	0	-0.35	cfa-miR-130a
BMPR2	**1**	0	1	0	**1**	0	1	0	-0.35	cfa-miR-130a

9.3.18 miR-1843

Target Gene	Conserved sites				Poorly conserved sites				Total context+ score	Representative miRNA
	Total	8mer	7mer-m8	7mer-1A	Total	8mer	7mer-m8	7mer-1A		
PCDH7	**1**	1	0	0	**1**	1	0	0	-0.64	cfa-miR-1843
COL3A1	**0**	0	0	0	**1**	1	0	0	-0.46	cfa-miR-1843
ESAM	**0**	0	0	0	**2**	0	2	0	-0.38	cfa-miR-1843

9.3.19 miR-197

Target Gene	Conserved sites				Poorly conserved sites				Total context+ score	Representative miRNA
	Total	8mer	7mer-m8	7mer-1A	Total	8mer	7mer-m8	7mer-1A		
ADAMTS5	**1**	1	0	0	**4**	0	2	2	-0.79	cfa-miR-197
AFAP1L2	**0**	0	0	0	**2**	1	1	0	-0.65	cfa-miR-197
HTR7	**1**	1	0	0	**1**	0	1	0	-0.58	cfa-miR-197
ITGAM	**0**	0	0	0	**2**	1	0	1	-0.5	cfa-miR-197
CTNND1	**1**	1	0	0	**0**	0	0	0	-0.4	cfa-miR-197
HTR2C	**0**	0	0	0	**1**	1	0	0	-0.4	cfa-miR-197
CTSL1	**0**	0	0	0	**1**	1	0	0	-0.37	cfa-miR-197
PCDH18	**0**	0	0	0	**1**	1	0	0	-0.36	cfa-miR-197
LAMC1	**0**	0	0	0	**1**	1	0	0	-0.35	cfa-miR-197
COL5A2	**0**	0	0	0	**2**	0	1	1	-0.32	cfa-miR-197
LRPAP1	**0**	0	0	0	**1**	1	0	0	-0.32	cfa-miR-197

9.3.20 miR-143

Target Gene	Conserved sites				Poorly conserved sites				Total context+ score	Representative miRNA
	Total	8mer	7mer-m8	7mer-1A	Total	8mer	7mer-m8	7mer-1A		
FNDC7	**0**	0	0	0	**3**	2	1	0	-0.69	cfa-miR-143
ITGAL	**0**	0	0	0	**2**	1	1	0	-0.38	cfa-miR-143
FGF9	**1**	1	0	0	**0**	0	0	0	-0.38	cfa-miR-143
CLDN1	**0**	0	0	0	**1**	1	0	0	-0.3	cfa-miR-143
ITGA6	**1**	1	0	0	**1**	0	0	1	-0.3	cfa-miR-143
COL6A5	**0**	0	0	0	**2**	0	1	1	-0.28	cfa-miR-143
FLNB	**0**	0	0	0	**3**	0	2	1	-0.27	cfa-miR-143

9.3.21 miR-872

Target Gene	Conserved sites				Poorly conserved sites				Total context+ score	Representative miRNA
	Total	8mer	7mer-m8	7mer-1A	Total	8mer	7mer-m8	7mer-1A		
ACTC1	**0**	0	0	0	**1**	1	0	0	-0.39	cfa-miR-872
PCDHAC1	**0**	0	0	0	**1**	1	0	0	-0.37	cfa-miR-872
ECM2	**0**	0	0	0	**1**	1	0	0	-0.31	cfa-miR-872
ITGAV	**0**	0	0	0	**2**	1	1	0	-0.29	cfa-miR-872
ADAMTS19	**0**	0	0	0	**2**	0	1	1	-0.25	cfa-miR-872
COL14A1	**0**	0	0	0	**1**	0	1	0	-0.25	cfa-miR-872
ANGPTL3	**0**	0	0	0	**1**	0	1	0	-0.25	cfa-miR-872
POSTN	**0**	0	0	0	**1**	0	1	0	-0.24	cfa-miR-872

9.3.22 miR-545

Target Gene	Conserved sites				Poorly conserved sites				Total context+ score	Representative miRNA
	Total	8mer	7mer-m8	7mer-1A	Total	8mer	7mer-m8	7mer-1A		
HTR2C	**2**	0	2	0	**1**	0	1	0	-0.37	cfa-miR-545
SNAI2	**1**	1	0	0	**1**	0	0	1	-0.33	cfa-miR-545
MMP16	**0**	0	0	0	**1**	1	0	0	-0.26	cfa-miR-545